JOURNAL OF THE AERONAUTICAL SCIENCES

VOLUME 22 JULY, 1955 NUMBER 7

CONTENTS

Laminar Compressible Boundary Layer Along a Curved Insulated Surface.....I. FLÜGGE-LOTZ AND ARLO F. JOHNSON 445

On the Stability of the Laminar Boundary Layer in a Compressible Fluid.....D. W. DUNN AND C. C. LIN 455

The Unsteady Forces Due to Viscous Wakes in Turbomachines.....NELSON H. KEMP AND W. R. SEARS 478

The Design and Calibration of a Variable Mach Number Nozzle.....JOHN ROSÉN 484

On the Buckling of Stringer Panels, Including Forced Crippling.....P. P. BIJLAARD 491

Readers' Forum: "The Effect of the Temperature Dependence of King's 'Constant' A on the Hot-Wire Sensitivity Coefficient," by J. R. Ruetenik; "Optimum Stage for Axial Flow Turbines," by N. Van Le; "A Similarity Rule for the Interaction Between a Conical Field and a Plane Shock," by Y. H. Kuo; "Effect of High Advancing-Tip Mach Number on Helicopter Blade Flapping," by Kenneth B. Amer and H. Hirsch; "Analysis of Thermal Stresses in Conical Shells," by Marvin Stern; "Transient Stresses in Airfoils Under Blast Loading," by H. F. Ludloff and F. J. Marshall; "On a Stress Tensor for Turbulence," by Willis H. Braun; "The Obukhoff Spectrum of Homogeneous Isotropic Turbulence," by Knox Millsaps; "On the Normal Force Produced by Multifinned Tail Assemblies in Supersonic Flow," by J. Leith Potter, William D. Murphree, and Norman M. Shapiro; "Note on Velocity Fluctuations in Equilibrium Turbulent Shear Flow Along Solid Boundaries," by Heinrich B. Helmbold; "Limitations of Linear Theory in Predicting the Pressure Distribution on Triangular Wings," by Elliott D. Katzen; "A New Method of Solution of Equation of Compressible Flow," by Ezio Betti; "On Use of the General Bending Formula," by W. P. Rodden.502–516

Published by

INSTITUTE OF THE AERONAUTICAL SCIENCES, INC.

JOURNAL OF THE AERONAUTICAL SCIENCES

Editor: HUGH L. DRYDEN, *Director, NACA*
Associate Editor: ROBERT R. DEXTER
Managing Editor: RITA J. TURINO
Editorial Assistant: CAROLINE TAYLOR

Editorial Committee

Aerodynamics

Dean R. Chapman
Francis H. Clauser
Antonio Ferri
Alexander Flax
R. Paul Harrington
R. T. Jones
Carl Kaplan
H. W. Liepmann
C. C. Lin
H. F. Ludloff
Harold Luskin
John R. Markham
Clark B. Millikan
Shatswell Ober
W. Bailey Oswald
C. D. Perkins
Elliott G. Reid
H. J. E. Reid
Russell Robinson
George S. Schairer
G. B. Schubauer
W. R. Sears
John Stack
Theodore Theodorsen
Th. von Kármán

Air Transport

Charles Froesch
J. A. Herlihy
R. D. Kelly
Otto E. Kirchner
Jerome Lederer
John C. Leslie
R. Dixon Speas

Flight Testing

R. R. Gilruth
Melvin N. Gough
W. L. Howland
W. F. Milliken, Jr.
E. G. Stout

Structures and Materials

W. B. Bleakney
E. W. Conlon
John E. Duberg
E. C. Hartmann
N. J. Hoff
Samuel Levy
J. F. McBrearty
Alfred S. Niles
W. Ramberg
F. R. Shanley
C. R. Strang
S. Timoshenko
H. S. Tsien

Rotating Wing Aircraft

F. B. Gustafson
K. H. Hohenemser
Bartram Kelley
R. B. Maloy
Ralph McClarren
R. H. Miller
R. H. Prewitt
Igor I. Sikorsky

Vibration and Flutter

Lee Arnold
M. A. Biot
R. L. Bisplinghoff
William Bollay
Chieh-Chien Chang
J. P. Den Hartog
I. E. Garrick
Martin Goland
Theodore Theodorsen

Aircraft Design

W. E. Beall
E. H. Heinemann
Hall L. Hibbard
Richard Hutton
C. L. Johnson
A. A. Kartveli
E. G. Stout
F. K. Teichmann
Robert J. Woods

Electronics in Aviation

Welcome W. Bender
K. C. Black
M. V. Kiebert, Jr.
David S. Little
S. B. Rogers
Paul Rosenberg
L. M. Sherer

Physiologic Problems

H. G. Armstrong
Louis H. Bauer
Robert J. Benford
W. Randolph Lovelace, II
Ross A. MacFarland

Fuels and Oils

D. P. Barnard
J. H. Doolittle
Graham Edgar
R. T. Goodwin
A. M. Rothrock

Flight Propulsion

George W. Brady
Frank W. Caldwell
L. S. Hobbs
E. E. Johnson
Joseph Keenan
R. P. Kroon
Hans Reissner
Abe Silverstein
C. Fayette Taylor
E. S. Taylor
P. B. Taylor
E. S. Thompson
H. S. Tsien

Instruments

Allan G. Binnie
Charles H. Colvin
Frank R. Cook
C. S. Draper
S. G. Eskin
O. E. Esval
C. F. Savage
R. C. Sylvander

Meteorology

C. F. Brooks
D. M. Little
F. W. Reichelderfer
K. C. Spengler

SUBSCRIPTION RATES

JOURNAL OF THE AERONAUTICAL SCIENCES, Published Monthly.—United States and Possessions: 1 Year, $12.00; Single Copies, $1.50. Foreign Countries Including Canada (American Currency Rates): 1 Year, $13.00; Single Copies, $1.50.

AERONAUTICAL ENGINEERING REVIEW, Published Monthly.—United States and Possessions: 1 Year, $3.00; Single Copies, $0.50. Foreign Countries Including Canada (American Currency Rates): 1 Year, $3.50; Single Copies, $0.50.

Notices of change of address should be sent to the Institute at least 30 days prior to actual change of address.

Manuscripts for publication, proofs, and all correspondence should be addressed to the Editorial Office of the JOURNAL.

Correspondence regarding subscriptions may be addressed to Publication Office, 20th and Northampton Sts., Easton, Pa., or to the Editorial Office of the JOURNAL OF THE AERONAUTICAL SCIENCES, 2 East 64th Street, New York 21, N.Y.

Copyright, 1955, by the Institute of the Aeronautical Sciences, Inc.

Entered as Second Class Matter at the Post Office, Easton, Pa., May 1, 1937. Acceptance for mailing at a special rate of Postage provided for in the Act of August 24, 1912. Authorized April 29, 1937.

JOURNAL OF THE AERONAUTICAL SCIENCES

VOLUME 22 JULY, 1955 NUMBER 7

Laminar Compressible Boundary Layer Along a Curved Insulated Surface*

I. FLÜGGE-LOTZ† AND ARLO F. JOHNSON‡

Stanford University

ABSTRACT

Several approximate methods exist for computing the compressible laminar boundary-layer flow along a curved surface with given pressure gradient and given wall temperature. The boundary-layer flow for given pressure gradient and insulated wall is an essentially different problem, because for Prandtl Number unequal to one the wall temperature is unknown and a rather accurate computation of this temperature is desirable. In this paper a method is developed for solving the laminar compressible boundary layer over insulated bodies of arbitrary shape via the integrated momentum and energy equations and the expression of velocity and temperature profiles by polynomials. Examples are worked out for a flat plate which is compared with Crocco's solution, for an arbitrary pressure distribution which is compared with the solution of Flügge-Lotz and Eichelbrenner, for a biconvex airfoil, and for an inflected wall. The method gives results accurate to a few per cent so long as the flow is accelerating. Like the Pohlhausen technique—its counterpart in incompressible flow—it is less accurate in decelerating flows and predicts separation too far downstream. The time required to calculate the drag coefficient, boundary-layer thickness, velocity, and temperature profiles at any given section using this method is of the order of a few hours.

The solutions presented indicate that compressibility has an appreciable effect on velocity, temperature, drag, and boundary-layer thickness. Prandtl Number variation appears to create a significant change only in the temperature profile.

A method that Gruschwitz developed to solve the same problem is briefly discussed at the end of this paper.

NOTATION

x	=	arc length along the wall, ft.
y	=	coordinate normal to the wall, ft.
u	=	velocity in the x direction, ft. per sec.
v	=	velocity in the y direction, ft. per sec.
ρ	=	fluid density, slugs per ft.^{3}
p	=	fluid pressure, lb. per sq.ft.
μ	=	absolute viscosity, slugs per ft. sec.
ν	=	μ/ρ kinematic viscosity, sq.ft. per sec.
τ	=	$\mu(\partial u/\partial y)$ viscous shear stress, lb. per sq.ft.
c_p	=	specific heat at constant pressure, sq.ft. per sec.^{2} °R.
c_v	=	specific heat at constant volume, sq.ft. per sec.^{2} °R.
γ	=	c_p/c_v (1.4 for air) ratio of the specific heats
T	=	absolute temperature, °R.
i	=	c_pT (perfect gas) enthalpy, sq.ft. per sec.^{2}
j	=	$i + (u^2/2)$ total specific energy, sq.ft. per sec.^{2}
k_T	=	thermal conductivity, lb. per sec. °R.
Pr	=	$(\mu c_p)/(k_T)$, Prandtl Number
R_1	=	gas constant in the equation of state
C	=	empirical constant in the Sutherland Equation, °R.
C_1	=	C/T_0, modified Sutherland constant
a	=	speed of sound, ft. per sec.
M	=	u/a, Mach Number
m	=	$[(\gamma - 1)/2]\ M_e^2 = u_e^2/2i_e$ compressibility variable
C_d	=	local drag coefficient
C_D	=	total drag coefficient
θ	=	$\int_0^{y_e} \frac{\rho u}{\rho_e u_e}\left(1 - \frac{u}{u_e}\right) dy$ momentum thickness, ft.
δ^*	=	$\int_0^{y_e} \left(1 - \frac{\rho u}{\rho_e u_e}\right) dy$ displacement thickness, ft.
u_r	=	u/u_e, velocity ratio
ρ_r	=	ρ_e/ρ, density ratio
T_r	=	T/T_e, temperature ratio
η	=	normalized y coordinate
δ	=	boundary-layer "thickness" used in defining η, ft.
a_0, a_1, a_2, etc.	=	coefficients in the velocity polynomial
b	=	ρ_e/ρ_w, basic parameter in the density polynomial
$b, b_1, b_2, \ldots, b_5$	=	coefficients in the density polynomial [Eq. (15)]
$d, d_1, d_2, \ldots, d_5$	=	coefficients in the density polynomial [Eq. (16)]
λ	=	basic parameter in the velocity polynomial

Received April 7, 1954.

* This study is part of a research project at Stanford University sponsored by the Office of Naval Research [Contract N6-onr-251 Task Order 6 (NR-035-104)].

† Lecturer, Department of Mechanical Engineering, Stanford University.

‡ Formerly, Graduate Student at Stanford University. Now, Associate Professor, Department of Mechanical Engineering, University of Utah.

X = $(b'u_e)/(bu'_e)$, abbreviated notation for this ratio
κ = alternate parameter to λ
L = characteristic length, ft.
Re = $(u_0 L)/\nu_0$, Reynolds Number, based on the reference values
f_1, f_2, etc. = functions of λ
B = tabulated function of λ and R
R = $(b-1)/m$, abbreviated notation of the given ratio
ΔB = tabulated function of λ
k_1 = constant associated with the isentropic energy equation

Subscripts and Superscripts

e = value in the flow just external to the boundary layer
w = value at the wall
0 = value at the reference point in the flow (free-stream values have been taken here)
sep. = value at the separation point
stag. = value at the stagnation point
$'$ = $\partial/\partial x$
$''$ = $\partial^2/\partial x^2$

Variables in Dimensionless Form

$x_d = x/L$
$y_d = (y\sqrt{Re})/L$
$u_d = u_e/u_0$
$T_d = T_e/T_0$
$b_d' = Lb'$
$u_d' = (Lu_e')/u_0$
$\rho_d = \rho_e/\rho_0$
$\nu_d = \nu_e/\nu_0$
$\theta_d^2 = (\theta^2 Re)/L^2$
$\theta_d^{2\prime} = (\theta^{2\prime} Re)/L$

Introduction

THE PROBLEM ATTACKED HERE, the so-called "thermometer problem" of compressible flow, had been previously solved with the help of finite differences by Flügge-Lotz and Eichelbrenner,[1] but since their solution is laborious, the present work is offered as an approximate solution that will give satisfactory accuracy with a reasonable expenditure of time. The line of attack follows that conceived by von Kármán. executed by Pohlhausen,[2] and refined by Holstein and Bohlen[3] for the corresponding incompressible fluid case, Because of its length, the mathematical development can be presented here only in skeleton form. One may find its detailed development and discussion in reference 4.

Basic Relations in the Boundary Layer

To solve the boundary-layer problem exactly, one must satisfy the following equations:

(1) Equation of conservation of mass:

$$[(\partial/\partial x)\ (\rho u)] + [(\partial/\partial y)\ (\rho v)] = 0 \qquad (1)$$

Note that this consideration is limited to two-dimensional flow. These results can be extended to the three-dimensional flow about axially symmetric bodies by the method of Mangler.[5]

(2) Momentum equation:

$$[\rho u(\partial u/\partial x)] + [\rho v(\partial u/\partial y)] = -(\partial p/\partial x) + (\partial \tau/\partial y) \qquad (2)$$

This equates flow-wise (x) components of force to momentum change. The equation for y components degenerates to the form

$$\partial p/\partial y = 0 \qquad (3)$$

because of the extreme thinness of the boundary layer and the deductions that follow therefrom.

(3) The energy equation, expressed in alternate forms:

$$[\rho u(\partial j/\partial x)] + [\rho v(\partial j/\partial y)] = (\partial/\partial y)\ (u\tau) + (\partial/\partial y)\ [k_T(\partial T/\partial y)] \qquad (4a)$$

$$= (1/Pr)\ (\partial/\partial y)\ [\mu(\partial j/\partial y)] - [(1-Pr)/Pr]\ (\partial/\partial y)\ (u\tau) \qquad (4b)$$

It is derived under the usual assumption that there is no appreciable exchange of energy in the x direction. Because μ and k_T vary with temperature, while Pr is constant for a given fluid, Eq. (4b) proves preferable for mathematical analysis. It reveals by inspection the particular solution, j = constant when $Pr = 1$, which fits the physical boundary conditions of flow over an insulated wall.

(4) Equation of state for a perfect gas:

$$p = R_1 \rho T \qquad (5)$$

(5) Viscosity-temperature relations:

$$(\mu/\sqrt{T})\ [1 + (C/T)] = \text{const.} \qquad (6)$$

where $C = 203$ for air, T in degrees Rankine.

$$\rho\mu = \rho_e \mu_e \qquad (7)$$

Eq. (6) is the Sutherland empirical relation which nicely fits experimental data. Because of its awkward form, it will be used only to evaluate $\mu(T)$ for the potential flow just outside the boundary layer. Passing at constant x through the boundary layer, we shall substitute the simpler Eq. (7). Crocco,[6] substantiated by Howarth,[7] found that for the flat plate this substitution wrought no appreciable effect on temperatures and velocities, only a minor overestimating effect on drag. We assume the pressure gradient on our curved surfaces will not magnify these errors appreciably.

Boundary Conditions

The boundary conditions for these differential equations are:

(a) No slip at, or flow through, the wall—i.e., $u_w = v_w = 0$

(b) Insulated wall, $(\partial T/\partial y)_w = 0$

(c) Asymptotic transition of velocity and temperature from boundary layer to potential flow, $u_r \to 1$, $T_r \to 1$.

It is assumed that the velocity u_e (x) is known. For a body of given shape, this function will be calculated by the theory of frictionless fluid or else evaluated experimentally.

Mathematical Development: Satisfying Average Momentum and Energy Relations

The coupled, nonlinear differential equations [Eqs. (1), (2), and (4)] force one to conclude that the problem cannot be solved in exact form with a reasonable expenditure of calculation effort. The method of Flügge-Lotz and Eichelbrenner, which is nearly exact, requires a calculation point by point, in both x and y increments, of the basic equations using finite differences. The work involved is prohibitive. If we take averages in the y direction and seek only to satisfy the equations governing such averages, the y increment is thereby in effect extended to the entire width of the boundary layer and only x-wise steps need to be taken.

The averaging is done by multiplying each term of Eqs. (2) and (4) by dy and integrating with respect to y through the boundary layer, using Eq. (1) to eliminate v. The integration $\int_0^{y_e}$ [Eq. (2)] dy yields

$$\tau_w/\rho_e = v_e{}^2\theta' + u_e u_e'\theta[2 - M_e{}^2 + (\delta^*/\theta)] \quad (8)$$

The integration $\int_0^{y_e}$ [Eq. (4)] dy yields

$$\frac{\partial}{\partial x}\int_0^{y_e} \rho u(j_e - j)\, dy = 0$$

which for the insulating wall is

$$\int_0^{y_e} \rho u(j_e - j)\, dy = 0$$

Replacing j by $i + (u^2/2)$ and normalizing y through the substitution (first suggested by Dorodnitzyn)

$$\eta = \int_0^y \frac{dy}{\rho_r} \Big/ \int_0^{y_e} \frac{dy}{\rho_r} = \frac{1}{\delta}\int_0^y \frac{dy}{\rho_r} \quad (9)$$

(i.e., $\rho_r\delta\, d\eta = dy$) we obtain the energy relation in the form

$$\int_0^1 u_r(\rho_r - 1)\, d\eta = m\int_0^1 u_r(1 - u_r{}^2)\, d\eta \quad (10)$$

This peculiar way of normalizing y requires both explanation and justification. The simpler substitution $\eta = y/y_e$ would give $\eta = 0$ when $y = 0$, $\eta \to 1$ when $y \to y_e$, as does our substitution, and appears preferable because of its simplicity. However, such a substitution would yield approximate velocity profiles that do not change shape with Pr and M_e, as they must (Fig. 1).

Although Prandtl Number does not appear in Eqs. (8) and (10), it does exert its influence through the ρ_r term, as will presently be seen.

Introduction of Velocity and Density Polynomials: Accelerated Flow

Equations (8) and (10) become amenable to solution if we can find expressions for u_r and ρ_r involving only two unknown parameters. For the accelerated flow—

FIGURE 1

Effect of Mach Number and Prandtl Number on Flat Plate Velocity Profiles

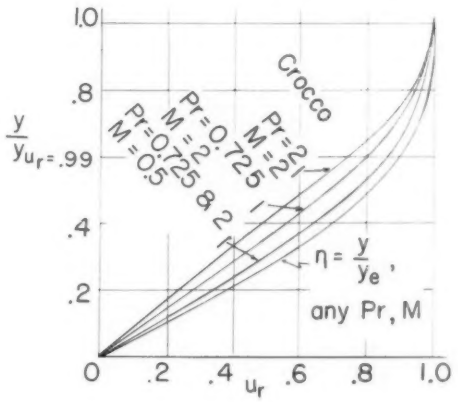

i.e., from the stagnation point to the point of minimum pressure—let us assume

$$u_r = a_0 + a_1\eta + a_2\eta^2 + a_3\eta^3 + a_4\eta^4 \quad (11)$$

and apply the boundary conditions:

At the wall satisfy (1) the condition of no slip ($u = 0$) and (2) the differential momentum equation [Eq. (2)].

At $\eta = 1$ simulate an asymptotic approach of u_r to unity: (3) $u_r = 1$; (4) $\partial u_r/\partial\eta = 0$; and (5) $\partial^2 u_r/\partial\eta^2 = 0$. Eq. (11) then becomes

$$u_r = \eta(2 - 2\eta^2 + \eta^3) + (\lambda\eta/6)(1 - \eta)^3 \quad (12)$$

where

$$\lambda = [(b\delta^2)/\nu_e]u_e' \quad (13)$$

It is the fundamental parameter of this profile.

At $Pr = 1$, $j = j_e$ or $i + (u^2/2) = i_e + (u_e{}^2/2)$, which yields the relation

$$\rho_r = 1 + m(1 - u_r{}^2) \quad (14)$$

Thus we require an eighth-degree density polynomial to be consistent with u_r.

$$\rho_r = b + b_1\eta + \ldots + b_8\eta^8 \quad (15)$$

Since we do not wish to specify eight boundary conditions, we also write it in alternate form.

$$\rho_r = 1 + m(1 - u_r{}^2) + (1 - Pr)(d + d_1\eta + \ldots + d_5\eta^5) \quad (16)$$

and apply the following boundary conditions:

At the wall satisfy (1) the condition of no heat transfer; (2) the differential energy equation [Eq. (4)]; and (3) $\partial/\partial y$ [Eq. (4)].

At $\eta = 1$ simulate an asymptotic approach of ρ_r to unity: (4) $\rho_r = 1$ and (5) $\partial\rho_r/\partial\eta = 0$.

Eq. (15) becomes

$$\rho_r - 1 = (b-1)(1 - 5\eta^4 + 4\eta^5) + PrX\{[\lambda(12+\lambda)]/36\}\eta^3(1-\eta)^2 - Pr\,m\,[(12+\lambda)/36]\eta^2(1-\eta)^2 \times [12(1+2\eta) + \lambda(1-2\eta)] + m\{[\eta^4(1-\eta)^2]/36\}[36(1+2\eta-\eta^2) + 12\lambda(2-\eta)(1-\eta) - \lambda^2(6-4\eta+\eta^2)] \quad (17)$$

The density (or temperature)* profile is seen to depend upon the following variables: Pr (constant for a given fluid); $m = [(\gamma-1)/2]M_e^2$ (compressibility variable); λ (basic profile parameter); and X [$X = (b'u_e)/(bu_e')$]. This last variable, X, exerts through b' a controlling influence on the variation of temperature along the wall. When $Pr = 1$, $X = 2m$, showing X to be another manifestation of compressibility effect.

At this point a few words need to be said about the choice of boundary conditions for the u_r and ρ_r polynomials.

Experience in the comparable Pohlhausen method for incompressible fluid has shown that a different choice of boundary conditions (e.g., impose $\partial^3 u_r/\partial\eta^3$ in addition to $\partial^2 u_r/\partial\eta^2 = 0$, or in lieu of it at $\eta = 1$) may greatly change the predicted location of the separation point and, to a small degree, reshape the velocity profiles. Therefore careful attention should be given to this point, and boundary conditions should be chosen which lead to best agreement with those exact solutions that are available. A study by Mangler[8] on this point augmented our own calculations and comparisons and led to the choice indicated. The experience of Flügge-Lotz and Eichelbrenner on this same problem led to the inclusion of the third condition for the ρ_r profile $\{\partial/\partial y$ [Eq. (4)] satisfied at the wall$\}$. It brings our variable X, thence b', into the solution and thereby gives a control of temperature variation along the wall ($b = \rho_w/\rho_e = T_e/T_w$) which appears essential but is not otherwise obtained. Note that no attempt is made to assign separate thicknesses to the thermal and kinetic boundary layers. In each case, it is assumed that temperature and velocity attain potential value at the same point, $\eta = 1$. However, velocity, with three outer boundary conditions, is required to approach its potential value more rapidly than temperature, with only two outer boundary conditions. After all, an artificiality must be introduced when finite "thickness" is assigned to the layers that are actually asymptotic in profile, and the above device is at least as reasonable as the carrying of separate thermal and kinetic boundary-layer "thicknesses," and much simpler mathematically.

* Since $\partial p/\partial y = 0$, $\rho_r = T_r$.

Velocity and Density Polynomials: Decelerated Flow

On the basis of our studies of choice of boundary conditions it was concluded that a better prediction of separation point would result if for decelerating flow—from the point of minimum pressure to the separation point—we change to a different velocity polynomial:

$$u_r = a_1\eta + \ldots + a_5\eta^5 \quad (18)$$

One additional boundary condition is imposed: Satisfy $\partial/\partial y$ [Eq. (2)] at the wall.† Putting in the boundary conditions, Eq. (18) becomes

$$u_r = (\eta/3)(5 - 5\eta^3 + 3\eta^4) + (\lambda\eta/4)(1-\eta)^3(1+\eta) \quad (19)$$

† Imposing this additional boundary condition on the accelerating flow is found to *decrease* accuracy there, contrary to what one might expect.

Table 1

For $Pr = 1$

λ	κ	f_1	$f_2 + f_3 + f_4$	$2(\theta/\delta)a_1$
12	0.0948	−0.095	1.043	0.711
11	0.0941	−0.091	1.038	0.709
10	0.0919	−0.080	1.023	0.703
9	0.0882	−0.061	0.997	0.693
8	0.0831	−0.034	0.963	0.679
7.8	0.0819	−0.027	0.956	0.677
7.6	0.0807	−0.020	0.948	0.674
7.4	0.0794	−0.013	0.940	0.670
7.2	0.0781	−0.006	0.932	0.666
7	0.0767	0.002	0.923	0.662
6.8	0.0752	0.010	0.914	0.659
6.6	0.0737	0.019	0.904	0.655
6.4	0.0721	0.028	0.893	0.651
6.2	0.0705	0.037	0.882	0.647
6	0.0689	0.046	0.872	0.643
5	0.0599	0.098	0.816	0.620
4	0.0497	0.158	0.754	0.595
3	0.0385	0.225	0.688	0.567
2	0.0264	0.299	0.618	0.536
1	0.0135	0.381	0.545	0.504
0	0	0.470	0.470	0.470
0	0	0.414	0.414	0.414
−1	−0.0157	0.506	0.316	0.355
−2	−0.0316	0.604	0.225	0.293
−3	−0.0469	0.704	0.143	0.229
−4	−0.0610	0.804	0.072	0.165
−5	−0.0735	0.900	0.019	0.101
−6	−0.0835	0.987	−0.016	0.039

TABLE 2

For $Pr = 0.725$

λ	κ	f_1	f_2	$f_3 + 0.725 f_4$	B	ΔB
10	0.0919	−0.080	0.384	0.626	10.32	67.7
9	0.0882	−0.061	0.389	0.596	7.56	70.4
8	0.0831	−0.034	0.395	0.558	4.80	73.3
7.8	0.0819	−0.027	0.396	0.550	4.25	73.9
7.6	0.0807	−0.020	0.398	0.541	3.70	74.5
7.4	0.0794	−0.013	0.399	0.532	3.14	75.2
7.2	0.0781	−0.006	0.400	0.522	2.59	75.9
7	0.0767	0.002	0.401	0.512	2.04	76.6
6.8	0.0752	0.010	0.403	0.501	1.48	77.3
6.6	0.0737	0.019	0.404	0.490	0.93	78.0
6.4	0.0721	0.028	0.406	0.479	0.38	78.7
6.2	0.0705	0.037	0.407	0.468	−0.18	79.4
6	0.0689	0.046	0.408	0.457	−0.73	80.2
5	0.0599	0.098	0.416	0.395	−3.51	84.1
4	0.0497	0.158	0.425	0.326	−6.28	88.6
3	0.0385	0.225	0.434	0.251	−9.06	93.7
2	0.0264	0.299	0.445	0.171	−11.85	99.4
1	0.0135	0.381	0.457	0.087	−14.64	106.0
0	0	0.470	0.470	0	−17.43	113.7
0	0	0.414	0.414	0	−14.43	122.2
−1	−0.0157	0.506	0.413	−0.095	−16.50	153.8
−2	−0.0315	0.604	0.414	−0.189	−18.59	181.0
−3	−0.0468	0.704	0.417	−0.275	−20.68	225.1
−3.5	−0.0540					257.3
−4	−0.0610	0.804	0.423	−0.350	−22.79	301.9
−4.2	−0.0636					324.7
−4.4	−0.0662					351.5
−4.6	−0.0687					383.4
−4.8	−0.0711					422.1
−5	−0.0734	0.900	0.431	−0.412	−24.92	470.2
−5.1	−0.0745					498.8
−5.2	−0.0756					531.3
−5.3	−0.0767					568.6
−5.4	−0.0778					611.7
−5.5	−0.0788					662.2
−5.6	−0.0798					722.2
−5.7	−0.0808					794.5
−5.8	−0.0818					883.6
−5.9	−0.0827					995.9
−6	−0.0836	0.987	0.441	−0.456	−27.07	1141.8
−6.05	−0.0840					1232.5
−6.1	−0.0844					1339.2
−6.15	−0.0849					1466.6
−6.2	−0.0853					1621.3
−6.25	−0.0857					1813.0

See Table 1 for $2(\theta/\delta)a_1$.

The boundary conditions for the density profile are not changed, but, since it must now be a tenth-degree polynomial, several terms are altered, giving

$$\rho_r - 1 = (b-1)(1 - 5\eta^4 + 4\eta^5) + PrX[\lambda(20 + 3\lambda)/72]\eta^3(1-\eta)^2 - Pr\, m[(20 + 3\lambda)/12]\eta^2(1-\eta)^2 \times [(5/3)(1 + 2\eta) + (\lambda/12)(3 - 2\eta)] + m\{[\eta^4(1-\eta)^2]/144\}[-16(30 - 4\eta - 8\eta^2 - 12\eta^3 + 9\eta^4) + 24\lambda(5 + 5\eta - 3\eta^2 - 5\eta^3 + 3\eta^4) + 9\lambda^2(1 - 4\eta + \eta^2 + 2\eta^3 - \eta^4)] \quad (20)$$

Eqs. (17) and (20) may be checked by noting that they revert to Eq. (14) when we let $Pr = 1$, for which case $b - 1 = X/2 = m$.

Simplifying the Integrated Momentum and Energy Equations

The velocity and density polynomials may now be substituted into Eqs. (8) and (10) to yield

$$d\theta^2/dx = [\nu_e/(bu_e)][f_1 + (b-1)f_2 + m(f_3 + Pr\, f_4)] \quad (21)$$

$$db/dx = (bm/u_e)(u_e'/\lambda)[B + (1 - R)\Delta B] \quad (22)$$

where $f_i(\lambda)$, $B(\lambda, Pr)$, and $\Delta B(\lambda, Pr)$ are known functions that have been calculated and tabulated in Tables 1, 2, and 3.

These equations will be of more general application if all terms are rendered dimensionless:

$$d\theta_d^2/dx_d = [\nu_d/(bu_d)][f_1 + (b-1)f_2 + m(f_3 + Pr\, f_4)] \quad (23)$$

$$db/dx_d = (bmu_d'/u_d\lambda)[B + (1 - R)\Delta B] \quad (24)$$

In these equations u_d, u_d', ν_d, and m are known from the potential flow. Variables λ, θ_d, and b are to be evaluated as functions of x_d. One additional relationship is needed. It arises out of Eq. (13):

$$\lambda\theta^2/\delta^2 = \theta^2 u_e' b/\nu_e = \kappa \quad (25)$$

Since $\theta/\delta = \int_0^1 (u_r - u_r^2)\, d\eta$, the group $[\lambda(\theta^2/\delta^2)]$ is a function of λ only. We designate it κ for convenience. In dimensionless form,

$$\kappa = \theta_d^2 u_d' b/\nu_d \quad (26)$$

TABLE 3

For any Pr

λ	f_2	f_4	g_3
10	0.590	0.049	45.51
9	0.565	0.043	45.51
8	0.531	0.037	45.52
7.8	0.523	0.036	45.53
7.6	0.515	0.035	45.53
7.4	0.507	0.034	45.53
7.2	0.498	0.033	45.54
7	0.489	0.032	45.54
6.8	0.479	0.031	45.55
6.6	0.469	0.030	45.55
6.4	0.459	0.028	45.56
6.2	0.448	0.027	45.56
6	0.437	0.026	45.57
5	0.379	0.020	45.61
4	0.314	0.015	45.65
3	0.243	0.011	45.71
2	0.166	0.007	45.78
1	0.085	0.003	45.85
0	0	0	45.94
0	0	0	38.05
−1	−0.094	−0.002	36.23
−2	−0.187	−0.003	34.45
−3	−0.273	−0.003	32.69
−4	−0.349	−0.002	30.98
−5	−0.411	−0.001	29.33
−6	−0.456	−0.000	27.72

$B = [2\lambda - (1 - Pr)g_3]/Pr$.
$\Delta B\ (Pr = x) = (0.725/x)\Delta B\ (Pr = 0.725)$.
See Table 2 for $f_1, f_2, \Delta B\ (Pr = 0.725)$. See Table 1 for $2(\theta/\delta)a_1$.

METHOD OF SOLUTION

The solution of a given boundary-layer problem may now be made by the following steps:

(1) Determine $u_e(x)$ for the body in question (evaluate experimentally or calculate by the theory of frictionless flow).

(2) Evaluate reference values T_0 and u_0 at some selected reference point in the flow, such as the undisturbed free stream.

(3) Express the velocity $u_e(x)$ in dimensionless form, $u_d(x_d)$.

(4) Calculate the constants

$$C_1 = 203/T_0$$

$$k_1 = 2c_pT_0/u_0^2 = 1/m_0$$

where c_p is expressed in (ft. lb.) (slug)$^{-1}$ (°R.)$^{-1}$. The value 5,920 is suggested for air.

(5) Calculate the potential flow quantities

$$m = u_d^2/(1 + k_1 - u_d^2)$$

$$T_d = (1 + k_1 - u_d^2)/k_1$$

$$\nu_d = (1/T_d)\ [(1 + C_1)/(T_d + C_1)]$$

(6) Evaluate the initial values for b, b_d', λ, κ, θ_d^2, $\theta_d^{2\prime}$. If the calculations are initiated at the stagnation point, these will be found to be (for details see reference 4, p. 84–86)

$$\left.\begin{aligned} b &= 1 \\ b_d' &= 0 \\ \lambda &= 7.05 \\ \kappa &= 0.0770 \\ \theta_d^2 &= 0.0770\ (\nu_d/u_d') \\ \theta_d^{2\prime} &= -0.0653\ [(\nu_d u_d'')/(u_d')^2] \end{aligned}\right\} \qquad (27)$$

where the values of ν_d, $u_d' = \partial u_d/\partial x_d$, and $u_d'' = \partial^2 u_d/\partial x_d^2$ are those at the stagnation point.

If the calculations are initiated at some other point, it may be necessary to have—presumable from experiment—velocity and density profiles $u(y)$ and $\rho(y)$ at two points closely adjacent (a distance Δx apart) from which to calculate these initial values. Use the defining equations

$$\left.\begin{aligned} b &= \rho_e/\rho_w \\ b_d' &= \partial b/\partial x_d \\ \lambda &= \frac{b\delta^2 u e'}{\nu_e} \text{ where } \delta = \int_0^{y_e} \frac{\rho}{\rho_e}\,dy \\ \kappa &= \lambda(\theta/\delta)^2 = \lambda[(37/315) - (\lambda/945) - (\lambda^2/9072)]^2 \\ \theta_d &= \sqrt{\frac{u_0}{\nu_0 L}} \int_0^{y_e} \frac{\rho u}{\rho_e u_e}\left(1 - \frac{u}{u_e}\right) dy \\ \theta_d^{2\prime} &= d\theta_d^2/dx_d \end{aligned}\right\} \qquad (28)$$

For supersonic flows around airfoils with sharp nose there will, of course, be no stagnation point. It will probably be satisfactory in such cases to use the initial values $b = 1$; $b_d' = 0$; $\lambda = \kappa = \theta_d^2 = \theta_d^{2\prime} = 0$.

(7) Choose an arbitrary small increment Δx_d and calculate θ_d^2 and b at the station x_d (initial) + Δx_d by finite-difference equations of the form

$$z(w + \Delta w) = z(w) + z'(w)\cdot\Delta w$$

Greater accuracy will be obtained if the average value of b_d' (and $\theta_d^{2\prime}$) over the increment Δx_d is used instead of the initial value as indicated in the above equation. This, however, involves some trial-and-error calculations since b_d' and $\theta_d^{2\prime}$ at $x_d + \Delta x_d$ are not known until calculations for the given increment of Δx_d are completed.

(8) Calculate at x_d (initial) + Δx_d the remaining variables κ, $\theta_d^{2\prime}$, and b_d' from the equations

$$\kappa = \theta_d^2 u_d' b/\nu_d$$

$$\theta_d^{2\prime} = [\nu_d/(bu_d)]\ [f_1 + (b - 1)f_2 + m(f_3 + Pr\, f_4)]$$

where f_{1-4} are functions of κ or λ, tabulated in Tables 1, 2, or 3;

$$b_d' = [(bmu_d')/(u_d\lambda)]\ [B + (1 - R)\Delta B]$$

where B and ΔB are tabulated in the same tables.

(9) Calculate the wall temperature T_w from

$$T_w = T_d T_e b \qquad (29a)$$

(10) Calculate the local skin-friction drag coefficient from

$$C_d\sqrt{Re} = 2(\theta/\delta)a_1(\nu_d/\theta_d)u_d T_d^{s/2} \qquad (29b)$$

where $2(\theta/\delta)a_1$ is a function of κ found in Table 1.

All quantities are now known at station x_d + Δx_d. Choose additional increments in x_d and repeat steps 7–10 for each. See the end of this paper for examples of these calculations. It will be observed that at the point of minimum pressure ($x_d = 1.67$ in the Flügge-Lotz example) there occur discontinuities in the functions f_1, f_2, ΔB, and B, causing slight irregularities in

the values of $\theta_d^{2\prime}$, b_d', and $C_d\sqrt{Re}$. A change in the form of the velocity and density polynomial at the minimum pressure point causes these discontinuities. The computer should terminate a Δx_d increment at the minimum pressure point so that he will not need to interpolate tabulated values of f_1, f_2, etc., over an interval including these discontinuities. Otherwise this point requires no special treatment.

(11) Locate the separation point at the value of x_d for which $\kappa = -0.0890$. Calculation difficulties at the separation point make it expedient to terminate our calculations short of the separation point and then locate $x_{d\,(\text{sep.})}$ by extrapolation of the curve $x_d(\kappa)$.

Since only the wall temperature is appreciably affected by the value of the Prandtl Number (see p. 453) if this temperature is not needed the calculations may be made under the assumption that $Pr = 1$. For this mathematically simpler case, $b = 1 + m$ and can be calculated *a priori*, obviating the calculations of b_d' and b in steps 6, 7, and 8. Step 9 is eliminated completely since $T_w = T_0\,(1 + m_0) = \text{const.}$ for $Pr = 1$.

Examples and Summary

The thinness of the boundary layer makes it almost impossible to obtain experimental data sufficiently accurate and definitive to afford a means of checking the theory. Velocity profiles can be measured, but it is extremely difficult to measure temperatures accurately. We can only test our results against those of more mathematically exact theory insofar as it exists. The flat plate case has been satisfactorily solved by a number of workers. Crocco has done extensive work on this case. For the curved surface there is the Flügge-Lotz, Eichelbrenner report. Due to the lengthy computations entailed, they have calculated essentially one example, for the case $Pr = 1$, although there are a few results for $Pr = 0.7$. We shall compare results with these two cases. Beyond that our calculations must stand alone until other exact solutions appear for further check.

The Flat Plate

The flat plate is assumed to be extremely thin and set at zero angle of attack so that the pressure gradient will be zero. It follows that $u_d' = \lambda = \kappa = 0$, $u_d = T_d = \nu_d = 1$, $m = \text{const.}$ Evaluate Eq. (23) at $\lambda = 0$ noting from Tables 2 and 3 the values $f_1 = f_2 = 0.470$, $f_3 = f_4 = 0$:

$$d\theta_d^2/dx_d = 0.470$$

Integrating with respect to x_d we obtain

$$\theta_d^2 = 0.470\,x_d + \text{const.}$$

where the constant is zero since $\theta_d = 0$ when $x_d = 0$, measuring x_d from the beginning of boundary-layer formation—i.e., from the leading edge of the plate. Evaluate Eq. (24) at $\lambda = 0$, using Tables 2 and 3:

$$db/dx_d = bm(u_d'/u_d\lambda)\,(\{[45.94(Pr - 1)]/Pr\} + \{1 - [(b - 1)/m]\}\,[(0.725/Pr)\,113.7]) \quad (30)$$

The ratio $u_d'/\lambda = 0/0$ is evaluated through its alternate expression [cf. Eq. (25)]

$$u_e'/\lambda = (\kappa/\lambda)\,[\nu_e/(\theta^2 b)]$$

or in dimensionless form, using also Eq. (28),

$$u_d'/\lambda = (\kappa/\lambda)\,[\nu_d/(\theta_d^2 b)] = (37/315)^2\,[1/(0.470 x_d b)] \quad (31)$$

Eq. (30) is a simple differential equation in the form

$$db/dx_d = (1/x_d)\,(bk_2 + k_3)$$

for which the only finite solution is

$$b = -k_3/k_2 = 1 + m\,(0.4428 + 0.5572\,Pr)$$

Observe that $b = 1 + m$ for $Pr = 1$, as it should. The wall temperature comes from this relation since

$$b = \rho_e/\rho_w = T_w/T_e$$

At $Pr = 0.725$ (air),

$$T_w = T_e\,(1 + 0.8468\,m)$$

Crocco finds the exact relation to be

$$T_w = T_e\,(1 + 0.8513\,m)$$

Our approximate theory is here in error by 0.2 per cent for $M_e = 2$, or $m = 0.8$. If M_e is lower and/or Prandtl Number is nearer unity, the error will be still less.

The local drag coefficient is calculated, with the aid of Eq. (29b), to be

$$C_d\sqrt{Re} = 0.6854/\sqrt{x_d}$$

The total drag coefficient is then

$$C_D\sqrt{Re} = \frac{1}{x_d}\int_0^{x_d} C_D\sqrt{Re}\,dx_d = \frac{1.371}{\sqrt{x_d}}$$

Crocco gets $C_D\sqrt{Re} = 1.328/\sqrt{x_d}$. It is interesting to note that this value is the same as that obtained by Blasius for the incompressible case. In other words, the drag of the insulated flat plate at zero angle of attack is unaffected by Mach and Prandtl Numbers. Our approximate theory overestimates drag by 3.2 per cent.

To compare velocity and temperature profiles, use the following relation which derives from Eqs. (9) and (13),

$$y_d = \sqrt{\frac{\lambda\nu_d}{bu_d'}}\int_0^{\eta}\rho_r\,d\eta \quad (32)$$

Using Eqs. (31) (17), and (32) we obtain

$$y_d = 5.84\,[\eta + m((0.4428 + 0.5572\,Pr)\times\{\eta - \eta^5 + (2/3)\eta^6\} - 4\,Pr\{(\eta^3/3) - [(3/5)\eta^5] + (\eta^6/3)\} + (\eta^5/5) - [(4/7)\eta^7] + (\eta^8/2) - (\eta^9/9))]$$

Combined with Eqs. (12) and (17), this evaluates $u_r(y_d)$ and $\rho_r(y_d)$. Calculations have been made for air, $Pr = 0.725$, and the results compared with Crocco's profiles in Fig. 2.

FIGURE 2

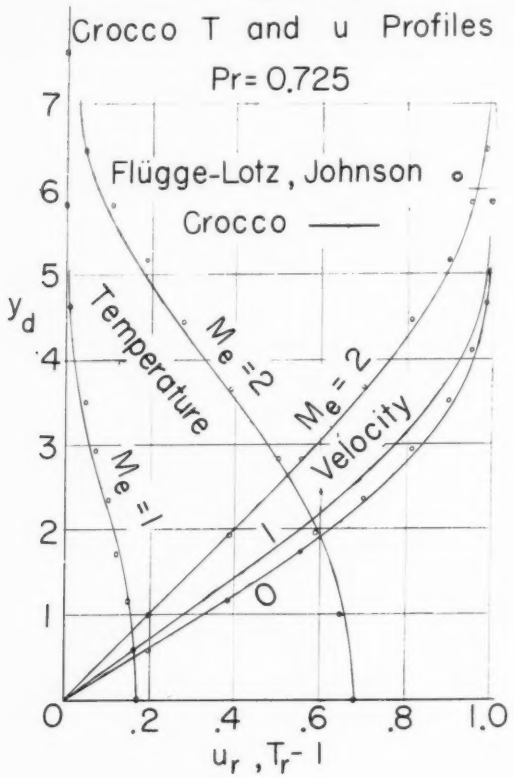

FIGURE 3

Accuracy of the Approximate Method

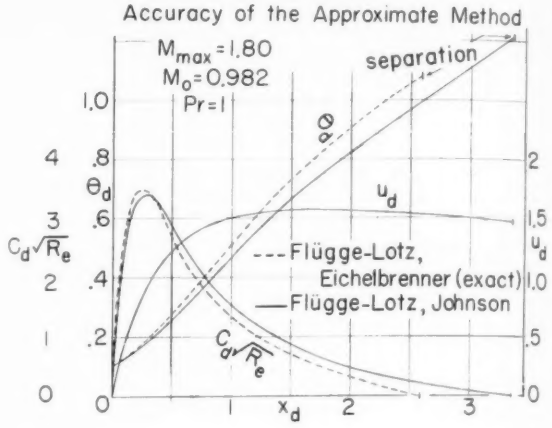

FIGURE 4

Velocity and Temperature Profiles

Flügge-Lotz Example,

Accelerating Flow

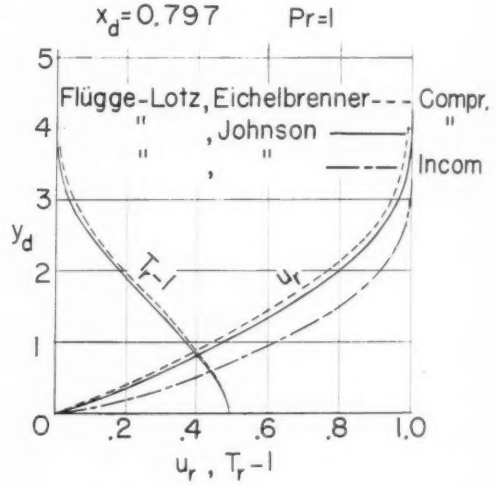

FIGURE 5

Velocity and Temperature Profiles

Flügge-Lotz Example, Decelerating Flow

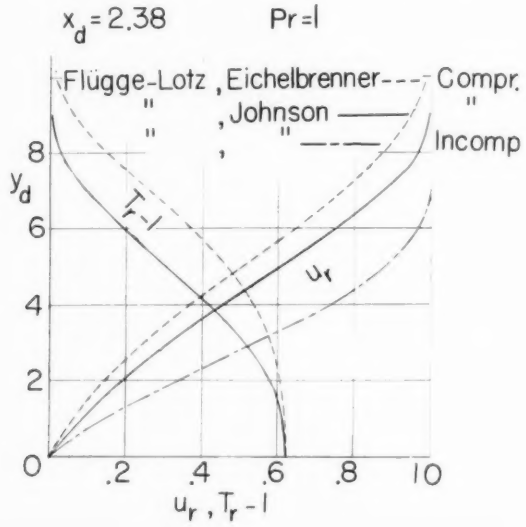

FIGURE 6

Compressibility Effect

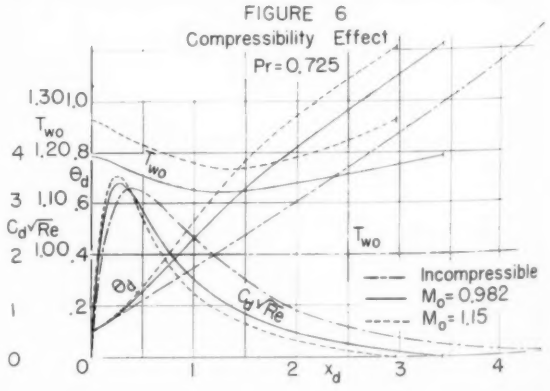

Flügge-Lotz Example

In the Flügge-Lotz-Eichelbrenner report, one example—for $Pr = 1$—had been completed. The authors chose a velocity distribution that would incorporate a number of the characteristic features of flows over aerodynamic bodies. The velocity starts from a stagnation point, has a region of accelerated flow, reaches a maximum velocity, and then has a region of decelerated flow which persists until separation of the boundary layer occurs. The shape of body over which this velocity distribution would occur was not ascertained. In that report the reference values are those at the stagnation point, with reference velocity u_0 taken as the speed of sound in the stagnant fluid.

We shall make a number of calculations based on this example and variations of it. It is thought convenient to reference the example to the free-stream conditions. The velocity is then given by the analytic expression

$$u_d = [x_d(x_d + 5)]/(x_d + 1)^2$$

and the reference values are $u_0 = 997$ ft. per sec.; $T_0 = 435°$R.; and $\nu_0 = 2.091 \times 10^{-4}$ sq.ft. per sec. By means of our calculations we shall show for this example (1) accuracy of our approximate method; (2) effect of compressibility; (3) effect of Prandtl Number; and (4) effect of velocity gradient u_d'.

(*1*) *Accuracy of Our Approximate Method.*—Our first calculation is made for conditions identical with those taken in the Flügge-Lotz calculation. Since the latter may be considered to be exact, a comparison of the results serves to measure the accuracy of our approximate method. In Fig. 3 the drag and momentum thickness are compared ($Pr = 1$). Also separation is located at the point where the drag drops to zero. The momentum thickness is about 10 per cent low. The separation point is 31 per cent too far aft, and this is largely responsible for an overestimation of drag over the major portion of the curve.

A comparison of velocity and density (or temperature) profiles was also made at approximately the mid-region of accelerated flow and of decelerated flow. Figs. 4 and 5 portray these results. There is also added the velocity profile for incompressible flow, calculated for the same velocity distribution. Temperature is, of course, constant in the incompressible flow, and the $(T_r - 1)$ line would coincide with the y axis. It is seen that an extremely satisfactory accuracy is obtained in the accelerated flow. The approximation is somewhat rough for decelerated flow, although our method is set up so that the wall value of T_d is given exactly [at $b = (T_r)_w = 1 + m$] for the case $Pr = 1$. It will be almost exact for other values of Prandtl Number.

Local drag per unit area, $\tau_w = [\mu(\partial u/\partial y)]_w$, will depend on $(T_r)_w$, which fixes μ_w, and on $(\partial u/\partial y)_w$. The good reproduction of $(T_r)_w$ means that if there is any inaccuracy of drag prediction it is due to the error in the velocity profile slope at the wall.

(*2*) *Effect of Compressibility.*—Some effect of compressibility may already be seen in Figs. 4 and 5. The velocity profile of the compressible flow is changed appreciably from that of the incompressible flow. The boundary layer becomes thicker in the studied cases. In order to study further the influence of compressibility, new examples were added and the variables that characterize the boundary layer (θ_d, C_D, and $T_{w0} = T_w/T_0$) were plotted.

First the basic example for $Pr = 0.725$ was calculated. In addition, the comparable incompressible case was calculated after setting $m = 0$, $T_d = \nu_d = 1$. A third case was formed by increasing the reference velocity by approximately 17 per cent. Dimensionless velocity $u_d(x_d)$ remained unchanged in the three cases, as did reference temperature T_0. Fig. 6 presents the results. It is seen that every variable compared feels a major compressibility influence. We recognize, of course, that this is not a comparison of boundary layers over the same body traveling at different speeds, since the form of the velocity variation $u_d(x_d)$ would be altered by a change of speed of travel. However, the comparison is certainly of qualitative value.

It may be added that increasing the free-stream Mach Number by 17 per cent—from 0.982 to 1.15—while holding $u_d(x_d)$ the same was accompanied by an increase in maximum local Mach Number from 1.80 to 2.27, a 26 per cent increase.

(*3*) *Effect of Prandtl Number.*—The preceding examples were recalculated at $Pr = 1$ (except for the incompressible case where Prandtl Number has no significance and does not enter the calculations). The results of Crocco show that greater Prandtl Number effect will be encountered at the higher speeds. Therefore, we have compared the cases, in Fig. 7, at the higher Mach Number to magnify any Prandtl Number effects. It is seen that there is no appreciable alteration of momentum thickness, drag, or separation point by going from $Pr = 1$ to the value for air, $Pr = 0.725$. In addition, two completely supersonic flows (not shown

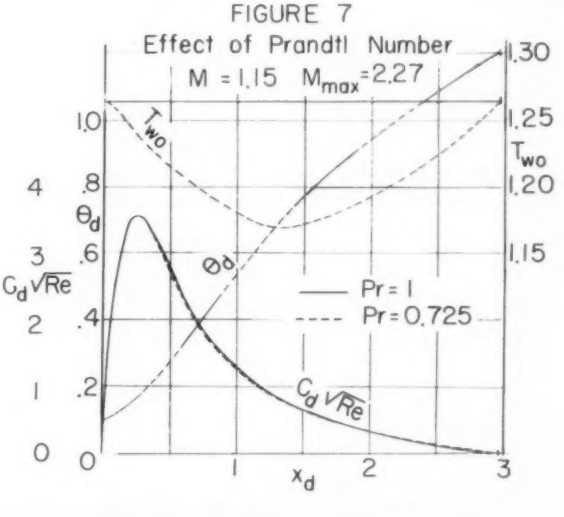

FIGURE 7

FIGURE 8

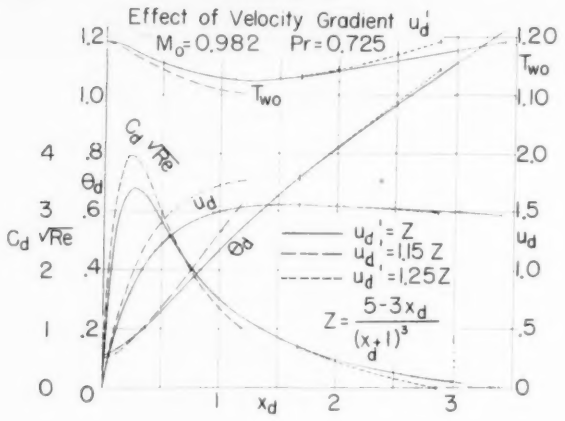

in this paper) have also been calculated—shock-wave effects have been ignored—for $Pr = 1$ and 0.725. They further support the conclusion that the Prandtl Number affects only the temperature to an appreciable degree. This is a pleasant discovery, since it means that for most purposes we may make our calculations at $Pr = 1$, which is a much simpler and less tedious calculation than for $Pr \neq 1$. Prandtl Number does alter wall temperature ratio T_{w0}. At $Pr = 1$ the ratio remains constant at $T_{w0} = 1 + m_0$. At $Pr < 1$ this ratio has the same value at the stagnation and separation points but dips to lower values in between. We must not conclude from the small percentage wise variation of T_{w0} that here again the Prandtl Number effect will be of no practical importance. In the example shown the minimum value of T_{w0} is only 7.4 per cent below its stagnation value, but a 7 per cent decrease could amount to 70° for $M_0 = 4$, say. This would be of considerable importance in calculating the temperature of a pilot's canopy.

(4) *Effect of Velocity Gradient* u_d'.—It is readily seen that increasing the reference velocity while holding velocity ratio $u_d = u_e/u_0$ unchanged results in an increase in u_e at a given value of x and therefore corresponds to a numerical increase in u_e' at all points except the minimum pressure point where it is zero. Thus the method employed above in ascertaining compressibility effects is as much a measure of the effect of the slope of the $u_e(x)$ curve as it is of compressibility.

A more clear-cut manifestation of slope effect will be found in holding the reference values constant while increasing the value of u_d. Partial examples were made for the two cases:

$$u_d = 1.15\left\{[x_d(5 + x_d)]/(x_d + 1)^2\right\}$$

for $0 \leqslant x_d \leqslant 1.2$.

$$u_d = 1.25\left\{[x_d(5 + x_d)]/(x_d + 1)^2\right\} - 0.390$$

for $1.67 \leqslant x_d \leqslant (x_d)_{sep.}$. The first shows the effect of an increase in u_e' in the accelerating part of the boundary layer. The second reveals the influence of an increased deceleration. To give a smooth transition from the basic $u_d(x_d)$ curve, this latter alteration was begun at the point of zero slope u_d' with the same values of u_d and θ_d which were found for the basic case. Fig. 8 shows the results and reveals an extremely strong slope influence in the region of accelerated flow. The separation point is materially advanced by increased adverse pressures.

Limitations

(1) No attempt has been made to account for boundary-layer shock-wave interaction.

(2) Under conditions of high positive velocity gradients, or sustained gradients of moderate magnitude, the proposed method may break down both mathematically and physically. The formal calculations may require a value of κ greater than 0.0948. But κ reaches a peak value at 0.0948 ($\lambda = 12$) and further computations cannot be made. Physically, values of $\lambda > 12$ are unsupportable because they will give boundary-layer velocities greater than the exterior velocity at the same cross section of flow. Nevertheless, while some practical cases may not be amenable to solution by the above method, there are many more which can be solved with good accuracy and reasonable expenditure of time.

Comparison with the Method of Gruschwitz

Gruschwitz[9] studied the same problem at approximately the same time but published it earlier. He assumes different thicknesses for the velocity and the temperature layers, and, by an ingenious method, he avoids the trouble that usually is caused by employing two different thicknesses. He takes as his polynomials $u_r = f_1(\eta)$ and $\rho_r(1 - u_r) = f_2(\eta)$. The latter polynomial is required to satisfy the outer boundary conditions, $f_2 = \partial f_2/\partial\eta = \partial^2 f_2/\partial\eta^2 = 0$. But it satisfies these by virtue of the character of u_r and places no requirement upon ρ_r to reach unit value when u_r does. Thus he can make allowance for the difference in thermal and kinetic thicknesses while carrying just one thickness through his calculations. There is a serious disadvantage to this method, however: He loses control of the ratio ρ_r and has no assurance it will reach unity or its slope will become zero at any point. Calculations of his density profiles were made for several reasonable cases, and it was found that ρ_r is not well approximated; it can even become negative near the outer edge in some cases. The fact that in his second polynomial the region of objectionable values of ρ_r occurs where $1 - u_r$ is extremely small minimizes its harmful effect on the rest of his results. In fact, he achieves in the region of accelerated flow better agreement with the exact Flügge-Lotz example than do the present authors. Considering the renegade action of ρ_r, one cannot help feeling that the agreement might be only a coincidence peculiar to this example. Certainly its radical departure from physical reality forms

(*Continued on page 490*)

On the Stability of the Laminar Boundary Layer in a Compressible Fluid*

D. W. DUNN† AND C. C. LIN‡

Massachusetts Institute of Technology

ABSTRACT

A more complete theory is developed for the stability of the laminar boundary layer in a compressible fluid, removing some limitations and modifying certain general conclusions in the earlier treatment of Lees and Lin. The main changes are the inclusion of three-dimensional disturbances and the demonstration that, in many cases, the stability characteristics depend on temperature fluctuations (contrary to previous conclusions). The former change is made possible by a more careful analysis and simplification of the basic equations of the disturbances; the latter modification is found through improved solutions of these equations.

At high supersonic free-stream velocities, the relation for the characteristic values is found to be dependent on temperature fluctuations and the boundary conditions imposed on them, except for three-dimensional disturbances traveling very obliquely to the direction of the free stream. For subsonic and slightly supersonic velocities, where the wave speed of the disturbances is usually not large, the earlier conclusion of Lees and Lin is still valid—i.e., temperature fluctuations are unimportant for the stability problem.

For the boundary-layer flow over a flat surface, three-dimensional disturbances are found to be of little importance at low subsonic free-stream Mach Numbers, since they usually have a higher minimum critical Reynolds Number than two-dimensional ones, except possibly under conditions of extreme surface cooling. As the Mach Number increases, three-dimensional disturbances become significant under conditions that are less and less extreme, until finally, at a Mach Number between one and two, they begin to play the leading role in many cases of practical interest.

At supersonic free-stream Mach Numbers the boundary layer can never be *completely* stabilized by cooling with respect to *all* three-dimensional disturbances. There is always present a class of unstable three-dimensional disturbances no matter how low the temperature of the solid surface becomes. However, in many cases, surface cooling is still a very effective means of stabilizing the boundary layer.

Numerical results illustrating these conclusions are presented for the case of the boundary layer on a flat plate.

Received February 10, 1954. Revised and received November 18, 1954.

* Part of the material in this paper is contained in a thesis submitted by D. W. Dunn in partial fulfillment of the requirements for the degree of Doctor of Philosophy at the Massachusetts Institute of Technology. Some of the conclusions given in a preliminary version of the paper[13] have been somewhat revised and extended. The numerical results remain the same.

The work was begun 1951–1952 while D. W. Dunn was holding a scholarship from the Research Council of Ontario. It was later completed with the support of the Office of Naval Research, under Contract N5 ori-07872. Some of the numerical calculations were carried out by W. V. Caldwell, also with the support of the Office of Naval Research, under Contract N5 ori-60.

† Formerly, Department of Mathematics, Massachusetts Institute of Technology. Now at the Department of Aeronautics, School of Engineering, The Johns Hopkins University.

‡ Professor of Mathematics, Massachusetts Institute of Technology.

(1) INTRODUCTION

IN RECENT YEARS there has been considerable interest in the theory of boundary-layer stability for compressible fluids. Most of the recent work on the subject has been based on the original theoretical investigations of Lees and Lin.[1, 2] As has been pointed out on several occasions, there are certain inadequacies in this basic theory which limit its significance and which in some cases make unreliable the results of numerical calculations based on it. The purpose of the present investigation is to clarify some of these problems and, in general, to gain further insight into the stability theory for the laminar boundary layer in a compressible fluid.

One of the chief limitations of the theory up to now has been consideration of only two-dimensional disturbances by analogy with the procedure for an incompressible fluid. Squire[3] has shown by means of a transformation of the equations of the problem that for an incompressible fluid every three-dimensional disturbance is equivalent to a two-dimensional one at a lower Reynolds Number. Therefore, for an incompressible fluid the minimum critical Reynolds Number for two dimensional disturbances is the minimum critical Reynolds Number for all disturbances, so that the restriction to two-dimensional disturbances is justified. If an attempt is made to prove a similar result for a compressible fluid, it is found that the equations obtained by making the usual approximations (see reference 1) are too complicated to permit a transformation of the type used by Squire. In the present work an order-of-magnitude analysis of the terms in the complete equations for a three-dimensional disturbance is carried out. A consistent approximation scheme based on this now yields simplified equations of the same order of accuracy as the usual ones, but with fewer terms, so that a transformation to equations of the same form as for a two-dimensional disturbance is possible. However, these transformed two-dimensional equations are not the equations of a proper two-dimensional disturbance, so that no direct conclusion regarding the importance of three-dimensional disturbances can be made. For a compressible fluid the properties of three-dimensional disturbances have to be found by means of a more elaborate investigation than for an incompressible fluid. The transformed two-dimensional

equations lead to a considerable simplification mathematically, however.

It is found in the present investigation that for subsonic free-stream Mach Numbers three-dimensional disturbances are not of much importance, but for supersonic Mach Numbers they may play a leading role in certain circumstances. In particular, for supersonic sonic Mach Numbers there is always present a class of unstable three-dimensional disturbances no matter how low the temperature of the solid surface is, so that complete stabilization of the boundary layer in such cases, as predicted in reference 2, is impossible in the strict sense.

It is known that at high Mach Numbers the usual form of the boundary-layer theory becomes inaccurate,[4, 5] so there is some question as to the proper form of the stability theory in such cases. An investigation of this problem[6] has shown that, as long as the proper velocity and temperature profiles for the mean flow are used, the simplified stability equations derived in this paper are still valid as a first approximation at high Mach Numbers. However, in such cases the accuracy of a first approximation may not be great, so that higher approximations and thus more complicated equations may have to be considered.†

Various limitations to some of the approximations made in the theoretical developments of reference 1 have been brought out. In fact, as pointed out in reference 7, the original theory of reference 1 has sometimes been used in situations in which it was not intended to be valid. This theory was formulated with the restriction to small values of the wave speed c, so that, strictly speaking, its range of reliability is limited to values of the Mach Number not too much larger than unity. In particular, the viscous solutions of reference 1 are accurate first approximations only in the immediate neighborhood of the point where $w = c$. However, at high Mach Numbers, c is often large in the stability calculations, so that, in order to satisfy conditions at the solid boundary, the viscous solutions have to be accurate far away from this point. For an incompressible fluid, Tollmien[8] obtained viscous solutions that are uniformly accurate all across the boundary layer. This work has been extended to the case of a compressible fluid, and a new mathematical formulation of the stability problem in terms of the new viscous solutions has been obtained. In the present paper the modified formulas for the calculation of the characteristic values are given. The detailed mathematical discussion will be presented elsewhere.

The conclusion reached in reference 1—that the relation for the characteristic values is independent of the temperature fluctuations and the boundary conditions imposed on them—is now found to be restricted to subsonic and slightly supersonic Mach Numbers in general. At high Mach Numbers it is true only for three-dimensional disturbances whose direction of propagation is at a large angle with the free-stream direction. In all other cases the form of the relation for the characteristic values depends on the boundary condition for the temperature fluctuations at the solid boundary. However, for very small values of the wave number, the relation again takes on a simple form much like that of the earlier theory. This situation, which corresponds to very low frequency fluctuations, occurs in the limiting case of complete stabilization of the boundary layer by cooling, for example. Thus, it is still possible to obtain the critical temperature ratios for complete stabilization by fairly simple numerical calculations. In all cases at high Mach Numbers when the wave number is not small, the relation for the characteristic values is more complicated.

† As an example of the increase in complication, in a second approximation terms must be retained whose coefficients involve the z-component of the basic flow velocity, so that to this order of approximation the flow cannot be considered to be parallel. This conclusion was reached independently in reference 6 and in an investigation by Cheng.[12]

(2) General Formulation of Problem

The basic differential equations for the motion of a compressible fluid, in Cartesian tensor notation, are as follows:

Equation of motion

$$(\partial u_i/\partial t^*) + [u_j(\partial u_i/\partial x_j)] = (1/\rho^*)\,(\partial \tau_{ij}/\partial x_j) \quad (2.1)$$

Equation of continuity

$$(\partial \rho^*/\partial t^*) + (\partial/\partial x_j)\,(\rho^* u_j) = 0 \quad (2.2)$$

Equation of energy

$$\rho^* C_v\{(\partial T^*/\partial t^*) + [u_j(\partial T^*/\partial x_j)]\} = (\partial/\partial x_j)\,[k^*(\partial T^*/\partial x_j)] + \tau_{ij} e_{ij} \quad (2.3)$$

Equation of state

$$p^* = R^* \rho^* T^* \quad (2.4)$$

In these equations e_{ij} is the rate-of-strain tensor and τ_{ij} is the stress tensor, defined in the following way

$$e_{ij} = (1/2)\,[(\partial u_i/\partial x_j) + (\partial u_j/\partial x_i)] \quad (2.5)$$

$$\tau_{ij} = 2\mu^* e_{ij} + [(2/3)\,(\lambda^* - \mu^*)e_{kk} - p^*]\delta_{ij} \quad (2.6)$$

All quantities are dimensional, as defined in the List of Symbols (p. 477). The coefficients of viscosity μ^* and λ^*, the coefficient of heat conductivity k^*, the specific heats C_p and C_v, and the Prandtl Number σ are considered to be functions of the temperature alone. The gravitational force terms are omitted, since they can be shown to be negligible for the large values of the Froude Number to be expected in most practical problems (see reference 1).

We consider a time-independent basic flow and a small time-dependent disturbance. Thus, any quantity $Q(x_i, t^*)$ may be written as the sum of a part $\bar{Q}(x_i)$ and a part $Q'(x_i, t^*)$:

$$Q(x_i, t^*) = \bar{Q}(x_i) + Q'(x_i, t^*) \quad (2.7)$$

We are interested in determining whether the disturb-

ances represented by Q' are stable or unstable—that is, whether they decrease or increase with time. Both the quantities, Q in the disturbed motion and $\bar{Q}$ in the steady motion, satisfy Eqs. (2.1) to (2.4). Thus, if expressions of the form of Eq. (2.7) for all the variables are inserted into these equations and quadratic terms in the small disturbance quantities are neglected, the following system of linearized equations for the fluctuations Q' is obtained:

$$\bar{u}_j(\partial\bar{u}_i/\partial x_j)\rho^{*\prime} + \bar{\rho}^*\{(\partial u_i'/\partial t^*) + [(\partial\bar{u}_i/\partial x_j)u_j'] + [\bar{u}_j(\partial u_i'/\partial x_j)]\} = \partial\tau_{ij}'/\partial x_j \quad (2.8)$$

$$(\partial\rho^{*\prime}/\partial t^*) + (\partial/\partial x_j)(\bar{u}_j\rho^{*\prime} + u_j'\bar{\rho}^*) = 0 \quad (2.9)$$

$$\bar{u}_j\frac{\partial\bar{T}^*}{\partial x_j}\rho^{*\prime} + \bar{\rho}^*\left(\frac{\partial T^{*\prime}}{\partial t^*} + \frac{\partial\bar{T}^*}{\partial x_j}u_j' + \bar{u}_j\frac{\partial T^{*\prime}}{\partial x_j}\right) = \frac{1}{\bar{C}_v}\frac{\partial}{\partial x_j}\left[\frac{\bar{C}_p\bar{\mu}^*}{\bar{\sigma}}\frac{\partial T^{*\prime}}{\partial x_j} + \left(\frac{C_p\mu^*}{\sigma}\right)'\frac{\partial\bar{T}^*}{\partial x_j}\right] + \frac{1}{\bar{C}_v}(\bar{\tau}_{ij}e_{ij}' + \tau_{ij}'\bar{e}_{ij}) + \left(\frac{1}{C_v}\right)'\frac{\partial}{\partial x_j}\left(\frac{\bar{C}_p\bar{\mu}^*}{\bar{\sigma}}\frac{\partial\bar{T}^*}{\partial x_j}\right) + \left(\frac{1}{C_v}\right)'\bar{\tau}_{ij}\bar{e}_{ij} \quad (2.10)$$

$$p^{*\prime}/\bar{p}^* = (\rho^{*\prime}/\bar{\rho}^*) + (T^{*\prime}/\bar{T}^*) \quad (2.11)$$

The quantities e_{ij}', τ_{ij}', $(C_p\mu^*/\sigma)'$, $(1/C_v)'$, $\lambda^{*\prime}$, and $\mu^{*\prime}$ are given by

$$e_{ij}' = (1/2)[(\partial u_i'/\partial x_j) + (\partial u_j'/\partial x_i)] \quad (2.12)$$

$$\tau_{ij}' = 2(\bar{\mu}^*e_{ij}' + \mu^{*\prime}\bar{e}_{ij}) + [(2/3)(\bar{\lambda}^* - \bar{\mu}^*)e_{kk}' + (2/3)(\lambda^{*\prime} - \mu^{*\prime})\bar{e}_{kk} - p^{*\prime}]\delta_{ij} \quad (2.13)$$

and

$$\left.\begin{aligned}(C_p\mu^*/\sigma)' &= \overline{(d/dT^*)(C_p\mu^*/\sigma)}T^{*\prime}\\ (1/C_v)' &= \overline{(d/dT^*)(1/C_v)}T^{*\prime}\\ \lambda^{*\prime} &= \overline{(d\lambda^*/dT^*)}T^{*\prime}\\ \mu^{*\prime} &= \overline{(d\mu^*/dT^*)}T^{*\prime}\end{aligned}\right\} \quad (2.14)$$

Equations (2.8) to (2.11) form a system of linear partial differential equations for the fluctuations. The coefficients are known functions given by the steady flow.

(3) Stability of Parallel and Nearly Parallel Flows

When the fluid is incompressible, the basic steady flow can be strictly parallel, as in the case of two-dimensional flow through a channel. The formation of the stability problem is then simple. For compressible fluids, however, there is no such simple basic flow. Flows satisfying the boundary-layer approximation are the closest to parallel flows. It will be shown that for such flows the stability problem is essentially the same as that for a parallel flow which agrees locally with the basic flow of the boundary-layer type.

For proving the theorem in Section (4) and for application to boundary layers in three-dimensional flow, the development will be made in a somewhat more general manner than usual. We consider a semi-infinite flat plate in an oblique incoming stream. The free stream has components of velocity U_1 and U_3 parallel to the plate, and the flow inside the boundary layer is parallel to the free stream at each location (x_1, x_3). Indeed, the boundary layer can be described in terms of strips parallel to the direction of the resultant free stream. Each strip behaves like a flat plate with the leading edge normal to the resulting stream. The location of the leading edge coincides with that of the particular strip in question. Thus, if s is the distance of a point from the leading edge in the direction of the free stream, the boundary-layer thickness δ at that point is given by

$$\delta/s = 0(R_s^{-1/2}) = 0(R^{-1}) \quad (3.1)$$

where

$$R_s = (s\sqrt{U_1^2 + U_3^2})/\bar{\nu}_1^* \quad (3.2)$$

$$R = R_\delta = (\delta\sqrt{U_1^2 + U_3^2})/\bar{\nu}_1^* \quad (3.3)$$

and $\bar{\nu}_1^*$ is the kinematic viscosity in the free stream. As is well known, the quantities $\bar{Q}$ associated with the basic flow satisfy the following order-of-magnitude relations (if the free-stream Mach Number is not too large):

$$(\partial\bar{Q}/\partial x_2):\quad [(\partial\bar{Q}/\partial x_1)\text{ or }(\partial\bar{Q}/\partial x_3)] = 0(R_s^{1/2}) = 0(R) \quad (3.4)$$

$$(\bar{u}_1\text{ or }\bar{u}_3):\quad \bar{u}_2 = 0(R_s^{1/2}) = 0(R) \quad (3.5a)$$

$$\bar{T}^* = 0(\bar{T}_1^*),\quad \bar{\rho}^* = 0(\bar{\rho}_1^*),\quad \bar{\mu}^* = 0(\bar{\mu}_1^*) \quad (3.5b)$$

We shall now simplify the equations for the small fluctuations by means of analogous considerations regarding the fluctuations and their derivatives. From physical considerations and also from the mathematical nature of the boundary-value problem associated with the system of disturbance equations [Eqs. (2.8) to (2.11)], it may be expected that the fluctuations have the typical boundary-layer type behavior in a region adjacent to the solid boundary. That is, near to the boundary, viscous effects and therefore the highest order derivatives in the direction normal to the solid surface are important, and changes in the normal direction are much more rapid than in any direction parallel to the surface.

It should first be recognized that the fluctuations have a general length scale of the order of the boundary-layer thickness, so that

$$(1/Q')(\partial Q'/\partial x_1) = (1/\bar{Q})(\partial\bar{Q}/\partial x_1)\,0(R) \quad (3.6)$$

In the viscous region next to the surface, the characteristic length in the x_2 direction (normal direction) is much smaller and is obtained by considerations analogous to the usual boundary-layer arguments for the basic flow. It is clear from Eq. (2.8) that the equation of motion for u_1' contains a term of the form $\bar{\rho}^*\bar{u}_1\partial u_1'/\partial x_1$ from the inertial terms and a term of the form $\bar{\mu}^*\partial^2u_1'/\partial x_2^2$ from the viscous terms. Thus, if these terms are to be

of the same order, x_2-derivatives must be larger than x_1-derivatives. Now,

$$\bar{\rho}^*\bar{u}_1(\partial u_1'/\partial x_1) = 0[(\bar{\rho}_1^* U_1 u_1'/\delta] \quad (3.7)$$

$$\bar{\mu}^*(\partial^2 u_1'/\partial x_2^2) = 0[\bar{\mu}_1^*(u_1'/\delta^2)R^{2n}] \quad (3.8)$$

where R^n is a factor indicating the difference of order of magnitude between x_1 and x_2 derivatives:

$$(\partial Q'/\partial x_2): \quad [(\partial Q'/\partial x_1) \text{ or } (\partial Q'/\partial x_3)] = 0(R^n) \quad (3.9)$$

A comparison of Eqs. (3.7) and (3.8) gives $n = 1/2$. The relation (3.9) is now comparable to Eq. (3.4) with R_s replaced by R_δ. The relation analogous to Eq. (3.5a) is

$$(u_1' \text{ or } u_3'): \quad u_2' = 0(R^{1/2}) \quad (3.10)$$

An examination of the equations also gives the following relations [which are used in Section (4)]:

$$T^{*\prime}/\bar{T}_1^* = 0(u_1'/U_1), \quad \rho^{*\prime}/\bar{\rho}_1^* = 0(u_1'/U_1) \quad (3.11)$$

Therefore we have a boundary-layer phenomenon associated with the fluctuations within the boundary layer for the mean flow. In a thin layer next to the solid surface with thickness of the order of $\delta R^{-1/2}$ the fluctuations have the viscous behavior characterized by rapid variation in the x_2-direction, while outside this layer they are usually independent of viscosity since the viscous terms in the equations are usually unimportant there. In general, the order-of-magnitude relations (3.9) and (3.10) are valid only in the viscous layer at the solid surface, while outside it the velocity fluctuations are all of the same order of magnitude and the characteristic length in all directions is the same—that is, of the order of the boundary-layer thickness δ.

In all of these order-of-magnitude estimates $0(R^{1/2})$ may denote a quantity not actually of the order of magnitude of $R^{1/2}$ in the strict sense, but smaller. Such a situation occurs in certain layers of the fluid where it is shown by a more complete analysis (see reference 6) that $0(R^{1/2})$ is replaced by $0(R^{1/3})$. In fact, when the disturbance is analyzed into periodic components [see Section (5)] and the ordinary differential equations for the amplitudes of these components examined, it is found that such a layer ("critical layer") always occurs at the x_2-location in the boundary layer where the wave speed in the x_1-direction of the particular component considered is equal to the component of the velocity of the basic flow in that direction. There is the possibility that in certain cases this critical layer (where viscosity is also always important) may occur outside the viscous layer at the solid surface described above. In such cases, relation (3.9) with $0(R^{1/2})$ replaced by $0(R^{1/3})$ will also be valid in the critical layer, so that variations through this layer in the x_2-direction will also be extremely rapid, just as in the layer at the wall. The order-of-magnitude analysis of the disturbance equations carries through in just the same way, so that it is not necessary for present purposes to consider the more complicated properties of the solutions of these equations.

(4) Simplified Equations for Small Disturbances in Flows of the Boundary-Layer Type

By making use of the boundary-layer approximations outlined above [corresponding to relations (3.4), (3.5), (3.9), (3.10), and (3.11)] it can be shown that the equations for the small disturbances can be simplified to the following:

$$\bar{\rho}^*\left(\frac{\partial u_1'}{\partial t^*} + \bar{u}_1\frac{\partial u_1'}{\partial x_1} + \bar{u}_3\frac{\partial u_1'}{\partial x_3} + u_2'\frac{\partial \bar{u}_1}{\partial x_2}\right) = -\frac{\partial p^{*\prime}}{\partial x_1} + \bar{\mu}^*\frac{\partial^2 u_1'}{\partial x_2^2} \quad (4.1)$$

$$\bar{\rho}^*\left(\frac{\partial u_2'}{\partial t^*} + \bar{u}_1\frac{\partial u_2'}{\partial x_1} + \bar{u}_3\frac{\partial u_2'}{\partial x_3}\right) = -\frac{\partial p^{*\prime}}{\partial x_2} + \bar{\mu}^*\frac{\partial^2 u_2'}{\partial x_2^2} \quad (4.2)$$

$$\bar{\rho}^*\left(\frac{\partial u_3'}{\partial t^*} + \bar{u}_1\frac{\partial u_3'}{\partial x_1} + \bar{u}_3\frac{\partial u_3'}{\partial x_3} + u_2'\frac{\partial \bar{u}_3}{\partial x_2}\right) = -\frac{\partial p^{*\prime}}{\partial x_3} + \bar{\mu}^*\frac{\partial^2 u_3'}{\partial x_2^2} \quad (4.3)$$

$$\frac{\partial \rho^{*\prime}}{\partial t^*} + \bar{u}_1\frac{\partial \rho^{*\prime}}{\partial x_1} + \bar{u}_3\frac{\partial \rho^{*\prime}}{\partial x_3} + u_2'\frac{\partial \bar{\rho}^*}{\partial x_2} = -\bar{\rho}^*\Delta' \quad (4.4)$$

$$\bar{\rho}^* C_v\left(\frac{\partial T^{*\prime}}{\partial t^*} + \bar{u}_1\frac{\partial T^{*\prime}}{\partial x_1} + \bar{u}_3\frac{\partial T^{*\prime}}{\partial x_3} + u_2'\frac{\partial \bar{T}^*}{\partial x_2}\right) = -\bar{p}^*\Delta' + \bar{k}\frac{\partial^2 T^{*\prime}}{\partial x_2^2} \quad (4.5)$$

$$p^{*\prime}/\bar{p}^* = (\rho^{*\prime}/\bar{\rho}^*) + (T^{*\prime}/\bar{T}^*) \quad (4.6)$$

where

$$\Delta' = (\partial u_1'/\partial x_1) + (\partial u_2'/\partial x_2) + (\partial u_3'/\partial x_3) \quad (4.7)$$

Equation (4.5) can also be written in the form

$$\bar{\rho}^*\left(\frac{\partial T^{*\prime}}{\partial t^*} + \bar{u}_1\frac{\partial T^{*\prime}}{\partial x_1} + \bar{u}_3\frac{\partial T^{*\prime}}{\partial x_3} + u_2'\frac{\partial \bar{T}^*}{\partial x_2}\right) = \frac{1}{C_p}\left(\frac{\partial p^{*\prime}}{\partial t^*} + \bar{u}_1\frac{\partial p^{*\prime}}{\partial x_1} + \bar{u}_3\frac{\partial p^{*\prime}}{\partial x_3}\right) + \frac{\bar{\mu}^*}{\sigma}\frac{\partial^2 T^{*\prime}}{\partial x_2^2} \quad (4.8)$$

where $\sigma = C_p\bar{\mu}^*/\bar{k}^*$. These equations are correct except for terms $0(R^{-1/2})$.

A few typical steps in the process of simplification are discussed below:

Example 1.—In the inertial terms of the equations of motion we have terms of the kind $\bar{u}_1(\partial u_1'/\partial x_1) + \bar{u}_2(\partial u_1'/\partial x_2)$. Only the first term is included in Eq. (4.1). This is justified by the fact that

$$\bar{u}_2(\partial u_1'/\partial x_2): \quad \bar{u}_1(\partial u_1'/\partial x_1) = (\bar{u}_2/\bar{u}_1)\,[(\partial u_1'/\partial x_2)/(\partial u_1'/\partial x_1)] \quad (4.9)$$

which is $0(R^{-1})$ outside the viscous layer and $0(R^{-1/2})$ inside the viscous layer, according to Eqs. (3.4), (3.5), (3.9), and (3.10).

Example 2.—None of the terms arising from the dissipation function $(\tau_{ij}e_{ij} + p^*\partial u_i/\partial x_i)$ are included in Eq. (4.5). This is justified as follows. The typical terms of the largest order which could contribute to Eq. (4.5) are

$$\mu^{*\prime}(\partial\tilde{u}_1/\partial x_2)^2 + 2\bar{\mu}^*(\partial\tilde{u}_1/\partial x_2)\,(\partial u_1'/\partial x_2) + \ldots$$

Their orders of magnitude can be estimated by comparing them with $\bar{\mu}^*(\partial\tilde{u}_1/\partial x_2)^2$, which is the largest term in the dissipation function for the mean flow. Thus,

$$\mu^{*\prime}(\partial\tilde{u}_1/\partial x_2)^2 = (\mu^{*\prime}/\bar{\mu}^*)\bar{\mu}^*(\partial\tilde{u}_1/\partial x_2)^2 \quad (4.10)$$

$$2\bar{\mu}^*(\partial\tilde{u}_1/\partial x_2)\,(\partial u_1'/\partial x_2) = 2[(\partial u_1'/\partial x_2)/(\partial\tilde{u}_1/\partial x_2)]\bar{\mu}^*(\partial\tilde{u}_1/\partial x_2)^2 \quad (4.11)$$

On the other hand, the term $\bar{\rho}^*\tilde{u}_1 C_v \partial T^{*\prime}/\partial x_1$ retained on the left-hand side of Eq. (4.5) can be estimated as follows:

$$\bar{\rho}^*\tilde{u}_1\, C_v(\partial T^{*\prime}/\partial x_1) = \bar{\rho}^*\tilde{u}_1 C_v[(\partial\bar{T}^{*\prime}/\partial x_1)/(\partial\bar{T}^*/\partial x_1)]\,(\partial\bar{T}^*/\partial x_1) \quad (4.12)$$

Now, from the energy equation for the basic flow, $\bar{\rho}^*\tilde{u}_1 C_v(\partial\bar{T}^*/\partial x_1)$ is of the same order as the dissipation term $\bar{\mu}^*(\partial\tilde{u}_1/\partial x_2)^2$. Consequently, the various quantities given by Eqs. (4.10)–(4.12) are in the ratios $1:1:R$ outside the viscous layer and in the ratios $1:R^{1/2}:R$ within the viscous layer. We are therefore justified in neglecting the first two quantities, which are the largest contribution of the dissipation function to Eq. (4.5).

In addition to the approximations just described, we can also neglect the x_1 and x_3 dependence of the quantities in the basic flow, which determine the coefficients in Eqs. (4.1) to (4.6). This approximation, which has been repeatedly discussed by various writers on the stability problem, depends on the boundary-layer nature of the mean flow and can be shown to be equivalent to neglecting terms of the order of R^{-1} (see references 6, 8, and 10).

The system of Eqs. (4.1) to (4.6) is essentially of the form expected from a strictly parallel flow. One important characteristic of the system is the absence of dissipative terms in the energy equation. This makes it possible, as we shall see in Section (5), to reduce the problem for a three-dimensional disturbance to a two-dimensional problem. In previous investigations such a reduction was not possible because of certain terms retained in the equations for the disturbances that prevent a proper transformation. Such terms are now shown to be negligible.

The discussion up to now has been restricted to the case of moderate Mach Numbers, for which relations (3.1), (3.4), and (3.5) are valid. For very high supersonic Mach Numbers, the order-of-magnitude relations in the boundary layer corresponding to relations (3.1), (3.4), and (3.5) are different (see reference 5), and, consequently, those for the disturbances corresponding to Eqs. (3.9), (3.10), and (3.11) are different. An order-of-magnitude analysis (see reference 6) similar to that described for the case of low Mach Numbers shows that the disturbance equations are again, in the first approximation, of just the same form as Eqs. (4.1) to (4.6). The proper velocity and temperature distributions given by a modified boundary-layer theory (see reference 4) would have to be used, of course, at very high Mach Numbers. The error estimate for the neglected terms in the disturbance equations is now different, however, being expressed not in terms of R but in terms of a Reynolds Number

$$R_0 = (\bar{\nu}_1^*/\bar{\nu}_0^*)R \quad (4.13)$$

based on fluid properties at some representative temperature $\bar{T}_0^*$ *inside* the boundary layer. Since $\bar{T}_0^*$ is roughly proportional to M_1^2 at high Mach Numbers, R_0 is much less than R in such cases. Consequently, the errors committed in the simplified equations [which are $0(R_0^{-1/2})$] might not be very small at high Mach Numbers.

The present analysis is carried out for any boundary layer over a flat surface, whether there is a pressure gradient or not. Thus, the results are valid, not only for the zero pressure-gradient flow over a flat plate, but also for the flows over wedge-shaped profiles. Although a pressure gradient is associated with the latter flows at subsonic Mach Numbers, terms due to pressure gradient do not appear explicitly in the disturbance equations to the accepted order of approximation.†

Although the simplified equations [Eqs. (4.1) to (4.6)] are obtained by rather crude order-of-magnitude arguments, an *a posteriori* check verifies that the approximations made are valid in the stability investigation of the boundary layer over a solid surface.‡

(5) Periodic Solutions of the Equations for Small Disturbances

The Eqs. (4.1) to (4.7) contain x_1, x_3, and t^* only through the partial derivatives, so that solutions of the form

$$Q' = q(x_2)\exp\,[i(\alpha_1 x_1 + \alpha_3 x_3 - \alpha_1 c^* t^*)] \quad (5.1)$$

are possible. It may be expected that a disturbance of a fairly general nature can be analyzed into normal modes of this type, with α_1 and α_3 real and c^* in general complex. A normal mode is damped if $c_i^* < 0$, neutral if $c_i^* = 0$, and self-excited if $c_i^* > 0$.

Evidently solutions of the form (5.1) may be regarded as waves propagating in a direction in the (x_1, x_3) plane specified by the numbers (α_1, α_3) (with changing amplitude in time if c^* is complex).

Consider in particular the case $\alpha_3 = 0$. Then, the terms involving the x_3-derivatives drop out of the Eqs. (4.1) to (4.7), and the equations for u_1', u_2', $p^{*\prime}$, $\rho^{*\prime}$, $T^{*\prime}$ are exactly the same as if the component $\tilde{u}_3$ of the basic

† A more careful examination is necessary when there is surface curvature. Preliminary results indicate that for most three-dimensional disturbances curvature effects are negligible when the curvature is small, but that for those disturbances with propagation direction nearly normal to the free-stream direction [see Section (5)] additional terms have to be retained in Eq. (4.2).

‡ Free boundary layers (such as wakes and jets) are excluded from all of the above discussion. The effect of viscosity on the stability of such flows is quite different. Further investigation of these cases is being carried out.

flow were zero. Thus, for waves propagating in the x_1-direction only the component $\bar{u}_1$ of the basic flow (besides the distributions of the scalar quantities $\bar{p}^*$ and $\bar{T}^*$) has any influence. Now, a rotation of the coordinate system in the (x_1, x_3) plane will not change the system of Eqs. (4.1) to (4.7). Hence, we may conclude that for waves propagating in any direction only the component of the basic flow in that direction has to be considered, in addition to the distributions of the scalar quantities. *Every periodic three-dimensional disturbance may be treated in terms of a corresponding two-dimensional problem.* One need only take the proper component of velocity in the basic flow to carry out the simplification.

If we reduce the above equations to dimensionless forms, it is clear that the waves propagating in the direction of the resultant free-stream velocity are associated with the Reynolds Number R and the Mach Number M_1 of the basic flow. For a wave propagating at an angle Θ relative to this direction, these numbers are reduced to

$$\tilde{R} = R \cos \Theta, \quad \tilde{M}_1 = M_1 \cos \Theta \tag{5.2}$$

A direct transformation verifying this statement will be given in the next section.

The advantage of the present treatment lies in its generality and simplicity. Whether the incoming stream is oblique or normal to the leading edge of the flat plate makes no difference in the discussion. When specialized to the incompressible case, the present results cover both the original work of Squire[3] and the case of an oblique incoming flow discussed by Kuethe.[9] For two-dimensional parallel flows, Squire obtained a set of transformation formulas leading to a conclusion equivalent to Eq. (5.2). Supplementary discussions are required in Squire's method. Kuethe, dealing with the case of the oblique incoming stream by Squire's method, noted the variation of "effective" Reynolds Number with different directions. He did not, however, arrive at the conclusion reached here that the maximum "effective" Reynolds Number is reached by waves propagating in the direction of the free stream. Consequently, these waves first give rise to instability as the Reynolds Number of the flow is increased.

(6) Equations for the Amplitude Functions

Consider now the stability of a two-dimensional boundary layer over a flat plate coinciding with the (x_1, x_3) plane and introduce the dimensionless variables given in the List of Symbols (p. 477). The free-stream velocity is now U_1, since $U_3 = 0$. The free-stream reference quantities δ, U_1, $\bar{\rho}_1^*$, $\bar{T}_1^*$, $\bar{p}_1^*$, $\bar{\mu}_1^*$ are evaluated at a fixed point $x_1 = x_1^0$—that is, at a definite distance from the leading edge of the plate—in the part of the boundary layer that is of interest.

The dimensionless velocity and temperature distributions, $w = \bar{u}_1/U_1$ and $T = \bar{T}^*/\bar{T}_1^*$, depend on a number of factors—in particular, the boundary conditions at the wall and the free-stream Mach Number M_1.

We consider a small disturbance of the boundary layer in the manner discussed previously, with solutions of the form

$$Q'(x, y, z, t) = q(y) \exp [i(\alpha x + \beta z - \alpha c t)] \tag{6.1}$$

for the disturbance quantities, as indicated in the List of Symbols. When relations of the type [Eq. (6.1)] are inserted into Eqs. (4.1) to (4.7), the following equations for the amplitude functions f, ϕ, h, π, r, θ are obtained:

$$\rho[i\alpha(w - c)f + w'\alpha\phi] = -[(i\alpha)/(\gamma M_1^2)]\pi + (\mu/R)f'' \tag{6.2}$$

$$\rho[i\alpha^2(w - c)\phi] = -[1/(\gamma M_1^2)]\pi' + (\mu/R)\alpha\phi'' \tag{6.3}$$

$$\rho[i\alpha(w - c)h] = -[(i\beta)/(\gamma M_1^2)]\pi + (\mu/R)h'' \tag{6.4}$$

$$i\alpha(w - c)r + \rho'\alpha\phi + \rho(i\alpha f + i\beta h + \alpha\phi') = 0 \tag{6.5}$$

$$\rho[i\alpha(w - c)\theta + T'\alpha\phi] = -(\gamma - 1)(i\alpha f + i\beta h + \alpha\phi') + [(\gamma\mu)/(\sigma R)]\theta'' \tag{6.6}$$

$$\frac{\pi}{p} = \frac{r}{\rho} + \frac{\theta}{T} \tag{6.7}$$

where a prime now refers to differentiation with respect to y.

The combination of terms $\alpha f + \beta h$ suggests its replacement by a new variable $\tilde{\alpha}\tilde{f}$. Indeed, the following transformations convert Eqs. (6.2) to (6.7) to those of an equivalent two-dimensional problem:

$$\left.\begin{aligned} \alpha f + \beta h &= \tilde{\alpha}\tilde{f} \\ \alpha\phi &= \tilde{\alpha}\tilde{\phi} \\ \alpha\pi &= \tilde{\alpha}\tilde{\pi} \\ \alpha r &= \tilde{\alpha}\tilde{r} \\ \alpha\theta &= \tilde{\alpha}\tilde{\theta} \\ c &= \tilde{c} \\ \sqrt{\alpha^2 + \beta^2} &= \tilde{\alpha} \\ \alpha R &= \tilde{\alpha}\tilde{R} \\ \alpha M_1 &= \tilde{\alpha}\tilde{M}_1 \end{aligned}\right\} \tag{6.8}$$

The two-dimensional equations are:

$$\rho[i\tilde{\alpha}(w - c)\tilde{f} + w'\tilde{\alpha}\tilde{\phi}] = -[(i\tilde{\alpha})/(\gamma\tilde{M}_1^2)]\tilde{\pi} + (\mu/\tilde{R})\tilde{f}'' \tag{6.9}$$

$$\rho[i\tilde{\alpha}^2(w - c)\tilde{\phi}] = -[1/(\gamma\tilde{M}_1^2)]\tilde{\pi}' + (\mu/\tilde{R})\tilde{\alpha}\tilde{\phi}'' \tag{6.10}$$

$$i\tilde{\alpha}(w - c)\tilde{r} + \rho'\tilde{\alpha}\tilde{\phi} + \rho(i\tilde{\alpha}\tilde{f} + \tilde{\alpha}\tilde{\phi}') = 0 \tag{6.11}$$

$$\rho[i\tilde{\alpha}(w - c)\tilde{\theta} + T'\tilde{\alpha}\tilde{\phi}] = -(\gamma - 1)(i\tilde{\alpha}\tilde{f} + \tilde{\alpha}\tilde{\phi}') + [(\gamma\mu)/(\sigma\tilde{R})]\tilde{\theta}'' \tag{6.12}$$

$$\tilde{\pi}/p = (\tilde{r}/\rho) + (\tilde{\theta}/T) \tag{6.13}$$

Evidently the transformations [Eqs. (6.8)] are equivalent to Eq. (5.2) with $\cos \Theta = \alpha/\sqrt{\alpha^2 + \beta^2}$, so that Θ does in fact give the direction of propagation of the waves, Eq. (6.1). The dimensionless wave speed

c is not changed, which indicates that the phase velocity in the x-direction is actually sec Θ times the phase velocity in the direction of the wave normal.

To complete the analysis, it is necessary to verify the equivalence of the boundary conditions. In the stability problem the boundary conditions are homogeneous, so that there is no difficulty in this respect. The homogeneous boundary conditions of the three-dimensional problem clearly transform to the proper homogeneous boundary conditions of the equivalent two-dimensional problem. For forced oscillations, however, it is obvious that the equivalence would have to be more carefully examined.

We have now shown that the boundary value problem associated with the system of Eqs. (6.2) to (6.7) for a three-dimensional disturbance is equivalent to that associated with the system of two-dimensional Eqs. (6.9) to (6.13). Thus the stability problem for three-dimensional disturbances can always be formulated as a two-dimensional problem which is mathematically the same as that for two-dimensional disturbances. It should be realized, however, that the equivalence is purely mathematical since Eqs. (6.9) to (6.13) *do not represent a proper two-dimensional disturbance.* There is a decisive difference between the present results and those of Squire for an incompressible fluid. In the latter case, because the Mach Number does not enter, it is possible to transform the equations for a three-dimensional disturbance to equations that *actually do represent a real two-dimensional disturbance at a lower Reynolds Number.* It is then possible to conclude that three-dimensional disturbances can be ignored when the minimum critical Reynolds Number is being investigated. For a compressible fluid this is not true because of the necessity of transforming the free-stream Mach Number. It is not even true that every three-dimensional disturbance is equivalent to a two-dimensional one with a modified Mach Number as well as Reynolds Number, because with a reduced Mach Number the velocity and temperature distributions would also have to be modified. In the equivalence discussed above these distributions must remain the same.

To apply the results of a two-dimensional analysis to the three-dimensional problem we may use the transformations (6.8), with the quantities $\tilde{q}$ associated with the two-dimensional problem. It is convenient, therefore, to think of three-dimensional disturbances as waves propagating in various directions. For each value of $\bar{M}_1$—that is, for each value of the direction angle of the waves—the stability problem is investigated by means of Eqs. (6.9) to (6.13) with the usual methods of the two-dimensional theory. Thus, for each value of $\bar{M}_1$ there is a neutral curve in the $(\tilde{\alpha}, \bar{R})$ plane which transforms to one in the (α, R) plane by means of the transformation (6.8). The family of all such neutral curves, for all possible values of $\bar{M}_1$ in the range $0 \leq \bar{M}_1 \leq M_1$, gives the stability characteristics of three-dimensional disturbances.

(7) Formulation of the Characteristic-Value Problem

Having established a two-dimensional formulation of the problem for three-dimensional disturbances, we may make use of the theory of Lees and Lin[1] for further investigations. However, some modifications are necessary when the wave speed of the disturbance is not small compared with the free-stream speed. For supersonic free-stream velocities this is usually the most important case. Detailed mathematical discussions of the necessary modifications will be given in a separate paper. Here we shall merely give a summary of the theoretical arguments and indicate how the final formulas differ from the existing ones. For a brief outline of the mathematical theory see the Appendix.

To determine the analytical nature of the system of Eqs. (6.9) to (6.13), it is convenient to introduce the variables

$$\left.\begin{aligned} Z_1 &= \tilde{f} \\ Z_2 &= \tilde{f}' \\ Z_3 &= \tilde{\phi} \\ Z_4 &= \tilde{\pi}/\bar{M}_1^2 \\ Z_5 &= \tilde{\theta} \\ Z_6 &= \tilde{\theta}' \end{aligned}\right\} \tag{7.1}$$

Then the equations transform to a system of *six* equations of the first order. The latter, when reduced to normal form, have coefficients analytic in the independent variable y and the parameters $\bar{M}_1^2$, $\tilde{\alpha}\bar{R}$, $\tilde{\alpha}^2$, and c.

Six homogeneous boundary conditions must be satisfied for a natural oscillation. These are given by

$$\left.\begin{aligned} &\tilde{f}, \tilde{\phi}\ \tilde{\theta} \text{ bounded as } y \to \infty \\ &\tilde{f}(0) = \tilde{\phi}(0) = 0 \\ &a\tilde{\theta}'(0) + b\tilde{\theta}(0) = 0 \end{aligned}\right\} \tag{7.2}$$

where a and b are constants depending upon $\tilde{\alpha}$, c, Θ and the physical properties of the gas and the adjacent solid wall (see Appendix).

The condition of boundedness for $y \to \infty$ can be put into an analytical form with the aid of the differential equations [Eqs. (6.9) to (6.13)]. For large y, viscosity effects become negligible, so that the terms of order $1/R$ can be neglected, and the equations reduce to

$$(d/dy)\left\{[(w-c)\tilde{\phi}' - w'\tilde{\phi}]/[T - \bar{M}_1^2(w-c)^2]\right\} - \left\{[\tilde{\alpha}^2(w-c)]/T\right\}\tilde{\phi} = 0 \tag{7.3}$$

For $y \to \infty$ this is easily seen to become

$$\left.\begin{aligned} &\tilde{\phi}'' - \beta^2\tilde{\phi} = 0 \\ &\beta^2 = \tilde{\alpha}^2[1 - \bar{M}_1^2(1-c)^2] \end{aligned}\right\} \tag{7.4}$$

Equation (7.4) has two solutions $\exp(\pm\beta y)$, where (for real c) β denotes the positive square root

$$\beta = \tilde{\alpha}\sqrt{1 - \bar{M}_1^2(1-c)^2} \tag{7.5}$$

Thus, for real c the condition of boundedness at infinity is automatically satisfied if

$$c < 1 - (1/\tilde{M}_1) \tag{7.6}$$

In this case, the characteristic values are continuous, and the solutions represent disturbances whose phase velocity in the (x, z) plane is supersonic relative to the component of the free-stream velocity in the direction of propagation of the disturbances in this plane. These supersonic disturbances correspond to sound waves propagating into or out of the boundary layer (see reference 1).

For subsonic disturbances with

$$c > 1 - (1/\tilde{M}_1) \tag{7.7}$$

the solution of Eq. (7.3) which is bounded at infinity is $\exp(-\beta y)$. Therefore the boundary condition for $y \to \infty$ is

$$\tilde{\phi}'/\tilde{\phi} \to -\beta \text{ as } y \to \infty \tag{7.8}$$

In this case the characteristic values are discrete and are determined from a secular equation which can be reduced to the form

$$E(\tilde{\alpha}, c, \tilde{M}_1^2) = F(z) \{1 + \Delta\} \tag{7.9}$$

In this equation, $F(z)$ is the function of Tietjens defined by

$$F(z) = 1 + \left\{ \int_\infty^{-z} \zeta^{2/3} H_{1/3}^{(1)} \left[\frac{2}{3} (i\zeta)^{3/2} \right] d\zeta \div z \int_\infty^{-z} \zeta^{1/2} H_{1/3}^{(1)} \left[\frac{2}{3} (i\zeta)^{3/2} \right] d\zeta \right\} \tag{7.10}$$

where

$$z = (\tilde{\alpha}\tilde{R})^{1/3} \left(\frac{3}{2} \int_0^{y_c} \sqrt{\frac{c - w}{\nu}}\, dy \right)^{2/3} \tag{7.11}$$

and the function $E(\tilde{\alpha}, c, \tilde{M}_1^2)$ is given by

$$\left(\frac{c - w}{\nu} \right)_w^{-1/2} \left[\frac{3}{2} \int_{y_c}^0 \sqrt{\frac{c - w}{\nu}}\, dy \right] E(\tilde{\alpha}, c, \tilde{M}_1^2) = \begin{vmatrix} \tilde{\phi}_{1w} & \tilde{\phi}_{11}' + \beta\tilde{\phi}_{11} \\ \tilde{\phi}_{2w} & \tilde{\phi}_{21}' + \beta\tilde{\phi}_{21} \end{vmatrix} \div \begin{vmatrix} [(T_w\tilde{\phi}_{1w}' + \tilde{M}_1^2 w_w' c\tilde{\phi}_{1w})/(T_w - \tilde{M}_1^2 c^2)] & \tilde{\phi}_{11}' + \beta\tilde{\phi}_{11} \\ [(T_w\tilde{\phi}_{2w}' + \tilde{M}_1^2 w_w' c\tilde{\phi}_{2w})/(T_w - \tilde{M}_1^2 c^2)] & \tilde{\phi}_{21}' + \beta\tilde{\phi}_{21} \end{vmatrix} \tag{7.12}$$

The quantities $\tilde{\phi}_{1w}$, $\tilde{\phi}_{2w}$ are the wall values and $\tilde{\phi}_{11}$, $\tilde{\phi}_{21}$ the free-stream values of two linearly independent solutions of Eq. (7.3).

The function $\Delta = \Delta(\tilde{\alpha}, c, \tilde{M}_1^2, a, b, z, \sigma)$, whose analytical definition is given in the Appendix, depends on both the inviscid and viscous solutions of the disturbance equations and on the thermal boundary condition in Eq. (7.2).

The principal difference between the present formulation and that given by Lees and Lin[1] is in the presence of the function Δ. The appearance of this new term in the secular equation is due essentially to the fact that we are now placing no restriction on the value of c. In fact, for finite values of T_w,† Δ can always be written as

$$\Delta = \{ [(\gamma - 1)\tilde{M}_1^2 c^2]/T_w \} \Delta_1 \tag{7.13}$$

where Δ_1 is another function depending on the same quantities as Δ which is 0(1) at most. Thus, it is clear that Δ is always negligible when c is small. On the other hand, at high Mach Numbers, when c is usually large, Δ is in general 0(1) and cannot be neglected, since the value of Δ_1 depends on the thermal boundary condition and is therefore small only in very special cases.

In reference 1 it was concluded that the characteristic value problem is independent of the temperature fluctuations and the boundary conditions imposed on them. The present considerations show that this conclusion is of general validity only when c is small, since it is only then that Δ can be neglected without any restriction being placed on the value of Δ_1. For practical purposes, this limits the range of validity of the conclusion to subsonic and slightly supersonic Mach Numbers, when c is not large in most cases of interest. For example, the error corresponding to the neglect of Δ for an insulated wall at $M_1 = 1.6$ can be estimated from Eq. (7.13) to be about 10 per cent (on taking $c \approx 1 - 1/M_1$). This is still not very large, considering the usual order of accuracy of the asymptotic theory. However, for somewhat higher Mach Numbers the error increases rapidly.

The preceding conclusion is true in an extremely restricted sense at high Mach Numbers—namely, for those disturbances whose direction of propagation is at a large angle with the free-stream direction so that $\tilde{M}_1$ is small. For these, it is clear that Δ is again negligible without any restriction being placed on the value of Δ_1.

In the cases just discussed the secular equation reduces to

$$E(\tilde{\alpha}, c, \tilde{M}_1^2) = F(z) \tag{7.14}$$

which has a form much like that in the theory of reference 1. In all other cases, the form of this relation depends on the thermal boundary condition in Eq. (7.2).

A detailed analysis of the thermal boundary condition leads to the important conclusion that *when the wave number $\tilde{\alpha}$ is very small the relation for the characteristic values again reduces to Eq. (7.14), since Δ_1 then becomes negligible.* Such a situation corresponds to very low frequency fluctuations, since the time-frequency is given by $\tilde{\alpha}c \cos\Theta$. An important example is the limiting case of complete stabilization of the boundary layer by cooling, for which all values of $\tilde{\alpha}$ on the neutral curve must approach zero in the limit [see Section (10)]. Thus, the critical temperature ratios for complete stabilization can still be obtained by fairly simple calculations with the use of Eq. (7.14).

† The exceptional case $T_w = 0$ is discussed in the Appendix.

In all cases at high Mach Numbers when the wave number is not small, the relation for the characteristic value is more complicated than Eq. (7.14). We shall not consider these more complicated situations any further here and shall limit all subsequent calculations in this paper to situations in which Eq. (7.14) is a valid approximation. The detailed presentation of the extended theory will be given in future communications.

An examination of Eq. (7.14) shows that it reduces to the corresponding relation given by Lees and Lin for small c but that it is somewhat different for large c because of the changes in the definition Eq. (7.11) for z and the first factor in Eq. (7.12). The results of the previous theory are reproduced by assuming c to be small and keeping only the first term in each of the power series expansions of $(w - c)$ and ν about y_c. In the supersonic case, when c is not small, such a procedure does not represent a good approximation for our purposes.† For a discussion of the differences between results obtained by the present and older theories, see Section (10).

(8) Determination of the Curves of Neutral Stability for Oblique Waves

Consider oblique waves with direction angle arc cos $\tilde{M}_1/M_1$, where $\tilde{M}_1$ is some value in the range $0 \leq \tilde{M}_1 \leq M_1$. The condition (7.14) for the characteristic values $(\tilde{\alpha}, \tilde{R}, c)$ can be transformed to

$$\Phi(z) = (1 + \lambda)\left\{(u + iv)/[1 + \lambda(u + iv)]\right\} \tag{8.1}$$

with $\Phi(z) \equiv 1/[1 - F(z)]$, where z, λ, and $u + iv$ are given by

$$\tilde{\alpha}\tilde{R} = z^3\left(\frac{3}{2}\int_0^{y_c}\sqrt{\frac{c - w}{\nu}}\,dy\right)^{-2} \tag{8.2a}$$

$$\lambda(c) = \frac{3}{2}\frac{w_w'\nu_w^{1/2}}{c^{3/2}}\int_0^{y_c}\sqrt{\frac{c - w}{\nu}}\,dy - 1 \tag{8.2b}$$

$$u + iv = 1 + (w_w'c/T_w)\left\{[\phi_{21}' + \tilde{\alpha}\sqrt{1 - \tilde{M}_1^2(1 - c)^2}\phi_{21}]/[\phi_{11}' + \tilde{\alpha}\sqrt{1 - \tilde{M}_1^2(1 - c)^2}\,\phi_{11}]\right\} \tag{8.2c}$$

and ϕ_{11}, ϕ_{21}, ϕ_{11}', ϕ_{21}' are as defined by Eqs. (8.6a)–(8.6d).

For some purposes it is more convenient to solve Eq. (8.1) for $u + iv$, so that

$$u + iv = \Psi_r(z, c) + \Psi_i(z, c) \tag{8.3}$$

where

$$\Psi_r(z, c) = [(1 + \lambda)\Phi_r - \lambda(\Phi_r^2 + \Phi_i^2)] \div \left\{[1 + \lambda(1 - \Phi_r)]^2 + \lambda^2\Phi_i^2\right\} \tag{8.4a}$$

$$\Psi_i(z, c) = [(1 + \lambda)\Phi_i]/\left\{[1 + \lambda(1 - \Phi_r)]^2 + \lambda^2\Phi_i^2\right\} \tag{8.4b}$$

Before discussing the determination of the neutral curve we shall write down the required formulas and make certain transformations that are useful in the calculations. The quantities ϕ_{11} and ϕ_{21} are the free-stream values of two linearly independent solutions of the inviscid equation

$$(d/dy)\left\{[(w - c)\phi' - w'\phi]/[T - \tilde{M}_1^2(w - c)^2]\right\} - \tilde{\alpha}^2[(w - c)/T]\phi = 0 \tag{8.5}$$

These two solutions may be obtained as power series in $\tilde{\alpha}^2$, as described in reference 1, so that

$$\phi_{11} = (1 - c)\sum_{n=0}^{\infty}\tilde{\alpha}^{2n}\tilde{H}_{2n} \tag{8.6a}$$

$$\phi_{21} = (1 - c)\sum_{n=0}^{\infty}\tilde{\alpha}^{2n}\tilde{K}_{2n+1} \tag{8.6b}$$

$$\phi_{11}' = (1 - c)\left[\frac{1 - \tilde{M}_1^2(1 - c)^2}{(1 - c)^2}\right]\sum_{n=1}^{\infty}\tilde{\alpha}^{2n}\tilde{H}_{2n-1} \tag{8.6c}$$

$$\phi_{21}' = (1 - c)\left[\frac{1 - \tilde{M}_1^2(1 - c)^2}{(1 - c)^2}\right]\sum_{n=0}^{\infty}\tilde{\alpha}^{2n}\tilde{K}_{2n} \tag{8.6d}$$

where

$$\left.\begin{aligned}\tilde{H}_0 = 1,\quad \tilde{H}_1 = \int_0^1\frac{(w - c)^2}{T}\,dy,\quad \tilde{H}_2 = \int_0^1\frac{T - \tilde{M}_1^2(w - c)^2}{(w - c)^2}\,dy\int_0^y\frac{(w - c)^2}{T}\,dy,\\ \tilde{H}_3 = \int_0^1\frac{(w - c)^2}{T}\,dy\int_0^y\frac{T - \tilde{M}_1^2(w - c)^2}{(w - c)^2}\,dy\int_0^y\frac{(w - c)^2}{T}\,dy, \ldots\end{aligned}\right\} \tag{8.7a}$$

$$\left.\begin{aligned}\tilde{K}_0 = 1,\quad \tilde{K}_1 = \int_0^1\frac{T - \tilde{M}_1^2(w - c)^2}{(w - c)^2}\,dy,\quad \tilde{K}_2 = \int_0^1\frac{(w - c)^2}{T}\,dy\int_0^y\frac{T - \tilde{M}_1^2(w - c)^2}{(w - c)^2}\,dy,\\ \tilde{K}_3 = \int_0^1\frac{T - \tilde{M}_1^2(w - c)^2}{(w - c)^2}\,dy\int_0^y\frac{(w - c)^2}{T}\,dy\int_0^y\frac{T - \tilde{M}_1^2(w - c)^2}{(w - c)^2}\,dy, \ldots\end{aligned}\right\} \tag{8.7b}$$

For values of c that are not too large, the integrals (8.7a) and (8.7b) can be put into forms that are more suitable for calculation purposes. For example, in $\tilde{K}_2$ we use the relation

† The approximation is worse in ν than in $(w - c)$.

$$\int_0^y \frac{T - \tilde{M}_1^2(w-c)^2}{(w-c)^2}\,dy = \int_0^1 \frac{T - \tilde{M}_1^2(w-c)^2}{(w-c)^2}\,dy - \int_y^1 \frac{T - \tilde{M}_1^2(w-c)^2}{(w-c)^2}\,dy \quad (8.8)$$

to transform $\tilde{K}_2$ into

$$\tilde{K}_2 = \tilde{H}_1\tilde{K}_1 - \tilde{N}_2 \quad (8.9)$$

where

$$\tilde{N}_2 = \int_0^1 \frac{(w-c)^2}{T}\,dy \int_y^1 \frac{T - \tilde{M}_1^2(w-c)^2}{(w-c)^2}\,dy$$

Thus $\tilde{N}_2$ has an integrand

$$\frac{(w-c)^2}{T}\int_y^1 \frac{T - \tilde{M}_1^2(w-c)^2}{(w-c)^2}\,dy \quad (8.10)$$

which is not numerically large for any value of y, so that $\tilde{N}_2$ may be expected to be numerically smaller than $\tilde{K}_2$. Similar transformations are made for the other integrals as follows:

$$\left.\begin{aligned} \tilde{K}_n &= \tilde{K}_1\tilde{H}_{n-1} - \tilde{N}_n, \qquad n \geq 3 \\ \tilde{N}_2 &= \tilde{H}_2 \\ \tilde{H}_n &= \tilde{H}_2\tilde{H}_{n-2} - \tilde{M}_n, \qquad n \geq 3 \end{aligned}\right\} \quad (8.11)$$

In general, $\tilde{M}_n$, and $\tilde{N}_n$ will be numerically smaller than the corresponding $\tilde{H}_n$ and $\tilde{K}_n$ for small c. The preceding transformations were first used in the stability theory for incompressible fluids,[10] where c is usually fairly small, and then extended to the case of compressible fluids.[2] Obviously they are not useful for reasonably large values of c, in which case other transformations may be more appropriate. This situation occurs for large enough Mach Numbers—for M_1 greater than about two, perhaps. When M_1 becomes very large, in fact, c is often very close to unity.

The relation (8.2c) may now be written as

$$u + iv = \frac{w_w'c}{T_w}\left\{\tilde{K}_1 + [T_w/(w_w'c)] + (1/\tilde{\alpha})G(\tilde{\alpha}, c)\right\} \quad (8.12)$$

where

$$G(\tilde{\alpha}, c) = (1 - \tilde{H}_2\tilde{\alpha}^2)\left\{\left[\frac{\sqrt{1 - \tilde{M}_1^2(1-c)^2}}{(1-c)^2} \times \left(1 - \sum_1^\infty \tilde{\alpha}^{2n}\tilde{N}_{2n}\right) - \sum_1^\infty \tilde{\alpha}^{2n+1}\tilde{N}_{2n+1}\right] \div \left[\left(1 - \sum_2^\infty \tilde{\alpha}^{2n}\tilde{M}_{2n}\right) + \frac{\sqrt{1 - \tilde{M}_1^2(1-c)^2}}{(1-c)^2} \times \left(\tilde{\alpha}\tilde{H}_1 - \sum_1^\infty \tilde{\alpha}^{2n+1}\tilde{M}_{2n+1}\right)\right]\right\} \quad (8.13)$$

If $G(\tilde{\alpha}, c)$ is expanded as a power series in $\tilde{\alpha}$, the real and imaginary parts of Eq. (8.12) are given by the following expressions in the case of real c:

$$u = (w_w'c/T_w)\left\{\tilde{K}_{1r} + [T_w/(w_w'c)] + (k/\tilde{\alpha})\,[1 - k\tilde{H}_1\tilde{\alpha} + (k^2\tilde{H}_1^2 - 2\tilde{H}_{2r})\tilde{\alpha}^2 - +]\right\} \quad (8.14)$$

$$v = (w_w'c/T_w)\,[\tilde{K}_{1i} + (k/\tilde{\alpha})\,(-2\tilde{H}_{2i}\tilde{\alpha}^2 + - \ldots)] \quad (8.15)$$

where

$$k = [1 - \tilde{M}_1^2(1-c)^2]^{1/2}\,(1-c)^2$$

Such series expressions are expected to be good approximations when $k\tilde{\alpha}$ is small. This is true for all cases at subsonic and slightly supersonic Mach Numbers, but at high supersonic Mach Numbers it appears to hold only for cases of extreme cooling since otherwise k may be very large.

In the present work we shall neglect all terms of order $\tilde{\alpha}^2$ in Eqs. (8.14) and (8.15) for the sake of simplicity, so that

$$u = (w_w'c/T_w)\left\{\tilde{K}_{1r} + [T_w/(w_w'c)] + (k/\tilde{\alpha})\,(1 - k\tilde{H}_1\tilde{\alpha})\right\} \quad (8.16a)$$

$$v = v_0(c) \equiv (w_w'c/T_w)\tilde{K}_{1i} \quad (8.16b)$$

In the calculations of reference 2 the same approximation [Eq. (8.16b)] for v is used, but terms of order $\tilde{\alpha}^3$ are retained in the relation (8.14) for u. The results show, however, that often the error corresponding to the neglect of terms of order $\tilde{\alpha}^2$ in Eq. (8.16a) is no larger than that in Eq. (8.16b). In any event, the approximations (8.16a) and (8.16b) appear to be reasonably adequate for all subsonic and slightly supersonic Mach Numbers, with errors within the limits of error of the asymptotic theory. Moreover, they are very accurate at *any* Mach Number *when* $\tilde{\alpha}$ *is very small* (which occurs, for example, when cooling at the solid surface is sufficient). [See Section (10)]. For Mach Numbers greater than about two, however, this is true only for cases of extreme cooling. The present approximations, therefore, are probably not accurate at such high Mach Numbers in most cases of practical importance, and the method of numerical calculation may have to be revised.†

Now let us consider the procedure for finding the characteristic values $(\tilde{\alpha}, \tilde{R}, c)$ on the neutral curve. The various steps can be illustrated most clearly by geometrical considerations, with the aid of the condition for the characteristic values in the form of Eq. (8.3) rather than Eq. (8.1).

For the values of c that occur in the calculations, $\lambda(c)$ is always small, so that $\Psi_r(z, c)$ and $\Psi_i(z, c)$ are approximated fairly closely by $\Phi_r(z)$ and $\Phi_i(z)$. In fact, for $c = 0$, $\Psi_r(z, 0) = \Phi_r(z)$ and $\Psi_i(z, 0) = \Phi_i(z)$. Therefore, for each value of c, the graphs of Ψ_r and Ψ_i against z have much the same shapes as those of Φ_r and Φ_i, respectively (see Fig. 1). The maximum $\Psi_{im}(c)$ on the graph of $\Psi_i(z, c)$ against z is generally close to the maximum value $\Phi_i = 0.580$ at $z = 3.22$ on the Φ_i curve.

† All existing calculations suffer from limitations of this kind. In some investigations, numerical calculations were carried out by using methods adequate only for small c and α, even though the resulting values of these quantities were not small. Such results must be treated with reserve.

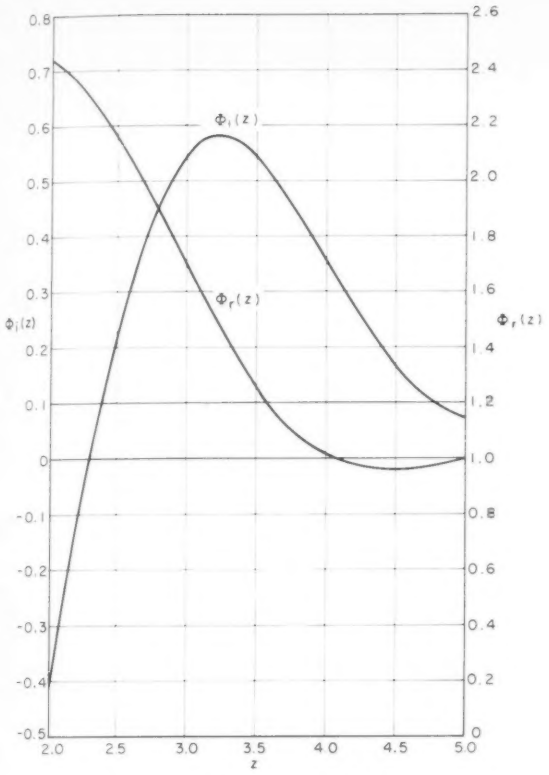

FIG. 1. The Functions $\Phi_r(z)$ and $\Phi_i(z)$.

For Mach Numbers that are not greater than about two, the graph of $v_0(c)$ against c has one of the typical forms shown in Fig. 2a (which is plotted from the data given in reference 2). In general, the greater the cooling—that is, the lower the wall temperature—the higher the v_0 curve is in the (c, v_0) plane. For larger Mach Numbers the v_0 curves may have more complicated shapes, as indicated in Fig. 2b. For the present, we shall consider only Mach Numbers for which the curves have the simple behavior shown in Fig. 2a.

The pairs of values $(\tilde{\alpha}, \tilde{R})$ are to be found for a series of real values of c. The minimum value of c for subsonic Mach Numbers is $c = 0$, and for supersonic Mach Numbers it is either $c = 0$ or $c = 1 - 1/\bar{M}_1$ if $\bar{M}_1 > 1$.

For each value of c, relation (8.3) is solved for z and u with the aid of Eq. (8.16b). First, z is obtained by solving $v_0(c) = \Psi_i(z, c)$, which is equivalent to finding the value of z corresponding to the point of intersection of the curve $\Psi_i(z, c)$ against z with a straight line parallel to the z-axis at a distance $v_0(c)$ from it. From the behavior of the graph of $\Psi_i(z, c)$ [which is similar to the graph of $\Phi_i(z)$ in Fig. 1], we see that if $v_0(c) < 0$ there is one intersection point (one value of z), and if $v_0(c) > 0$ there are generally two intersection points (two values of z) if $v_0(c)$ is not too large. For some value of c large enough it is clear that the straight line will be just tangent to the corresponding graph of $\Psi_i(z, c)$ at its maximum point, and for larger values of c there will be no intersection points at all. This maximum value of c, therefore, is given by the intersection of the graph of $\Psi_{i_m}(c)$ with that of $v_0(c)$ (see Figs. 2). Corresponding to it there is just one value of z. With the value of z determined, $u = \Psi_r(z, c)$ is obtained from the graph of $\Psi_r(z, c)$ [which is similar to the graph of $\Phi_r(z)$ in Fig. 1]. Then $\tilde{\alpha}$ follows by solving Eq. (8.16a), since all the quantities in this equation besides $\tilde{\alpha}$ are now known functions of c, and finally $\tilde{R}$ is obtained from Eq. (8.2a). The corresponding values (α, R) are then determined by means of the transformations (6.8). The points (α, R) for all possible values of c give the curve of neutral stability in the (α, R) plane.

Evidently $z(c)$ and $u(c)$ could be obtained graphically as just described by drawing graphs of $\Psi_r(z, c)$ and $\Psi_i(z, c)$ against z for each value of c. However, for the purpose of the numerical calculations it is more convenient and more accurate to solve the two real relations obtained from Eq. (8.1) for z and u by an iteration procedure with the aid of the tabulated values of $\Phi_r(z)$ and $\Phi_i(z)$ (see Table 1), as described in reference 2. The maximum value of c and the corresponding values of z and u can also be found accurately by an iteration method (see reference 13).†

Present calculations are carried out for the boundary layer on a flat plate at a Mach Number of $M_1 = 1.6$

† A detailed discussion of the procedure for the numerical calculations described in this and following sections and complete tables of various functions used in the calculations are given in reference 13.

TABLE 1
The Functions $\Phi_r(z)$, $\Phi_i(z)$, $\Phi_r'(z)$, $\Phi_i'(z)$

z	$\Phi_r(z)$	$\Phi_i(z)$	$\Phi_r'(z)$	$\Phi_i'(z)$
1.0	0.80630	-2.60557		
1.1				
1.2	1.77012	-2.29854	3.71	2.781
1.3			2.54	
1.4	2.26836	-1.71669	1.505	2.937
1.5			.850	2.633
1.6	2.44985	-1.18600	.4245	2.384
1.7			.1390	2.127
1.8	2.48104	- .75892	- .06428	1.907
1.9			- .2140	1.726
2.0	2.43927	- .41253	- .3337	1.573
2.1			- .4377	1.443
2.2	2.35196	- .12342	- .5333	1.325
2.3			- .6242	1.213
2.4	2.22724	+ .11916	- .7108	1.1007
2.5			- .7912	.9833
2.6	2.06929	.31558	- .8625	.8564
2.7			- .9209	.7254
2.8	1.88566	.46043	- .9627	.5853
2.9			- .9850	.4414
3.0	1.68938	.54872	- .9853	.2978
3.1			- .9640	.1590
3.2	1.49726	.58082	- .9223	.0296
3.3			- .8629	- .0867
3.4	1.32516	.56401	- .7893	- .1862
3.5			- .7054	- .2695
3.6	1.18429	.51074	- .6151	- .3332
3.7			- .5222	- .3786
3.8	1.07982	.43560	- .4302	- .4067
3.9			- .3422	- .4193
4.0	1.01118	.35220	- .2609	- .4189
4.1			- .1865	- .4060
4.2	.97361	.27133	- .1172	- .3793
4.3			- .0625	- .3538
4.4	.96056	.20038	- .01470	- .3225
4.5			- .0061	
4.6	.95989	.13601	+ .0034	
4.7			+ .0476	
4.8	.97659	.09503	+ .1794	
4.9				
5.0	.99582	.07266		

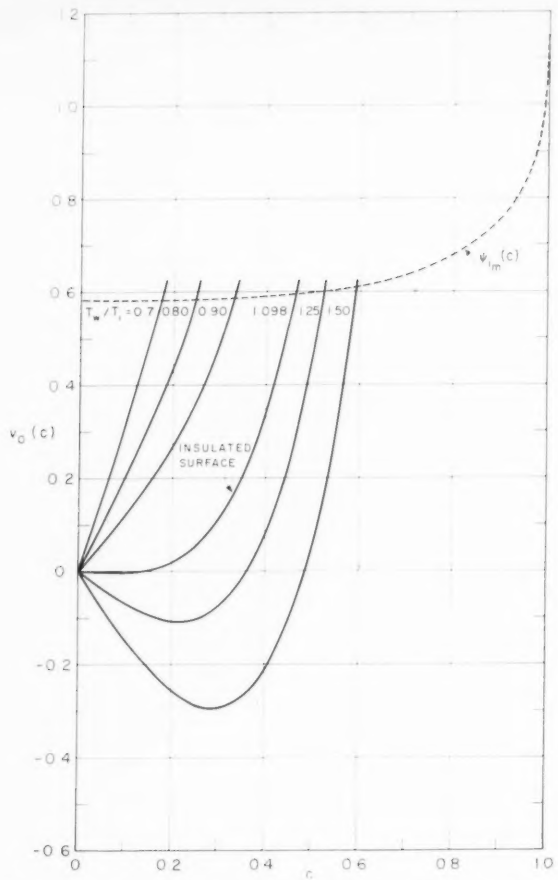

FIG. 2a. The function $v_0(c)$ versus c for various ratios T_w/T_1 of wall to free-stream temperature at a free-stream Mach Number of $M_1 = 0.7$.

and ratio of wall to free-stream temperature of $T_w/T_1 = 1.073$. This temperature ratio is the critical ratio below which the boundary layer is completely stable with respect to two-dimensional disturbances [see Section (10)]. The Prandtl Number is given the value 0.75, and, for simplicity of calculation, the viscosity coefficient is taken to be directly proportional to the absolute temperature, with the constant of proportionality chosen so as to give the correct result at the wall. This procedure for the viscosity coefficient is known to be a good approximation in the case of the boundary layer itself when the Mach Number is not too large. Although it probably is not as accurate in the stability calculations, estimates show that it does not significantly alter the general trend of the results.

In Table 3, α, α_x, α_θ, R, R_x, R_θ are tabulated as functions of c for several values of $\tilde{M}_1$ in the range $0 < \tilde{M}_1 < 1.6$, where α_x and R_x are wave number and Reynolds Number based on a reference length x_1 (the distance from the leading edge of the plate) and α_θ and R_θ are those based on the momentum thickness as reference length.

In Fig. 3 neutral curves in the $(\alpha_\theta, R_\theta)$ plane are shown for the three cases $\tilde{M}_1 = 1.4$, 1.0, 0.6 corresponding to direction angles of 29.0°, 51.3°, 68.0°, respectively.

The approximation is now made that the minimum critical Reynolds Number is very close to the value of R corresponding to the maximum value of c. This was found to be true in previous investigations for an incompressible fluid[10] and for a compressible fluid.[2] The neutral curves in Fig. 3 show that in the present case it is also an excellent approximation, with only a slight error. The minimum critical Reynolds Number R_{xc} approximated in this way is plotted against the direction angle of the oblique waves in Fig. 4 and tabulated in Table 4. As might have been expected, R_{xc} becomes infinite at direction angles of 0° and 90°. The minimum value of R_{xc} occurs at $\tilde{M}_1 = 1.030$ (corsponding to a direction angle of 49.9°) and is given by $R_{xc} = 1.64 \times 10^6$. This value $R_{xc} = 1.64 \times 10^6$, therefore, is the minimum critical Reynolds Number for all three-dimensional disturbances in this particular case.

(9) The Dependence of the Minimum Critical Reynolds Number on the Direction of Propagation of the Waves

For those cases in which the approximations (8.16a) and (8.16b) are sufficiently accurate, it is possible to derive fairly simple analytical results for the directional dependence of the minimum critical Reynolds Number —that is, dependence on the parameter $\tilde{M}_1$. By solving Eq. (8.16a) for $\tilde{\alpha}$ we have

$$\tilde{\alpha} = \tilde{\alpha}_0/(1 + k\tilde{H}_1\tilde{\alpha}_0) \tag{9.1}$$

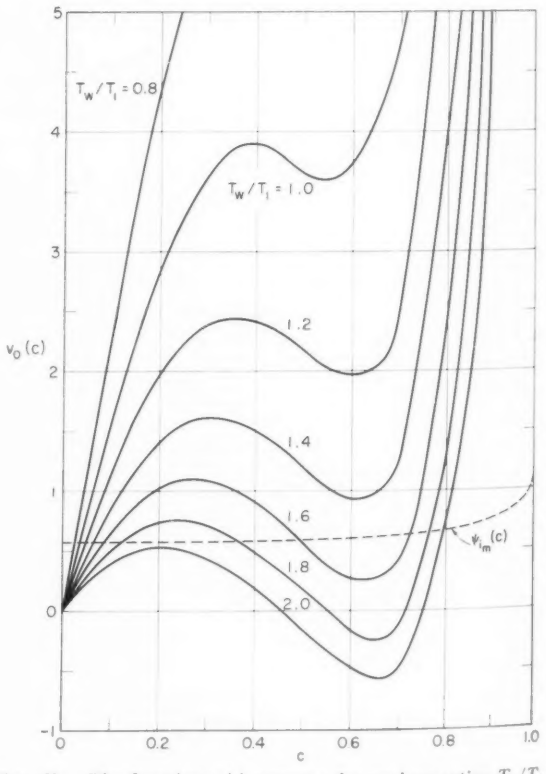

FIG. 2b. The function $v_0(c)$ versus c for various ratios T_w/T_1 of wall to free-stream temperature at a free-stream Mach Number of $M_1 = 4$.

where

$$\tilde{\alpha}_0 = \left[\frac{w_w'c}{T_w}\frac{\sqrt{1-\tilde{M}_1^2(1-c)^2}}{(1-c)^2}\right] \div \left[u - \frac{w_w'c}{T_w}\left(\tilde{K}_{1r} + \frac{T_w}{w_w'c}\right)\right] = \frac{(w_w'c/T_w)k}{u-\tilde{L}} \quad (9.2)$$

Then the minimum value of R on the neutral curve in the (α, R) plane is given, with the aid of Eqs. (6.8) and (8.2a), by

$$R_c = \frac{M_1}{\tilde{M}_1}\tilde{R}_c = \frac{M_1}{\tilde{M}_1} z^3 \left(\frac{3}{2}\int_0^{y_c}\sqrt{\frac{c-w}{p}}\,dy\right)^{-2} \times \frac{1+k\tilde{H}_1\tilde{\alpha}_0}{\tilde{\alpha}_0} \quad (9.3)$$

where c is approximated by the maximum permissible value of c described previously. Once the particular boundary-layer flow is specified—i.e., the functions $w(y)$ and $T(y)$—this value of c and therefore $z(c)$, $u(c)$, and all the other functions of c in Eq. (9.3) are determined. For small λ, previous discussions show that c is given approximately by $v_0(c) \approx 0.580$, and also that $z(c) \approx 3.22$, $u(c) \approx 1.48$ (see Fig. 1).

We now have

$$R_c = K\{[1 + (\tilde{M}_1\tilde{\alpha}_0)] + (k\tilde{H}_1/\tilde{M}_1)\} \quad (9.4)$$

where K depends on the given boundary-layer flow but is *independent of* $\tilde{M}_1$. In order to determine the dependence on $\tilde{M}_1$ of the other quantities entering into R_c, we note that

$$\tilde{H}_1 = \int_0^1 \frac{(w-c)^2}{T}\,dy = H_1 \quad (9.5)$$

is independent of $\tilde{M}_1$, and, with the use of Eqs. (8.7b) and (9.2), that

$$u - \tilde{L} = u - L - (w_w'c/T_w)(M_1^2 - \tilde{M}_1^2) \quad (9.6)$$

where

$$L = \frac{w_w'c}{T_w}\left[Re\int_0^1 \frac{T - M_1^2(w-c)^2}{(w-c)^2}\,dy + \frac{T_w}{w_w'c}\right] \quad (9.6a)$$

Then, with the aid of the definition for k, Eq. (9.4) can be written as

$$R_c = (A + B\tilde{M}_1^2)/[\tilde{M}_1\sqrt{1-\tilde{M}_1^2(1-c)^2}] \quad (9.7)$$

where

$$A = K\left((1-c)^2\{[T_w/(w_w'c)](u-L) - M_1^2\} + [H_1/(1-c)^2]\right) \quad (9.8a)$$

$$B = K[(1-c)^2 - H_1] \quad (9.8b)$$

The quantities A, B, and c are independent of $\tilde{M}_1$ and are determined from the distributions $w(y)$ and $T(y)$ of velocity and temperature, respectively, in the boundary layer.

From Eq. (9.7) we find

$$dR_c/d\tilde{M}_1 = \{\tilde{M}_1^2[2A(1-c)^2 + B] - A\}/\{\tilde{M}_1^2 \times [1-\tilde{M}_1^2(1-c)^2]^{3/2}\} \quad (9.9)$$

Therefore

$$dR_c/d\tilde{M}_1 = 0$$

when

$$\tilde{M}_1 = 1/\sqrt{2(1-c)^2 + (B/A)} \quad (9.10)$$

and

$$dR_c/d\tilde{M}_1 < 0 \quad (9.11)$$

when

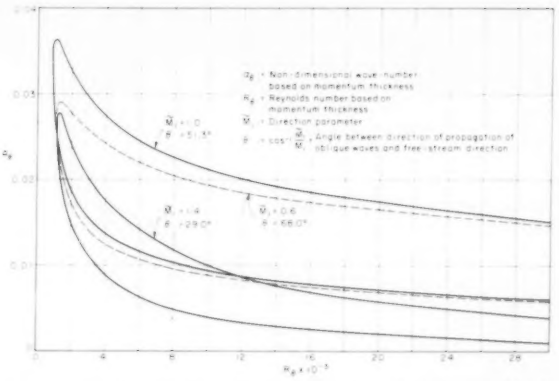

FIG. 3. Curves of neutral stability at a free-stream Mach Number of $M_1 = 1.6$ and a ratio of wall to free-stream temperature of $T_w/T_1 = 1.073$.

TABLE 2(a)

The Function $v_0(c)$ for Various Ratios of Wall to Free-Stream Temperature at a Free-Stream Mach Number of 0.7

The function $v_0(c)$; $M_1 = 0.7$, $\rho\mu = 1$, $\sigma = 1$

$T_w/T_1 = 0.70$		$T_w/T_1 = 0.80$		$T_w/T_1 = 0.90$		$T_w/T_1 = 1.098$		$T_w/T_1 = 1.25$	
c	v_0	c	v_0	c	v_0	c	v_0	c	v_0
.0262	.0625	.0237	.0486	.0433	.0517	.0353	−.0009	.0364	−.0237
.0521	.1645	.0472	.0965	.0863	.1028	.0705	−.0024	.0692	−.0470
.0777	.2466	.0705	.1443	.1291	.1568	.1058	−.0025	.1040	−.0698
.1030	.3297	.0937	.1925	.1714	.2173	.1410	.0000	.1389	−.0868
.1281	.4146	.1168	.2417	.2135	.2865	.1764	.0090	.1738	−.1021
.1529	.5023	.1397	.2926	.2551	.3746	.2114	.0248	.2088	−.1085
.1701	.5661	.1625	.3457	.2963	.4805	.2464	.0501	.2439	−.1057
.1726	.5754	.1851	.4017	.3366	.5428	.2813	.0872	.2789	−.0917
		.2075	.4614	.3268	.5742	.3161	.1389	.3138	−.0641
		.2298	.5253			.3505	.2082	.3485	−.0203
		.2498	.5592			.3847	.2985	.3831	.0427
		.2475	.5801			.4185	.4137	.4174	.1286
						.4352	.4821	.4512	.2614
						.4652	.5270	.4846	.3859
						.4559	.5790	.5092	.5184
								.5190	.5779

TABLE 2(b)

The Function $v_0(c)$ for Various Ratios of Wall to Free-Stream Temperature at a Free-Stream Mach Number of 4.0

The function $v_0(c)$; $M_1 = 4$, $\rho\mu = \rho_w\mu_w$, $\sigma = 0.75$

c \ T_w/T_1	0.8	1.0	1.2	1.4	1.6	1.8	2.0
0.1	2.275	1.572	1.144	.858	.654	.502	.385
0.2	4.367	2.856	1.976	1.409	1.019	.735	.521
0.3	5.830	3.632	2.388	1.605	1.083	.710	.433
0.4	6.571	3.888	2.406	1.498	.899	.480	.177
0.5	6.207	3.645	2.164	1.192	.563	.133	−.172
0.6	6.828	3.741	1.969	.925	.264	−.179	−.487
0.7	9.095	4.809	2.557	1.245	.422	−.135	−.496
0.8	18.98	10.94	6.676	4.172	2.587	1.365	.793
0.9	84.3	52.6	35.5	25.3	18.71	14.23	11.00
0.95	343	218	150.8	110.0	83.6	65.6	52.6

TABLE 3

Wave speeds, wave numbers, and Reynolds Numbers for Neutral Subsonic Disturbances at a Free-Stream Mach Number of 1.6 and Ratio of Wall to Free-Stream Temperature of 1.073

(a) $\tilde{M}_1 = 0.6$, $M_1 = 1.6$, $T_w/T_1 = 1.073$

c	α	$Rx10^{-4}$	α_θ	$R_\theta x10^{-3}$	α_x	$R_x x10^{-6}$
0	0	∞	0	∞	∞	∞
.15	.0515	40.7	.00534	42.1	512	4240
.175	.0642	21.3	.00665	22.1	334	1110
.2	.0779	12.2	.00807	12.7	233	365
.25	.110	4.82	.0114	5.00	129	56.7
.275	.129	3.23	.0134	3.35	102	25.5
.325	.178	1.63	.0184	1.69	70.8	6.52
.3625	.231	1.09	.0239	1.13	61.7	2.92
.375	.268	1.05	.0278	1.09	68.8	2.70
.3625	.278	1.40	.0288	1.45	94.7	4.76
.325	.253	2.63	.0262	2.73	162	16.9
.275	.208	6.23	.0216	6.45	317	94.8
.25	.186	9.89	.0193	10.3	450	239
.2	.144	28.2	.0149	29.2	988	1938
0	0	∞	0	∞	∞	∞

Table 3 (Continued)

(b) $\tilde{M}_1 = 1.0$, $M_1 = 1.6$, $T_w/T_1 = 1.073$

c	α	$Rx10^{-4}$	α_θ	$R_\theta x10^{-3}$	α_x	$R_x x10^{-6}$
0	0	∞	0	∞	∞	∞
.05	.00869	4980	.000900	5160	10600	$606x10^6$
.1	.0264	249	.00273	258	1600	151000
.15	.0515	40.7	.00534	42.2	513	4050
.175	.0671	20.4	.00695	21.1	335	1017
.2	.0849	11.2	.00880	11.6	233	307
.25	.128	4.44	.01330	4.28	130	41.8
.275	.155	2.70	.0161	2.79	103	17.8
.3	.186	1.84	.0193	1.90	83.6	8.25
.325	.222	1.31	.0230	1.35	70.9	4.17
.35	.267	.969	.0277	1.00	63.3	2.30
.3625	.295	.856	.0306	.887	61.7	1.79
.375	.343	.822	.0355	.852	68.8	1.65
.3625	.349	1.11	.0362	1.15	95.0	3.02
.35	.337	1.40	.0350	1.45	115	4.76
.325	.307	2.17	.0318	2.25	163	11.5
.3	.274	3.38	.0284	3.50	227	27.9
.275	.241	5.39	.0250	5.58	318	71.0
.25	.209	8.81	.0217	9.13	449	189
.2	.151	26.8	.0156	27.8	990	1760
.15	.0993	109	.0103	113	2640	28900
.1	.0553	748	.00573	775	10120	$137x10^6$
.05	.0193	19180	.00200	19900	90300	$9x10^8$
0	0	∞	0	∞	∞	∞

Table 3 (Continued)

(c) $\tilde{M}_1 = 1.4$, $M_1 = 1.6$, $T_w/T_1 = 1.073$

c	α	$Rx10^{-4}$	α_θ	$R_\theta x10^{-3}$	α_x	$R_x x10^{-6}$
.2857	0	∞	0	∞		∞
.2875	.0219	17.18	.00227	17.80	92.0	721
.292	.0421	8.63	.00436	8.94	88.8	182
.3	.0662	5.17	.00686	5.36	83.7	65.3
.325	.125	2.33	.0129	2.41	70.9	13.2
.35	.183	1.41	.0189	1.46	63.3	4.89
.3625	.216	1.17	.0224	1.21	61.8	3.35
.375	.263	1.07	.0272	1.11	68.8	2.81
.3625	.250	1.55	.0259	1.61	94.9	5.87
.35	.225	2.09	.0233	2.17	115	10.7
.325	.166	4.01	.0172	4.15	163	39.3
.3	.0936	9.92	.00969	10.28	227	241
.292	.0605	17.05	.00627	17.67	252	711
.2875	.0318	34.5	.00329	35.7	268	2904
.2857	0	∞	0	∞		∞

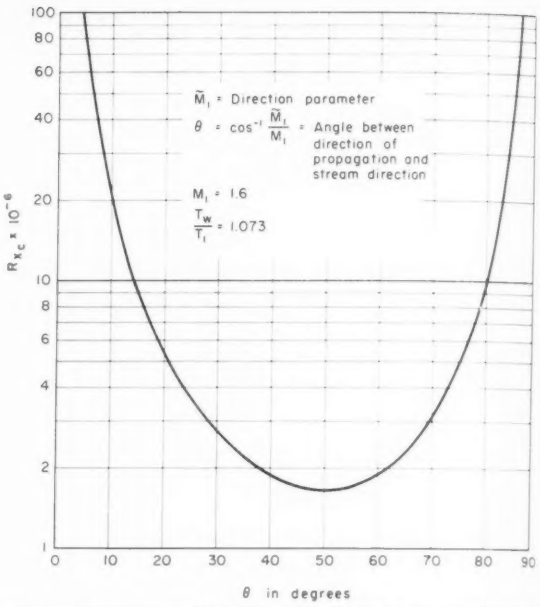

FIG. 4. Minimum critical Reynolds Number versus direction of propagation of oblique waves.

TABLE 4

Minimum Critical Reynolds Numbers and Direction Angles for Oblique Waves at a Free-Stream Mach Number of 1.6 and Ratio of Wall to Free-Stream Temperature of 1.073

$M_1 = 1.6$, $T_w/T_1 = 1.073$

Direction angle = $\cos^{-1}\tilde{M}_1/M_1$

$\tilde{M}_1$	$\cos^{-1}\tilde{M}_1/M_1$	$R_{x_c} x10^{-6}$
0	90°	∞
.1	86.4	75.1
.2	82.8	19.2
.4	75.5	5.23
.6	68.0	2.70
.8	60.0	1.89
1.0	51.3	1.65
1.030	49.9	1.64
1.2	41.4	1.80
1.4	29.0	2.81
1.5	20.4	5.08
1.576	10	19.6
1.594	5	76.7
	0	∞

$$\bar{M}_1 < 1/\sqrt{2(1-c)^2 + (B/A)}$$

Since $0 \leq \bar{M}_1 \leq M_1$ it follows that

$$M_1\sqrt{2(1-c)^2 + (B/A)} < 1 \qquad (9.12)$$

is the condition that all three-dimensional disturbances have a *higher* minimum critical Reynolds Number than two-dimensional ones. Thus, if it can be shown that the parameter $C = M_1\sqrt{2(1-c)^2 + (B/A)}$ for a specified boundary-layer flow is less than unity, then three-dimensional disturbances are more stable and are not very important in the stability problem.

In Table 5 and Fig. 5 are given the results of calculations of C as a function of M_1 for an insulated flat plate from $M_1 = 0$ to $M_1 = 2.4$ and of C as a function of T_w/T_1 at a Mach Number of $M_1 = 0.7$ from $T_w/T_1 = 0.70$ to $T_w/T = 1.25$. For the insulated plate, it is clear that three-dimensional disturbances are more stable than two up to a Mach Number of about 1.8 when they become slightly more unstable. The fact that C decreases and again becomes less than unity when M_1 increases beyond 1.8 may not be of much significance because of the large errors at such Mach Numbers due to the approximations used in the deductions.†

(10) The Influence of Surface Cooling on Boundary-Layer Stability

The problem of boundary-layer stability at supersonic speeds is different from that at subsonic speeds in one important respect—there is always a class of oblique waves (those with $1 < \bar{M}_1 \leq M_1$) for which the values of c are bounded away from zero (i.e., $c \geq 1 - 1/\bar{M}_1 > 0$). This leads to interesting consequences in the case of surface cooling.

Let us first consider strictly two-dimensional disturbances (for which $\bar{M}_1 = M_1$), since the situation is then somewhat simpler. The minimum value of c on the neutral curve is $1 - 1/M_1$, and the maximum value is given by $v_0(c) = \Psi_{im}(c)$—that is, it is the value of c corresponding to the intersection point of the graph of $v_0(c)$ with that of $\Psi_{im}(c)$ (see Figs. 2). For sufficiently small T_w/T_1, $v_0(c) > 0$ for $c = 1 - 1/M_1$ and $v_0(c)$ is monotonically increasing for $c > 1 - 1/M_1$. Also, further decreases in T_w/T_1 raise the whole of the v_0 curve higher in the (c, v_0) plane. This behavior of the v_0 curve is typical for Mach Numbers up to $M_1 = 7.48$.‡ For Mach Numbers greater than $M_1 = 7.48$, no amount of cooling is sufficient to raise the v_0 curve sufficiently to make $v_0(c)$ positive at $c = 1 - 1/M_1$.

We see, therefore, that in this range of Mach Numbers, for T_w/T_1 small enough, the range of values of c on the neutral curve is bounded below by $1 - 1/M_1$ and above by an upper limit given by $v_0(c) = \Psi_{im}(c)$, which can be made as close to $1 - 1/M_1$ as desired by making T_w/T_1 smaller. Thus, there is a critical temperature ratio $(T_w/T_1)_c$ given by $v_0(1 - 1/M_1) = \Psi_{im}(1 - 1/M_1)$ for which the whole neutral curve disappears. This can be seen by solving Eq. (8.16a) for $\tilde{\alpha}$ and noting that $\tilde{\alpha} \to 0$ as $c \to 1 - 1/M_1$. Therefore, when $T_w/T_1 \to (T_w/T_1)_c$, all values of c on the

TABLE 5

The Function $C = M_1\sqrt{2(1-c)^2 + B/A}$ for Various Mach Numbers and Rates of Heat Transfer

Table 5(a)

The function $C = M_1\sqrt{2(1-c)^2 + B/A}$ for zero heat transfer; $\sigma = 1$, $\rho/\mu = 1$.

M_1	0	0.5	0.9	1.3	1.7	2.472
C	0	0.455	0.759	0.941	1.006	0.885

Table 5(b)

The function $C = M_1\sqrt{2(1-c)^2 + B/A}$ for various temperature ratios at $M_1 = 0.7$; $\sigma = 1$, $\rho/\mu = 1$

T_w/T_1	0.70	0.80	0.90	1.25
C	0.871	0.797	0.722	0.544

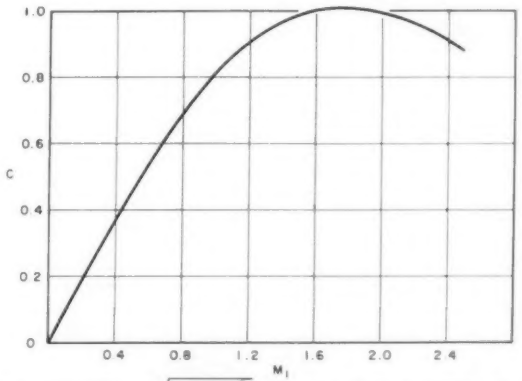

THE FUNCTION $C = M_1\sqrt{2(1-c)^2 + \frac{B}{A}}$ FOR ZERO HEAT TRANSFER AT VARIOUS MACH NUMBERS

FIGURE 5(a)

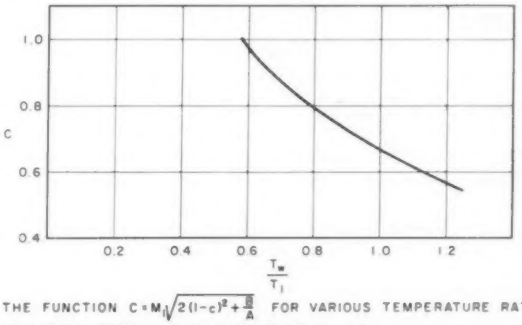

THE FUNCTION $C = M_1\sqrt{2(1-c)^2 + \frac{B}{A}}$ FOR VARIOUS TEMPERATURE RATIOS AT A FREE-STREAM MACH NUMBER OF $M_1 = 0.7$

FIGURE 5(b)

† It should be emphasized that, because of the use of the approximate relations (8.16a) and (8.16b), the results of this section are in most practical cases valid only for Mach Numbers not too much larger than unity. Their implications in regard to the influence of surface cooling at low Mach Numbers are discussed at the end of the next section.

‡ The actual value of this upper limit to the Mach Number depends on the value of the Prandtl Number and the particular viscosity law used. The value $M_1 = 7.48$ corresponds to a Prandtl Number of 0.75 and a linear viscosity-temperature relationship.

TABLE 6
Critical Temperature Ratios for Complete Stability with Respect to Two-Dimensional Disturbances for Free-Stream Mach Numbers from 1 to 8

$\sigma = 0.75, \quad \rho\mu = \rho_w\mu_w$

M_1	T_w/T_1
1	0
1.1	.582
1.2	.766
1.25	.827
1.5	1.018
2	1.262
2.5	1.453
3	1.590
3.5	1.678
4	1.700
4.5	1.641
5.	1.548
6	1.146
6.5	.842
7	.453
7.25	.240
7.48	0

neutral curve approach $1 - 1/M_1$, so that all values of $\tilde{\alpha} \to 0$ and all values of $\tilde{R} \to \infty$.

It is to be noticed that in this limiting situation relations (8.16a) and (8.16b) become *exact* since the errors are $0(\tilde{\alpha}^2)$, so that the relation

$$v_0[1 - (1/M_1)] = \Psi_{im}[1 - (1/M_1)] \qquad (10.1)$$

for the critical temperature ratio $(T_w/T_1)_c$ is exact.

When $T_w/T_1 < (T_w/T_1)_c$ evidently $v_0(c) > \Psi_{im}(c)$ for $c \geq 1 - 1/M_1$, so that no solution is possible, at least for small α. The inequality $T_w/T_1 \leq (T_w/T_1)_c$ is usually interpreted as the condition for the complete stabilization of the boundary layer with respect to two-dimensional disturbances.† The preceding arguments are essentially the same as those used by Lees.[2]

Calculations have been carried out to determine the variation of $(T_w/T_1)_c$ with M_1 for the boundary layer on a flat plate with Prandtl Number equal to 0.75 and viscosity coefficient directly proportional to absolute temperature. The results are tabulated in Table 6, and the curve of critical temperature ratio against Mach Number for two-dimensional disturbances is shown in Fig. 6. Since the critical temperature ratio approaches zero at $M_1 = 7.48$, no amount of cooling is sufficient to completely stabilize the boundary layer with respect to two-dimensional disturbances when $M_1 \geq 7.48$. The present numerical results do not differ appreciably from those of Van Driest,[11] even though corrected viscous solutions [which enter into the determination of $\lambda(c)$ and thus of $\Psi_{im}(c)$] are used. The explanation is probably traceable to the fact that $v_0(c)$ is so extremely sensitive to variations in T_w/T_1 that small errors in Ψ_{im} in Eq. (10.1) do not affect the solution T_w/T_1 much.‡

The conclusions depend, of course, strongly on the value of the Prandtl Number and the particular viscosity-temperature relationship used.[11] However, for the same reason as given above, it is not likely that the use of the present viscous solutions would significantly alter the results for these other cases obtained in reference 11.

Now consider oblique waves with direction angle arc cos $\tilde{M}_1/M_1$, where $1 < \tilde{M}_1 < M_1$. Just as in the case of strictly two-dimensional disturbances, there is again the possibility of completely stabilizing the boundary layer with respect to oblique waves propagating in this direction for small enough T_w/T_1. The arguments carry through much as before except for one complication due to the fact that when the Mach Number is large the curve $v_0(c)$ against c may have an inflection point and thus a maximum and minimum in the interval $0 < c < 1$ (see Fig. 2b). Thus, even when T_w/T_1 is small enough for the relation

$$v_0[1 - (1/\tilde{M}_1)] = \Psi_{im}[1 - (1/\tilde{M}_1)] \qquad (10.2)$$

to hold, the corresponding $v_0(c)$ may *not* be monotonically increasing for $c > 1 - 1/\tilde{M}_1$, when $\tilde{M}_1$ is small

† This interpretation will be discussed later.

‡ Van Driest's computations, in addition to the use of the inaccurate $\lambda(c)$ of reference 1, also involve what is essentially an approximation for $\Psi_{im}(c)$ in terms of $\lambda(c)$. It is interesting to observe that if the exact procedure of calculation is used, in combination with the inaccurate value of $\lambda(c)$ given by reference 1, several critical cooling ratios will be found for each value of $c = 1 - 1/M_1$. This has been pointed out by Bloom.[14] However, with the present function $\lambda(c)$ whose influence is small, such difficulties do not arise.

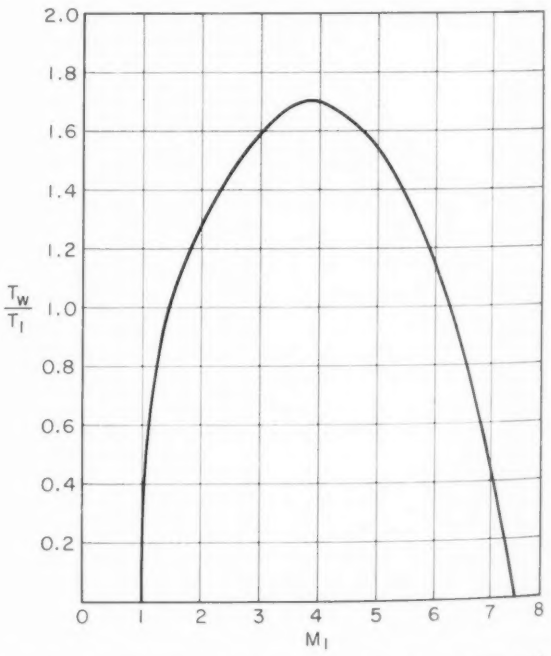

FIG. 6. Critical temperature ratios for complete stability with respect to two-dimensional disturbances.

enough.† There could still be values of $c > 1 - 1/\tilde{M}_1$ for which $v_0(c) < \Psi_{im}(c)$ (see Fig. 2b), so that a neutral curve might still exist. We shall make the tentative assumption‡ that the critical temperature ratio, below which the boundary layer is completely stable with respect to oblique waves with direction angle arc cos $\tilde{M}_1/M_1$, is the largest T_w/T_1 for which

$$v_0(c) \geq \Psi_{im}(c), \quad c \geq 1 - (1/\tilde{M}_1) \qquad (10.3)$$

This value of T_w/T_1 is evidently the one for which the corresponding $v_0(c)$ curve is just tangent near its minimum point to the $\Psi_{im}(c)$ curve (see Fig. 2b).

Obviously if $\tilde{M}_1 \leq 1$ the minimum value of c on the neutral curve is just $c = 0$. Therefore, it is not possible by any amount of cooling to completely stabilize the boundary layer with respect to oblique waves with direction angles greater than arc cos $1/M_1$. The limiting directions are thus the normals to the Mach lines in a plane parallel to the solid surface.

For the boundary layer on a flat plate at a Mach Number $M_1 = 4$ with Prandtl Number equal to 0.75 and a linear viscosity temperature relation, the critical temperature ratio T_w/T_1 has been calculated as a function of direction angle arc cos $\tilde{M}_1/M_1$ and plotted as a full-line curve in Fig. 7. The calculations are carried out by first finding T_w/T_1 as a function of $\tilde{M}_1$ from Eq. (10.2). The resulting values of T_w/T_1 when plotted against arc cos $\tilde{M}_1/M_1$ give a curve with a maximum and a minimum for $\tilde{M}_1$ in the range $0 < \tilde{M}_1 < M_1$. The proper curve for the critical temperature ratio is then obtained by drawing a horizontal tangent to this curve at its minimum point (thus cutting off the dashed part around the maximum point in Fig. 7).** The numerical results are listed in Table 7.

Figure 7 shows that for a temperature ratio $T_w/T_1 = 1.700$ all two-dimensional disturbances are completely stabilized, and, for a somewhat smaller ratio $T_w/T_1 = 1.474$, the three-dimensional disturbances corresponding to oblique waves with direction angles from 0° to 74.3° are completely stabilized. The critical temperature ratio T_w/T_1 decreases to zero rapidly, however, when the direction angle increases from 74.3° to arc cos $1/M_1 = 75.5°$.

When the temperature ratio T_w/T_1 is as low as 1.474, therefore, all oblique waves are stabilized except those with direction angles greater than 74.3°. Estimates of the minimum critical Reynolds Number of the latter (all of which have extremely small values of the wave speed c) show that $R_c \sim 10^6$ or $R_{x_c} \sim 10$.[12] Since such large values of the Reynolds Number are often far beyond the range of practical importance, it follows that if the wall temperature ratio can be reduced to as low a value as 1.474 the boundary layer will be highly stabilized from the practical point of view. However, since the boundary layer is sensitive to changes in T_w/T_1, even a small increase above $T_w/T_1 = 1.474$ might make the boundary layer relatively unstable.

For each value of M_1 up to $M_1 = 7.48$ it is probable that the nature of the oblique waves is about the same as at $M_1 = 4$; that is, for a sufficiently small temperature ratio T_w/T_1, it is possible to completely stabilize oblique waves with direction angles less than arc cos $1/M_1$ but not those with larger direction angles.

At the present time the state of knowledge regarding the general problem of boundary-layer stability at high Mach Numbers is mainly restricted to such results as the preceding regarding complete stabilization by cooling. It is only in such limiting cases, for which $\tilde{\alpha}$

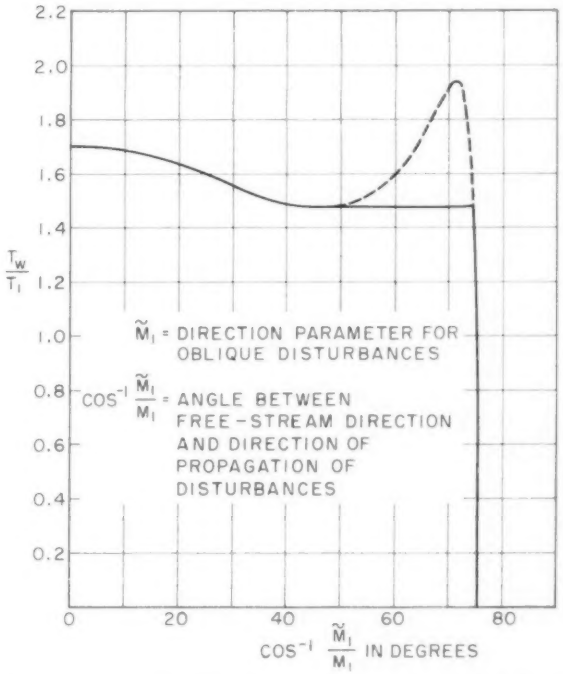

FIG. 7. Critical temperature ratios for complete stability with respect to three-dimensional disturbances at a free-stream Mach Number of $M_1 = 4$.

TABLE 7

Critical Temperature Ratios for Complete Stability with Respect to Three-Dimensional Disturbances at a Free-Stream Mach Number of 4

$M_1 = 4$, $\cos \tilde{M}_1/M_1$ = direction angle, $\rho/\mu = \rho_w/\mu_w$, $\sigma = 0.75$

$\tilde{M}_1$	$\cos\tilde{M}_1/M_1$	T_w/T_1	$\tilde{M}_1$	$\cos \tilde{M}_1/M_1$	T_w/T_1
4.	0°	1.700	1.429	69.1°	1.885
3.61	25.4°	1.600	1.25	71.8	1.935
3.33	33.7	1.540	1.143	73.5	1.800
2.67	48.1	1.474	1.096	74.1	1.600
2.5	51.3	1.483	1.068	74.5	1.400
2.0	60.0	1.585	1.051	74.8	1.200
1.968	60.5	1.700	1.036	75.0	1.000
1.667	65.4	1.740	1.026	75.2	0.800
1.567	66.9	1.800	1.000	75.5	0

† This difficulty does not occur when $\tilde{M}_1$ is as large as M_1, at least for the boundary layer on a flat plate.

‡ This assumption seems the most reasonable one to make, but whether or not it is always justified will depend on results of calculation of neutral curves for large values of $\tilde{\alpha}$. See comments further on in this section.

** This is equivalent to the use of the condition mentioned in connection with relation (10.3). The exact significance of the dashed part of the curve is not yet entirely understood.

TABLE 8

The Functions $\lambda(c)$, $\psi_{i_m}(c)$ for $\rho\mu = \rho_w\mu_w$, $\sigma = 0.75$ and Zero Pressure Gradient

c	$\lambda(c)$	$\psi_{i_m}(c)$	c	$\lambda(c)$	$\psi_{i_m}(c)$
0	0	.58114	.6	.0273	.61307
.1	$.11520\times10^{-3}$	.58216	.7	.0462	.63625
.2	$.9237\times10^{-3}$	.58251	.8	.0769	.67622
.3	3.136×10^{-3}	.58529	.9	.1298	.75297
.4	.0068	.58891	.95	.1775	.83165
.5	.0152	.59868	1.0	.320	1.15

approaches zero in the limit, that the present calculation procedures are satisfactory.

It should be emphasized that for high Mach Numbers the proper interpretation of the critical temperature ratios calculated by present methods is not completely certain. All that is known in any particular case is that for a temperature ratio *slightly* above the critical value a neutral curve exists at all points of which $\tilde{\alpha}$ is very small, and, when the temperature ratio is reduced to the critical value, this neutral curve recedes to infinite values of $\tilde{R}$ with all values of $\tilde{\alpha}$ on it approaching zero at the same time. It is possible that if we start with a temperature ratio *considerably* above the critical value and allow it to approach the latter the neutral curve might split into two branches, one of which disappears in the limit as described above, *while the other continues to exist at finite values of* $\tilde{\alpha}$ *and* $\tilde{R}$. In order to determine whether or not this is so, a method would have to be devised to allow the calculation at high Mach Numbers of neutral curves for values of $\tilde{\alpha}$ which are not very small.

For Mach Numbers not too much larger than unity, the situation is clearer, since neutral curves can be calculated by existing methods for finite values of $\tilde{\alpha}$ and thus for all temperature ratios. It appears that in these cases the possibility suggested above does *not* occur and the *entire* neutral curve disappears in the limit so that the critical temperature ratios actually do correspond to complete stabilization of the boundary layer with respect to the particular class of disturbances under consideration.

For low Mach Numbers (up to about $M_1 = 2$), the theoretical results of Section (9), which are then satisfactory approximations, also provide considerable useful information. The numerical calculations indicate that the parameter C increases as T_w/T_1 decreases (see Fig. 5). Thus, the effect of cooling a flat plate at a given Mach Number is evidently to make three-dimensional disturbances relatively more unstable, so that with sufficient cooling some of them can actually become more unstable than two-dimensional disturbances. Since C for an insulated plate increases from $C = 0$ at $M_1 = 0$ to a value close to unity when $M_1 \approx 2$, it appears that the amount of cooling required to make any of the three-dimensional disturbances more unstable than two-dimensional ones is extreme at low subsonic Mach Numbers but gradually becomes less and less extreme as M_1 increases, until, at a Mach Number of the order of two, little is required. In particular, at $M_1 = 0.7$, the wall temperature ratio must be reduced below $T_w/T_1 = 0.58$ (see Fig. 5).

It is known that at subsonic Mach Numbers cooling of the solid surface is effective in stabilizing the boundary layer if only two-dimensional disturbances are considered.[2] The preceding remarks indicate that probably this conclusion is still valid even if three-dimensional disturbances are considered, since the latter usually have a higher minimum critical Reynolds Number than two-dimensional disturbances (except under conditions of extreme cooling).

Even at the moderate supersonic Mach Numbers when three-dimensional disturbances begin to play the leading role, cooling still has an important stabilizing effect, although complete stabilization at supersonic Mach Numbers as predicted in reference 2 is impossible in the strict sense, according to the present theory. For example, estimates show that for an insulated flat plate at $M_1 = 1.6$, R_{x_c} is of the order of 10^5, whereas the calculated results show that for a cooled plate at the same Mach Number $M_1 = 1.6$, with a temperature ratio $T_w/T_1 = 1.073$ which is just small enough for two-dimensional disturbances to be completely stabilized, R_{x_c} is of the order of 10^6.

(11) CONCLUSIONS

(a) An order of magnitude analysis of the complete linearized equations for a three-dimensional disturbance superimposed on a two-dimensional boundary layer shows that they can be reduced to much simpler equations in the first approximation. These simplified equations are still valid at high free-stream Mach Numbers if correct velocity and temperature profiles for the boundary layer in such cases are used. At very high Mach Numbers, however, the accuracy of a first approximation may not be great, so that higher order approximations (and therefore more complicated equations with more terms retained) may have to be considered.

(b) The present equations for a three-dimensional disturbance transform to equations that have the same form mathematically as those for a two-dimensional disturbance but which do not, however, correspond to a real two-dimensional disturbance. Although no direct conclusion regarding the importance of three-dimensional disturbances is now possible, the use of these transformed two-dimensional equations leads to a considerable mathematical simplification of the theory.

(c) Corrected viscous solutions have been obtained which lead to a new formulation of the stability theory. The conclusion reached by Lees and Lin—that the relation for the characteristic values is independent of the temperature fluctuations and the boundary conditions imposed on them—is now found to be restricted in general validity to subsonic and slightly supersonic Mach Numbers and is true only in a restricted sense—namely, for very obliquely traveling waves at high Mach Numbers. At high Mach Numbers the relation for the

characteristic values depends in general on the thermal boundary conditions. It is found, however, that for very small values of the wave number the relation again has the same simple form as at low Mach Numbers. In all cases at high Mach Numbers when the wave number is not small, the relation is more complicated. The detailed mathematical development of this improved theory is to be presented elsewhere.

(d) Consideration of the present analytical and numerical results suggests that probably three-dimensional disturbances are of little importance at subsonic free-stream Mach Numbers, since they usually have a higher minimum critical Reynolds Number than two-dimensional ones, except possibly under conditions of extreme surface cooling. However, further numerical calculations for oblique waves in this range of Mach Numbers would be useful.

(e) As the Mach Number increases, three-dimensional disturbances enter the picture under conditions which become less and less extreme, until finally for free-stream Mach Number M_1 between one and two they begin to play the leading role in many problems of practical interest.

(f) At supersonic free-stream Mach Numbers, the boundary layer can never be completely stabilized with respect to *all* three-dimensional disturbances. Although oblique waves whose directions of propagation are at an angle less than arc cos $1/M_1$ with the free-stream direction can be completely stabilized by sufficient cooling when M_1 is not too large, those whose directions of propagation are at a greater angle cannot.

(g) The graph of critical temperature ratio (below which strictly two-dimensional disturbances are completely stabilized) versus Mach Number (Fig. 6) is not significantly different from that found by Van Driest,[11] in spite of the corrections to the viscous solutions. Although these corrections are very important for the accurate determination of the curve of neutral stability at supersonic Mach Numbers, they are not as important for the determination of the critical temperature ratios.

(h) For Mach Numbers up to about two, cooling of the solid surface is effective in stabilizing the boundary layer. For higher Mach Numbers, reliable calculations of the minimum critical Reynolds Number over wide ranges of the wall temperature ratio have not yet been made; but this general conclusion would probably remain unchanged for Mach Numbers up to six, say.

(i) Little more can be said about the problem of boundary-layer stability at Mach Numbers greater than two, since the present methods of numerical calculation for the curve of neutral stability (and thus the minimum critical Reynolds Number) do not appear to be adequate in such cases. When c and $\tilde{\alpha}$ are both large, there are difficulties in working with the more complicated relation for the characteristic values and also in evaluating the inviscid solutions of the disturbance equations. These problems are being studied further.

(j) At very high Mach Numbers there is an even more serious difficulty than the preceding—namely, that the present asymptotic theory, which is essentially a first-order theory, may in itself be inaccurate [as pointed out in paragraph (a) above]. More information about this matter will be provided by numerical results (including estimates of certain parameters) for high Mach Numbers, which can be obtained as soon as the difficulties mentioned above in paragraph (i) are resolved.

(k) It is believed that the approximate method of calculation of the neutral curve described in Section (8) is adequate up to a Mach Number of the order of two, especially in cases involving cooling, when c and $\tilde{\alpha}$ are both small. Additional neutral curves for the oblique waves in this range of Mach Numbers or perhaps further calculations of the type described in Sections (9) and (10) would be of considerable value. It might also be of interest to determine in a few typical cases the effect of using a more accurate approximation than Eq. (8.16a) by keeping terms of higher order in $\tilde{\alpha}$, as Lees has done.[2]

(l) For practical purposes, the transition Reynolds Number is much more important than the minimum critical Reynolds Number. Thus, information concerning the rate of amplification of the boundary-layer disturbances after they enter the unstable region would be extremely useful. Further investigations are being directed toward developing the amplification theory for three-dimensional disturbances, which may be somewhat different from that for strictly two-dimensional disturbances.

(m) Applications of any of the present theory to cases involving finite wall curvature should be made with caution. Although there are no restrictions regarding pressure gradient, the basic equations derived here are strictly correct only for flow over a flat surface. Although curvature effects are usually extremely small for moderate values of the direction angle of the disturbances (see references 6 and 15), they may become important for values of this angle approaching 90°. For example, whereas the present theory predicts an infinite minimum critical Reynolds Number for disturbances with direction angle of 90°, it might be expected from the work of Görtler[16] that for small but finite concave curvature such disturbances would be unstable at finite Reynolds Numbers.

Appendix

Derivation of the Relation for the Characteristic Values

The basic relation (7.9) is obtained as the practical form of the secular equation on which all subsequent deductions and calculations are based. A complete derivation involves a detailed study of the asymptotic solutions of the system of Eqs. (6.9) to (6.13) and will be presented elsewhere. Here we shall merely outline the major steps and point out the nature of the approximations involved.

For large values of $\tilde{\alpha}\tilde{R}$ and finite values of $(y - y_c)$, formal expansions give rise to solutions of the following three types:

(a) Two solutions for which each of the functions has an asymptotic form

$$Z_i(y) = Z_i^{(0)}(y) + [1/(\tilde{\alpha}\tilde{R})]Z_i^{(1)}(y) + \ldots \quad \text{(A1)}$$

(b) Two solutions for which each of the functions has an asymptotic form

$$\left.\begin{aligned} Z_i(y) &= \{\exp [\pm(\tilde{\alpha}\tilde{R})^{1/2}P]\}\ [\bar{Z}_i^{(0)} + (\tilde{\alpha}\tilde{R})^{-1/2}\bar{Z}_i^{(1)} + \ldots] \\ P(y) &= \int_{y_c}^{y} [(w - c)/\nu]^{1/2}\, dy \end{aligned}\right\} \quad \text{(A2)}$$

(c) Two solutions for which each of the functions has an asymptotic form

$$\left.\begin{aligned} Z_i(y) &= \{\exp [\pm(\tilde{\alpha}\tilde{R})^{1/2}Q]\}\ [\hat{Z}_i^{(0)} + (\tilde{\alpha}\tilde{R})^{-1/2}\hat{Z}_i^{(1)} + \ldots] \\ Q(y) &= \int_{y_c}^{y} [\sigma(w - c)/\nu]^{1/2}\, dy \end{aligned}\right\} \quad \text{(A3)}$$

In the above, y_c is the point where $w = c$. The approximate solution $Z_i^{(0)}(y)$ is the inviscid approximation and has the exponential behavior $\exp [\pm\beta y]$ for large y, as discussed in Section (7).

Consider the case of real c. It is clear that, if the solution is to remain bounded at infinity, only the negative signs are allowed in *all* the exponentials. Thus, we have *one* permissible solution from each of the three types, (a), (b), and (c). Let us denote these solutions by

(a) $(\tilde{f}, \tilde{\phi}, \tilde{\theta}) = (F, \Phi, \Theta)$
(b) $(\tilde{f}, \tilde{\phi}, \tilde{\theta}) = (f_3, \phi_3, \theta_3)$
(c) $(\tilde{f}, \tilde{\phi}, \tilde{\theta}) = (f_5, \phi_5, \theta_5)$

To satisfy the conditions at the wall, i.e.,

$$\tilde{f} = \tilde{\phi} = 0, \quad a\tilde{\theta}' + b\tilde{\theta} = 0 \quad \text{(A4)}$$

where a and b are given constants, we must have

$$a\begin{vmatrix} F(0) & f_3(0) & f_5(0) \\ \Phi(0) & \phi_3(0) & \phi_5(0) \\ \Theta'(0) & \theta_3'(0) & \theta_5'(0) \end{vmatrix} + b\begin{vmatrix} F(0) & f_3(0) & f_5(0) \\ \Phi(0) & \phi_3(0) & \phi_5(0) \\ \Theta(0) & \theta_3(0) & \theta_5(0) \end{vmatrix} = 0 \quad \text{(A5)}$$

Actual calculations reveal that the general orders of magnitudes of the functions are given by [see Eq. (A9)]

$$\left.\begin{aligned} (F, \Phi, \Theta) &\sim (1, 1, 1) \\ (f_3, \phi_3, \theta_3) &\sim (1, \epsilon, 0) \\ (f_5, \phi_5, \theta_5) &\sim (0, \epsilon, 1) \end{aligned}\right\} \quad \text{(A6)}$$

to the order of $\epsilon = (\tilde{\alpha}\tilde{R})^{-1/2}$. Hence, we obtain

$$\Phi(0)/F(0) = [\phi_3(0)/f_3(0)]\,(1 + \Delta) \quad \text{(A7)}$$

where

$$\Delta = \frac{a\Theta'(0) + b\Theta(0)}{F(0)}\,\frac{\theta_5(0)}{a\theta_5'(0) + b\theta_5(0)}\,\frac{\phi_5(0)}{\theta_5(0)}\,\frac{f_3(0)}{\phi_3(0)} \quad \text{(A8)}$$

We shall consider Δ in more detail later and just observe at this point that it is always 0(1) at most.

From Eq. (A6), it follows that $\phi_3(0)/f_3(0) = 0(\epsilon)$, which shows that in the limit $\epsilon \to 0$ Eq. (A7) reduces to the inviscid formulation $\Phi(0) = 0$, as it should.

On the basis of the general nature of the solutions (A1), (A2), and (A3) and because of the orders of magnitude of the solutions as shown in Eq. (A6), we may refer to these solutions as (a) the inviscid solution, (b) the viscous solution of velocity variation, and (c) the viscous solution of thermal variation.

For practical purposes it is found to be desirable to use asymptotic forms of the viscous solutions which remain accurate even for $(y - y_c) \to 0$. For example, for the viscous solution of velocity variation, detailed studies give

$$\left.\begin{aligned} f_3 &= A(y)\int_{\infty}^{\zeta} \zeta^{1/2} H_{1/3}^{(1)}\left[\frac{2}{3}(i\zeta)^{3/2}\right] d\zeta \\ \phi_3 &= (\tilde{\alpha}\tilde{R})^{1/3} B(y)\int_{\infty}^{\zeta} d\zeta \int_{\infty}^{\zeta} \zeta^{1/2} H_{1/3}^{(1)}\left[\frac{2}{3}(i\zeta)^{3/2}\right] d\zeta \end{aligned}\right\} \quad \text{(A9)}$$

where

$$B(y) = -i\left(\frac{w - c}{\nu}\right)^{-1/2}\left[\frac{3}{2}\int_{y_c}^{y}\left(\frac{w - c}{\nu}\right)^{1/2} dy\right] A(y) \quad \text{(A10)}$$

and

$$\zeta = (\tilde{\alpha}\tilde{R})^{1/3}\left[\frac{3}{2}\int_{y_c}^{y}\left(\frac{w - c}{\nu}\right)^{1/2} dy\right]^{2/3} = (\tilde{\alpha}\tilde{R})^{1/3}\left(\frac{3P}{2}\right)^{2/3} \quad \text{(A11)}$$

This solution agrees asymptotically with Eq. (A2) when ζ is large but is also valid for small ζ. Furthermore, if each of the integrals (A10) and (A11) is evaluated in the neighbourhood of y_c by retaining only the first term in the power series expansion of the integrand, the solution given in reference 1 is obtained. An improved version of the viscous solution of thermal variation may also be developed.*

By substituting Eq. (A9) into Eq. (A7), the relation (7.9) can be easily obtained. The only additional step is to express $\Phi(y)$ as a linear combination of two linearly independent inviscid solutions $\phi_1(y)$ and $\phi_2(y)$—i.e., two such solutions of Eq. (7.3)—and then to require that this linear combination shall be proportional to $\exp [-\beta y]$ for $y \geq 1$, where $y = 1$ corresponds to the edge of the boundary layer.

Now let us return to Eq. (A8) for Δ and investigate the conditions under which it may be neglected and those under which it must be retained. It may be shown that, for T_w bounded away from zero,† Eq. (A8) becomes

$$\Delta = [(\gamma - 1)\bar{M}_1^2 c/T_w]\,\{\{a[(T_w'c - T_w w_w')/T_w]\} + bc\}\,\{[\theta_5(0)]/[a\theta_5'(0) + b\theta_5(0)]\}\,\chi(z, \sigma) \quad \text{(A12)}$$

where $\chi(z, \sigma)$ is a function depending on the viscous solutions which is always 0(1) (z is defined by Eq.

* The improved solutions are obtained by extending a method of Tollmien in the incompressible case.[8] Their use does not alter any of the order-of-magnitude estimates in the present discussion.

† The exceptional case $T_w \to 0$ is to be considered later.

(7.11) and σ is the Prandtl Number). It might be mentioned that the factor c in the first term is due to $\phi_5(0)$ being proportional to c.

In reference 1 the conclusion was reached that the characteristic-value problem is independent of the temperature fluctuations and the boundary conditions imposed on them, to the order of accuracy of the theory. From Eqs. (A7) and (A12) it is clear that this will be true when Δ can be neglected without any restrictions being placed on the values of a and b. Since the factors multiplying $(\gamma - 1)\bar{M}_1^2 c/T_w$ in Eq. (A12) are all $0(1)$ at most, it follows that the conclusion is valid in two main cases:

$$c \ll 1 \tag{A13}$$

which was considered in Reference 1, and

$$\bar{M}_1^2 \ll 1 \tag{A14}$$

which corresponds to oblique waves with direction angles close to 90°.

Case (A13) covers most practical situations at subsonic and slightly supersonic Mach Numbers, when c is usually not large. Case (A14) extends the conclusion to very obliquely traveling disturbances at high Mach Numbers.

It might be remarked that since $\phi_5(0)$ is proportional to c and since the theory of reference 1 was restricted to values of c of order ϵ, it is understandable that the preceding conclusion should be a natural consequence of the asymptotic theory [in which quantities $0(\epsilon)$ are neglected], as developed in reference 1.

In all situations at high Mach Numbers when Eq. (A14) does not hold, the exact form of Eq. (A7) depends on a knowledge of the thermal boundary conditions—i.e., a knowledge of the constants a and b. If it is observed that $\theta_5'(0)/\theta_5(0) = 0(1/\epsilon)$, an examination of Eq. (A12) shows that three cases may be distinguished:

$$b/a = 0(1), \quad \Delta = 0(\epsilon) \tag{A15}$$

$a/b = 0(\epsilon)$

$$\Delta = [(\gamma - 1)\bar{M}_1^2 c^2/T_w]\,\{[\theta_5(0)]/[(a/b)\theta_5'(0) + \theta_5(0)]\}\,\chi(z, \sigma) \tag{A16}$$

$a/b = 0(\epsilon^2)$

$$\Delta = [(\gamma - 1)\bar{M}_1^2 c^2/T_w]\,\chi(z, \sigma) \tag{A17}$$

In case (A15), Δ may again be neglected, so that Eq. (A7) again reduces to the same simple form as at low Mach Numbers. In the other two cases, Δ cannot be neglected, and in Eq. (A16), moreover, a new parameter a/b enters into the theory.

It may be noted that when Δ is not $0(\epsilon)$, it is always of the form

$$\Delta = [(\gamma - 1)\bar{M}_1^2 c^2/T_w]\,\Delta_1 \tag{A18}$$

where $\Delta_1 = 0(1)$. Thus, the error in neglecting Δ on the basis of small c is somewhat smaller than might have been expected from the discussion regarding condition (A13).

To determine the proper form of the thermal boundary condition (A4) and thus the values of the constants a and b in practical situations, an analysis of the heat conduction problem in the medium below the interface between the gas and solid wall is necessary. Since this is straightforward but fairly lengthy, we shall just give the final conclusions here for a few typical cases.

Consider a boundary-layer flow of a gas extending from the solid surface at $y = 0$ to $y = \infty$, and suppose that from $y = 0$ to $y = -h_1$ is a thin metal wall, from $y = -h_1$ to $y = -h$ a channel through which a cooling liquid is flowing, and finally from $y = -h$ to $y = -\infty$ an insulating material. Although the problem is considerably idealized, it illustrates some of the essential features in certain cases of interest. For this problem, it can be shown that the condition for the temperature fluctuations in the boundary layer is given by

$$\theta'(0) - \{\omega - [(1/k)\,(dk/dT)\,(\partial T/\partial y)]_w\}\theta(0) = 0 \tag{A19}$$

where

$$\omega = \omega_m \frac{k_m}{k_0}\left\{\left[\left(1 + S\frac{k_l\omega_i}{k_m\omega_m}\right) - \left(1 - S\frac{k_l\omega_i}{k_m\omega_m}\right)e^{-2\omega_m h}\right]\Big/\left[\left(1 + S\frac{k_l\omega_i}{k_m\omega_m}\right) + \left(1 - S\frac{k_l\omega_i}{k_m\omega_m}\right)e^{-2\omega_m h}\right]\right\} \tag{A20}$$

in which the various quantities appearing are defined as follows:

$$\frac{1}{S} = \frac{k_l\omega_i}{k_l\omega_l}\left\{\left[\left(1 + \frac{k_l\omega_i}{k_l\omega_l}\right)e^{-2\omega_l(h_1 - h)} + \left(1 - \frac{k_l\omega_i}{k_l\omega_l}\right)\right]\Big/\left[\left(1 + \frac{k_l\omega_i}{k_l\omega_l}\right)e^{-2\omega_l(h_1 - h)} - \left(1 - \frac{k_l\omega_i}{k_l\omega_l}\right)\right]\right\} \tag{A21}$$

$$\omega_m^2 = -i\alpha c\,(\rho_m c_m/k_m) \tag{A22}$$

with corresponding definitions for ω_l and ω_i. The symbols ρ_m, c_m, and k_m denote density, specific heat, and thermal conductivity, respectively. The subscripts 0, m, l, and i refer to gas at $y = 0$, metal, liquid, and insulator, respectively. The quantity αc is the nondimensional time frequency of the fluctuations [see Eq. (6.1)].

Relation (A20) is appropriate for a *cooled wall*. It reduces to

$$\omega = \omega_m(k_m/k_0) \tag{A23}$$

for high frequencies, and to

$$\omega = \omega_i(k_i/k_0) \tag{A24}$$

for low frequencies. The case of low frequencies is of most interest here. In Section (10) it is shown that if the simple eigenvalue relation (7.14) obtained by neglecting Δ is used, then in the limiting case of complete stabilization $\tilde{\alpha} \to 0$ everywhere on the neutral curve. Since the frequency is given by $\alpha c = \tilde{\alpha} c \cos\Theta$,

where Θ is the direction angle of the waves, it follows that $\omega \to 0$ in the limit and thus from Eq. (A15) that Δ is indeed negligible. Thus, we see that the use of the simple relation (7.14) in calculating the critical temperature ratios is justified.

The definition of ω for an *insulated wall* is easily obtained from Eq. (A20) by letting $h_1 = h$. For high frequencies this also reduces to Eq. (A23). If there is no metal layer so that the insulator extends right to the surface, $h = 0$, and ω is given by

$$\omega = \omega_i(k_i/k_0) \tag{A25}$$

for all frequencies.

In all cases at high Mach Numbers when a neutral curve exists, $\tilde{\alpha} = 0(1)$, $c = 0(1)$, are reasonable estimates. Then, on taking $\cos\Theta = 0(1)$, we find that Eqs. (A23) and (A25) are accurate approximations and that ω is *extremely large*. This is true of Eq. (A23) even when $\tilde{\alpha} = 0(10^{-2})$, say. Thus, in most cases of interest at high Mach Numbers when cooling is not sufficient to give complete stabilization, ω is extremely large, and the relation for the characteristic values is that corresponding to Eq. (A17).

The exceptional case $T_w \to 0$ has not been considered so far. This occurs in the calculations of the critical temperature ratios for $\tilde{M}_1 \to 1$ and for $M_1 \to 7.48$ (see Figs. 6 and 7). We may justify the procedure of using the simple relation (7.14) for these calculations *a posteriori*—that is, we assume Eq. (7.14) to hold in these limiting cases and then check the consequences to see if they are consistent with the assumption. In the case $\tilde{M}_1 \to 1$, $c = 1 - 1/\tilde{M}_1 \to 0$, and an examination of Eqs. (10.2) and (8.16b) shows that $T_w \propto c$. Then Eq. (A12) shows that Δ is now $0(c)$, so that the procedure is justified. In the case $M_1 \to 7.48$, c remains finite, and relations (10.1) and (8.16b) imply that $K_{1_c} = 0$—i.e., that $[d/dy(w'/T)]_c = 0$. This indicates that the solution obtained by the use of Eqs. (7.14) or (8.1) reduces to that obtained from an inviscid formulation. On the other hand, the more accurate relation (7.9), when put into the form (8.1), has $\Phi(z)$ replaced by $[1 - F(z)\,(1 + \Delta)]^{-1}$. At the same time, Eq. (A12) shows that $\Delta = 0(1/T_w)$. It can be shown that for Δ with such a behavior the more accurate relation also leads to the inviscid solution in the limit $T_w \to 0$. Thus, the results obtained by the use of Eq. (7.14) are again justified.

Summarizing our main conclusions, we have found that for very low frequencies the boundary condition for the temperature fluctuations is

$$\theta'(0) + [(1/k)\,(dk/dT)\,(\partial T/\partial y)]_w\,\theta(0) = 0 \tag{A26}$$

and the corresponding secular equation is

$$E(\tilde{\alpha}, c, \tilde{M}_1^2) = F(z) \tag{A27}$$

while for very high frequencies, the boundary condition is

$$\theta(0) = 0 \tag{A28}$$

and the corresponding secular equation is

$$E(\tilde{\alpha}, c, \tilde{M}_1^2) = F(z)\{1 + [(\gamma - 1)\tilde{M}_1^2 c^2/T_w] \times \chi(z, \sigma)\} \tag{A29}$$

The boundary conditions (A26) and (A28) are actually just what would be expected physically, as the following considerations will show. In the stability theory, the temperature fluctuations are essentially natural oscillations originating in the boundary layer. Although these fluctuations can penetrate into the adjacent medium (gas, liquid, solid, etc.), they must go to zero at large enough distances. For very low frequencies, it is clear that such fluctuations will go far into the surrounding medium before dying out. Thus, for low enough frequencies, the change in amplitude will be negligible over distances in the solid of the order of the boundary-layer thickness, so that the fluctuating part of the heat flux will be negligible. Therefore, since the left-hand side of Eq. (A26) is proportional to the latter quantity expressed in terms of boundary-layer properties at the wall, relation (A26) will hold closely.

On the other hand, for very high frequencies the thermal inertia of the medium will prevent the fluctuations at any given location from reaching the maximum amplitude attained near the origin of the disturbance. Thus, the amplitude will die away to zero within a short distance inside the solid wall, for example.* Ultimately, for high enough frequencies, even the amplitude at the surface will become negligible, so that the condition $\theta(0) = 0$ will be a very accurate approximation.

References

[1] Lees, L., and Lin, C. C., *Investigation of the Stability of the Laminar Boundary Layer in a Compressible Fluid*, NACA TN 1115, 1946.

[2] Lees, L., *The Stability of the Laminar Boundary Layer in a Compressible Fluid*, NACA Report No. 876, 1947 (formerly TN 1360).

[3] Squire, H. B., *On the Stability for Three-Dimensional Disturbances of Viscous Fluid Flow Between Parallel Walls*, Proc. Roy. Soc. (London), Vol. A142, pp. 621–628, 1933.

[4] Lees, L., and Probstein, R. F., *Hypersonic Viscous Flow over a Flat Plate*, Princeton University, Aeronautical Engineering Laboratory, Report No. 195, April, 1952.

[5] Shen, S. F., *On the Boundary-Layer Equations in Hypersonic Flow*, Journal of the Aeronautical Sciences, Vol. 19, No. 7, pp. 500–501, July, 1952.

[6] Dunn, D. W., Thesis for Ph.D., Massachusetts Institute of Technology, June, 1953.

[7] Lin, C. C., *On the Stability of the Boundary Layer with Respect to Disturbances of Large Wave Velocity*, Journal of the Aeronautical Sciences, Vol. 19, No. 2, pp. 138–139, February, 1952.

[8] Tollmien, W., *Asymptotische Integration der Störungsdifferentialgleichung ebener laminarer Strömungen bei hohen Reynoldschen Zahlen*, Zeitschrift für Ang. Math. und Mech., Vols. 25–27, pp. 33–50, 70–83, 1947.

[9] Kuethe, A. M., *Some Aspects of Boundary-Layer Transition and Flow Separation on Cylinders in Yaw*, Proceedings of the Mid-western Conference on Fluid Dynamics, 1st conference, May, 1950, pp. 44–55; J. W. Edwards, Ann Arbor, Mich., 1951.

* This "surface-layer effect" or "skin effect" is well known in other problems involving temperature fluctuations.

[10] Lin, C. C., *On the Stability of Two-Dimensional Parallel Flows*, Parts I, II, III; Quart. Appl. Math., Nos. 2, 3, 4; pp. 117–142, pp. 218–234, pp. 277–301, 1945–1946.

[11] Van Driest, E. R., *Calculation of the Stability of the Laminar Boundary Layer in a Compressible Fluid on a Flat Plate with Heat Transfer*, Journal of the Aeronautical Sciences, Vol. 19, No. 12, pp. 801–812, December, 1952.

[12] Cheng, Sin-I, *On the Stability of Laminar Boundary Layer Flow*, Quart. Appl. Math., Vol. 11, No. 3, pp. 346–350, October, 1953.

[13] Dunn, D. W., and Lin, C. C., *On the Stability of the Laminar Boundary Layer in a Compressible Fluid*, (Preliminary Report), Department of Mathematics, Massachusetts Institute of Technology, December, 1953.

[14] Bloom, M., *On the Calculation of Laminar Boundary-Layer Stability*, Journal of the Aeronautical Sciences, Vol. 21, No. 3, pp. 207–210, March, 1954.

[15] Görtler, H., *Über den Einflusz der Wandkrümmung auf die Entstehung der Turbulenz*, Zeit für Ang. Math. und Mech., Vol. 20, pp. 138–147, 1940.

[16] Görtler, H., *Über eine Dreidimensionale Instabilität Laminarer Grenzschichten an Konkaven Wänden*, Nachr. Ges. Wiss., Göttingen, Vol. 2, pp. 1–26, 1940 (Translated as NACA TM 1375, 1954).

List of Symbols

Dimensional quantities	Nondimensional quantities	Reference quantities
Positional co-ordinates		
(1) x_1	x	δ
(2) x_2	y	δ
(3) x_3	z	δ
Time		
(4) t^*	t	δ/U_1
Velocity components		
(5) $u_1 = \bar{u}_1 + u_1'$	$w(y) + f(y) \exp [i(\alpha x + \beta z - \alpha c t)]$	U_1
(6) $u_2 = \bar{u}_2 + u_2'$	$v(y) + \alpha\phi(y) \exp [i(\alpha x + \beta z - \alpha c t)]$	U_1
(7) $u_3 = u_3'$	$h(y) \exp [i(\alpha x + \beta z - \alpha c t)]$	U_1
Density		
(8) $\rho^* = \bar{\rho}^* + \rho'^*$	$\rho(y) + r(y) \exp [i(\alpha x + \beta z - \alpha c t)]$	$\bar{\rho}_1^*$
Pressure		
(9) $p^* = \bar{p}^* + p'^*$	$p(y) + \pi(y) \exp [i(\alpha x + \beta z - \alpha c t)]$	$\bar{p}_1^*$
Temperature		
(10) $T^* = \bar{T}^* + T'^*$	$T(y) + \theta(y) \exp [i(\alpha x + \beta z - \alpha c t)]$	$\bar{T}_1^*$
Viscosity coefficients		
(11) $\mu^* = \bar{\mu}^* + \mu'^*$	$\mu(y) + \overline{(d\mu/dT)}\,\theta(y) \exp [i(\alpha x + \beta z - \alpha c t)]$	$\bar{\mu}_1^*$
(12) $\lambda^* = \bar{\lambda}^* + \lambda'^*$	$\lambda(y) + \overline{(d\lambda/dT)}\,\theta(y) \exp [i(\alpha x + \beta z - \alpha c t)]$	$\bar{\mu}_1^*$
Thermal conductivity		
(13) $k^* = \bar{k}^* + k'^*$	$[\mu(y)/\sigma(y)] + \overline{(d/dT)\,(\mu/\sigma)}\theta(y) \exp [i(\alpha x + \beta z - \alpha c t)]$	$C_p\bar{\mu}_1^*$
Wave numbers of the disturbance		
(14) α_1	$\begin{cases} \alpha \\ \alpha\theta \\ \alpha_r \end{cases}$	δ^{-1} θ^{*-1} x_1^{-1}
(15) α_2	β	δ^{-1}
Wave velocity of the disturbance		
(16) c^*	c	U_1
Specific heat at constant volume		
(17) C_v	1	C_v
Specific heat at constant pressure		
(18) C_p	γ	C_v
Gas constant per gram		
(19) R^*	$\gamma - 1$	C_v
Acceleration due to gravity		
(20) g	$1/F^2$	U_1^2/δ
Momentum thickness of boundary layer		
(21) $\theta^* = \int_0^\infty \rho w(1 - w)\, dx_2$		
Reynolds Number		
(22) Based on boundary layer thickness δ	$R = \bar{\rho}_1^* U_1 \delta/\bar{\mu}_1^*$	
(23) Based on momentum thickness θ^*	$R_\theta = \bar{\rho}_1^* U_1 \theta^*/\bar{\mu}_1^*$	
(24) Based on distance x_1 from leading edge	$R_x = \bar{\rho}_1^* U_1 x_1/\bar{\mu}_1^*$	
Mach Number		
(25)	$M_1 = U_1/\sqrt{\gamma_1 R^* \bar{T}_1^*}$	
Froude Number		
(26)	$F = U_1/\sqrt{g\delta}$	
Prandtl Number		
(27)	$\sigma = C_p\mu^*/k^*$	

(a) A bar (———) denotes mean value, a prime denotes fluctuation. The subscript 1 refers to the value at the edge of the boundary layer at the particular x-location considered, and the subscript w refers to wall value. The subscripts r and i denote the real and imaginary parts of a quantity, respectively.

(b) The nondimensional mean quantities $u_1(x_1, x_2)/U_1$, $u_2(x_1, x_2)/U_1$, $\bar{\rho}(x, y)$, $\bar{p}(x, y)$, . . . are represented as functions of y alone—that is, as $w(y)$, $v(y)$, $\rho(y)$, $p(y)$, . . . , respectively. This corresponds to an approximation depending on the boundary-layer nature of the mean flow [see Section (4)].

(c) The quantities C_p, C_v, μ, λ, k, σ, γ are all considered to be functions of T only. The fluctuation Q' of any such quantity Q is given by $Q' = \overline{dQ/dT}\, T'$.

(d) For moderate Mach Numbers and rates of heat transfer C_p, C_v, γ, σ vary only slightly in the boundary layer. They are therefore regarded as constants equal to their free-stream values in the numerical calculations.

(e) The reference length δ is the boundary-layer thickness at the particular value of x considered. Its definition is somewhat arbitrary and may be taken in any convenient manner. In the present numerical computations it is taken to be the value of x_2 at which $u_1/U_1 = 0.999$.

The Unsteady Forces Due to Viscous Wakes in Turbomachines

NELSON H. KEMP* AND W. R. SEARS†
Cornell University

ABSTRACT

The configuration of viscous wakes of cascade blades is approximated from single airfoil experiments. The unsteady force and moment on a downstream blade passing through such wakes is then calculated on the basis of the theory of isolated thin airfoils in nonuniform motion. The results indicate that the force is nearly proportional to the profile-drag coefficient of the upstream blades. For typical values of this coefficient and conventional cascade geometry the unsteady forces arising from passage through viscous wakes are of about the same size as those due to aerodynamic interference between the moving blade rows, previously estimated.

SYMBOLS

b	= axial distance between centerlines of stator and rotor rows (Fig. 2)
b'	= axial distance between trailing edge of stator row and leading edge of rotor row $b' = b - c_s \cos \alpha_s - c_r \cos (\beta - \alpha_s)$
c	= airfoil half-chord
d	= pitch of blades in direction of rotation of turbomachine
q	= dynamic pressure, $(1/2)\rho V^2$
t	= time
u	= perturbation velocity component in the stream direction
v	= nonsteady upwash induced at airfoil
x	= coordinate along airfoil, measured from mid-chord, positive toward trailing edge
y	= coordinate perpendicular to x, positive upward
x', y'	= oblique coordinate system (Fig. 2)
C_D	= profile drag coefficient
C_L	= lift coefficient, $L/(1/2)\rho V^2 2c$
C_M	= moment coefficient, $M/(1/2)\rho V^2(2c)^2$
G	= coefficient of nonsteady upwash induced at rotor blade, Eqs. (28) and (29)
K	= dimensionless half-width of viscous wake Eq. (21)
K_n	= modified Bessel function of the second kind
L	= lift, positive upward
M	= moment about airfoil center, positive in the stalling direction
$\Re$	= real part
$S(\omega)$	= $\{i\omega[K_0(i\omega) + K_1(i\omega)]\}^{-1}$
U	= rotational speed of rotor, positive downward
V	= speed of stream relative to airfoil
Y	= half-width of viscous wake
α	= angle of stagger of blades (Fig. 2)
β	= angle between stator and rotor blades
ν	= circular frequency, radians per sec.
ρ	= gas density
σ	= solidity of cascade, $2c/d$
ω	= reduced frequency, $\nu c/V$

Subscripts

s	= stator
r	= rotor
T	= total effect due to all viscous wakes
c	= center of viscous wake
∞	= free stream
0	= taken constant along rotor blade

Superscripts

rv	= effects on rotor blade due to viscous stator wakes
s	= stator

Received September 25, 1954.

* National Science Foundation Fellow. Now at Research Department, United Aircraft Corporation, East Hartford, Conn.
† Director, Graduate School of Aeronautical Engineering.

INTRODUCTION

IN AN EARLIER INVESTIGATION[1] an approximate calculation was made of the forces and moments that act on the blades of a turbomachine due to their passage through the disturbed fields of flow of adjacent blade rows. The extreme complexity of the problem made it necessary to introduce several important approximations. First, the calculation was restricted to the case of an elementary stage consisting of a stator and rotor. Second, the familiar approximations of unsteady thin-airfoil theory were adopted. Finally, the theory adopted was a first-order one based on the assumption, later confirmed, that the fluctuation of blade circulation is always small compared to the mean value.

Within these approximations, calculations were carried out to determine the fluctuations of the lift, moment, and circulation due to passage through the potential-flow field of the adjacent row of blades. For the downstream ("rotor") row, this included the effects of passage through the sheet-vortex wakes of the upstream ("stator") blades, although this is, to be sure, a "second-order" effect in the spirit of the approximations mentioned above. The fluctuations of lift, in particular, were worked out for typical stage geometries and were found to be appreciable.

In the work just described, no account was taken of the effects of viscous wakes. This is, of course, an obvious shortcoming of the investigation, since such wakes are always present in a real fluid, and one may even imagine that the viscous-wake effects are larger than the purely potential-flow effects that were considered. The authors' purpose, however, was to consider these phenomena separately. The present paper reports on a study of the viscous-wake effects. Their evaluation involves additional approximations, as will be explained, although the mathematical details are actually somewhat simpler than in the earlier task.

In outline, the present work involves the following steps.

(1) The flow downstream of a cascade of blades with viscous wakes will be represented by an inviscid shear flow. The velocity profile of the wake behind each blade is made to resemble the results of measurements behind isolated airfoils.

(2) The theory of thin airfoils in unsteady flow is applied to calculate the force and moment resulting from passage through such a series of wakes—i.e., gusts. As is often the case, the presence of vorticity in the oncoming stream is neglected in making this application

In view of the small-perturbation type of approximation that is inherent in thin-airfoil theory, it is consistent to add together the fluctuating forces, moments, and circulations calculated here and in the earlier paper.[1] Naturally, to be precise one would add these various terms in proper phase—e.g., superimpose them as complex numbers before taking real parts. As an upper limit, however, one might simply add their absolute values. The absolute values are easier to compute and are the numerical values presented in the graphs and tables of this report and the earlier one.

Description of the Viscous Wakes

The model adopted here for the viscous wakes of cascade blades is based upon the experimental results of Silverstein, Katzoff, and Bullivant,[2] who measured the wakes of airfoils and generalized their results. It will be assumed that the wake behind each blade is the same as the wake behind an isolated airfoil. Since the wakes are relatively narrow, compared to the blade spacing, in the region of the adjacent downstream row, this assumption seems justified.

As a further simplification, the wake will be considered to consist only of an inviscid, symmetrical, shear perturbation of the undisturbed stream. It will be recalled that all other perturbations due to the upstream airfoils have been included in the previous study;[1] thus, in a small-perturbation theory, only the introduction of the wake disturbance into the free stream is required here.

Silverstein, Katzoff, and Bullivant have shown that the half-width of the wake, Y, may be calculated from the following formula

$$Y = 0.68\sqrt{2}C_D^{1/2}c(x/c - 0.7)^{1/2} \qquad (1)$$

where c is the airfoil half-chord, x is measured along the wake axis (free-stream direction) rearward from the center of the airfoil (see Fig. 1), and C_D is the airfoil profile-drag coefficient. If q_c is the dynamic pressure at the center of the wake and q_∞ that in the free stream, reference 2 also shows that

$$1 - (q_c/q_\infty) = (4.84C_D^{1/2})/(x/c - 0.4) \qquad (2)$$

Finally, the wake velocity profile is also given in the same reference in terms of the dynamic pressure q as

$$\frac{1 - q/q_\infty}{1 - q_c/q_\infty} = \cos^2\left(\frac{\pi}{2}\frac{y}{Y}\right) \qquad (|y| \leqq Y) \qquad (3)$$

where y is the coordinate perpendicular to the stream

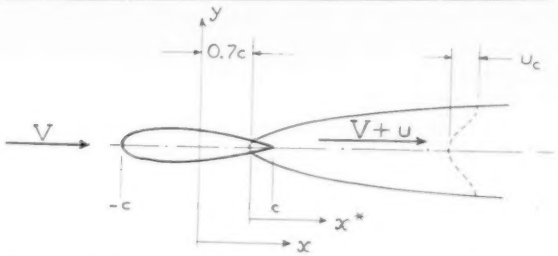

Fig. 1. Viscous wake of an airfoil according to reference 2.

(see Fig. 1). Eqs. (1), (2), and (3) completely define the wake.

In order to convert the wake equations from dynamic pressure to velocity, the small perturbation assumption is used. Let u denote the perturbation velocity in the x-direction, which is the only velocity perturbation considered, as has been mentioned above. Since the free-stream velocity is also in the x-direction, one has, assuming $u \ll V$,

$$1 - (q/q_\infty) = 1 - [(V + u)^2/V^2] \approx -2(u/V) \qquad (4)$$

In view of Eq. (4), Eqs. (2) and (3) become relations for the perturbation velocity at the center of the wake, u_c, and the wake velocity profile:

$$u_c/V = -(2.42C_D^{1/2})/(x/c - 0.4) \qquad (5)\dagger$$

$$u/u_c = \cos^2[(\pi/2)(y/Y)] \qquad (|y| \leqq Y) \qquad (6)$$

In order to simplify the mathematical analysis, the cosine wake profile of Eq. (6) will be replaced by a profile in the form of a Gaussian error curve that has the same momentum flow. The momentum flow in the wake is proportional to the square of the velocity, $(V + u)^2 \approx V^2 + 2u$. The momentum flow across any section therefore depends on $\int u\,dy$ taken across the wake, and it is this integral that will be made the same for the cosine profile and the assumed Gaussian profile. For the former the integral is

$$\int_{-Y}^{Y} \cos^2\left(\frac{\pi}{2}\frac{y}{Y}\right) dy = Y \qquad (7)$$

The Gaussian profile may be written $u/u_c = \exp[-(ky/Y)^2]$, where the constant k is to be determined by the momentum flow condition. The integral is

$$\int_{-Y}^{Y} \exp[-(ky/Y)^2]\,dy = \frac{Y}{k}\int_{-k}^{k} e^{-\eta^2}\,d\eta = \frac{\sqrt{\pi}\,Y}{k}\left(\frac{2}{\sqrt{\pi}}\int_0^k e^{-\eta^2}\,d\eta\right) \qquad (8)$$

The expression in parentheses is the well-known error function denoted by erf (k), and comparison of Eqs. (7)

† The reader will easily verify that the velocity perturbation u_c according to this formula may be so large (say 40 per cent of V) just behind the airfoil as to cast doubt on the validity of the small perturbation approximation. However, the perturbation attenuates downstream and rapidly in the cross-stream direction [Eq. (6)], and it is therefore hoped that the approximation is reasonably well justified. The small disturbance theory appears to be the only theory available for this type of investigation.

and (8) shows that for the momentum flows to be equal, k must satisfy

$$k/\sqrt{\pi} = \text{erf}(k) \tag{9}$$

Now, erf $(\sqrt{\pi}) = 0.9878$, so a satisfactory approximate solution to Eq. (9) is $k = \sqrt{\pi}$, and the new velocity profile to be used in place of Eq. (6) will be taken as

$$u/u_c = \exp\,[-\pi(y/Y)^2] \tag{10}$$

This expression closely approximates Eq. (6) in the range $-Y \leqq y \leqq Y$, and, although it extends to infinity, its values for $|y| > Y$ are negligibly small.

For convenience a new coordinate x^* along the wake axis is introduced in Eqs. (1) and (5). It is defined by

$$x^* \equiv x - 0.7c \tag{11}$$

and in terms of x^* the wake half-width and velocity at the center become

$$Y = 0.68\sqrt{2c}(C_D x^*/c)^{1/2} \tag{12}$$

$$u_c/V = -(2.42C_D{}^{1/2})/(x^*/c + 0.3) \tag{13}$$

Eqs. (10), (12), and (13) completely define the wake to be used in this analysis of the nonsteady effects on a rotor blade moving through the viscous wakes of the upstream row of stator blades. Before this analysis is begun, it should be noted that the ratio of wake half-width to airfoil half-chord is small. For a value of C_D typical of compressor blades, say 0.02, Eq. (12) shows that at $x = 1.2c$,

$$x^*/c = 0.5, \quad Y/c \approx 0.1$$

and at $x = 3c$,

$$x^*/c = 2.3, \quad Y/c \approx 0.2$$

Thus, if the airfoil is a turbomachine blade, its wake is still relatively narrow compared to its chord and, presumably, compared to the circumferential blade spacing, in the region of the next blade row.

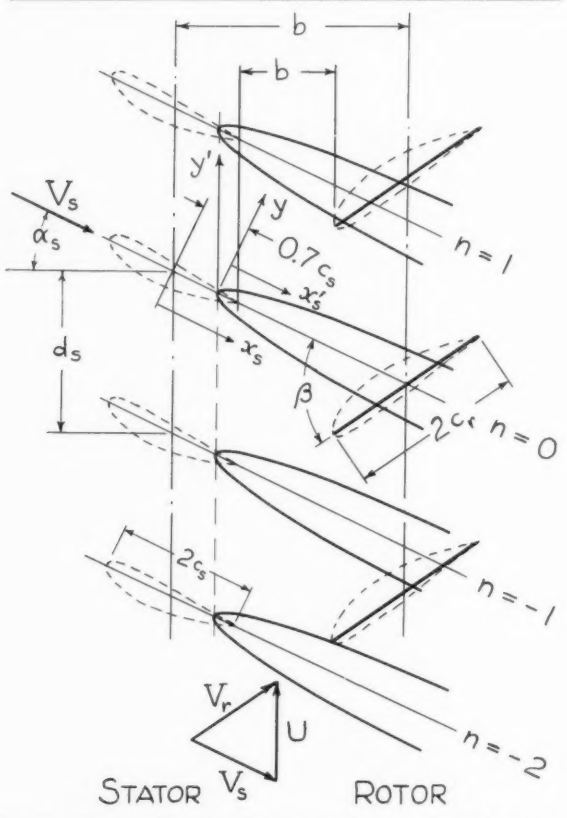

FIG. 2. Diagram denoting stator and rotor cascades and stator-blade wakes.

APPLICATION TO TURBOMACHINE

The viscous-wake model described in the previous section will now be applied to find approximately the nonsteady effects experienced by a blade in the rotor row of a turbomachine as it passes through the viscous wakes shed by the blades of the upstream stator row. First, an approximate expression for the nonsteady upwash experienced by the rotor blade is obtained. Then the concepts and results of nonsteady thin-airfoil theory are used to find the lift and other nonsteady quantities associated with this upwash.

The problem may be visualized with the aid of Fig. 2. This represents a stage of a typical turbomachine as an infinite cascade of two-dimensional stator blades followed by a similar rotor row moving downward relative to the stator with velocity U. The stator blades have chord $2c_s$, spacing d_s, and stagger α_s which represents the swirl of the incoming flow whose velocity is V_s. The rotor blades have chord $2c_r$ and have mean chord lines in the direction of the relative flow, V_r, which makes an angle β with the velocity V_s. The distance between the centerlines of the stator and rotor rows is b. It is assumed that each stator blade sheds a viscous wake of the form described in Eqs. (10), (12), and (13), where c, V and x^* now have the subscript s, and C_D is to be read $C_D{}^s$, the stator-blade profile drag coefficient. The wakes are symmetrical about the direction of V_r, as shown.

Velocity Induced at Rotor

Since the rotor blade moves along a line oblique to the x_s (or x_s^*) axis, it is convenient to introduce oblique coordinates x', y' as shown in Fig. 2, where the y' axis is parallel to the direction of rotor motion. The relation between x_s^*, y and x', y' is given by

$$x_s^* = x' - y' \sin \alpha_s, \quad y = y' \cos \alpha_s \tag{14}$$

This simply means that the coordinate x' is always measured from a vertical line (the y' axis) in Fig. 2. But, as has been seen above, the wake is narrow in the region of interest, so that y'/x' is small in the wake itself, and one may write, approximately,

$$x_s^* = x', \quad y = y' \cos \alpha_s \tag{15}$$

This approximation simplifies the analysis because it retains the simple dependence of the wake half-width

and centerline velocity on only one coordinate—i.e., from Eqs. (12) and (13),

$$Y = 0.68\sqrt{2}c_s(C_D{}^s x'/c_s)^{1/2} \tag{16}$$

$$u_c/V_s = -(2.42\sqrt{C_D{}^s})/(x'/c_s + 0.3) \tag{17}$$

The velocity profile from Eq. (10) is now

$$u/u_c = \exp\{-\pi[(y' \cos \alpha_s)/Y]^2\} \tag{18}$$

Eq. (18) gives the profile of the wake shed from the center stator blade in Fig. 2 (the zero-th blade). Each stator blade sheds such a wake, so that the pattern is repeated infinitely many times in the y'-direction. The profile of the wake shed from the nth stator blade may be found from Eq. (18) by replacing y' by $y' - nd_s$. To obtain the total velocity field of all the wakes, one then sums over n from $-\infty$ to ∞. The result is the total perturbation velocity field due to all the wakes, u_T.

$$\frac{u_T}{u_c} = \sum_{n=-\infty}^{\infty} \exp\left[-\pi\left(\frac{\cos \alpha_s}{Y}\right)^2 (y' - nd_s)^2\right] \tag{19}$$

The assumption that the configuration of wakes behind a cascade can be described by superposition of isolated-airfoil wakes is, of course, approximate. As is often the case, the simplicity afforded by this approximation is attended by a certain complication—namely, Eq. (19), as it stands, does not satisfy the principle of continuity of the axial flow through the stage. Because of the periodic nature of the flow in the y'-direction and the fact that a shear flow with only one velocity perturbation component has been assumed, continuity requires that the integral of the total perturbation velocity u_T vanish when taken over a period in the y'-direction. Therefore, a constant equal to the average value of u_T in Eq. (19) should be subtracted from the right side of that equation. However, the next step in the analysis is to expand the right side of Eq. (19) in a Fourier series, and the constant term in this expansion will be just the constant that should be subtracted. Thus, continuity will be satisfied if the constant term is simply dropped. This is the procedure to be followed.

Eq. (19) can be transformed into a complex Fourier series by means of the Poisson Summation Formula,[3] which states that for suitable $f(n)$

$$\sum_{n=-\infty}^{\infty} f(n) = \sum_{m=-\infty}^{\infty} \int_{-\infty}^{\infty} f(z)e^{-2\pi imz}\, dz \tag{20}$$

To apply this to Eq. (19) it is necessary to evaluate the integral

$$\int_{-\infty}^{\infty} \exp\,[-K^2(y'/d_s - z)^2]e^{-2\pi imz}\, dz$$

where

$$K^2 \equiv \pi \cos^2 \alpha_s(d_s/Y)^2 \tag{21}$$

After introduction of a new variable, $\xi \equiv (y'/d_s - z)K$, and completion of the square on the exponent, the integral is

$$\frac{1}{K} \exp\left(-2\pi im\, \frac{y'}{d_s} - \frac{\pi^2 m^2}{K^2}\right) \times \int_{-\infty}^{\infty} \exp\left[-\left(\xi - \frac{im\pi}{K}\right)^2\right] d\xi = \frac{\sqrt{\pi}}{K} \exp\left(-2\pi im\, \frac{y'}{d_s} - \frac{\pi^2 m^2}{K^2}\right) \tag{22}$$

With this result, the application of the Poisson Summation Formula to Eq. (19) gives

$$\frac{u_T}{u_c} = \frac{\sqrt{\pi}}{K} \sum_{m=-\infty}^{\infty} \exp\left(-2\pi im\, \frac{y'}{d_s} - \frac{\pi^2 m^2}{K^2}\right) = \frac{\sqrt{\pi}}{K}\left\{1 + \Re\left[\sum_{m=1}^{\infty} 2 \exp \times \left(-2\pi im\, \frac{y'}{d_s} - \frac{\pi^2 m^2}{K^2}\right)\right]\right\} \tag{23}$$

where $\Re$ denotes the real part. The constant term in Eq. (23) is the average value of u_T/u_c, which must be dropped to satisfy continuity, as explained above, so that u_T/u_c is to be written

$$\frac{u_T}{u_c} = \frac{2\sqrt{\pi}}{K} \sum_{m=1}^{\infty} \exp\left(-2\pi im\, \frac{y'}{d_s} - \frac{\pi^2 m^2}{K^2}\right) \tag{24}$$

The real part is implied from here on.

The time dependence of the y'-coordinate of a fixed point x_r of the rotor blade can be obtained from Fig. 2. The coordinate x_r is measured rearward from the center of the rotor blade, and the time origin, $t = 0$, is taken in the position shown in Fig. 2—i.e., when the center of the rotor blade lies on the extended chord line of the zero-th stator blade. It is seen from the figure that

$$y' = U(x_r/V_r - t) \tag{25}$$

U is the downward velocity of the rotor blade, and V_r is the velocity relative to it.

The velocity u_T is in the direction of x_s, which makes an angle β with the rotor blade, so that the component giving upwash at the blade is $-u_T \sin \beta$. Therefore, the upwash at the rotor blade, v^{rr}, is, from Eqs. (24) and (25)

$$v^{rr} = -u_c \sin \beta\, \frac{2\sqrt{\pi}}{K} \sum_{m=1}^{\infty} \exp\left[-\frac{\pi^2 m^2}{K^2}\right] e^{i\nu_r m(t - x_r/V_r)} \tag{26}$$

Here ν_r is the circular frequency with which the rotor blades pass the stator blades, defined by $\nu_r \equiv 2\pi U/d_s$.

Besides the explicit dependence on x_r exhibited in the last exponential of Eq. (26), there is a dependence through u_c and K, both of which depend on x' and therefore on x_r. The relation between x' and x_r is $x' = b \sec \alpha_s - 0.7c_s + x_r V_s/V_r$. With this relation, one can write

$$\frac{x'}{c_s} = \frac{c_r}{c_s}\left(\frac{b}{c_r} \sec \alpha_s + \frac{x_r}{c_r}\, \frac{V_s}{V_r}\right) - 0.7 \tag{27}$$

It is this expression for x'/c_s which must be used in u_c and K and which gives them their dependence on x_r.

Now that the nonsteady upwash v^{re} has been obtained, the nonsteady effects caused by the viscous stator wakes at the rotor blade can be found by applying nonsteady thin-airfoil theory to an airfoil with this upwash. However, the dependence of v^{re} on x_r just discussed makes this process complicated. Since the theory outlined so far is an approximate one, another approximation, which makes the application of nonsteady airfoil theory to v^{re} simple, will be introduced. Namely, it is assumed that the variation of u_c and K with x_r does not have a large effect on v^{re}, so that in these two quantities x_r/c_r may be taken fixed at some appropriate value between 1 and -1. In other words, in calculating the variation of v^{re} along the rotor-blade chord, one assumes some mean values for the quantities u_c and K. The consequences of this assumption are investigated in the numerical calculations reported in the next section.

If the fixed value of x_r in u_c and K is denoted by x_{r0} and the corresponding value of x' from Eq. (27) is x_0', then use of Eqs. (21), (16), and (17) in Eq. (26) yields the following expression for v^{re}:

$$v^{re}(x_r, t) = \frac{1}{2\pi} V_r \sum_{m=1}^{\infty} G_m{}^{re} e^{i\nu_r m(t - x_r/V_r)} \qquad (28)$$

where

$$G_m{}^{re} \equiv 4\pi \frac{V_s}{V_r} \frac{2.42\sqrt{C_D{}^s}\sin\beta}{x_0'/c_s + 0.3} \frac{0.68\sigma_s}{\sqrt{2}\cos\alpha_s} \times \sqrt{\frac{C_D{}^s x_0'}{c_s}} \exp\left[-\pi m^2 \left(\frac{0.68\sigma_s}{\sqrt{2}\cos\alpha_s}\right)^2 \frac{C_D{}^s x_0'}{c_s}\right] \qquad (29)$$

Here σ_s denotes the stator row solidity $2c_s/d_s$, and x_0'/c_s is given by Eq. (27) with $x_r = x_{r0}$.

Nonsteady Lift, Moment, and Wake of Rotor

The calculation of the nonsteady aerodynamic quantities induced at a thin airfoil by a relative upwash of the form of v^{re} can be easily obtained from the results of a paper by Sears.[4] There it is shown that if a thin airfoil experiences at nonsteady upwash of the form

$$v = v_0 e^{i\nu(t - x/V)} \qquad (30)$$

the lift and the moment about the mid-chord are given by

$$L(t) = 2\pi c V v_0 S(\omega) e^{i\nu t}$$
$$M(t) = L(t)/2c \qquad (31)$$

Here v_0 is a constant independent of x, which may be complex, V is the stream velocity, c is the half-chord (not the chord as in reference 4), x is measured rearward from mid-chord, and $S(\omega)$ is a complex function of the reduced frequency $\omega \equiv \nu c/V$, which was shown in reference 5 to be

$$S(\omega) = \{i\omega[K_0(i\omega) + K_1(i\omega)]\}^{-1} \qquad (32)$$

where K_0 and K_1 are modified Bessel functions of the second kind.

The application of this isolated-airfoil result to a cascade blade is consistent with the idea of a "first-order" theory, as previously mentioned. It is assumed that the effects of passage through viscous wakes are small compared to steady effects. Thus, in calculating nonsteady quantities, the induced effects of other blades of the rotor cascade and of the stator cascade are neglected. This approximation, of course, limits the validity of the results to cascades of relatively low solidity.

Since each term of v^{re} is of exactly the same form as v in Eq. (30) and since the problem is a linear one due to the restriction to thin airfoils, the result of Eq. (31) can be applied term-by-term to v^{re} to find the lift and moment of the rotor blade. If lift and moment coefficients defined by

$$C_L{}^{re}(t) \equiv [L^{re}(t)]/[(1/2)\rho V_r{}^2 2c_r]$$
$$C_M{}^{re}(t) \equiv [M^{re}(t)]/[(1/2)\rho V_r{}^2 (2c_r)^2]$$

are used, the lift and moment at the rotor due to v^{re} are

$$C_L{}^{re}(t) = \sum_{m=1}^{\infty} G_m{}^{re} S(m\omega_r) e^{im\nu_r t}$$
$$C_M{}^{re}(t) = (1/4) C_L{}^{re}(t) \qquad (33)$$

where c_r is the rotor half-chord and ω_r is the rotor reduced frequency, $\nu_r c_r/V_r$.

Thus, the lift and moment coefficients are obtained as sums of harmonic components. In flutter and vibration analyses, for example, the magnitudes of the harmonics themselves are of primary importance, rather than their sum.

Other nonsteady aerodynamic quantities associated with v^{re}, such as the nonsteady circulation and nonsteady vortex wake shed by the blade, can be found by standard methods of nonsteady thin-airfoil theory (see, for instance, references 6 and 1).

Numerical Calculations and Conclusions

A few sample calculations of $C_L{}^{re}$ have been made in order (1) to obtain the order of magnitude of the lift on a rotor blade due to its passage through the viscous wakes shed by the stator blades, (2) to evaluate the effect on this lift of $C_D{}^s$, the stator profile drag coefficient, and (3) to investigate the sensitivity of the results to the choice of x_{r0}/c_r, the point on the rotor blade at which the constant wake width $2V$ and velocity at the wake center u_c are evaluated.

The geometric parameters taken are thought to be typical of present-day axial-flow compressors and are the same as those used in the earlier calculation of nonsteady interference effects in a turbomachine stage.[1] They are

$$\sigma_s = 1$$
$$c_r/c_s = 1$$
$$\alpha_s = 45°$$
$$\beta = 90°$$
$$b'/c_r = 0.2$$

where $b' = b - c_s\cos\alpha_s - c_r\cos(\beta - \alpha_s)$, the axial distance from stator trailing edge to rotor leading edge

TABLE 1

ABSOLUTE VALUES OF FIRST TWO HARMONICS OF ROTOR LIFT COEFFICIENTS

x_{r0}/c_r	C_D^s	$\lvert C_{L1}^{rv}\rvert$	$\lvert C_{L2}^{rv}\rvert$
−1/2	0.01	0.029	0.020
	0.02	0.057	0.037
+1/2	0.01	0.023	0.014
	0.02	0.045	0.026

Two typical values were taken for C_D^s—namely, $C_D^s = 0.01, 0.02$. For each, the first two terms of the series for C_L^{rv}—i.e., the first two harmonic components—were obtained.

To test the importance of the choice of x_{r0}, two values—namely, $c_r/2$ and $-c_r/2$—are used in every case. This means that, in calculating the variation of the upwash velocity over the rotor-blade chord, the quantities u_e and K have been evaluated at the $^3/_4$-chord and the $^1/_4$-chord stations, respectively. The results are shown in Table 1 where the absolute value $\lvert C_{Lm}^{rv}\rvert$ of the first two harmonics, $m = 1, 2$, of C_L^{rv} are tabulated.

The convergence of the series in C_L^{rv}—that is, the rapidity of decrease of successive harmonics—is not as rapid as might appear from the fact that the convergence factor in G_m^{rv} [Eq. (29)] is exp $(-m^2\pi^2/K^2)$. Although for large m this factor will decrease rapidly, for small m it is extremely close to unity because π^2/K^2 is proportional to C_D^s, which is small. In fact, for the cases calculated, π^2/K^2 is of order 10^{-2}. Therefore, the second harmonic is smaller than the first by a factor of only about two.

The effect of the C_D^s term in the exponent of C_{Lm}^{rv} is seen to be fairly small, because the results for the two different values of C_D^s are in about the same ratio as the respective drag coefficients—namely, 1/2. It seems, therefore, that the lift produced at the rotor due to its passage through the viscous wakes shed by the stator blades is nearly proportional to the profile drag coefficient of the stator blades.

The large change in x_{r0}/C_r from $-1/2$ to $1/2$ produced changes of the order of 25 per cent in $\lvert C_{Lm}^{rv}\rvert$. Thus, the approximation involved in taking constant values of u_e and K seems to be justified for practical purposes.

The results given in Table 1 may be compared with similar results given in reference 1 for the nonsteady effects at a rotor blade due to the relative motion of the circulation carried by the stator blades. Since typical compressor blades operate at steady lift coefficients of about unity, the values of $\lvert C_{Lm}^{rv}\rvert$ may be compared with the magnitudes of the ratio of nonsteady to steady lift on a rotor blade given in Fig. 7 of reference 1. If this is done, it is seen that the first harmonics ($m = 1$) are of about the same size for $C_D^s = 0.02$, while the second harmonics ($m = 2$) of C_L^{rv} are larger than those given in reference 1. This is because the convergence is slower here than was the case there. It therefore appears that, at the higher stator profile-drag coefficients, the viscous-wake effects on a rotor blade are of about equal importance with the circulation-induced effects discussed in reference 1.

REFERENCES

[1] Kemp, N. H., and Sears, W. R., *Aerodynamic Interference Between Moving Blade Rows*, Journal of the Aeronautical Sciences, Vol. 20, No. 9, pp. 585–598, September, 1953.

[2] Silverstein, A., Katzoff, S., and Bullivant, W. K., *Downwash and Wake Behind Plain and Flapped Airfoils*, NACA Rep. 651, 1939.

[3] Madelung, E., *Die Mathematischen Hilfsmittel Des Physikers*, Julius Springer, Berlin, 1936 (also Dover Publications, New York, 1943), p. 28, Eq. (18).

[4] Sears, W. R., *Some Aspects of Non-Stationary Airfoil Theory and Its Practical Application*, Journal of the Aeronautical Sciences, Vol. 8, No. 3, pp. 104–188, January, 1941.

[5] Kemp, N. H., *On the Lift and Circulation of Airfoils in Some Unsteady-Flow Problems*, Journal of the Aeronautical Sciences, Vol. 19, No. 10, p. 713, October, 1952.

[6] von Kármán, Th., and Sears, W. R., *Airfoil Theory for Non-Uniform Motion*, Journal of the Aeronautical Sciences, Vol. 5, No. 10, pp. 379–390, August, 1938.

IAS Twenty-Fourth Annual Meeting

Hotel Sheraton-Astor, New York City, January 23–27, 1956

The Meetings Committee is planning sessions on Aerodynamics, Aeroelasticity, Structures, Rotating Wing, Aircraft Design, Meteorology, etc.

Authors wishing to have papers considered for presentation at this meeting should submit outlines or short abstracts to the Meetings Committee, 2 East 64th St., New York 21, N.Y., no later than September 1, 1955.

The Design and Calibration of a Variable Mach Number Nozzle

JOHN ROSÉN*

Division of Steam Engineering at The Royal Institute of Technology
Stockholm, Sweden

SUMMARY

A method of designing a symmetric Mach Number nozzle with adjustable flexible walls has been developed. The continuous variation of the Mach Number is controlled by one single screw mechanism, which in a defined manner simultaneously affects the coordinates and derivatives of the inlet and throat curvatures up to the inflection point. The flexible part of the curvature between the inflection point and the test section consists of a spring, with linear thickness distribution, rigidly clamped at the level of the test section (150×150 mm.^{2} = 5.9 in. $\times$ 5.9 in.). Due to small curvatures and a suitable choice of the linear thickness distribution of the flexible part of the wall, a good Mach Number distribution (± 0.015 or less) has been realized within the whole Mach Number range from 1.5 to 2.5.

INTRODUCTION

THE EVER INCREASING DEMAND for a more advanced wind tunnel technique explains the keen interest recently shown in the development of devices for continuous variation of the Mach Number. Some of these tunnels fitted with such devices can be characterized by their working principles, as for instance, the sliding-block type, the flexible-wall nozzles and the Drougge wedge.

The investigation described below concerns a small flexible-wall tunnel (150×150 mm.^{2} at the test section). To avoid the complicated mechanism generally characteristic of these constructions, a new method was found for affecting the flexible walls in a well-defined motion by means of one single screw mechanism. The purpose of this tunnel is to study the Mach Number effect in some processes which previously were very difficult, or even impossible, to study in a setup of conventional fixed-wall nozzles. As a comparison, some prominent features of the variable nozzle design will be mentioned:

(1) All measurements can be recorded continuously as a function of the Mach Number.

(2) The time-wasting nozzle changes are eliminated.

(3) The starting of the tunnel can be performed smoothly.

(4) Instructive films can be taken over complicated processes, visualizing the influence of Mach Number.

Some important investigations which could easily be carried out with such a device are:

(A) The pressure recovery for supersonic diffusors running at different Mach Numbers and the cause of instabilities which generally occurs at lower mass flow ratios.

(B) Some hysteresis effects associated with the starting conditions for supersonic diffusors.

(C) The regulation of an air intake when diverging from the design Mach Number.

Received June 1, 1954.

* Civilingenjör, now with Svenska Flygmotor Aktiebolaget, Aerodynamiska avdelningen, Trollhättan, Sweden.

SYMBOLS

x, y	=	coordinates according to Fig. 1
X, Y, Z	=	coordinates according to Fig. 7
M	=	Mach Number
P	=	load
σ	=	stresses

Subscripts

t	=	test section value according to the Foelsch method
1	=	test section value according to the spring calculation (see further Figs. 1–7)

NOZZLE DESIGN

A Mach Number range from 1.5 to 3.0† was selected as being the most interesting range for future needs. A flexible symmetrical nozzle was chosen, the following conditions being imposed for the contour:

(1) At Mach Number 2.5 the nozzle profile approximately corresponds to a Foelsch profile.

(2) In the whole Mach Number range only small curvatures are allowed.

(3) To get a rigid system the spring has to be short and strong.

(4) In order to avoid the pressure changing sign along the flexible part of the wall, communication is established between the test section and the space outside the springs.

(5) The springs are rigidly clamped at the level of the test section.

(6) The inlet and throat contours IOBA up to the inflection point (A) at the supersonic side are made out of one solid block.

(7) Corrections for the boundary-layer increment have been estimated at 0.60°.

Theoretical Treatment

The Foelsch method was applied for designing a Mach Number nozzle the contour of which should correspond to the elastic line of a spring, flexible downstream of the inflection point (A) and rigid upstream of it. The Mach Number (M_t) at which this should happen

† The Mach Number range 2.5–3.0 is to be examined at Svenska Flygmotor AB, Trollhättan, Sweden.

was chosen as 2.500, when the maximum slope angle φ_1 was to be 7.0°. (See Fig. 3.) The radius (R) at the throat is 400 mm. and the part between B and A is straight. The data given above are sufficient for determining the nozzle profile.

$$\Theta_t = 39.14° \qquad \tau_t = \frac{r_t}{r_0} = \frac{y_t}{y_0} = 2.6367 \qquad M_t = 2.500$$

$$\Theta_1 = \Theta_t - \varphi_1 = 32.14° \qquad \tau_1 = \frac{r_1}{r_0} = \frac{A_1}{A_0} = 2.0355 \qquad M_1 = 2.217$$

$y_t = 75$ mm.

$y_0 = 28.44$ mm.

$$y_1 = y_0 \cdot \frac{\sin \varphi_1}{\varphi_1} \cdot \frac{A_1}{A_0} = 57.76 \text{ mm.}$$

The coordinates of the contour are given by the equation

$$x - x_1 = r \cos (\Theta_t - \Theta) - r_1 \cos \varphi_1 + 1 \cos (\Theta_t - \Theta + \beta) \quad (1)$$

$$y = r \sin (\Theta_t - \Theta) + 1 \sin (\Theta_t - \Theta + \beta) \quad (2)$$

where

$r_1 = y_1/\sin \varphi_1 = 473.91$ mm.
$r_0 = r_1/\tau_1 = 232.82$ mm.
$x_1 = r_1 \cos \varphi_1 = 470.38$ mm.
$l = M \cdot r(\theta - \Theta_1)$

The coordinates between A and F are presented in Table 1. Due to the fact that y_0 and y_t are known at a given Mach Number the following values can be determined

$$\kappa = (y_1 - y_0)/\sin \varphi_1 = 240.51 \text{ mm.}$$

Because the radius (R) at the throat is 400 mm.:

$$\lambda = \kappa - R\, tg(\varphi_1/2) = 216.04 \text{ mm.}$$

The x-coordinate at the throat is

$$x_0 = [(y_0 + R) \cos \varphi_1 - R]/\sin \varphi_1 = 207.21 \text{ mm.}$$

The coordinates of the point B are

$$x_B = x_0 + R \sin \varphi_1 = 255.96 \text{ mm.}$$
$$y_B = y_0 + R\,(1 - \cos \varphi_1) = 31.43 \text{ mm.}$$

TABLE 1
The Nozzle Shape According to Foelsch
$\varphi_1 = 7°$ and $M_t = 2.500$

Point	ξ	x', mm.	y, mm.
O	−0.835	000	28.44
B	−0.681	48.7	31.42
A	0.0	263.2	57.75
	0.035	274.3	59.09
	0.091	292.0	61.07
	0.180	320.0	63.88
	0.307	359.8	67.24
	0.442	402.3	70.10
	0.587	448.0	72.41
	0.744	497.6	74.04
F	1.000	578.5	75.00

The total length l' from the throat to the test section then is

$$l' = x_t - x_0 = 578.52 \text{ mm.}$$

The part IOBA of the contour is a solid block, which is fixed in relation to the tangent through the inflection point. If now the flexible part of the wall between A and F is considered as the elastic line of a beam with linear thickness distribution acted upon by a point load at A and with its end clamped at the level of the test section, the following conditions must be satisfied in order to have the elastic line osculating to the Foelsch profile. The coordinates and derivatives at A and F must be equivalent. If now the thickness distribution is

$$h_\xi = h_0(1 + \beta\xi) \quad (3)$$

the differential equation of the elastic line of the beam (case A) will be

$$\delta'' \cdot \frac{Ebh_0^3}{12PL} = -\frac{\xi}{(1 + \beta\xi)^3} \quad (4)$$

$$\delta' \cdot \frac{Ebh_0^3}{12PL^2} = \frac{\xi}{2\beta(1 + \beta\xi)^2} + \frac{1}{2\beta^2(1 + \beta\xi)} + C_0 \quad (5)$$

$$\delta \cdot \frac{Ebh_0^3}{12PL^3} = -\frac{\xi}{2\beta^2\,(1 + \beta\xi)} + \frac{1}{\beta^3} \ln (1 + \beta\xi) + C_0\xi + C_1 \quad (6)$$

where

$b = 15.0$ cm.
$L = 31.50$ cm. (the projection of the Foelsch profile between A and F on the centerline)

The boundary conditions are

$$\delta'(1) = 0 \qquad \because C_0 = -\frac{1 + 2\beta}{2\beta^2(1 + \beta)^2} = f(\beta)$$

$$\delta(0) = 0 \qquad \because C_1 = 0$$

By comparison with the data from the Foelsch profile, the values of β and P/h_0^3 can be calculated.

$$\delta'(0) = \frac{12PL^2}{Ebh_0^3} \frac{1}{2\,(1 + \beta)^2} = tg\ 7.0° = 0.12278 \quad (7)$$

$$\delta(1) = \frac{12PL^3}{Ebh_0^3}\left[\frac{1}{\beta^3} \ln (1 + \beta) - \frac{2 + 3\beta}{2\beta^2\,(1 + \beta)^2}\right] = 1.725 \text{ cm.} \quad (8)$$

By dividing Eq. (7) by Eq. (8), P/h_0^3 is eliminated, and β becomes 2.46. In order to limit the stresses in the beam (Case A)

$$(\sigma)_{max.} = \frac{6PL\xi}{bh_0^2(1 + \beta\xi)^2} \leq 3{,}000 \text{ kp./cm.}^2 \quad (9)$$

$$\because \sigma'(\xi) = \frac{6PL\,(1 - \beta\xi)}{bh_0^2(1 + \beta\xi)^3} = 0 \quad \text{gives} \quad \xi = \frac{1}{\beta} = 0.4065$$

From Eqs. (7) and (9)

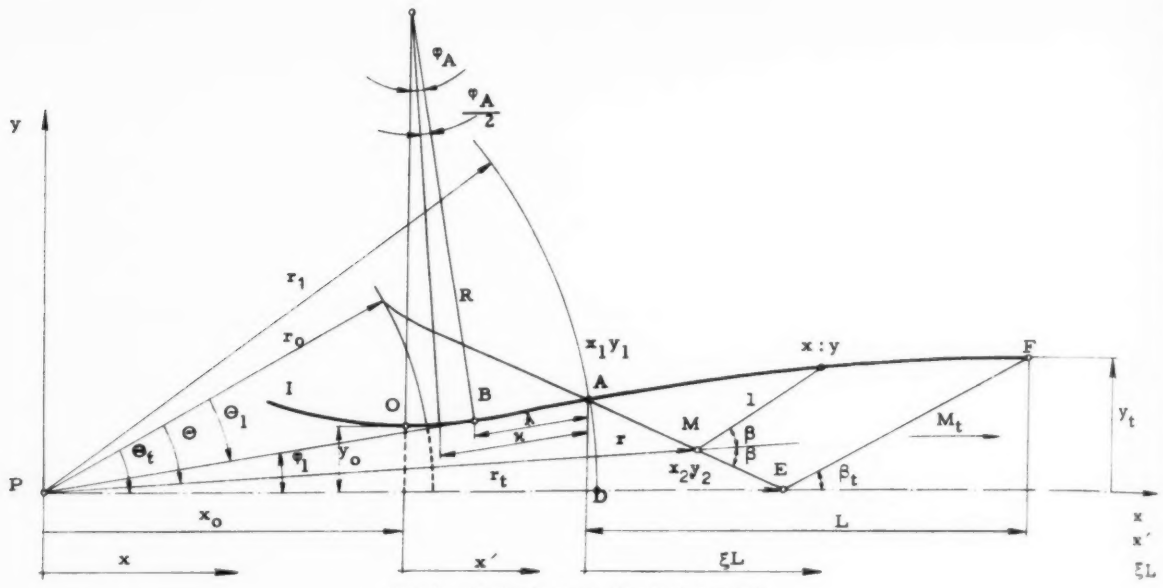

FIG. 1. Design features of a Foelsch profile.

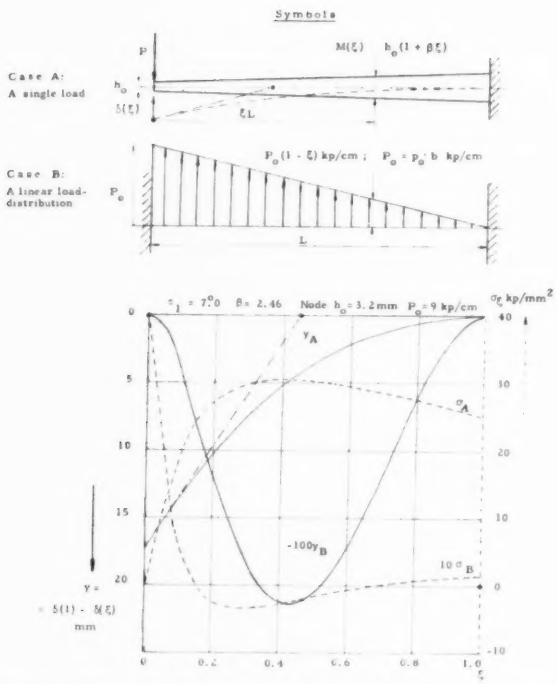

FIG. 2. Deflections and stresses due to loads according to cases A and B.

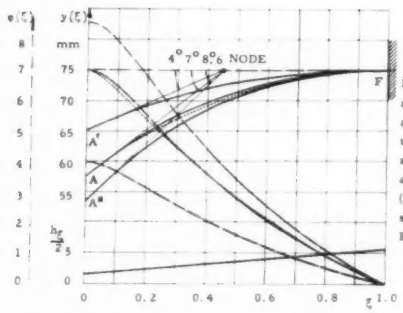

Fig 3. Deflections y(ξ) and slope angles φ(ξ) of a beam with linear thickness distribution, a single load at ξ = 0 and clamped at ξ = 1.0 (Aerodynamic nozzle shape according to Foelsch ----------)

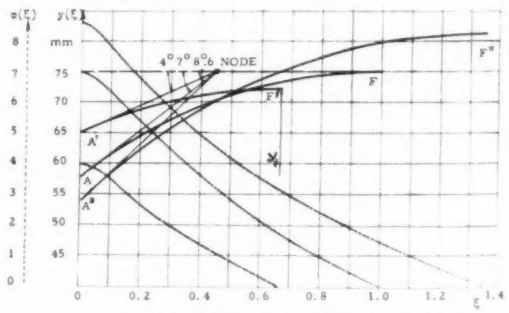

Fig. 4. Some aerodynamic nozzle contours osculating to the elastic lines of the spring at ξ = 0

According to the Foelsch method					According to the spring calculation				Divergences	
	M_t	y_t mm	ξ_t	$\varphi(1)°$		M_1	y_1 mm	$\varphi(\xi_t)°$	ΔM	Δy mm
F	2.500	75.00	1.000	0	F	2.500	75.00	0	0	0
F'	1.827	72.15	0.672	-	F	1.877	75.00	0.93	-0.05	-2.85
F''	3.128	81.23	1.354	1°43	F	3.048	75.00	-	+0.08	+6.23

TABLE 2
The Nozzle Shape According to the Spring Calculation
$\varphi_1 = 7°$ and $M_t = 2.500$

Point	ξ	$L\xi$, mm.	x', mm.	y_A, mm.	$\varphi^0(\xi)$	y_B, mm.	σ_A, kp./mm.^{2}	σ_B, kp./mm.^{2}	σ_T, kp./mm.^{2}
O	−0.835	...	0	28.44	0	0			
B	−0.681	...	48.75	31.42	7.00	0			
A	0	0	263.2	57.75	7.00	0	0	−4.06	−4.06
	0.05	15.7	278.9	...	6.84	...	...	...	...
	0.1	31.5	294.7	61.50	6.46	0.04	19.36	−0.61	18.75
	0.2	63.0	326.2	64.81	5.50	0.12	27.01	+0.23	27.24
	0.3	94.5	357.7	67.57	4.52	0.18	29.86	+0.34	30.20
	0.4	126.0	389.2	69.80	3.61	0.21	30.55	+0.29	30.84
	0.5	157.5	420.7	71.55	2.80	0.21	30.22	+0.18	30.40
	0.6	189.0	452.2	72.89	2.08	0.17	29.42	+0.08	29.50
	0.7	220.5	483.7	73.86	1.47	0.12	28.40	+0.01	28.41
	0.8	252.0	515.2	74.51	0.92	0.06	27.30	−0.05	27.25
	0.9	283.5	546.7	74.88	0.43	0.02	26.19	−0.09	26.10
F	1.0	315.0	578.2	75.00	0.00	0.0	25.11	−0.13	24.98

$h_0 = 0.32$ cm.

$P = 242.5$ kp.

(Further spring data are given in Table 2.)

The expansion curve between A and F has also to be taken into account. Assuming that a linearly decreasing pressure distribution exists along the spring between A and F, the load distribution can be written

$$q(\xi) = P_0 \cdot (1 - \xi) \tag{10}$$

and thus the elastic line becomes

$$\delta \cdot \frac{Ebh_0^3\beta^5}{6P_0L^4} = [2 + \beta + \beta^2\xi + 3\beta\xi + \beta^2\xi^2] \ln (1 + \beta\xi) - \beta(2 + \beta)\xi + [6\beta + 4\beta^2 - (6 + 9\beta + 3\beta^2) \cdot \ln (1 + \beta)]\xi^2 + [(4 + 5\beta + \beta^2) \ln (1 + \beta) - (4 + 3\beta)\beta]\xi^3 \tag{11}$$

In the above equation the following values have been used:

$\varphi_1 = 7.00°$
$b = 15$ cm.
$h_0 = 0.32$ cm.
$\beta = 2.46$
$L = 31.50$ cm.
$P_0 = p_0 \cdot b = 0.6 \cdot 15 = 9$ kp./cm.

At $M_t = 2.500$ this gives a maximum deflection of 0.21 mm. (See further Table 2.) The spaces outside the springs are evacuated by means of the jet in the test section but not to such an extent that the static pressure value there is reached. Therefore the deflection will be less than indicated above and will decrease with the Mach Number.

Within the approximation made in obtaining the differential equation for the elastic line of the spring, we make use of another outstanding feature. This is the node, defined as the center of convergence of the tangent from point A when this is deflected by a point load at A.

The general expression for the ξ-coordinate of the node is thus (see Fig. 8)

$$\xi_n = \frac{\delta(1)}{L\delta'(0)} = \frac{2(1 + \beta)^2}{\beta^3} \ln (1 + \beta) - \frac{2 + 3\beta}{\beta^2} \tag{12}$$

and in particular for $\beta = 2.46$, $\xi_n = 0.44647$. Because of this property a supporting arm with a bearing at the node and clamped at the point A will entirely control the system upstream of the point A. Because the point A moves in a circle and the spring cannot extend, a compensation spring is placed at the level of the test section. (See Figs. 5 and 6.) The maximum deflection (ϑ) of this spring is 0.25 mm.

These preliminary calculations first aimed at determining a theoretical nozzle profile for a certain Mach Number according to Foelsch, and then accommodating it to the elastic line of a spring.

The next step is to check the spring for another single load P—e.g., that corresponding to $\varphi_1 = 4.0°$. With the same curvature IOBA as before, the new elastic line between A′ and F can be calculated. The new test section Mach Number (M_1) becomes 1.877 if the boundary-layer correction is excluded. Upon this new IOBA′ profile it is possible to erect a Foelsch profile A′F′. This nozzle however is 10.33 cm. shorter and produces theoretically a Mach Number 0.05 lower than the corresponding spring nozzle. (See Tables 3 and 4 and Fig. 4.) Finally the discrepancy between the flexible-wall nozzle and the Foelsch profile has been checked at a value of $\varphi_1 = 8.60°$. (The results are given in Tables 5 and 6 and Figs. 3 and 4.)

DESCRIPTION

The entire nozzle contour is made out of one steel spring (material: Bofors S 145) with a minimum

TABLE 3
The Nozzle Shape According to the Spring Calculation
$\varphi_1 = 4.0°$

Point	ξ	x', mm	y_A, mm.	$\varphi^0(\xi)$
O	−0.773	0	49.12	0
B	−0.684	27.9	50.10	4.00
A′	0	243.4	65.17	4.00
	0.050	259.2	...	3.91
	0.100	274.9	67.31	3.69
	0.200	306.4	69.19	3.14
	0.300	337.9	70.76	2.58
	0.400	369.4	72.03	2.06
	0.500	400.9	73.03	1.60
	0.600	432.4	73.80	1.19
	0.700	463.9	74.35	0.83
	0.800	495.4	74.72	0.52
	0.900	526.9	74.93	0.25
F	1.000	558.4	75.00	0.00

σ_z = 120 kp./mm.^{2} (see Fig. 5). This spring is clamped at the test section and at the part upstream of A, joined by bolts to a supporting arm pivoted about the node. By this means a screw mechanism acting upon the supporting arm, via an articulation, entirely defines the curve IOBA within the whole Mach Number range. The supporting arm also has to prevent the spring from cracking as could happen if the pressure on the inlet surface were transmitted by the spring.

Due to the fact that the node is fixed and the lengths of the supporting arm and the spring are determined, a special device (see Figs. 5 and 6) is fitted in the test section to conserve the condition that the end of the spring is clamped though it changes axial position at different Mach Numbers. This device consists of a frame-spring mounted in such a way that the nozzle wall is pre-inclined 0.60°, approximately corresponding to the correction for the boundary-layer increment.

The compensation spring is further preset to give higher axial tension to the nozzle spring at lower Mach Numbers, thus giving negligible influence on the elastic line of the flexible wall at higher Mach Numbers. Due to the thickness distribution of the spring the elastic line has to be inclined 0.72° + 0.60° = 1.32°.

The screw mechanism consists of a symmetrically working gear system, which transmits the control forces via an articulation to the supporting arm at the level of the throat. The height of the throat can be read on a circular scale placed upon one gear, so that after calibration, the test section Mach Number can be arbitrarily adjusted from the outside during the run. Another device for Mach Number indication on photographs or films is mounted in the light beam of the schlieren system. At the inlet, a thin (1 mm.) spring is fixed with one end upon the nozzle block and the other on rollers running in tracks in the floor and bottom. The spring osculates to two contour blocks, one moving with the nozzle block and the other fixed to the floor and bottom. (See Figs. 5 and 9.)

TABLE 4
The Nozzle Shape According to Foelsch: IOBA′ as in Table 3

Point	ξ	x', mm.	y, mm.
O	−0.773	0	49.12
B	−0.684	27.9	50.10
A′	0	243.4	65.17
	0.044	257.4	66.10
	0.226	313.5	69.14
	0.318	343.6	70.31
	0.419	375.4	71.26
	0.525	408.8	71.82
F′	0.672	455.2	72.15

TABLE 5
The Nozzle Shape According to the Spring Calculation
$\varphi_1 = 8.6°$

Point	ξ	x', mm.	y_A, mm.	$\varphi^0(\xi)$
O	−0.868	0	16.93	0
B	−0.678	59.8	21.43	8.60
A″	0	273.4	53.73	8.60
	0.05	289.2	...	8.40
	0.1	304.9	58.36	7.95
	0.2	336.4	62.44	6.77
	0.3	367.9	65.84	5.56
	0.4	399.4	68.58	4.44
	0.5	430.9	70.75	3.45
	0.6	462.4	72.40	2.57
	0.7	493.9	73.60	1.80
	0.8	525.4	74.40	1.13
	0.9	556.9	74.86	0.53
F	1.0	588.4	75.00	0.0

TABLE 6
The Nozzle Shape According to Foelsch: IOBA″ as in Table 5

Point	ξ	x', mm.	y, mm.
O	−0.868	0	16.93
B	−0.678	59.8	21.43
A″	0	273.4	53.73
	0.069	295.1	56.88
	0.217	341.7	62.82
	0.392	396.8	68.52
	0.595	460.8	73.64
	0.835	536.6	77.84
	1.122	626.7	80.58
F″	1.354	700.1	81.23

SCHLIEREN SYSTEM

For flow visualization in the test section two separate schlieren systems are used, which work perpendicular to one another as in Fig. 10.

The principal of these two systems can be fed alternatively by continuous light or by a spark (1–2μsec). The change of light source is performed by a pneumatically controlled mirror to allow both continuous observation during the run and instantaneous photog-

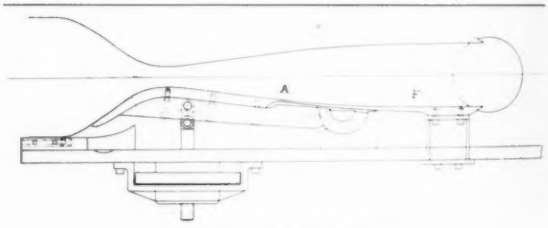

Fig. 5. Representation of nozzle assembly

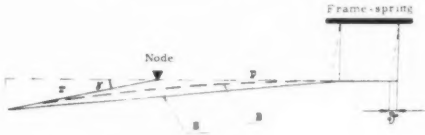

Fig. 6. Deformation of frame-spring

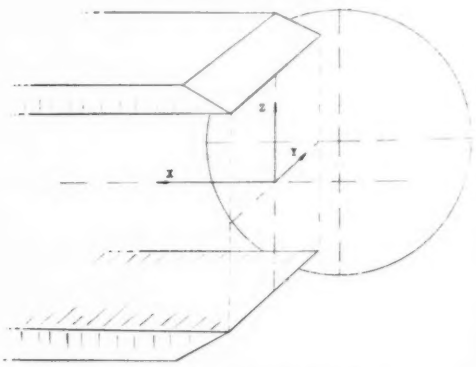

Fig. 7. Coordinate-system at test section

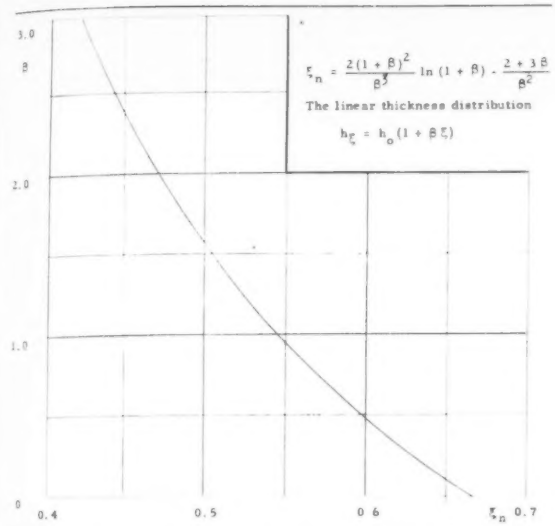

FIG. 8. The coefficient β versus the ξ-coordinate of the node.

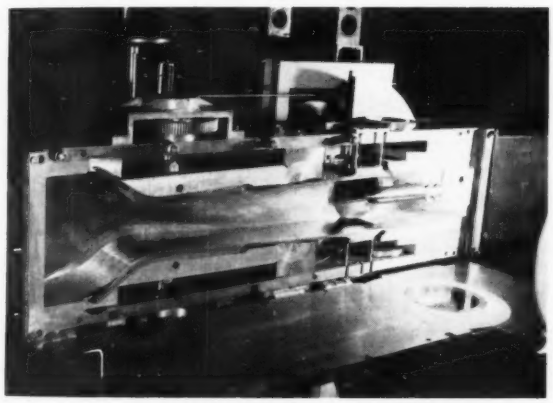

FIG. 9. Photograph of nozzle assembly.

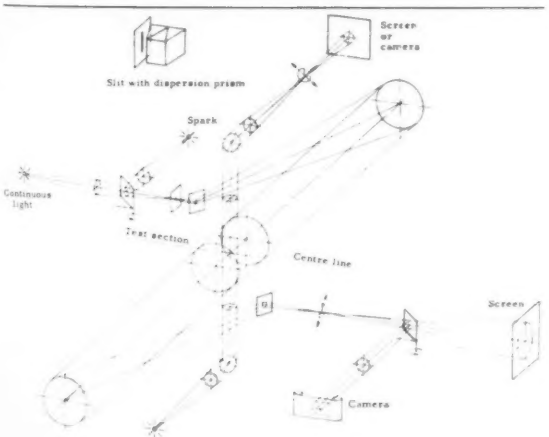

FIG. 10. Assembly drawing of schlieren system.

raphy. From the first slit the light beam passes via two spherical mirrors (250 mm. diameter and f = 500 mm.) to the second slit or cut-off edge. After that it goes to a large screen or via another pneumatically controlled mirror to a camera.

In order to take coloured schlieren photographs, a dispersion prism can be attached immediately after the slit. The schlieren edge is then replaced by a slit large enough to let one color through when the pressure is constant in the test section.

The vertical parallel light beam is produced by a spark in the focus of a lens of 80 mm. diameter and f = 1,000 mm. The camera side is optically identical and fitted with pneumatically controlled cutoff edges. (See Fig. 10.)

RESULTS AND DISCUSSION

The complete results of the tunnel calibrations are shown in Fig. 11. A compilation of the nozzle calibration results is given in Table 7, where the Mach Number divergences are shown for all Mach Numbers. The accuracy of measuring the Mach Number was determined from the scatter of test points obtained from several tests made under the same conditions. The

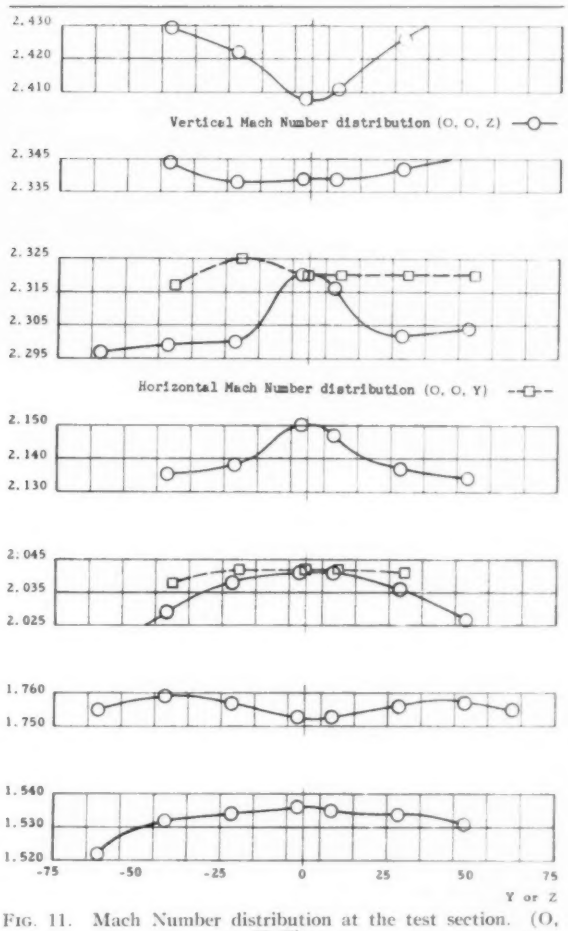

FIG. 11. Mach Number distribution at the test section. (O, Y, Z).

TABLE 7

Summary of Nozzle Calibration Results

(Because a fix diffuser was used during the calibration, the flow could sometimes separate before the exit of the nozzle. This explains why some values in Table 7 are excluded.)

Vertical rake: O, O, Z

M_1 theor. \ Z mm.	−62	−42	−22	−2	8	28	48	$M_{1\ med.}$	$M_{1\ max.}$
1.602	(1.522)	1.532	1.534	1.536	1.535	1.534	1.531	1.533	±0.003
1.833	1.755	1.759	1.757	1.753	1.753	1.756	1.757	1.756	±0.003
2.065		2.029	2.038	2.041	2.041	2.036	2.027	2.035	±0.008
2.160			2.138	2.150	2.147	2.137	2.134	2.141	±0.009
2.391	(2.296)	2.299	2.300	2.320	2.316	2.302	2.304	2.307	±0.013
2.450		2.344	2.338	2.339	2.339	2.342		2.340	±0.004
2.533		2.429	2.422	2.408	2.411	2.426		2.419	±0.011

Horizontal rake: O, Y, O

M_1 theor. \ Y mm.	−60	−40	−20	0	10	30	50	$M_{1\ med.}$	$M_{1\ max.}$
2.065		2.028	2.042	2.042	2.042	2.041			
2.261	(2.215)	2.229	2.230	2.230	2.229	2.231	2.224	2.229	±0.005
2.391		2.317	2.325	2.320	2.320	2.320	2.220	2.320	±0.005

error in the Mach Number measurement in the whole region was thus less than ±0.007.

The two springs are symmetrically mounted with an accuracy of ±0.02 mm., which explains the good horizontal Mach Number distribution (±0.005). The vertical Mach Number distribution is also good, especially for Mach Numbers lower than 2.00 (±0.008). This is obvious, due to the fact that the curvatures of the nozzle in this region are very small. Above Mach Number 2.00, however, the divergences become greater (±0.013) until the design Mach Number is reached (≈2.39, theoretically 2.50). For even higher Mach Numbers the divergences increase once again and the Mach Number profile also changes character. (See Fig. 11.)

CONCLUSIONS

A method of designing a symmetrical flexible-wall nozzle for continuous variation of the Mach Number has been developed by using small wall curvatures in the lower Mach Number region and by applying the Foelsch theory for a higher Mach Number (2.50). The results show the variation in Mach Number to be ±0.015 or less. The range of Mach Numbers from 1.5 to 2.5 was obtained by one single screw mechanism.

The length of the nozzle from the minimum section to the beginning of the experimental test section was approximately constant and measured 4.5 test section heights.

REFERENCES

[1] Dhawan, Satish and Roshko, Anatol, *A Flexible Nozzle for a Small Supersonic Windtunnel*, Journal of the Aeronautical Sciences, Vol. 18, No. 4, pp. 253–258, April, 1951.

[2] Foelsh, K., *A New Method of Designing Two-Dimensional Laval Nozzles*, North American Aviation, Inc. Report NA-46-235-2.

[3] Hilding, Lars O., *Lavalmunstycken*, Division of Steam Engineering, Royal Institute of Technology, Stockholm. Report KTHÅ 1/0.04.

Laminar Compressible Boundary Layer . . .

(*Continued from page 454*)

a weak foundation upon which to build an approximate method of solution.

REFERENCES

[1] Flügge-Lotz, I., and Eichelbrenner, E. A., *La Couche Limite Laminaire dans L'Écoulement Compressible le long d'une Surface Courbé*, ONERA, Rapport No. 1/694 A, 1948. (A short résumé of this paper is offered as appendix to the report: Gruschwitz, E., and Eichelbrenner, E. A., *Calcul Approché de la Couche Limite Laminaire en Écoulement compressible sur une Paroi non conductrice de la Chaleur*, ONERA, No. 47, Châtillon-sous-Bagneux, Seine, 1950).

[2] Pohlhausen, K., *Zur näherungsweisen Integration der Differentialgleichungen der laminaren Reibungschicht*, ZAMM 1, 1921.

[3] Schlichting, H., *Lecture Series "Boundary Layer Theory," Part I—Laminar Flows*, NACA T. M. 1217.

[4] Johnson, A. F., *Laminar Boundary Layer of a Compressible Fluid Passing over a Curved Insulated Surface*, Stanford University, Tech. Rep. No. HS-5, Navy contract N6-ONR-251 Task Order VI (NR-035-104).

[5] Mangler, W., *Zusammenhang zwischen ebenen und rotationssymmetrischen Grenzschichten in kompressiblen Flüssigkeiten*, ZAMM 28, 1948.

[6] Crocco, L., *Lo Strato Limite Laminare nei Gas*, Monografie Scientifiche di Aeronautica, No. 3, Rome, 1946.

[7] Howarth, L., *On the Solution of the Laminar Boundary Layer Equations*, Proc. Roy. Soc. Lond. A, No. 919, Vol. 164, 1938.

[8] Mangler, W., *Das Impulsverfahren zur näherungsweisen Berechnung der laminaren Reibungsschicht*, ZAMM 24, 1944.

[9] Gruschwitz, E., *Calcul Approché de la Couche Limite Laminaire en Écoulement compressible sur une Paroi non conductrice de la Chaleur* (see reference 1).

On the Buckling of Stringer Panels Including Forced Crippling*

P. P. BIJLAARD†

Bell Aircraft Corporation

ABSTRACT

The analysis considers the effective moment of inertia of the stiffeners when located on one side of the plate and the effective width of the plate at the unloaded edges. It is shown that the rigid beam webs supporting the unloaded edges of the plate greatly increase the effective width of the plate acting with the first stiffener.

Also considered in the analysis are the effects of shear deformation of the stiffener web and the flexibility of the attached flange of the stiffener; each may cause an approximate 10 per cent reduction in the effective moment of inertia in computing the critical stress for the case in which the column deflection of the stiffeners predominates.

An explicit formula is presented for the critical stress for buckling in the forced crippling mode, which is valid for panels having any number of stiffeners. A rapid method for computing the buckling stress is given.

NOMENCLATURE

a	= half wave length of buckles in the direction of the compressive force (X-direction)
b	= width of a bay
b_a	= distance between the rivet line and the middle plane of the stiffener web
c	= spring constant in case of buckling in the forced crippling mode in reference 6
e	= distance of middle plane of skin to axis of gravity of beam webs that bound a stringer panel
f	= effective flange width of stiffener
k	= $[(b^2t)/(\pi^2D)]\sigma$, buckling stress coefficient
n	= number of bays in a stringer panel
p	= pitch of rivets in attached stringer flange
s, q	= parameters in expression for k_2' in Eq. (61)
r	= radius of gyration
t	= plate thickness
u	= displacement in the X-direction
v	= displacement in the Y-direction
w	= deflection (in the Z-direction)
x, y	= coordinates
z	= distance of center of gravity of effective stiffener cross section to middle plane of skin
z_s	= distance of center of gravity of stiffener proper to middle plane of skin
A, C_1, C_2, C_3, C_4	= constants
A_e, A_s	= effective area of cross section of bounding beam webs and area of cross section of stiffeners proper, respectively
B	= nb, width of stringer panel
C	= spring constant or foundation modulus
D	= flexural rigidity of plate
E	= modulus of elasticity
G	= modulus of rigidity
I	= effective moment of inertia of stiffeners
I'	= effective moment of inertia of stiffeners, taking account of flexibility of attached stiffener flange
I''	= effective moment of inertia of stiffeners, taking account of shear deformation of stiffener web and of flexibility of attached stiffener flange
I_s	= moment of inertia of stiffeners proper
K_{cr}	= buckling stress coefficient for forced crippling applying for an infinite number of panels
L	= length of stringer panel
R	= $(c_{eq}b^3)/(\pi^4D)$, parameter in theory of buckling in the forced crippling mode
T	= excess tension in the skin in case of upward buckling of stringer panel
V	= transverse shear force in stiffener
X, Y, Z	= coordinate axes
α	= k_2'/k_1 in Eq. (60)
β	= a/b, ratio between half wave length and width of a bay
γ	= coefficient of interaction in method of split rigidities
δ	= A_s/bt
δ_e	= A_e/bt
ϵ	= quantity that is small with respect to unity
λ	= π/a
ν	= Poisson's ratio
σ	= normal stress
τ	= shear stress
θ	= coefficient of interaction in method of split rigidities
Φ	= Airy's stress function

Subscripts

b	= bending
cr	= critical
e	= effective
eq	= equivalent
f	= caused by bending of attached stiffener flange
fc	= forced crippling
g	= web beam
i	= infinite
m	= maximum deflection, amplitude
o	= refers to "outer" as additional subscript to b_e or f_2
s	= stiffener, except as additional subscript to k, b_e, or B_e, where it refers to "simply supported" or as subscript to C, where it refers to "shear"
u	= upper
w	= web

Received January 21, 1954. Revised and received November 29, 1954.

* This is part of a study undertaken by the author at the request of the Bell Aircraft Corporation. The author wishes to thank the Bell Aircraft Corporation for permission to publish these results and for the helpful advice and guidance given him by Messrs. Arthur Schnitt, Alexander Krivetsky, and George S. Johnston.

† Consultant. Also, Professor of Structural Engineering, Cornell University.

1, 2, 3 = refers to the number of stiffeners in the stringer panel

Introduction

The problem of buckling of stringer panels into the conventional mode has been treated in several publications.[1, 2, 3] However, at the writing of the subject report, none of the references offered any suggestions for the evaluation of the effective moment of inertia for an arbitrary number of stiffeners located on one side of a panel. This problem was brought to the attention of the author whose investigation resulted in a report on the effective moment of inertia of stiffeners in stiffened flat plate panels with 1, 2, 3, and an infinite number of stiffeners.[4] Recently, somewhat similar calculations were published in reference 5. Reference 5 assumes that the unloaded edges $y = 0$ and $y = nb$ of the skin are not restrained in the X-direction (Fig. 1), so that the shear stresses, τ_{xy}, are zero here. On the other hand, reference 4 takes into account, in a conservative way, the attachment between the skin and the beam webs. It also considers the flexibility of the attached stringer flange, which results in a decrease of the effective moment of inertia of the stiffeners.

In the present paper, formulas are derived for the effective moment of inertia of the stiffeners, taking into account the compatibility of the strains in the skin and beam webs OA and CD (Fig. 1) and the reduction of the effective moment of inertia of the stiffeners by the shear deformation of the stiffener web and by the flexibility of the attached stiffener flange. General formulas are given for buckling into the forced crippling mode, extending reference 6, which presupposes panels with a large number of stiffeners.

Determination of the Effective Moment of Inertia of the Stiffeners

The stringer panels considered are assumed to consist of a skin supported by stiffeners of equal cross section, located at equal distances b, and to be bounded by webs (Fig. 1). The panel is loaded by compressive stresses in the direction of the stiffeners.

The determination of the effective moment of inertia of the stiffeners which has to be taken into account in computing the buckling stress of the stringer panel reduces to that of determining the effective width of the skin which can be taken into account as flange of the stiffeners. This effective width will be computed for a plate (skin) with one stiffener (Fig. 2) and for a plate with an infinite number of stiffeners. From these cases those for plates with 2 and with 3 stiffeners will be derived. The effective moments of inertia of the stiffeners so determined will be reduced to take account of shear deformation of the stiffener web and of the flexibility of the attached stiffener flange.

Plate with One Stiffener

In this case (Fig. 2) the number of bays $n = 2$. It is assumed that plate and stiffener buckle in half waves a which vary sinusoidally in the X-direction, which assumption will subsequently be proved to be exact. Hence the deflection of the stiffener is

$$w_s = w_{sm} \sin \lambda x \tag{1}$$

where

$$\lambda = \pi / a \tag{2}$$

Assuming that in the half wave length as presented in Fig. 2 the stiffener is buckling upwards, at incipient buckling according to Fig. 2b excess tensile stresses σ_z will be introduced in the skin (plate). These stresses σ_x may vary in the Y-direction as shown in Fig. 2d. The entire state of stress in the skin will have to satisfy the differential equation (reference 7, page 25)

$$(\partial^4\Phi/\partial x^4) + \{2[\partial^4\Phi/(\partial x^2\partial y^2)]\} + (\partial^4\Phi/\partial y^4) = 0 \tag{3}$$

where Φ is Airy's stress function and

$$\left.\begin{aligned} \sigma_x &= \partial^2\Phi/\partial y^2 \\ \sigma_y &= \partial^2\Phi/\partial x^2 \\ \tau_{xy} &= -\partial^2\Phi/(\partial x\partial y) \end{aligned}\right\} \tag{4}$$

Eq. (3) is satisfied by

$$\Phi = Y \sin \lambda x \tag{5}$$

where Y is a function of y alone and λ is given by Eq. (2). Inserting Eq. (5) into Eq. (3), its general solution is (reference 7, page 45)

$$\Phi = (C_1 \cosh \lambda y + C_2 \sinh \lambda y + C_3 y \cosh \lambda y + C_4 y \sinh \lambda y) \sin \lambda x \tag{6}$$

The effective width b_{eo} of a bay of width b (Fig. 2d) is determined by the condition that, assuming the excess tensile force T in it to be equally distributed over the width b_{eo}, the strain in the X-direction should be equal to the actual strain at $y = 0$ (Fig. 2a), so that

$$T/(b_{eo}tE) = (\sigma_x - \nu\sigma_y)_{y=0}/E \tag{7}$$

The excess tension T in a bay, being introduced into it by the shear stresses τ_{xy} at $y = 0$, may be expressed as

$$T = t \int_0^x (\tau_{xy})_{y=0}\, dx \tag{8}$$

From Eqs. (4) and (6) τ_{xy} is proportional to $\cos \lambda x$. Let

$$(\tau_{xy})_{y=0} = A \cos \lambda x \tag{9}$$

Then from Eqs. (7), (8), and (9)

$$b_{eo} = (A/\lambda)\,[\sin \lambda x/(\sigma_x - \nu\sigma_y)_{y=0}] \tag{10}$$

Using Eqs. (4) and (6), this becomes

$$b_{eo} = A/\{\lambda^2[C_1(1 + \nu)\lambda + 2C_4]\} \tag{11}$$

From Eq. (11) the effective width b_{eo} is independent of x, so that the stiffener (stringer) will behave as if it had a flange of constant width $2b_{eo}$ along which the stress is equally distributed. Hence the stringer behaves as if it has a constant moment of inertia I. The assumed sinusoidal distribution of the skin deflection in the X-direction satisfies the differential equation for its deflection (reference 1, page 337)

$$D\nabla^4 w + t\sigma_x(\partial^2 w/\partial x^2) = 0 \tag{12}$$

From symmetry only half of the stiffener can be considered as support of the edge of the bay to the right (Fig. 2), so that from Eq. (r) on page 346 of reference 1 one of the boundary conditions of the skin at $y = 0$ is

$$1/2\, EI\, (\partial^4 w/\partial x^4) = -D\{(\partial^3 w/\partial y^3) + (2 - \nu)\, [\partial^3 w/(\partial x^2 \partial y)]\} - (1/2) A_s \sigma_x (\partial^2 w/\partial x^2) \tag{13}$$

where A_s is the cross section of the stringer proper. Since this boundary condition contains only even derivatives with respect to x, it is satisfied by a sinusoidal distribution in the X-direction of the deflections of stringer and skin. The other boundary conditions (Fig. 2), $\partial w/\partial y = 0$ at $y = 0$ and $w = 0$ and $\partial^2 w/\partial y^2 = 0$ at $y = b$, are independent of the distribution of the deflection in the X-direction. Hence the sinusoidal stringer deflection assumed in Eq. (1) is indeed correct.

The constants C_1 and C_4 in Eq. (11) have to be determined from the boundary conditions at $y = 0$ and $y = b$. One of the conditions at $y = 0$ is given by Eq. (9). The other condition is, from symmetry, that the displacements v in the Y-direction are zero, or rather, as was used in reference 8 for determining the effective width of the flanges of I beams, that the curvature of the edge $y = 0$ in the plane of the plate is zero:

$$(\partial^2 v/\partial x^2)_{y=0} = 0 \tag{14}$$

To express Eq. (14) in terms of Φ one obtains from Eqs. (4)

$$\tau_{xy} = G[(\partial u/\partial y) + (\partial v/\partial x)] = -\partial^2 \Phi/(\partial x \partial y)$$

where u is the displacement in the X-direction and G is the modulus of rigidity. Hence

$$\partial v/\partial x = -(1/G)\, [\partial^2 \Phi/(\partial x \partial y)] - (\partial u/\partial y)$$

$$\partial^2 v/\partial x^2 = -(1/G)\, [\partial^3 \Phi/(\partial x^2 \partial y)] - [\partial^2 u/(\partial x \partial y)] \tag{15}$$

In here $\partial u/\partial x$ may be expressed in terms of the strain ϵ_x, so that, using Eqs. (4),

$$\partial u/\partial x = \epsilon_x = (1/E)\, (\sigma_x - \nu\sigma_y) = (1/E)\, [(\partial^2 \Phi/\partial y^2) - \nu(\partial^2 \Phi/\partial x^2)] \tag{16}$$

After inserting this into Eq. (15), Eq. (14) can be written as

$$\big((1/G)\, [\partial^3 \Phi/(\partial x^2 \partial y)] + (1/E)\, \{(\partial^3 \Phi/\partial y^3) - \nu[\partial^3 \Phi/(\partial x^2 \partial y)]\}\big)_{y=0} = 0 \tag{17}$$

The outer edges $y = \pm b$ of the plate have a zero deflection w. They are assumed to be connected to edge members, running in the X-direction, with effective cross sections A_e (Figs. 2a and 2c). Here "effective cross section" means the cross section of a bar, concentrated at $y = b$ or $y = -b$, and in the plane of the plate, which has the same rigidity against elongation by a force at $y = \pm b$ and in the plane of the plate as the actual member. (The way to calculate A_e is shown in the Appendix.) Hence from Fig. 2e one of the boundary conditions at $y = b$ is

$$t\tau_{xy}\, dx - A_e\, d\sigma_x = 0$$

or

$$[t\tau_{xy} - A_e(d\sigma_x/dx)]_{y=b} = 0 \tag{18}$$

Further one has

$$(\sigma_y)_{y=b} = 0 \tag{19}$$

From the four boundary conditions, Eqs. (9), (17), (18), and (19), using Eqs. (4) and (6), one finds

$$\left.\begin{aligned} C_1 &= \frac{(1-\nu)\lambda b\delta_e \sinh 2\lambda b + (1+\nu)\lambda^2 b^2(1+2\delta_e) + (1-\nu)\sinh^2 \lambda b}{2\lambda^3 b + (2\lambda b\delta_e \coth \lambda b + 1)\lambda^2 \sinh 2\lambda b} A \\ C_2 &= -[(1-\nu)/2\lambda^2]A \\ C_3 &= -[(1+\nu)/2\lambda]A \\ C_4 &= \left(\frac{1-\nu}{2\lambda^2 b} + \frac{1+\nu}{2\lambda}\coth \lambda b\right)A - \frac{C_1}{b}\coth \lambda b \end{aligned}\right\} \tag{20}$$

where

$$\delta_e = A_e/(bt) \tag{21}$$

Insertion of C_1 and C_4 into Eq. (11) yields

$$b_{cr} = \frac{4\{\delta\,(1 + \cosh 2\lambda b) + [(\sinh 2\lambda b)/(2\lambda b)] + 1\}}{2(1+\nu)^2\lambda^2 b^2(2\delta_e + 1) + (5 - 2\nu + \nu^2) + (1+\nu)\,(3-\nu)\,(2\delta_e \lambda b \sinh 2\lambda b + \cosh 2\lambda b)}\, b \tag{22}$$

where

$$\left.\begin{aligned} \lambda b &= \pi/\beta \\ \beta &= a/b \end{aligned}\right\} \tag{23}$$

If $A_e = \delta_e = 0$, Eq. (22) reduces to

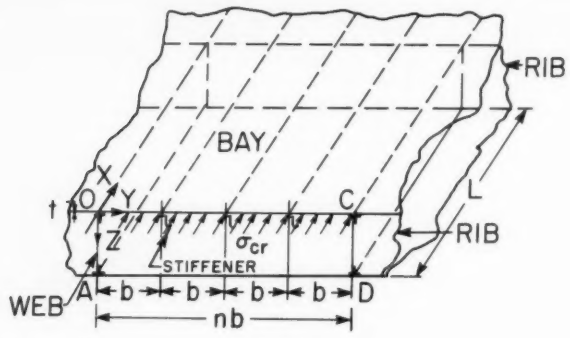

FIG. 1.

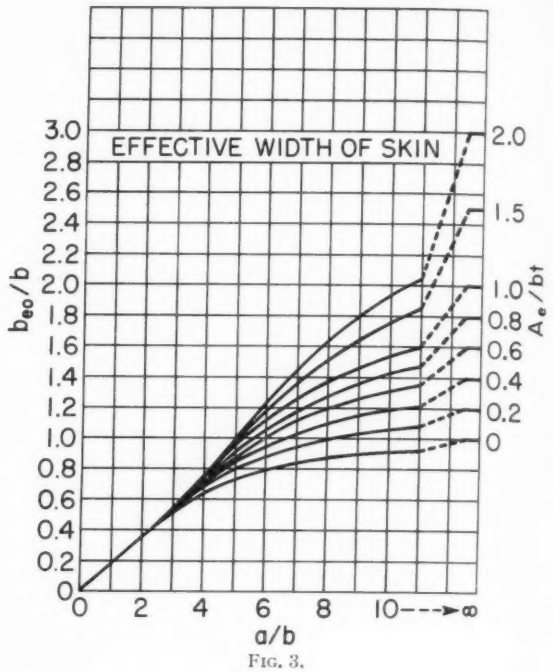

FIG. 3.

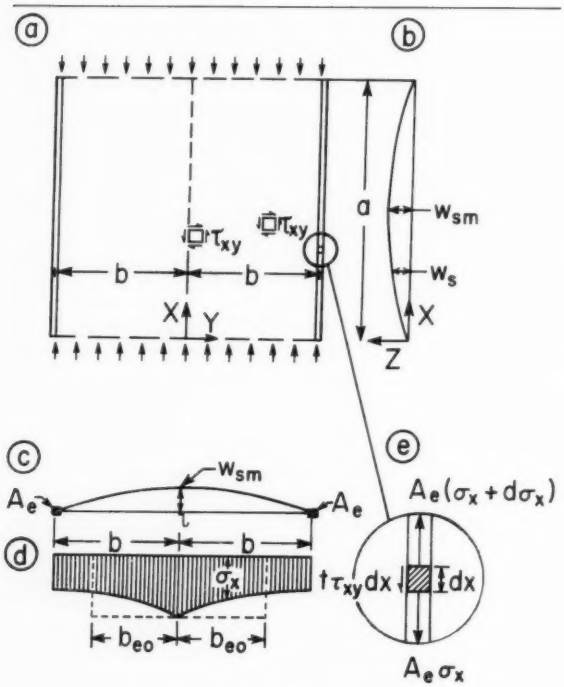

FIG. 2.

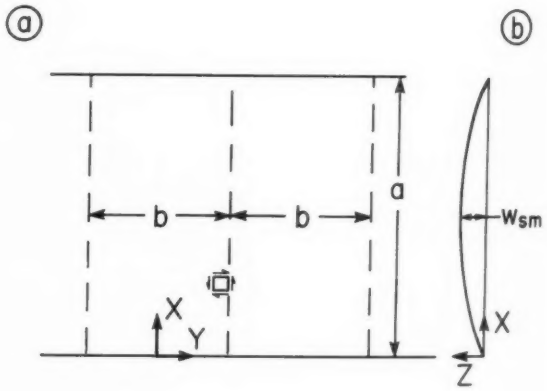

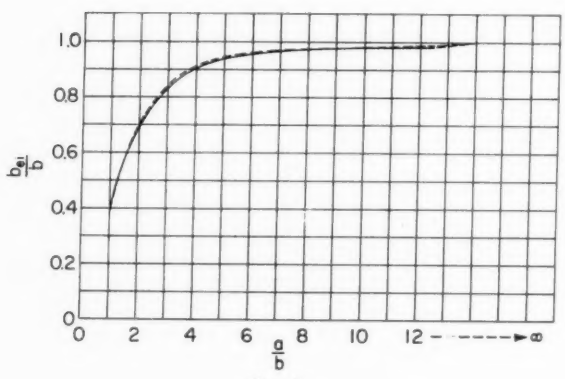

FIG. 5.

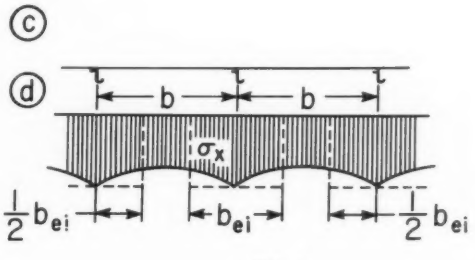

FIG. 4.

$$b_{e0} = \frac{2}{\lambda b} \frac{\sinh 2\lambda b + 2\lambda b}{(1+\nu)(3-\nu)\cosh 2\lambda b + 2(1+\nu)^2\lambda^2 b^2 + 5 - 2\nu + \nu^2} b \tag{24}$$

Eq. (22) is represented graphically in Fig. 3 for $A_e/(bt)$ between zero and two.

Plate with an Infinite Number of Stiffeners

Eqs. (1) and (6) also apply in this case (Fig. 4). Similarly to Eq. (7) the effective width b_{ei} is determined by the equation (Fig. 4)

$$T/(b_{ei}tE) = (\sigma_x - \nu\sigma_y)_{y=b/2}/E \tag{25}$$

where from Fig. 4 the tensile force T in a subpanel of width b is

$$T = -2t\int_0^x (\tau_{xy})_{y=b/2}\,dx \tag{26}$$

Assuming

$$(\tau_{xy})_{y=b/2} = -A\cos\lambda x \tag{27}$$

from Eqs. (25), (26), and (27), neglecting $\nu\sigma_y$ with respect to σ_x,

$$b_{ei} = (2A/\lambda)\,[\sin\lambda x/(\sigma_x)_{y=b/2}] \tag{28}$$

The reason for neglecting the influence of σ_y is the following. If at $x = 0$ a half wave, buckling upwards, is adjacent to a half wave that buckles downwards, from consideration of antisymmetry at $x = 0$ the displacement v in the Y-direction will be zero there. In other cases v at $x = 0$ will practically remain zero owing to restraint by the connection of the skin to a rib. With an infinite number of panels of width b a line $y = b/2$ will remain straight, so that then everywhere at $y = b/2$ the displacement v is zero. This means that the contraction in the Y-direction is restrained, so that for large a/b ratios the apparent modulus of elasticity for extension in the X-direction is increased from E to $E \div (1-\nu^2)$ as a consequence of the stresses $\sigma_y = \nu\sigma_x$ generated in the Y-direction. Since the effective width b_{ei} actually is used for cases where n is finite and the contraction in the Y-direction will be fully prevented only if nb is large with respect to a, lest b_{ei} is overestimated, the influence of σ_y was neglected in Eq. (28). Only for small β values, where σ_y is opposite in sign to σ_x, the influence of σ_y decreases b_{ei}, but the difference is negligible here.

From symmetry in the present case Eq. (6) reduces to

$$\Phi = (C_1\cosh\lambda y + C_4 y\sinh\lambda y)\sin\lambda x \tag{29}$$

Using Eqs. (4) and (29), Eq. (28) becomes

$$b_{ei} = 2A/\{\lambda^2[C_1\lambda\cosh(\lambda b/2) + C_4[2\cosh(\lambda b/2) + (\lambda b/2)\sinh(\lambda b/2)]]\} \tag{30}$$

The boundary conditions at $y = b/2$ are given by Eq. (27) and by the condition that the edge $y = b/2$ remains straight, as discussed above. Analogous to Eq. (17) this condition is

$$((1/G)\,[\partial^3\Phi/(\partial x^2\partial y)] + (1/E)\,\{(\partial^3\Phi/\partial y^3) - \nu[\partial^3\Phi/(\partial x^2\partial y)]\})_{y=b/2} = 0 \tag{31}$$

Using Eqs. (4) and (29) the conditions (27) and (31) yield

$$\left.\begin{aligned} C_1 &= \{[(1-\nu)\sinh(\lambda b/2) - (1+\nu)(\lambda b/2)\times \\ &\qquad \cosh(\lambda b/2)]/[2\lambda^2\sinh^2(\lambda b/2)]\}A \\ C_4 &= \{(1+\nu)/[2\lambda\sinh(\lambda b/2)]\}A \end{aligned}\right\} \tag{32}$$

Insertion of C_1 and C_4 into Eq. (30) gives

$$b_{ei} = ([4(\cosh\lambda b - 1)]/\{\lambda[(3+\nu)\times \sinh\lambda b - (1+\nu)\lambda b]\})b \tag{33}$$

where $\lambda b = \pi/\beta$. Eq. (33) is presented graphically in Fig. 5. It was also given as Eq. (101) in reference 6.

Plate with an Arbitrary Number of Stiffeners

For a plate with an arbitrary number of stiffeners the boundary conditions are less simple. For example, for the plate with two stiffeners in Fig. 6a, assuming it to buckle into one half wave in the Y-direction (Fig. 6b), the stresses or displacements at the edge $y = b/2$ of the center bay are not directly known. This edge neither remains straight, nor are the stresses σ_y equal to zero. It may be shown, however, that the stresses σ_y at the edges do not appreciably influence the effective width b_e. This may be done by comparing the case of an infinite number of stiffeners, dealt with in the preceding section, where the edge $y = b/2$ remained straight, with the case of a single bay reinforced by stiffeners at both edges, where at the edges $y = \pm b/2$ the stresses σ_y vanish (Fig. 6d). Also for this case Eqs. (29) and (30) may be used. The boundary conditions at $y = b/2$ are given by Eq. (27) and by

$$(\sigma_y)_{y=b/2} = 0 \tag{34}$$

Using Eqs. (4) and (29), Eqs. (27) and (34) yield

$$\left.\begin{aligned} C_1 &= -\{[b\sinh(\lambda b/2)]/[\lambda(\sinh\lambda b + \lambda b)]\}A \\ C_4 &= \{[2\cosh(\lambda b/2)]/[\lambda(\sinh\lambda b + \lambda b)]\}A \end{aligned}\right\} \tag{35}$$

These constants are similar to A_n and D_n in reference 8, referring to box and U beams under transverse loading, where the same boundary conditions [Eqs. (27) and (34)] apply, if in there $2b$, K_n, and α_n are replaced by b, A, and λ, respectively. Insertion of C_1 and C_4 into Eq. (30) gives the effective width

$$b_{es} = \{(\sinh\lambda b + \lambda b)/[\lambda b(\cosh\lambda b + 1)]\}b \tag{36}$$

where $\lambda b = \pi/\beta$. Eq. (36) is given in Fig. 5 by the dashed curve. Comparison with the solid curve for b_{ei} shows indeed that the influence upon the effective width of the stresses σ_y at the edges $y = \pm b/2$ is extremely little. This is partly due to the neglect of σ_y in Eq. (25), of which the reason was explained in the preceding section. Hence, in the case of an arbitrary

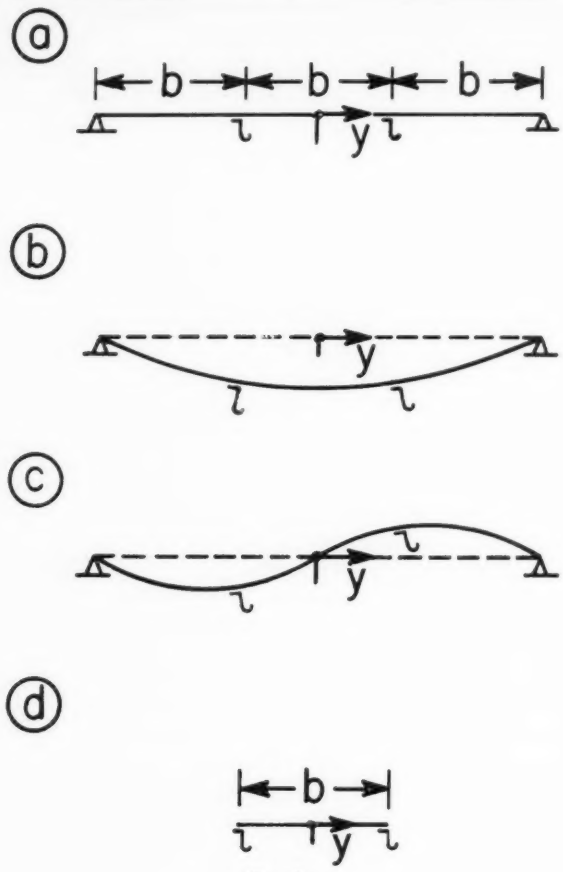

FIG. 6.

number of panels and assuming buckling into one half wave in the Y-direction, it will be appropriate to assume the effective width of the internal bays equal to b_{ei} from Eq. (33) and that of the external (outer) bays equal to b_{eo} from Eq. (22).

Effective Width of Stiffener Flanges

(*A*) *Plate with One Stiffener* ($n = 2$)—From the above section of the same title it is evident that the effective width of the stiffener flange is

$$f_{e1} = 2b_{eo} \tag{37}$$

where b_{eo} is given by Eq. (22) and Fig. 3. The way to determine A_e is shown in the Appendix.

(*B*) *Plate with Two Stiffeners* ($n = 3$)—For buckling with one half wave in the Y-direction (Fig. 6b) it follows from symmetry that the effective width of the flange of each stiffener is equal to the effective width b_{eo} of an outer bay plus half the effective width b_{ei} of the center panel, so that

$$f_{e2} = b_{eo} + (1/2)b_{ei} \tag{38}$$

where b_{eo} is given by Eq. (22) and Fig. 3 and b_{ei} is given by Eq. (33) and by the solid curve in Fig. 5. From reference 3 buckling into two half waves in the Y-direction is practically not governing. Since reference 3 deals with stiffeners with given flexural rigidities, this applies if for both modes (one and two half waves in the Y-direction) the effective width of the stiffener flange would be the same. Actually in the case of two half waves (Fig. 6c) from antisymmetry with respect to the line $y = 0$ the latter will not change in length, so that for each half wave it will act as a member with an infinite cross section A_e. Therefore, in the case of two half waves the effective width of the flange of each stiffener is larger than that from Eq. (38), so that buckling into two half waves in the Y-direction is still less likely to be governing.

(*C*) *Plate with Three Stiffeners* ($n = 4$)—For the same reasons as in the former case, also here only buckling with one half wave in the Y-direction is considered. For small ratios $\beta = a/b$ the excess normal stresses σ_x in the stiffener flanges (the plate) will not influence each other much, so that the effective flange width of the outer stiffeners is about

$$f_{3o} = b_{eo} + (1/2)b_{ei} \tag{39}$$

while that of the center stiffener is

$$f_{3c} = b_{ei} \tag{40}$$

From Figs. 3 and 5 it may be seen that for small ratios β the flange widths f_{3o} and f_{3c} will not differ much, so that also the effective moments of inertia of the stiffeners are practically equal. In that case, from reference 9, the deflection varies sinusoidally in the Y-direction, so that the deflections of the outer stiffeners are $(1/\sqrt{2})$ times the deflection of the center one. Since the internal work stored in the stiffeners is proportional to the square of their deflections, the influence of the moment of inertia of the outer stiffeners on the total internal work to be done at buckling is about $(1/\sqrt{2})^2 = {}^1/_2$ times that of the moment of inertia of the center stiffener. Hence, the moment of inertia of the two outer stiffeners together has about the same influence as that of the center stiffener alone. Therefore, the effective flange width of all stiffeners may be assumed to be the average of f_{3o} and f_{3c} from Eqs. (39) and (40), so that

$$f_{e3} = (1/2)b_{eo} + (3/4)b_{ei} \tag{41}$$

where b_{eo} and b_{ei} are given in Figs. 3 and 5. If, for example, $A_e = 0$, for large a/b ratios, from Figs. 3 and 5, $b_{eo} = b_{ei} = b$. From Eq. (41) this leads to a total flange width for the three stiffeners of 3.75 b, which is somewhat smaller than the actual total effective width of 4b.

(*D*) *Plate with an Infinite Number of Stiffeners*—From the above section with the same title the effective flange width of all stiffeners is

$$f_{ei} = b_{ei} \tag{42}$$

where b_{ei} is given by Eq. (30) and Fig. 5.

EFFECTIVE MOMENT OF INERTIA OF A STIFFENER

The flexural rigidity of the skin (plate) is fully accounted for in the action of the skin as a plate.

Therefore, in computing the effective moment of inertia of a stiffener the rigidity of the plate against extension alone is taken into account. If A_s, I_s, and z_s are the cross section and proper moment of inertia of the stiffener and the distance of its center of gravity from the middle plane of the plate, respectively, the center of gravity of the effective stiffener cross section is determined by the distance z (Fig. 7),

$$z = (A_s z_s)/(A_s + f_e t) \tag{43}$$

where f_e follows from Eqs. (37), (38), (41), or (42). Hence, the effective moment of inertia is

$$I = I_s + A_s(z_s - z)^2 + f_e t z^2 \tag{44}$$

Reduction of the Effective Moment of Inertia of a Stiffener by Shear Deformation of the Stiffener Web and Flexibility of the Attached Stiffener Flange

In the case of deformation by bending alone the restraining transverse force R acting on an element of the stiffener of length dx is (Fig. 8)

$$R_b = -dV = EI(d^4w_s/dx^4)\,dx \tag{45}$$

or, using Eq. (1),

$$R_b = \lambda^4 EI w_s\,dx \tag{46}$$

In the case of support of a stiffener, without any flexural rigidity, by an elastic foundation with a modulus C_b, the resisting transverse force per length dx would be $R_b = C_b w_s\,dx$, so that, by comparison with Eq. (46), the flexural rigidity of the stiffener is equivalent to a foundation modulus

$$C_b = \lambda^4 EI \tag{47}$$

The shear deformation of the plate was fully taken into account in calculating its effective width. The shear deformation of the stiffener web causes an angle rotation.

$$\gamma = dw_s/dx = 1.1[V/(A_w G)] \tag{48}$$

where V is the shear force (Fig. 8), A_w is the cross section of the stiffener web, and the factor 1.1 takes account of the variation of the shear stresses in the web in the vertical direction. From Eq. (48) and Fig. 8 the restraining force acting on an element of length dx, if only shear deformation of the web occurs, is

$$R_s = -dV = -(A_w G/1.1)\,(d^2w_s/dx^2)\,dx = \lambda^2(A_w G/1.1)w_s\,dx \tag{49}$$

Denoting the imaginary foundation modulus in the case of shear deformation by C_s, R_s would be $C_s w_s dx$, so that from Eq. (49)

$$C_s = \lambda^2(A_w G/1.1) \tag{50}$$

Hence, the plate may be assumed to be supported by two spring systems, built in series, with spring constants C_b and C_s. Therefore, the total stiffener deflection by a unit transverse load per unit length is

$$w = (1/C_b) + (1/C_s) = (C_b + C_s)/(C_b C_s) = 1/C_{bs}$$

so that the equivalent spring constant is

$$C_{bs} = (C_b C_s)/(C_b + C_s) \tag{51}$$

Using Eqs. (47), (50), and (51), with $G = E/(2 + 2\nu)$ and $\nu = 0.3$, comparison with Eq. (47) shows that the effective moment of inertia of the stiffener is reduced by shear deformation of the web to

$$I' = [1/(E\lambda^4)]C_{bs} = [(a^2 A_w)/(28I + a^2 A_w)]I \tag{52}$$

The reduction of I by shear may be as large as about 10 per cent. From Eq. (52) it will be smaller, the larger the half wave length a is. If in Fig. 9 curve k_{cr} represents k_{cr} in the equation

$$\sigma_{cr} = k_{cr}[(\pi^2 D)/(b^2 t)] \tag{53}$$

for the critical stress, where D is the flexural rigidity of

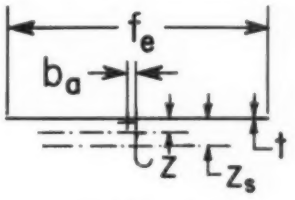

FIG. 7

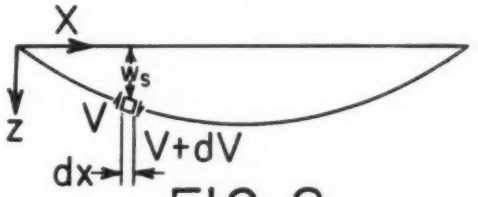

FIG. 8

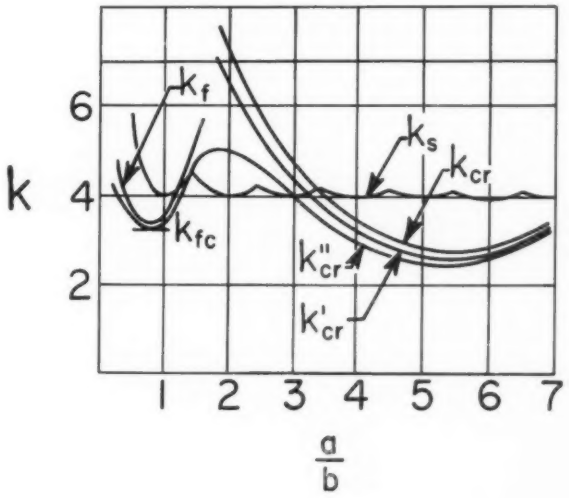

FIG. 9

the skin, without taking account of the reduction of I due to shear, curve k_{cr}' is that taking account of I' from Eq. (52).

If the skin were supported by a stiffener that is infinitely rigid against bending and shear, but with a thin flexible attached flange, its buckling stress coefficient would be given by curve k_f in Fig. 9. The actual buckling stress, taking account of all deformations, will be given by curve k_{cr}'', resulting from interaction of the curves k_f and k_{cr}'. This interaction curve has a similar form as the curve for σ_{cr}, resulting from interaction of the curves σ_1 and σ_2, for plate and column buckling, respectively, in Fig. 1 of reference 10. Curve k_{cr}'' in the present Fig. 9 has a minimum k_{fc} at a small a/b ratio. This is the buckling stress for forced crippling considered in reference 6. The right part of k_{cr}'', for larger a/b ratios, is slightly below the curve for k_{cr}'. This reduction of the long wave buckling stress by flexibility of the attached flange has to be considered here.

The equivalent spring constant C_f as a consequence of the flexibility of the flange is calculated as shown in reference 6 for c_{eq}, but without taking account of the deformation of the stiffener web in its own plane (Case c), which influence may be assumed to be taken into account in C_b and C_s. If only one or a few half waves can occur in the entire structure, it will be safer to assume C_f equal to c_u, referring to the upward half waves in reference 6. Hence, the total deflection by a unit transverse load per unit length, taking account of C_b, C_s, and C_f, is

$$w = (1/C_b) + (1/C_s) + (1/C_f) = 1/C_{bsf}$$

so that the equivalent spring constant is

$$C_{bsf} = (C_bC_sC_f)/(C_bC_s + C_sC_f + C_fC_b) \qquad (54)$$

Using Eqs. (47), (50), and (54) in comparison with Eq. (47) leads to a reduced effective moment of inertia of the stiffener

$$I'' = (1/E\lambda^4)C_{bsf} = \{(a^4A_wC_f)/[A_w(100EI + a^4C_f) + 28a^2IC_f]\}I \qquad (55)$$

Also, the reduction of I by flexibility of the attached flange may amount to about 10 per cent.

In order to avoid complicated calculations, C_f may be assumed to be equal to c_{eq}, as calculated for obtaining the graphs in Figs. 23 and 24 of reference 6, where panels with a large number of bays are considered and

$$R = (c_{eq}b^3)/(\pi^4D) \qquad (56)$$

so that

$$C_f = c_{eq} = (\pi^4D/b^3)R \qquad (57)$$

The pertinent values of R are given in Fig. 10 for various ratios p/b_a, $(b_a/t_s)/(b/t)$ and $(b_w/t_s)/(b/t)$, from which C_f can be calculated by Eq. (57). The distances b, t, b_a, b_w, and t_s are indicated in Fig. A3. Further p is the pitch of the rivets in the attached stringer flange. An example of such a calculation is given in the Appendix.

Buckling in the Forced Crippling Mode

In reference 9 a direct formula was derived for the buckling stress of stringer panels with any number of stiffeners by the method of split rigidities, using the more refined method of comparing the work done by the deflecting and restraining forces, in a way similar to that done in references 11 and 12. This formula yields results that are in practically complete accordance with those from the graphs of reference 3.

From Eq. (47) an elastic support with a foundation modulus c_{eq} is equivalent to support by a stiffener with a flexural rigidity.

$$(EI)_{eq} = c_{eq}/\lambda^4 \qquad (58)$$

and a cross section $A_s = 0$. Hence, the above mentioned formula for the buckling stress of stringer panels also applies for forced crippling if the flexural rigidity of the stiffeners is expressed by Eq. (58) and $A_s = 0$. This results in the following buckling stress coefficient k_{cr} in Eq. (53) [Eq. (93) of reference 9].

$$k_{cr} = k_0 + \{(1 + \alpha)/[2(1 - \gamma\theta)]\} \times \left[1 - \left(1 - \{[4(1 - \gamma\theta)\alpha]/(1 + \alpha)^2\}\right)^{1/2}\right] k_1 \qquad (59)$$

In Eq. (59)

$$\alpha = k_2'/k_1 \qquad (60)$$

whereas, from Eqs. (34) and (92) of reference 9,

$$\left.\begin{aligned} k_0 &= [(\beta/n^2) + (1/\beta)]^2 \\ k_1 &= R\beta^2 \\ k_2' &= s - (2/n^2) + [q - (1/n^4)]\beta^2 \end{aligned}\right\} \qquad (61)$$

where R is given by Eq. (56) and s, q, and $\gamma\theta$ depend on the number of bays, n, and are given in Table 1.

If in Eq. (59) the form within the square brackets is written conservatively as

$$1 - (1 - \epsilon)^{1/2} = 1 - [1 - (1/2)\epsilon] = (1/2)\epsilon$$

it reduces to

$$k_{cr} = k_0 + [(k_1k_2')/(k_1 + k_2')] \qquad (62)$$

With the present notations this formula is equivalent to Eq. (57) of reference 6, which, as was stated in its derivation on pages 25–29 of Part I of reference 6, is indeed conservative. For the case calculated on page 34 of Part II of reference 6, it was found that $R = 3.07$ and $\beta = 0.86$. Further n is infinite, so that from Table 1 of the present paper $s = 2.5$, $q = 5$, and $\gamma\theta = 0.707$. Hence, from Eq. (61)

$$k_0 = 1/\beta^2 = 1/0.86^2 = 1.35$$
$$k_1 = R\beta^2 = 3.07\ (0.86)^2 = 2.27$$
$$k_2' = s + q\beta^2 = 2.5 + 5(0.86)^2 = 6.2$$

so that from Eq. (59), $k_{cr} = 3.12$. This is only 2.5 per

Table 1

n	s	q	$\gamma\theta$
2	2.27	2.45	0.570
3	2.36	3.58	0.616
4	2.37	4.20	0.639
∞	2.5	5	0.707

cent more than $k_{cr} = 3.04$, found on page 34 of Part II of reference 6 from Eq. (57) of that reference.

An error of not more than 1 per cent is made if it is assumed that for any number of bays the minimum buckling stress occurs for the same half wave length as for an infinite number of bays. Hence, values R in the present Eq. (57) can be read from Fig. 10, while the half wave length $a = \beta b$ follows from the equation for β in the second column on page 27 of Part II of reference 6:

$$\beta = [(K_{cr}/2) - 0.0134K_{cr}^{2.5}]^{-1/2} \qquad (63)$$

where K_{cr} is the buckling coefficient for an infinite number of bays and can be read from Figs. 23 and 24 of reference 6 as a function of p/b_a, $(b_a/t_s)/(b/t)$ and $(b_w/t_s)/(b/t)$.* As stated in reference 6, the graphs in these figures were calculated for ratios $b/t = 25$ and $t_s/t = 0.5$ but can be used sufficiently accurately for $40 > b/t > 20$ and $0.6 > t_s/t > 0.4$. Hence, for any number of bays n, the buckling coefficient k_{cr} is given by Eq. (59), where α is given by Eq. (60), k_0, k_1, and k_2' by Eq. (61), and s, q, and $\gamma\theta$ are given in Table 1. An example of calculation is given in the Appendix.

Practical Determination of Buckling Stress of a Stringer Panel

To determine the buckling stress for long wave buckling (in contrast to forced crippling) of a stringer panel, one has first to estimate the half wave length for which it becomes a minimum. After estimating the effective flange width of the stiffeners and thus their EI, this can be done by examining, in the graphs of reference 3, the curves for constant EI/dD (in the present notations EI/bD) situated to the left of the dashed curves, where the abscissas represent the ratio a/b (for curves to the right of the dashed curves the abscissas represent $2a/b$, $3a/b$, etc., since in the present paper a denotes the half wave length). The actual minimum of σ_{cr} will occur with a ratio a/b which is a little smaller than that for which the curves in reference 3 show a minimum, since the effective moment of inertia increases with the ratio a/b. This is due to the larger effective flange width for larger ratios a/b as well as to the smaller reduction of the effective moment of inertia of the stiffeners by shear deformation of the stiffener web and by flexibility of the attached flange for larger a/b ratios.

For the ratio a/b so chosen, one calculates the effective flange width of the stiffeners from Eqs. (37), (38), (41), or (42), where b_{eo} and b_{et} are found from Figs. 3 and 5. The area A_e in Fig. 3 is calculated from Eq. (A3) as shown in the Appendix. Then the effective moment of inertia I of the stiffeners is computed from Eq. (44). This moment of inertia is reduced to I'' from Eq. (55) to take account of shear deformation of the stiffener web and flexibility of the attached flange.

* As follows from Eq. (180) of Part II, in the conservative equation for σ_{cr} on page 2 of Part I of reference 6, the middle solidus should be omitted, so that $\sigma_{cr} = 0.60\,E\,(t_s/b_a)\,(t/b)$.

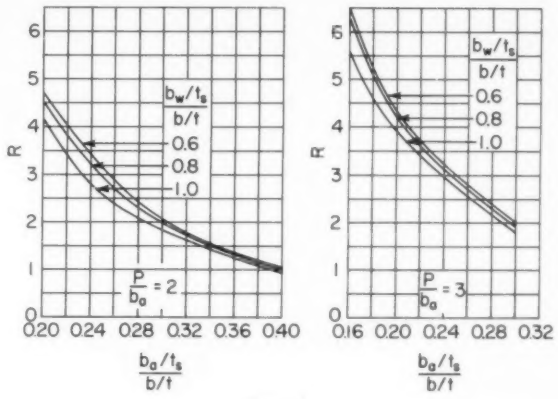

Fig. 10.

Finally k_{cr} is scaled from the graphs of reference 3, or computed from Eq. (32) of reference 9, in both cases using I'' from Eq. (55) instead of I. If one is not sure that the chosen ratio a/b leads to the smallest possible critical stress, one has to consider another ratio a/b. In most cases this will not be necessary, since only half wave lengths that are an integer part of the stringer length have to be considered.

If k_{cr} is higher than $k_s = 4$ for buckling of the bays as simply supported plates, indicated in Fig. 9, the latter value is governing.

Finally, one has to investigate whether or not a smaller buckling coefficient k_{fc} results from buckling into the forced crippling mode (Fig. 9). This computation has been worked out in reference 6 for a plate with an infinite number of stiffeners. In the preceding section this has been completed in order to use it also for cases with 1, 2, and 3 stiffeners. A numerical example of this calculation is given in the Appendix.

References

[1] Timoshenko, S., *Theory of Elastic Stability*, McGraw-Hill Book Company, Inc., New York, 1936.

[2] Barbre, R., *Beulspanningen in Rechteckplatten mit Längssteifen bei gleichmässiger Druckbeanspruchung*, Der Bauingenieur, Vol. 17, p. 268, 1936.

[3] Seide, P., and Stein, M., *Compressive Buckling of Simply Supported Plates with Longitudinal Stiffeners*, NACA TN 1825, March, 1949.

[4] Bijlaard, P. P., *Method of Determining the Effective Moment of Inertia of Stiffeners in Stiffened Flat Plate Analysis with 1, 2, 3 and Infinite Number of Stiffeners*, Bell Aircraft Corporation, Report No. 02-941-026, July, 1952.

[5] Seide, P., *The Effect of Longitudinal Stiffeners Located on One Side of a Plate on the Compressive Buckling Stress of the Plate-Stiffener Combination*, NACA TN 2873, January, 1953.

[6] Bijlaard, P. P., and Johnston, G. S., *Compressive Buckling of Plates Due To Forced Crippling of Stiffeners, Parts I and II*, Sherman M. Fairchild Fund Paper, No. FF-8, January, 1953.

[7] Timoshenko, S., *Theory of Elasticity*, McGraw-Hill Book Company, Inc., New York, 1934.

[8] Winter, G., *Stress Distribution in and Equivalent Width of Flanges of Wide, Thin-Wall Steel Beams*, NACA TN 784, 1940.

[9] Bijlaard, P. P., *Analysis of the Buckling of Stiffened Plates Having Any Number of Stiffeners*, Bell Aircraft Corporation, Report No. 02-984-013, July, 1953.

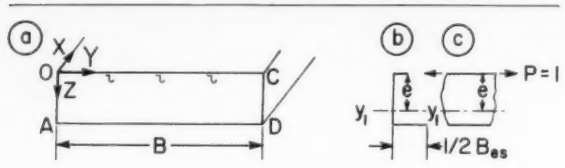

FIG. A1

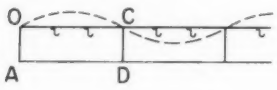

FIG. A2

[10] Bijlaard, P. P., and Fisher, G. P., *Interaction of Column and Local Buckling in Compression Members*, NACA TN 2640, March, 1952.

[11] Bijlaard, P. P., *Analysis of the Elastic and Plastic Stability of Sandwich Plates by the Method of Split Rigidities—III*, Journal of the Aeronautical Sciences, Vol. 19, No. 7, pp. 502–503, July, 1952.

[12] Bijlaard, P. P., and Fisher, G. P., *Column Strength of H-Sections and Square Tubes in Postbuckling Range of Component Plates*, NACA TN 2994, August, 1953.

Appendix

Computation of the Effective Cross Section A_e of the Webs

If panel OC buckles (Fig. A1, a), the webs OA and CD act as edge members. The effective edge member through O and running in the X-direction, should have the same rigidity against elongation in the X-direction, by a force through O in the X-direction, as the girder OA. Point O is located in the middle plane of the skin. To determine the width of the tension skin AD that can be considered to belong to the girders, it is observed that it has the same boundary conditions as the plate considered in Fig. 6d, so that its effective width B_{es} is given by Eq. (36), if there b is replaced by B (Fig. A1, a). Hence, the width of the tension skin belonging to the girders OA and CD is $(1/2)B_{es}$ (Fig. A1, b). B_{es}/B can be obtained from the dotted curve in Fig. 5, if in Fig. 5 the notations a/b and b_{es}/b are replaced by a/B and B_{es}/B. The axis of gravity of the cross section so obtained can be determined. Let it be located at a distance e below the middle plane of the compression skin (Fig. A1, b). The (fictitious) stress in such a section at $z = 0$ (Fig. A1, a), caused by a unit force P along the X-axis (Fig. A1, c), is

$$\sigma = (1/A_g) + (Me/I_g) \tag{A1}$$

where A_g and I_g are the cross section and the moment of inertia with respect to Y_1Y_1 (Fig. A1, b) of the girder. The bending moment M is equal to $Pe = e$. Inserting this into Eq. (A1) and requiring that the elongation, and thus the stress, at $z = 0$, is equal to that of a member with effective cross section A_e through O, one obtains

$$\sigma = (1/A_g) + (e^2/I_g) = 1/A_e \tag{A2}$$

or

$$A_e = I_g/(r_g^2 + e^2) \tag{A3}$$

where

$$r_g^2 = I_g/A_g \tag{A4}$$

If more girders are present (Fig. A2), at buckling, from antisymmetry in C, the superimposed elongation in the X-direction of the skin is zero, so that A_e is infinite. However, in O it is given by Eq. (A3), so that also here A_e should be assumed to be given by Eq. (A3) throughout.

Example of the Numerical Computation

(A) *Estimation of the Optimum Half Wave Length*

The data of the stringer panel considered are given in Fig. A3. Hence, $b = 2.5$ in., $b_a = 0.355$ in., $t = 0.102$ in., $b_w = 0.80$ in., $t_s = 0.040$ in., $b_f = 0.73$ in., $b_{ff} = 0.355$ in., $p = 0.75$ in., $d_s = 5/32$ in. The panel length is 12.5 in. The number of bays $n = 2$. The cross section of the stringer is found to be $A_s = 0.0754$ sq. in. Its proper moment of inertia $I_s = 0.008184$ in.^{4}. Estimating the effective flange width f_e of the stringer as $f_e = 2b = 5$ in., the flange section is $f_e t = 5(0.102) = 0.51$ sq.in. The distance z_s from the center of gravity of the stringer to the middle plane of the plate (Fig. 7) is 0.391 in. With these values one finds from Eq. (43) $z = [0.0754(0.391)]/[0.0754 + 0.51] = 0.0502$ in. Then from Eq. (44)

$$I = 0.008184 + 0.0754(0.391 - 0.0502)^2 + 0.51(0.0502)^2 = 0.018214 \text{ in.}^4$$

Further

$$D = Et^3/[12(1 - \nu^2)] = 0.0000972E$$

so that

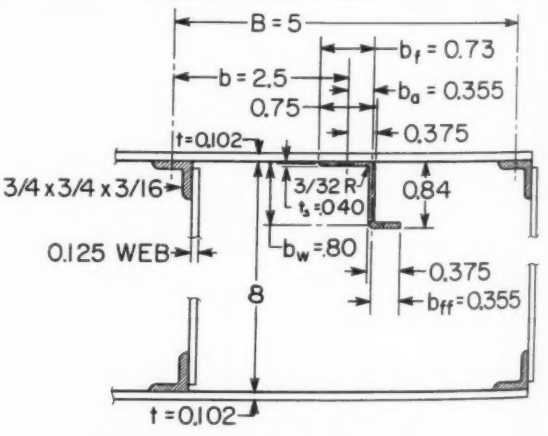

ALL RIVETS ARE 5/32" AT p = 3/4" SPACING.
DISTANCE BETWEEN RIBS IS 12.5 INCHES.
ALL MATERIAL IS 75 ST (SKIN & STRINGERS).

FIG. A3.

$$EI/(bD) = 0.018214E/[2.5(0.0000972E)] = 75$$

Assuming a reduction of the moment of inertia by shear deformation of the stringer web and by flexibility of the attached flange of about 15 per cent, one has $EI \div (bD) = 64$. Further, $\delta = A_s/(bt) = 0.0754/(2.5 \times 0.102) = 0.296$. Since, with a panel length of 12.5 in. and $b = 2.5$ in., the ratio $\beta = a/b$ can be only $12.5/2.5 = 5, 5/2, 5/3$, etc., it follows from the graphs on pages 12 and 13 of reference 3 that the smallest buckling stress will occur with $a = 12.5$ in. and $\beta = 5$.

(B) *Calculation of the Effective Cross Section A_e of the Webs*

The width of the lower (tension) skin (Fig. A3) is $B = 5$ in. The effective width is given by Eq. (36) if in there b is replaced by B. It is also given by the dashed curve in Fig. 5. With $a/B = 12.5/5 = 2.5$ from Fig. 5, the effective width $B_{es} = 0.78B$. Hence, the effective width of the tension skin belonging to a web is 0.39 (5) = 1.95 in. It is found that the axis of gravity of the web section so obtained (Fig. A4) is situated at a distance $e = 4.543$ in. below the middle plane of the compression skin. Its cross section is $A_g = 1.645$ in. and its moment of inertia I_g with respect to the axis Y_1Y_1 (Fig. A4) is 14.472 in.^{4}. Hence, $r_g^2 = I_g/A_g = 14.472 \div 1.645 = 8.8$ sq.in. Then from Eq. (A3)

$$A_e = 14.472/(8.8 + 4.543^2) = 0.4925 \text{ sq.in.}$$

so that $A_e/(bt) = 0.4925/0.255 = 1.93$ and $a/b = \beta = 5$. With these values from Fig. 3, $b_{eo} = b$.

(C) *Computation of the Reduced EI of the Stiffener*

With $b_{eo} = b$ the effective width of the stiffener flange from Eq. (37) is $f_{e1} = 2\ b_{eo} = 2b = 5$ in. This is the same effective width f_e as was assumed above (if this were not so, it would have to be checked whether with the newly found value f_{e1} and the resulting ratio $EI \div (bD)$ the same optimum half wave length a is found as above, which will generally be the case). Hence, $I = 0.018214$ in.^{4} as above. Further, in Eq. (55) $A_w = b_w t_s = 0.8 \times (0.04) = 0.032$ sq.in., $a = 12.5$ in., and C_f is given by Eq. (57), where R is found from Fig. 10 with $p/b_a = 0.75/0.355 = 2.11$, $b/t = 2.5/0.102 = 24.5$, $b_a/t_s = 0.355/0.040 = 8.87$, $(b_a/t_s)/(b/t) = 0.362$, $b_w/t_s = 0.80/0.040 = 20$, $(b_w/t_s)/(b/t) = 0.817$. One finds from Fig. 10 that $R = 1.30$, so that from Eq. (57) $C_f = (0.0000972E\ \pi^4/2.5^3) \times 1.3 = 0.00079E$. Insertion of a, A_w, I, and C_f into Eq. (55) gives a reduced moment of inertia $I'' = 0.837I$. Hence, from the above, with $EI/bD = 75$, $EI''/bD = 0.837\ (75) = 62.8$.

(D) *Computation of the Buckling Coefficient k_{cr}*

With the values found above—that is, $EI''/bD = 62.8$, $\delta = A_s/(bt) = 0.296$, $\beta = a/b = 5$, $n = 2$—from the graphs on pages 12 and 13 of reference 3, one finds $k_{cr} = 3.545$. The same value is found from Eq. (38) of reference 9.

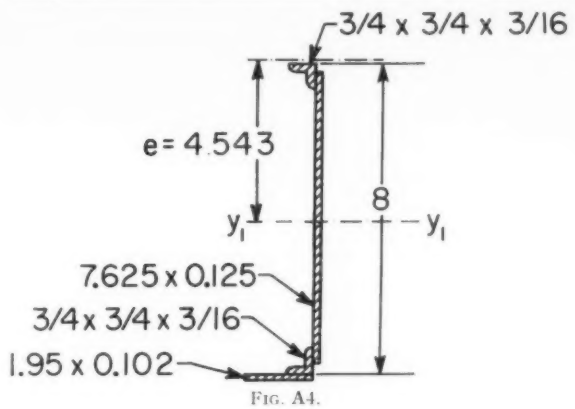

FIG. A4.

(E) *Buckling in the Forced Crippling Mode (Simplified Method)*

For the ratios $p/b_a = 2.11$, $(b_a/t_s)/(b/t) = 0.362$, and $(b_w/t_s)/(b/t) = 0.817$ as calculated above, as found above from Fig. 10, $R = 1.30$. From Figs. 23 and 24 of reference 6, with the same ratios, k_{cr} for an infinite number of bays is 2.08. Hence, from Eq. (63),

$$\beta = [1.04 - 0.0134(2.08)^{2.5}]^{-1/2} = 1.02$$

From Eqs. (61) and Table 1, with $n = 2$,

$$k_0 = [(1.02/4) + (1/1.02)]^2 = 1.528$$

$$k_1 = 1.3(1.02)^2 = 1.35$$

$$k_2' = 2.27 - (2/4) + [2.45 - (1/16)]1.02^2 = 4.25$$

$$\gamma\theta = 0.570$$

From Eq. (60) $\alpha = 4.25/1.35 = 3.15$. Hence, from Eq. (59),

$$k_{cr} = 1.528 + \{(1 + 3.15)/[2(1 - 0.57)]\} \times [1 - (1 - \{[4(1 - 0.57)3.15]/(1 + 3.15)^2\})^{1/2}] \times 1.35 = 2.67$$

(F) *More Accurate Calculation of the Buckling Stress for Forced Crippling*

An accurate calculation according to reference 6 leads to $R = 1.505$, 1.475, and 1.44 for $\beta = a/b = 0.93$, 1.005, and 1.08, respectively. With these values one finds from Eq. (59) $k_{cr} = 2.78$, 2.77, and 2.78, respectively, so that $k_{cr} = 2.77$ for the optimum value $\beta = 1.005$. Hence, the approximate value $k_{cr} = 2.67$ found above is 4 per cent conservative.

(G) *Minimum Buckling Stress*

The minimum buckling coefficient is that found for forced crippling. Using the approximate value $k_{cr} = 2.67$, which is calculated easily, the elastic buckling stress is

$$\sigma_{cr} = k_{cr}[(\pi^2 D)/(b^2 t)] = 2.67\ \{(0.0000972E\ \pi^2) \div [2.5^2(0.0102)]\} = 0.00401E = 43{,}000 \text{ lbs. per sq.in}$$

Actually for the material used (75S-T) this stress is within the plastic range. With $b/(t\sqrt{k_{cr}}) = 2.5 \div (0.102\sqrt{2.67}) = 15.0$, from Fig. 18 of reference 6, $\sigma_{cr} = 36{,}000$ *lbs. per sq.in.*

Readers' Forum

BRIEF REPORTS of investigations in the aeronautical sciences and discussions of papers published in the JOURNAL are presented in this special department. Publication is completed as soon as possible after receipt of the material. The Editorial Committee does not hold itself responsible for the opinions expressed by the correspondents.

The Effect of the Temperature Dependence of King's "Constant" A on the Hot-Wire Sensitivity Coefficient

J. R. Ruetenik
Senior Engineer, Aeroelastic and Structures Research Laboratory, Department of Aeronautical Engineering, MIT
January 12, 1955

IN A RECENT SERIES[1] of turbulence-level measurements (u') using a hot-wire anemometer the constant-*current*[2] and constant-*resistance*[3] methods of calibration gave sensitivity coefficients differing by 25 per cent over most of the velocity range (3 to 16 ft. per sec.). In both cases the wires were employed at essentially constant *current*.

The discrepancy was traced to the dependence of the coefficient A in King's Equation[4]

$$I^2R = [A(T) + B\sqrt{U}]\,(T - T_e) \tag{1}$$

on the wire temperature, T; I^2R is the rate of heat loss, U the air speed, and T_e the unheated wire temperature, taken as constant. This $A(T)$ effect, as hereafter called, had been identified and experimentally evaluated by King[4] but has been omitted in a number of interviewing investigations.[2, 3, 5, 6]

King empirically obtained in air

$$A = A_e[1 + c(T - T_e)] \tag{2}$$

where A_e is a constant, and $c = 0.00114$ at $T_e = 17°\text{C}$. To confirm Eq. (2) a 0.00015-in. diameter by 0.040-in. long platinum wire was calibrated at three "overheats": $a_w' = 0.4$, 0.7, and 1.0, where $a_w' \equiv (R - R_e)/R_e$. The air speed was 15 to 35 ft. per sec., and two wire orientations were tested: normal and inclined 40° to the stream. The comparison to Eq. (2) is shown in Fig. 1; B was assumed constant (justified by King and confirmed in the present test). The agreement is good.

The $A(T)$ effect will now be incorporated in the turbulence measurement. Since the completion of this investigation,[1] the author's attention has been directed to the elegant analysis by Betchov[7, 8] incorporating (1) the $A(T)$ effect as well as (2) the end losses. He applied Eq. (1) locally along the wire and derived corrections to the "perfect-wire" equations in terms of the "basic" data (wire dimensions and properties, A_e, etc.). The present report obtains a correction to the measurement of turbulence level in terms of quantities somewhat more readily measured in the laboratory by considering first-order differences from the mean operating conditions. The analysis includes (1) and (3) the second-degree term in the resistance law

$$R = R_f[1 + \alpha(T - T_f) + \beta(T - T_f)^2] \tag{3}$$

Item (2) is omitted, so the analysis evidently applies to wires with length-diameter ratios of 200 or greater (see reference 8).

It is convenient to adopt the symbols[9]

$$z \equiv \sqrt{U}/\{[A(T)/B] + \sqrt{U}\}$$
$$a_w \equiv (R - R_f)/R_f$$
$$a_e \equiv (R_e - R_f)/R_f$$

To apply Eq. (1) to turbulence measurement, the usual assumption of a quasi-equilibrium state of the flow field will be admitted. Eq. (1) is expanded in a Taylor's series keeping only first-order terms, in the manner of reference 3, giving

$$\Delta E/\bar{E} = -\{(a_w'z)/[2(1 + \Phi)]\}\,(\Delta U/\bar{U}) \tag{4}$$

where E is the voltage drop across the hot wire. The terms a_w', z, and Φ correspond to the mean conditions $\bar{E}$ and $\bar{U}$. Eq. (4) is identical to Eq. (12) of reference 3, for a constant-current wire, when $\Phi = 0$. Φ incorporates (1) and (3). For typical operation Φ can be approximated by

$$\Phi = a_w'(1 + a_w)\left[\frac{1 - z}{(\alpha/c) + a_w - a_e} - \frac{\beta}{\alpha^2}\right] \tag{5}$$

Eq. (5) is plotted in Fig. 2 for platinum and tungsten (α and β from reference 10). In reference 1 the Φ correction brought the two measurements within 5 to 10 per cent agreement.

The following remarks are in order:

(1) The Φ correction is generally larger for platinum due to α.

(2) For tungsten (3) tends to offset (1), but for platinum they are additive.

(3) Roughly $\Phi \sim a_w'$ for $a_w' < 0.5$. Since the signal is also proportional to a_w', it is not necessarily feasible to reduce a_w' to reduce Φ.

The writer would like to acknowledge the helpful discussions with Drs. Stanley Corrsin and Leslie S. G. Kovásznay.

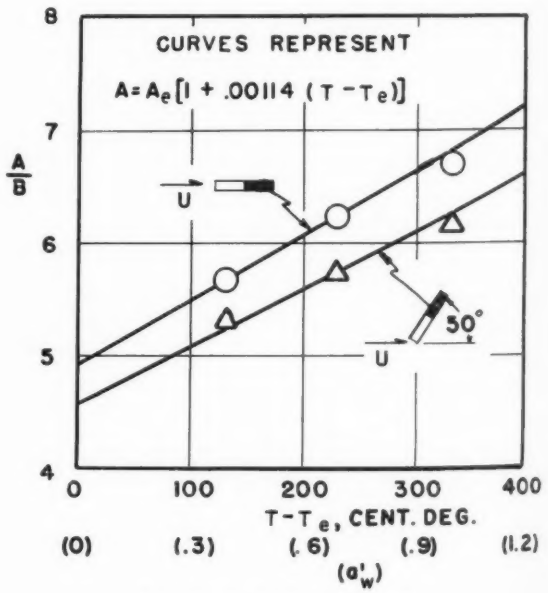

FIG. 1. Verification of Eq. (2).

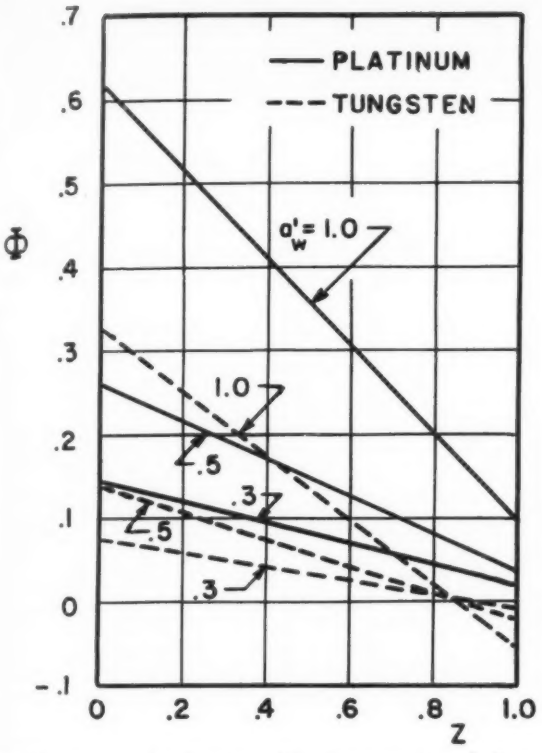

FIG. 2. Φ correction from Eq. (5). Parameter is a_w', T_t = 80 °F.

REFERENCES

[1] Ruetenik, J. R., *The Investigation of Equilibrium Flow in a Slightly Divergent Channel*, Diss. for degree of Dr. Engrg., The Johns Hopkins Univ., 1954 (final report for contract N-onr-248(33), Rep. I-19 of Dept. of Mech. Engrg.).

[2] Schubauer, G. B., and Klebanoff, P. S., *Theory and Application of the Hot-Wire Instruments in the Investigation of Turbulent Boundary Layers*, NACA Wartime Report W-86, 1946.

[3] Kovásznay, L. S. G., *Calibration and Measurement in Turbulence Research by the Hot-Wire Method*, Budapest, Hungary, 1943. (Translated as NACA TM 1130).

[4] King, L. V., *On the Convection of Heat from Small Cylinders in a Stream of Fluid: Determination of the Convection Constants of Small Platinum Wires with Applications to Hot-Wire Anemometry*, Phil. Trans. Roy. Soc. (London), Ser. A, Vol. 214, pp. 373–432, 1914.

[5] Dryden, H. L., and Kuethe, A. M., *The Measurement of Fluctuations of Air Speed by the Hot-Wire Anemometer*, NACA Rep. 320, 1929.

[6] Liepmann, H. W., and Laufer, J., *Investigations of Free Turbulent Mixing*, NACA TN 1257, 1947.

[7] Betchov, R., *Nonlinear Theory of a Hot-Wire Anemometer* (in French), Proc. Kon. Ned. Akad. Wet., Vol. 52, No. 3, pp. 195–207, 1949 (Translated as NACA TM 1346).

[8] Betchov, R., *Some Experiences Regarding the Nonlinearity of Hot Wires* (in French), Proc. Kon. Ned. Akad. Wet., Vol. 53, No. 4, pp. 195–207, 1950, (Translated as NACA TM 1223).

[9] Kovasznay, L. S. G., *Development of Turbulence-Measuring Equipment*, NACA TN 2839, 1953.

[10] *International Critical Tables*, 1st Edition, Vol. VI, p. 136, McGraw-Hill Book Company, Inc., 1929.

Optimum Stage for Axial Flow Turbines

N. Van Le

Aerodynamics Group, AiResearch Manufacturing Company, Los Angeles, Calif.

January 10, 1955

THE PROBLEM OF FINDING the stages of an axial flow turbine that would run at the highest efficiency under prescribed pressure ratio, diameter, speed and mass rate of flow has been approached on a trial basis, guided by experience.

A solution to this problem is presented, aiming at a systematic investigation, eliminating the cut and tried process and introducing possible use of computing equipment. Despite the three-dimensional flow pattern in turbines, their efficiency is calculated with mean values. On this basis, a turbine stage characterized by a velocity diagram and its *h-s* representation is considered in Fig. 1, with the definitions shown.

The stage efficiency η_{ST} can be calculated as

$$\eta_{ST} = W/W_r = h_{01} - h_{02}/h_{01} - h_{02ss} - C_2^2/2g \quad (1)$$

$$= \left[1 + \frac{\zeta_R (w_2/u)^2 + (T_2/T_1)(\zeta_s)(C_1/u)^2}{W/(u^2/2g)}\right]^{-1} \quad (2)$$

The ratio T_2/T_1 can generally be taken as equal to 1, or estimated from the degree of reaction of the turbine stage. The loss coefficients ζ_s, ζ_R, derived from test data, generally, form an integral system—for example, that of reference 1. The loss coefficients depend mainly on the turning angle, solidity, clearance, aspect ratio, Reynolds Number, etc. If a type of velocity diagram defined by its degree of reaction is selected, it is possible to

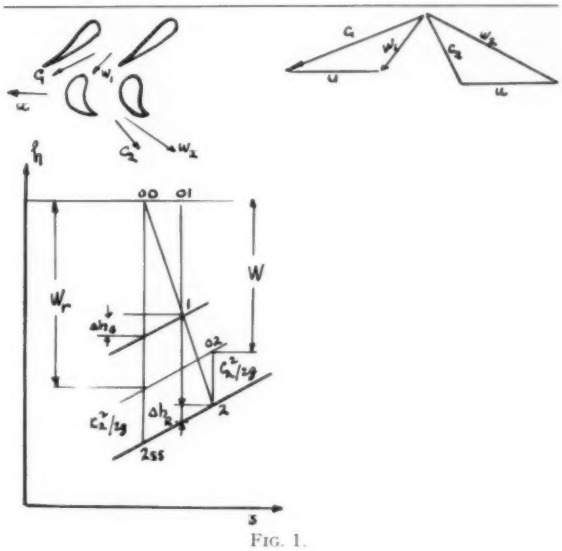

FIG. 1.

$W = h_{01} - h_{02}$, shaft work

$W_r = h_{01} - h_{2ss} - C_2^2/2g$, reversible work when the exit velocity C_2 is not assumed to be lost

$\zeta_s = \Delta h_s/(C_1^2/2g)$, loss coefficient in stator

$\zeta_R = \Delta h_R/(W_2^2/2g)$, loss coefficient in rotor

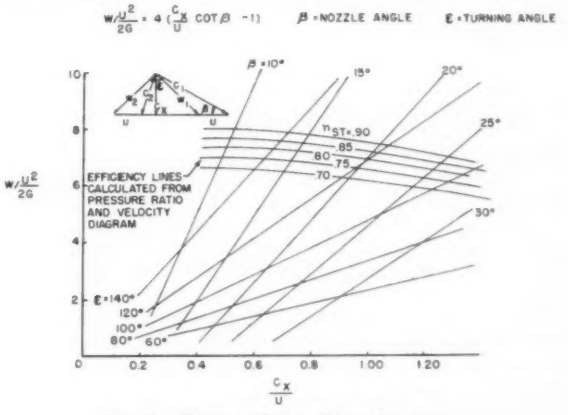

FIG. 2. Characteristics of impulse stage.

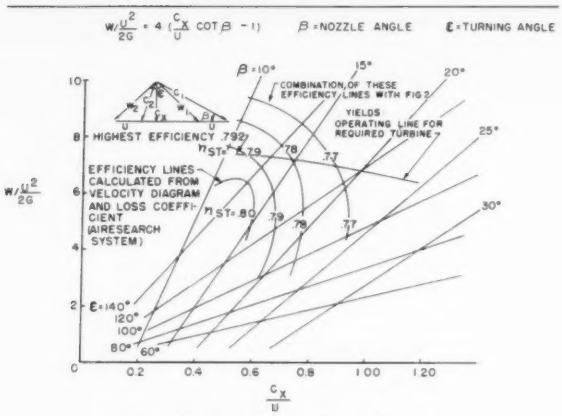

FIG. 3. Characteristics of impulse stage.

represent the characteristics of different combinations of this diagram. Fig. 2 shows a velocity diagram chart of the impulse type (zero reaction). For each point on this figure there is a corresponding velocity triangle which yields complete information for the calculation of ζ_s, ζ_R. Application of Eq. (2) permits the establishment of a map of lines of constant η_{ST}, Fig. 3. Now, every point on Fig. 2 yields also a shaft work W. From the given pressure ratio, the efficiency η_{ST} can be calculated with Eq. (1) independently of ζ_s, ζ_R. Lines of constant η_{ST} are then calculated and shown on Fig. 2.

Upon combining Figs. 2 and 3 and taking the intersects of lines of the same η_{ST}, a turbine that satisfies the prescribed conditions is found. It operates at the considered value of η_{ST}. The intersects constitute an operating line along which the efficiency is known and, therefore, the highest one can be selected, Fig. 3. No other combinations of velocity diagrams exist that would satisfy the problem.

By changing the degree of reaction, a new operating line is established. The combination of all these operating lines will permit the establishment of the absolute optimum turbine stage, defined by its degree of reaction and the parameter C_x/u.

It is readily seen that this method is adaptable to modern computing machines as any judgment based on experience is not involved. It is conceivable that different "unit" turbines corresponding to different sets of prescribed conditions can be investigated to establish relations between these units.

REFERENCE

[1] Ainley, D. G., *Performance of Axial-flow Turbines*, Internal Combustion Turbines, ASME Publication.

A Similarity Rule for the Interaction Between a Conical Field and a Plane Shock*

Y. H. Kuo
Graduate School of Aeronautical Engineering, Cornell University, Ithaca, N.Y.

January 14, 1955

IN THREE-DIMENSIONAL SUPERSONIC steady flow past an obstacle, it frequently happens that a conical field touches, and thereby interacts with, a plane shock, resulting in a phenomenon known as a "triple point." In the limit of infinitesimal shock strength, problems of this kind have been treated by linear theory, in which the "triple point" is disguised as a logarithmic singularity superposed on an algebraic one at the Mach cone. In reality, of course, the shock cannot change discontinuously but decays to zero strength under the action of the conical field through a definite region whose dimensions depend on the strength of the shock. Consequently, a correct description of this phenomenon necessitates a re-examination of the approximation assumed in the linear theory.

In the case of a weak shock, the flow behind it may still be considered as isentropic and irrotational. Let the velocity potential be φ in the cylindrical coordinate system (ρ, θ, z) in which z is in the free-stream direction. If the flow is conical, $\varphi = Uz[1 + f(r, \theta)]$ where $r = \beta\rho/z$ and $\beta = \sqrt{M_\infty^2 - 1}$; U and M_∞ are, respectively, the free-stream velocity and Mach Number. The differential equation satisfied by the function $f(r, \theta)$, according to Lighthill,[1] is

$$\{1 - r^2 - (\gamma + 1)M_\infty^2\beta^{-2}r^2[f - rf_r + (1/2)(f - rf_r)^2] - (\gamma - 1)M_\infty^2[f - rf_r + (1/2)(f - rf_r)^2 + (1/2)(r^2 + \beta^2)(f_r^2 + r^{-2}f_\theta^2)] + 2M_\infty^2 rf_r(1 + f - rf_r) - M_\infty^2\beta^2 f_r^2\}f_{rr} + [1 - (\gamma - 1)M_\infty^2(f - rf_r)] \times (r^{-1}f_r + r^{-2}f_{\theta\theta}) - 2M_\infty^2(r^{-2}f_\theta - r^{-1}f_{r\theta})f_\theta + C = 0 \quad (1)$$

Here C and γ stand for, respectively, the cubic terms of the exact equation, not containing f_{rr}, and the ratio of the specific heats. Subscripts denote partial differentiation. When the disturbances are small and no terms other than linear ones are kept, the coefficient of f_{rr} is approximated by $1 - r^2$ and the equation becomes linear. For such cases, $r = 1$ defines the singular Mach cone. It is no surprise that linear theory breaks down in the neighborhood of $r = 1$, inasmuch as the terms neglected are of the same order as $1 - r$. To remove the ambiguities inherent in the linear solution in that neighborhood, nonlinear terms are indispensable.

If the small parameter of the flow is α, such as the angle of attack of a wing, the shock strength, and so the velocity disturbances, will be of the order α. In the region of interaction let it be assumed that

$$\left.\begin{aligned} f &= (1/\beta)\alpha^l k^m F(\xi, \eta) \\ 1 - r &= (\alpha k)^m \xi \\ \theta - \theta_0 &= (\alpha k)^n \eta \end{aligned}\right\} \quad (2)$$

where θ_0 is a constant giving the location of the interaction zone and k is another constant to be determined. It is now assumed, on the basis of the fact that the interaction takes place far from the solid boundary, that the character of interaction—namely, the exponents l, m, and n—depends solely on the local conditions and the differential equation. Since the shock strength and the velocity disturbance $\varphi_z - U = U(f - rf_r)$ are both of order α, $l - m = 1$. If, in the coefficient of f_{rr}, $1 - r^2$ is of the same order as $f - rf_r$, then m must be unity. These two conditions uniquely define l to be 2. The first term of Eq. (1) is therefore $0(\alpha)$. Now if $f_{\theta\theta}$ is also of the first order, n must be 1/2. Therefore, by retaining only the first-order terms, Eq. (1) simplifies to

$$(2\xi - F_\xi)F_{\xi\xi} - F_\xi + F_{\eta\eta} = 0 \quad (3)$$

with

$$k = (\gamma + 1)M_\infty{}^4\beta^{-3}$$

This shows that the effect of the interaction would confine itself to a region that extends in the radial direction a distance of $0(\alpha)$ and subtends an angle of $0(\sqrt{\alpha})$ and that two flow fields described by $f_1(r, \theta)$ and $f_2(r, \theta)$ are similar if the product $k\alpha$ is the same for both cases. It is of interest to point out that, by a different interpretation of the variables, this similarity rule holds equally true for unsteady two-dimensional flow, such as the diffraction of a plane shock by a corner.

One of the boundary conditions that the solution to Eq. (3) must satisfy is the shock condition—namely, across the shock[1] (a) f is continuous, and, (b)

$$\Delta f_r = [2/(\gamma + 1)]\,[(\gamma - 1)(f - f_r) + 2M_\infty{}^{-2}f - 2f_r + 2M_\infty{}^{-4}\beta^2(r - 1) - M_\infty{}^{-4}\beta^2(dr/d\theta)^2] + \ldots \quad (4)$$

where Δf_r signifies the jump in f_r. From the similarity transformation, f is $0(\alpha^2)$ and therefore the shock condition reduces to

$$F_\xi = 4\xi + 2(d\xi/d\eta)^2 \quad (5)$$

* This study was sponsored by the Mechanics Branch of the Office of Naval Research.

if the disturbances in front of shock are zero.

If there is no disturbance outside the Mach cone and if both $(f - rf_r)$ and $1 - r$ near the Mach cone are of the order α^2, the same argument leads to the following similarity transformation

$$\left.\begin{aligned} f &= (1/\beta)k^3\alpha^1 F(\xi, \eta) \\ 1 - r &= (k\alpha)^2\xi \\ \vartheta - \vartheta_0 &= k\alpha\eta \end{aligned}\right\} \quad (6)$$

without affecting the validity of both Eq. (3) and Eq. (5).

The similarity considerations above show that in the (r, ϑ)-plane a three-dimensional purely supersonic conical flow in the neighborhood of both the "triple point" and the Mach cone $r = 1$ is governed by not a linear but a nonlinear differential equation of the mixed type, with the transitional line $F_\xi = 2\xi$ separating the elliptic and hyperbolic regions. These similarity rules lead us to conclude, without solving the differential Eq. (3), that the perturbed shock strength of a first-order plane shock can be expressed in the form

$$\Delta p/p_\infty = -[(\gamma M_\infty{}^2\alpha)/\beta] F_\xi(\xi, \eta) \quad (7)$$

with a shock curve of the form

$$1 - r = k\alpha\xi(\eta) \quad (7.1)$$

and that the shock strength of the Mach cone without disturbances in front of it has the form

$$\Delta p/p_\infty = -[(\gamma M_\infty{}^2 k\alpha^2)/\beta] F_\xi(\xi, \eta) \quad (8)$$

with a shock curve

$$1 - r = (k\alpha)^2\xi(\eta) \quad (8.1)$$

Two special solutions of Eq. (3) have been studied. They will be briefly discussed in the following:

(A) Suppose:

$$F = H(\mu) - 2\mu[\xi_0 + \sigma(1 - 2\sigma)(\eta + \eta_0)^2] + g(\eta) \quad (9)$$

and

$$\mu = \xi + \xi_0 + \sigma(\eta + \eta_0)^2$$

where $g(\eta)$ is a polynomial of degree 4 and ξ_0, η_0, and σ are constants. The differential equation for $H(\mu)$ is, from Eq. (3),

$$(2\mu - H')H'' - (1 - 2\sigma)H' - 4\sigma(1 - 2\sigma)\mu = 0 \quad (10)$$

where $H' = dH/d\mu$. This equation can be explicitly integrated with the result: for $6\sigma \neq 1$

$$(H' - 4\sigma\mu)[H' - (1 - 2\sigma)\mu]^{-(1 + 2\sigma)/[2(1 - 2\sigma)]} = \text{const.} \quad (11)$$

When $6\sigma = 1$, the solution can similarly be found and contains a logarithmic term.

If the constant σ lies in $-1/2 < \sigma < 1/2$, the integral curve (H', μ) will have a modal point at $\mu = 0$. For small μ, one branch is positive and the other is negative and intersects the singular line $H' = 2\mu$ at $\mu < 0$ with infinite slope. In the special case where there is no disturbance outside the Mach cone, $\sigma = 0$, then $F_\xi = H'(\mu)$. Thus, on the expansion side where $H' \geq 0$, the flow across the Mach cone is continuous. On the other hand, on the compression side where $H' < 0$, the flow across the Mach cone must be discontinuous with a shock strength from Eq. (8) proportional to $-k\alpha^2\beta^{-1}H'(\mu_0)$ and shock cone $1 - r = 4^{-1}(k\alpha)^2 H'(\mu_0)$ according to Eq. (5). These results seem to confirm Lighthill's earlier conclusions regarding the character of the shock in the case of a triangular wing with angle of attack, lying inside the Mach cone.

(B) By the similarity rule, assume

$$F = (\eta + \eta_0)^4 G(\zeta) \quad (12)$$

where

$$\zeta = \xi/(\eta + \eta_0)^2$$

With this form of solution, it is evident from the shock condition [Eq. (5)] that an admissible shock curve is $\zeta = \text{const.} = \zeta_0$. In the case of a conical field interacting with a shock, such as the tip Mach cone from a rectangular wing at angle of attack, the velocity disturbance F_ξ and the coordinates (ξ, η) of the "triple point" are, respectively, -1 and $(-1/2, 1/\sqrt{2})$ from the shock condition. With these values, it is easy to deduce $G'(\zeta_0) = 2\zeta_0$. The shock condition [Eq. (5)] then determines $\zeta_0 = -(1/4)$, from which it follows that $\eta_0 = 1/(\sqrt{2})$. One can conclude finally that the perturbed shock curve is $\xi = -(1/4)(\eta + 1/\sqrt{2})^2$ on which the shock strength decays according to $(\eta + 1/\sqrt{2})^2$.

The numerical integration of the resulting equation for G

$$(2\zeta + 4\zeta^2 - G')G'' - (1 + 10\zeta)G' + 12G = 0 \quad (13)$$

with the initial values $\xi = -(1/4)$, $G = (1/24)$, and $G' = -(1/2)$ shows, however, that the integral curve (G', ζ) forms a cusp after hitting the singular line $G' = 2\zeta + 4\zeta^2$ at $\zeta = 0$. The solution in this neighborhood is of the form $\sum_3^\infty C_m|\zeta|^{m/2}$. There is, at the moment, no evidence to support the existence of this singularity in the interaction zone, even though other properties of the solution are acceptable. Further exploration along this line is certainly desirable.

It might be mentioned, in passing, that in trying to solve the same problem, Legras[2] chose a similar shock curve as the initial line to construct a solution in power series. Unfortunately, his process has not been pursued far enough to determine whether this form of solution is actually possible. In the light of the new results, it seems to be a matter of fundamental importance that Legras' solution be reexamined.

References

[1] Lighthill, M. J., *The Shock Strength in Supersonic "Conical Fields,"* Phil. Mag., No. 11, pp. 1202–1223, 1949.

[2] Legras, J., *Nouvelles Applications de la méthode de Lighthill à l'etude des ondes de choc*, O.N.E.R.A., No. 66, 1953.

Effect of High Advancing-Tip Mach Number on Helicopter Blade Flapping

Kenneth B. Amer and H. Hirsch

Aircraft Division, Hughes Tool Company, Culver City, Calif.

January 14, 1955

References 1 and 2 discuss severe retreating-blade stall as the cause of helicopter rotor blades striking the fuselage or tail boom. The purpose of this note is to propose an additional, perhaps even more important, cause of blade striking, especially appropriate for modern helicopters.

Indications are that the blade-striking problem is becoming more severe with modern helicopters, and it is hypothesized that the blade-striking problem is accentuated by the current tendency toward operation at higher tip and forward Mach Numbers. Recent NACA data indicate that airfoils such as the commonly used NACA 0012 experience a forward shift in center of pressure with increasing Mach Number before the well-known large rearward shift occurs. It is believed that this forward shift in center

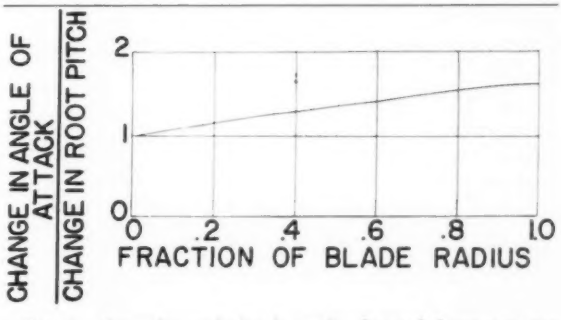

Fig. 1. Spanwise variation in angle of attack increment per unit root angle increment for a typical rotor blade. Advancing-tip Mach Number = 0.6.

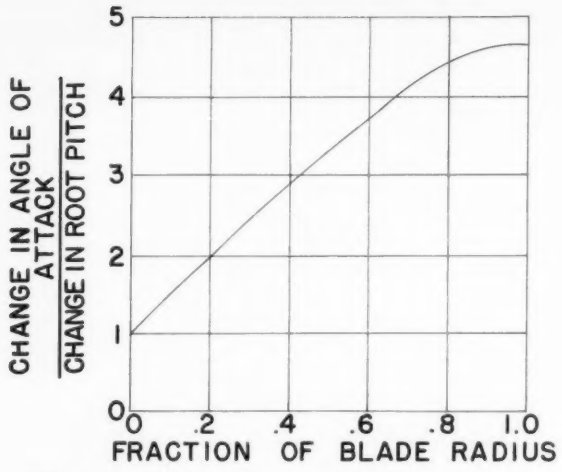

FIG. 2. Spanwise variation in angle of attack increment per unit root angle increment for a typical rotor blade. Advancing-tip Mach Number = 0.7.

of pressure, combined with the higher dynamic pressures associated with operation at higher advancing-tip Mach Numbers, results in a pitch-increasing twist of the blade on the advancing side and leads to a condition in which blade-striking occurs.

In order to indicate the manner in which the forward shift in airfoil center of pressure with increasing Mach Number twists the blade and leads to the blade-striking problem, a preliminary quasi-static study on a sample rotor blade was conducted. In this study, the effect on the blade of an increased in blade pitch on the advancing side (90° azimuth), such as would be caused by upward collective and/or rearward cyclic control motion, was computed. Figs. 1 and 2 present the results of this study in the form of the spanwise variation in angle of attack increment per unit root angle increment. The outboard angle of attack increment is greater than the root increment because of blade twist due to the lift increments near the tip acting forward of the center of gravity.

Fig. 1, for an advancing tip Mach Number of 0.6, shows a small increment in angle of attack change due to blade twist. Fig. 2, however, for an advancing tip Mach Number of 0.7, shows a large angle of attack increment due to blade twist. The large increase in blade twist indicated in Fig. 2, as compared to Fig. 1, occurs due to the forward shift in chordwise center of pressure associated with the increase in Mach Number and to the increased dynamic pressure. Also, it reflects the fact that at the higher advancing tip Mach Number, there is a significant destabilizing effect in that the blade twisting causes additional lift which, in turn, causes additional twisting.

Figs. 1 and 2 indicate that upward collective and/or rearward cyclic motion, which increases the blade angle of attack on the advancing side, may cause a large angle of attack increase at that position per unit control displacement under conditions of high advancing-tip Mach Number. This large increase in angle of attack would cause the blade to rise considerably in the forward position. Because the blade is operating in a centrifugal field, this large amount of flapping represents a large amount of potential energy. As the blade continues to rotate the potential energy is converted to downward kinetic energy and again to potential energy represented by an unusually large negative blade-flapping angle in the rearward position, where striking may occur. (This situation is aggravated by retreating-blade stalling, as discussed in references 1 and 2.) Thus, magnitudes of control motion that are safe at lower tip and forward speeds may become unsafe when higher tip and forward speeds are reached.

Assuming that blade twisting due to forward shift in center of pressure at high advancing-tip Mach Numbers is an important cause of the striking problem, it would appear desirable to design the blades of high-speed helicopters with the chordwise center of gravity moved forward about 3 per cent of chord from the usual position, at least over the outer 20 per cent of the span. This forward shift in blade chordwise center of gravity would eliminate the unstable cg-cp situation at high advancing-tip Mach numbers; thus, a fundamental cause of the blade-striking problem would be eliminated. At lower tip and forward Mach numbers, the cg-cp relation would be stable, which is acceptable from such standpoints as blade dynamic loads and flutter. It is recognized that the proposed shift in chordwise center of gravity would effect control loads at lower tip and forward speeds because of the separation of the center of gravity from the center of pressure. However, it can be shown that this effect is minor in relation to other sources of control loads.

The above hypothesis arose out of work on high-tip-speed rotors conducted under contract for the United States Air Force.

REFERENCES

[1] Stepniewski, W. Z., *On Down Flapping of a Stalled Helicopter Blade*, Journal of the Aeronautical Sciences, Vol. 21, No. 6, p. 428, June, 1954.

[2] Hohenemser, K. H., *Effect of Helicopter Blade Stall on Blade Flapping*, Journal of the Aeronautical Sciences, Vol. 21, No. 12, p. 861, December, 1954.

Analysis of Thermal Stresses in Conical Shells

Marvin Stern
Design Specialist, Convair, San Diego, A Division of General Dynamics Corporation, San Diego, Calif.
January 18, 1955

SUMMARY

The differential equations for the problem of induced thermal stresses in conical shells under axially symmetric temperature distribution are derived. Contrary to past analysis of this problem, the development presented herein allows for variations in temperature profile, Young's modulus, and skin thickness. The results appear as only two second-order linear differential equations that are relatively simple and allow for solution by machine methods for wide ranges of the above parameters.

INTRODUCTION

IN A RECENT PAPER[1] an idealized case of the subject problem has been analyzed. This past analysis will be extended here to include allowance for the following effects: (1) temperature profile to be arbitrary, (2) Young's modulus to vary as a function of temperature, and (3) skin thickness to vary arbitrarily.

The development in this analysis parallels that of Tsien in his treatment of the problem for heated flat plates.[2]

ANALYSIS

(I) *Displacements and Compatibility*

For displacements u in r direction and w in z direction (inward normal to surface) the strains at a distance z away from the median surface are:

$$\left.\begin{aligned} \epsilon_r &= (du/dr) - z[(d^2w)/(dr^2)] \\ \epsilon_\vartheta &= [(u/r) - (w/\tan\gamma)] - z(1/r)(dw/dr) \end{aligned}\right\} \quad (1.1)$$

Let $E(r, z)$ be the variable Young's modulus, ν the constant Poisson's ratio, and a the coefficient of thermal expansion. Then

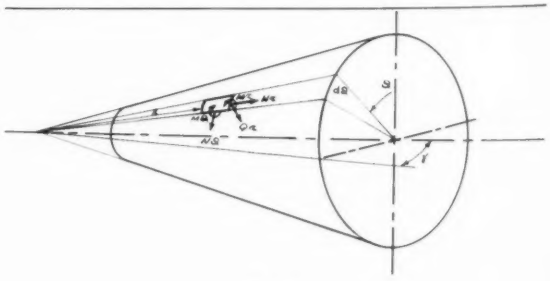

FIG. 1.

the stress-strain relations are:

$$\epsilon_r = \{1/[E(r, z)]\}\ (\sigma_r - \nu\sigma_\vartheta) + aT(r, z)$$
$$\epsilon_\vartheta = \{1/[E(r, z)]\}\ (\sigma_\vartheta - \nu\sigma_r) + aT(r, z)$$

Inverting yields:

$$\left.\begin{aligned}\sigma_r &= \{[E(r, z)]/(1 - \nu^2)\}\ (\epsilon_r + \nu\epsilon_\vartheta) - \{[E(r, z)]/(1 - \nu)\}aT(r, z)\\ \sigma_\vartheta &= \{[E(r, z)]/(1 - \nu^2)\}\ (\epsilon_\vartheta + \nu\epsilon_r) - \{[E(r, z)]/(1 - \nu)\}aT(r, z)\end{aligned}\right\} \quad (1.2)$$

In order to work with sectional forces and moments, set

$$\left.\begin{aligned}N_r &= \int \sigma_r\, dz\\ N_\vartheta &= \int \sigma_\vartheta\, dz\\ M_r &= \int \sigma_r z\, dz\\ M_\vartheta &= \int \sigma_\vartheta z\, dz\end{aligned}\right\} \quad (1.3)$$

Integrating Eqs. (1.2) and substituting Eqs. (1.1) and (1.3) yields,

$$\left.\begin{aligned}N_r &= D_0\left[\frac{du}{dr} + \nu\left(\frac{u}{r} - \frac{w}{r\tan\gamma}\right)\right] - D_1\left(\frac{d^2w}{dr^2} + \nu\frac{1}{r}\frac{dw}{dr}\right) - N_T\\ N_\vartheta &= D_0\left[\left(\frac{u}{r} - \frac{w}{r\tan\gamma}\right) + \nu\frac{du}{dr}\right] - D_1\left(\frac{1}{r}\frac{dw}{dr} + \nu\frac{d^2w}{dr^2}\right) - N_T\\ M_r &= D_1\left[\frac{du}{dr} + \nu\left(\frac{u}{r} - \frac{w}{r\tan\gamma}\right)\right] - D_2\left(\frac{d^2w}{dr^2} + \nu\frac{1}{r}\frac{dw}{dr}\right) - M_T\\ M_\vartheta &= D_1\left[\left(\frac{u}{r} - \frac{w}{r\tan\gamma}\right) + \nu\frac{du}{dr}\right] - D_2\left(\frac{1}{r}\frac{dw}{dr} + \nu\frac{d^2w}{dr^2}\right) - M_T\end{aligned}\right\} \quad (1.4)$$

where

$$\left.\begin{aligned}D_0(r) &= \frac{1}{1-\nu^2}\int E(r, z)\, dz\\ D_1(r) &= \frac{1}{1-\nu^2}\int E(r, z)z\, dz\\ D_2(r) &= \frac{1}{1-\nu^2}\int E(r, z)z^2\, dz\\ N_T(r) &= \frac{a}{1-\nu}\int E(r, z)T(r, z)\, dz\\ M_T(r) &= \frac{a}{1-\nu}\int E(r, z)T(r, z)z\, dz\end{aligned}\right\} \quad (1.5)$$

We choose our median surface for $z = 0$, dependent upon $E(r, z)$, so that $D_1 = 0$. Eqs. (1.5) reduce to

$$\left.\begin{aligned}N_r &= D_0\{(du/dr) + \nu[(u/r) - (w/r\tan\gamma)]\} - N_T\\ N_\vartheta &= D_0\{[(u/r) - (w/r\tan\gamma)] + [\nu(du/dr)]\} - N_T\\ M_r &= -D_2\{(d^2w/dr^2) + [\nu(1/r)\,(dw/dr)]\} - M_T\\ M_\vartheta &= -D_2\{(1/r)\,(dw/dr) + [\nu(d^2w/dr^2)]\} - M_T\end{aligned}\right\} \quad (1.6)$$

Eqs. (1.6) above give the representation of the net sectional forces and moments in terms of the two displacement variables u, w and the given thermal force and moment.

(II) *Static Equilibrium*

Static equilibrium of an element requires that

$$\left.\begin{aligned}(d/dr)\,(rN_r) - N_\vartheta &= 0\\ (d/dr)\,(rQ_r) + (N_\vartheta/\tan\gamma) &= 0\\ (d/dr)\,(rM_r) - M_\vartheta - rQ_r &= 0\end{aligned}\right\} \quad (2.1)$$

The normal shear term Q_r is eliminated in the following way. From the first two equations above we find

$$Q_r\tan\gamma + N_r = \text{const.}/r$$

Since $N_r = Q_r = 0$ at the boundaries, it follows that

$$N_r = -Q_r\tan\gamma$$

Therefore, our equilibrium equations become simply

$$\left.\begin{aligned}(d/dr)\,(rN_r) &= N_\vartheta\\ (d/dr)\,(rM_r) &= M_\vartheta - rN_r\cot\gamma\end{aligned}\right\} \quad (2.2)$$

(III) *Reduction to Two Equations in Two Unknowns*

The equilibrium Eqs. (2.2), together with Eqs. (1.6) which define forces in terms of displacements, will now be reduced to two second-order differential equations in terms of two dependent variables.

Introduce $\xi = dw/dr$ as one of the dependent variables and substitute the definitions of Eqs. (1.6) into the second of Eqs. (2.2).

$$(d/dr)D_2\{[r(d\xi/dr)] + \nu\xi\} + (d/dr)rM_T = D_2\{[(1/r)\xi] + [\nu(d\xi/dr)]\} + M_T + rN_r\cot\gamma$$

Expanding and collecting terms, the first of the required equations is obtained.

$$\frac{d^2\xi}{dr^2} + \left(\frac{1}{r} + \frac{d}{dr}\log D_2\right)\frac{d\xi}{dr} - \left(\frac{1}{r^2} - \frac{\nu}{r}\frac{d}{dr}\log D_2\right)\xi - \frac{\cot\gamma}{D_2}N_r = -\frac{1}{D_2}\frac{dM_T}{dr} \quad (3.1)$$

In order to obtain the second equation needed, we first invert the first two equations of Eqs. (1.4) to solve for u and du/dr.

$$u = \{r/[(1-\nu^2)D_0]\}\ (N_\vartheta - \nu N_r) + w\cot\gamma + \{r/[(1+\nu)D_0]\}N_T \quad (3.2)$$
$$du/dr = \{1/[(1-\nu^2)D_0]\}\ (N_r - \nu N_\vartheta) - \{1/[(1+\nu)D_0]\}N_T$$

The first of Eqs. (2.2) gives a substitution for N_ϑ in terms of N_r. Inserting this substitution and eliminating u from Eqs. (3.2) by differentiation, we find

$$\frac{d}{dr}\frac{r}{(1-\nu^2)D_0}\left(\frac{d}{dr}rN_r - \nu N_r\right) + \xi\cot\gamma + \frac{d}{dr}\frac{r}{(1+\nu)D_0}N_T = \frac{1}{(1-\nu^2)D_0}\left(N_r - \nu\frac{d}{dr}rN_r\right) - \frac{1}{(1+\nu)D_0}N_T$$

Expanding and collecting terms, the second of the required equations is obtained.

$$\frac{d^2N_r}{dr^2} + \left(\frac{3}{r} - \frac{d}{dr}\log D_0\right)\frac{dN_r}{dr} - \frac{(1-\nu)}{r}\frac{d}{dr}\log D_0N_r + \frac{(1-\nu)}{D_0r^2}\cot\gamma\,\xi = \frac{(1-\nu)}{r}\left[\left(\frac{d}{dr}\log D_0 - \frac{2}{r}\right)N_T - \frac{dN_T}{dr}\right] \quad (3.3)$$

(IV) *Collection of Equations*

Our two second-order differential equations in the two dependent variables ξ, N_r are

$$\left.\begin{aligned}(d^2\xi/dr^2) + f_1(r)\,(d\xi/dr) + f_2(r)\xi + f_3(r)N_r &= f_4(r)\\ (d^2N_r/dr^2) + f_5(r)\,(dN_r/dr) + f_6(r)N_r + f_7(r)\xi &= f_8(r)\end{aligned}\right\} \quad (4.1)$$

where the $f_i(r)$ are known functions of r given in Eqs. (3.1) and (3.3).

The boundary conditions are simply: at $r = r_1, r_2$,

$$N_r = 0$$
$$M_r = 0 = -D_2\{(d\xi/dr) + [(\nu/r)\xi]\} - M_T \quad (4.2)$$

(V) Simplification for Special Problem

It will be shown here that a simplification of Eqs. (4.1) results from application to one of the more typical of the subject problems.

Consider the cone subjected to a temperature distribution resulting from heat transfer through a laminar boundary layer. Further, assume that the cone has been optimally designed in the sense that the skin thickness variation has been proportioned so that the resulting heat flux distribution permits the outer and inner skin surfaces to be isotherms. To within a first-order approximation then, it is seen that the isotherm pattern is the same at all cross sections—i.e., the geometric picture of the isotherm pattern is merely scaled by the skin thickness $h(r)$.

Using this scalar magnification property, we set

$$z = h(r)\tau$$

so that $\int d\tau = 1$. The plate stiffness parameters become

$$\left.\begin{aligned} D_0(r) &= \int E(r, z)\, dz = \int E[T(\tau)]h(r)\, d\tau = \\ &\qquad h(r)\int E(\tau)d\tau = c_0 h(r) \\ D_2(r) &= \int E(r, z)z^2\, dz = \int E[T(\tau)]h^3(r)\tau^2\, d\tau = \\ &\qquad h^3(r)\int E(\tau)\tau^2\, d\tau = c_2 h^3(r) \end{aligned}\right\} \tag{5.1}$$

The logarithmic derivatives become

$$\left.\begin{aligned} (d/dr)\log D_0 &= (d/dr)\log h(r) \\ (d/dr)\log D_2 &= 3(d/dr)\log h(r) \end{aligned}\right\} \tag{5.2}$$

Further, since we have at our disposal the choice of temperature reference, we choose this reference so that the thermal normal force vanishes everywhere—i.e.,

$$\left.\begin{aligned} N_T(r) &= \frac{a}{1-\nu}\int E(r, z)T(r, z)\, dz \\ &= \frac{ah(r)}{1-\nu}\int E(\tau)T(\tau)\, d\tau \equiv 0 \end{aligned}\right\} \tag{5.3}$$

We are left with only the thermal moment, which is now

$$M_T(r) = \frac{ah^2(r)}{(1-\nu)}\int E(\tau)T(\tau)\tau\, d\tau = c_3 h^2(r) \tag{5.4}$$

Using Eqs. (5.1) through (5.4), the differential Eqs. (4.1) can be written in the following form:

$$\left.\begin{aligned} &\frac{d^2\xi}{dr^2} + \left(\frac{1}{r} + 3\frac{d}{dr}\log h\right)\frac{d\xi}{dr} - \left(\frac{1}{r^2} - 3\frac{\nu}{r}\frac{d}{dr}\log h\right)\xi - \\ &\qquad \frac{\cot\gamma}{c_2 h^3 N_r} = -\frac{2c_3}{c_2}\frac{1}{h}\frac{d}{dr}\log h \\ &\frac{d^2N_r}{dr^2} + \left(\frac{3}{r} - \frac{d}{dr}\log h\right)\frac{dN_r}{dr} - \frac{(1-\nu)}{r}\frac{d}{dr}\log hN_r + \\ &\qquad \frac{1-\nu^2\cot\gamma}{c_0 hr^2}\xi = 0 \end{aligned}\right\} \tag{5.5}$$

Eqs. (5.5) can be simplified still further by assuming that the optimally designed skin thickness variation can be approximated by a curve of the form

$$h(r) = br^{-n}$$

The resulting equations now become

$$\left.\begin{aligned} &\frac{d^2\xi}{dr^2} + \frac{1}{r}(1-3n)\frac{d\xi}{dr} - \frac{1}{r^2}(1+3\nu n)\xi - \\ &\qquad \frac{\cot\gamma}{b^3c_2}r^{3n}N_r = \frac{2nc_3}{bc_2}r^n \\ &\frac{d^2N_r}{dr^2} + \frac{1}{r}(3+n)\frac{dN_r}{dr} + \frac{1}{r^2}(1-\nu)nN_r + \\ &\qquad \frac{(1-\nu^2)\cot\gamma}{bc_0}r^{n-2}\xi = 0 \end{aligned}\right\} \tag{5.6}$$

The solutions to Eqs. (5.6) above can be easily approximated by series expansion.

REFERENCES

[1] Huth, J. H., *Thermal Stresses in Conical Shells*, Journal of the Aeronautical Sciences, Vol. 20, No. 9, pp. 613–616, September, 1953.

[2] Tsien, H. S., *Similarity Laws for Stressing Heated Wings*, Journal of the Aeronautical Sciences, Vol. 20, No. 1, pp. 1–11, January, 1953.

Transient Stresses in Airfoils Under Blast Loading*

H. F. Ludloff and F. J. Marshall
New York University and U.S. NOTS, China Lake, Calif.
January 24, 1955

THIS NOTE DEALS with the distribution of deflection, shear, and moment in a simplified airfoil model (beam), if the latter is struck by a strong, plane blast front. The airloads may be considered as known theoretically or experimentally. The type and intensity of the vibrations induced in the beam are to be derived.

Among the various possible geometrical arrangements, two may be pointed out as of particular theoretical and practical interest (see Fig. 1):

(I) Strong blast advancing almost perpendicularly to airfoil surface [at angle $(\pi/2) - \epsilon$]. Case I: The shock front will be split into two parts. The part moving along the upper surface will advance, as if against a shallow compression corner and experience a Mach reflection;† the shock moving along the lower surface will produce a weak expansion domain, as indicated.

* This problem originated from a discussion while the senior author was summer consultant at U.S. NOTS. This preliminary investigation is being supported, in part, by the Mechanics Branch of ONR.

† See Ting, L., and Ludloff, H. F., *Aerodynamics of Blasts*, Journal of the Aeronautical Sciences, Vol. 19, No. 5, pp. 317–328, May, 1952.

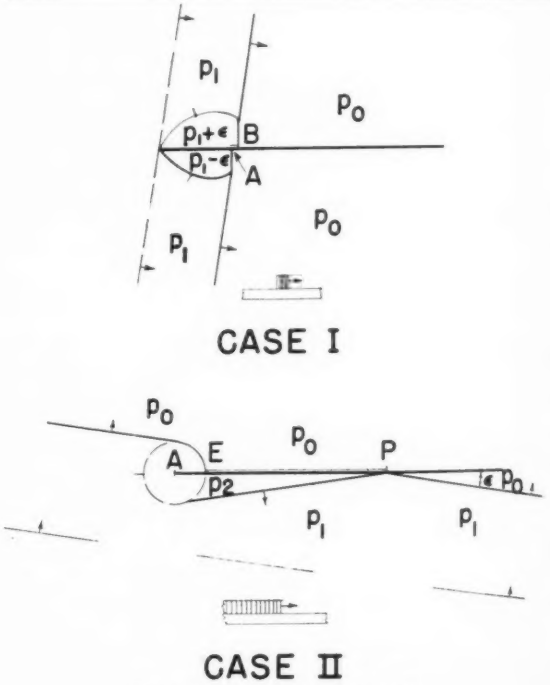

FIG. 1. Two cases of blast loads.

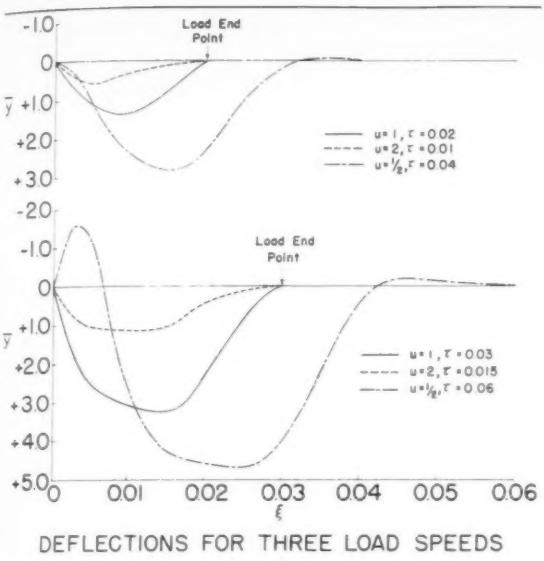

DEFLECTIONS FOR THREE LOAD SPEEDS

FIG. 2.

Both parts of the shock front will end perpendicularly on the airfoil surface, on places which are a *very small distance AB apart* from each other. Since either shock diffraction produces only small deviations from the undisturbed pressures behind the shock front, it is seen that a strong concentrated force $(p_1 + \epsilon - p_2)$ from above, will advance with shock speed U_s along the surface.

(II) Strong blast front advancing almost parallel to airfoil surface (at angle ϵ). Case II: In this case, the lower part of the shock front will experience a regular reflection producing an extremely high pressure load, p_2, on a restricted part AP of the lower surface. The upper part of the shock front will be diffracted and will become quite weak near the upper surface, E. Since P and E are increasingly far apart from each other, the airload acting from below is spread over an appreciable area AP. Now, the interesting feature is the fact that the end point of the load distribution, P, advances over the lower surface with a speed $U_s/\sin\epsilon$—i.e., at a *speed* which may be *well in excess* of the speed of propagation of the elastic waves produced in the *airfoil* (beam). In this case a discontinuous shear distribution will advance into the undisturbed part of the beam, similarly as a shock.

In either case, the flexural vibrations of the airfoil (beam) will play the predominant role. Since high frequencies are excited by blast loads, the rotatory inertia and shear have to be taken into account. In other words, the forced vibrations of "Timoshenko-beams" have to be computed. (As known, the velocity of elastic waves in such beams tends with decreasing wave length toward a finite limit.)

Thus, the analytic statement of the problem is to find solutions of the following differential equations:

$$z_\xi + i\cdot 2\lambda\cdot k_\tau = -q;\ z_\tau + i\cdot 2\lambda\cdot k_\xi - i\cdot 2\lambda\cdot z = 0;$$
$$\text{here } z = V + i\cdot 2\lambda\cdot\omega \text{ and } k = M + i\cdot 2\lambda\cdot\dot{y} \quad (1)$$

V = shear, M = bending moment, ω = angular velocity, y = transverse deflection. ξ, τ = dimensionless axial and time coordinates. $\lambda = L/2r_i$ is the beam length in radii of gyration.

For our loading

$$q = P \text{ for } 0 < \xi < u\cdot\tau$$
$$= 0 \text{ for } \quad \xi > u\cdot\tau$$

where the speed of the load (or load end point P respectively), u, may be larger or smaller than the limit speed of the elastic waves which is set equal to one.

Furthermore, there are two boundary conditions on either end of the beam, and four initial conditions.

The case of a concentrated moving load is easily deduced from the preceding case of distributed loading.

Solutions have been obtained in any one of the following three ways:

(1) by the classical method of expansion in eigenfunctions. Due to the discontinuity of the loading function, small wave lengths are excited with great intensity. Hence, the slow convergence of the series makes an evaluation of results prohibitive.

(2) by the method of characteristics which is applicable, because differential equations (1) are hyperbolic. This representation is very appropriate for numerical evaluation at early times.

(3) by application of the Laplace transform. In this representation, it turns out that the solutions can be represented by a finite number of terms, so that an analytic discussion as well as a numerical evaluation could be successfully carried out. The deflection curves $y(\xi, \tau)$ as well as the distribution of shear, bending moment and rotation have been derived for $u \gtrless 1$. This is comparable to supersonic, sonic, and subsonic conditions.

The analytic solutions obtained after (3) are of the form:

$$z(\xi, \tau) = P\int_0^\tau f_1(\tau - t)\cdot[\Phi - i\Psi]\,dt +$$
$$\frac{P}{2\lambda u}\cdot\int_0^\tau f_2(\tau - t)\cdot[i\Phi_\xi - \Psi_\xi]\,dt - U(\tau, \xi)\cdot f_3(\tau - \xi/u) \quad (2a)$$

and

$$K(\xi, \tau) = \frac{P}{2\lambda}\int_0^\tau f_4(\tau - t)\cdot[i\Phi_\xi + \Psi_\xi]\,dt -$$
$$\frac{P}{4\lambda^2 u}\cdot\int_0^t f_5(\tau - t)\cdot[\Phi_{\xi\xi} + i\Psi_{\xi\xi}]\,dt - U(\tau, \xi)\cdot f_6(\tau - \xi/u) \quad (2b)$$

Here

$$\Phi = U\cdot\Gamma;\ \Psi = \int_0^t U\Gamma\cdot J_1[2\lambda(t - \hat{t})]\cdot(t - \hat{t})^{-1}\,d\hat{t};\ \Gamma =$$
$$e^{i\lambda\tau}\cdot J_0[\lambda\cdot\sqrt{\tau^2 - \xi^2}];\ U(\tau, b) = 0 \text{ or } 1 \text{ for } \tau \gtrless b.$$

Discussion of these expressions is greatly simplified, if characteristic coordinates are employed.

Figs. 2 and 3 show the early development in time of the distribution of deflection $\bar{y} = y\cdot EI\cdot P^{-1}L^{-4}\cdot 10^6$ and shear $\bar{V} = V\cdot P^{-1}L^{-1}\cdot 10^2$. It is remarkable that for $u \geq 1$, the deflection is always downward, while for $u < 1$, there are two places (near the end of the elastic waves, and at one end of the wing) where the deflection is upward. It can be shown from Eqs. (2a) and (2b) that this is true for all times. Furthermore note that at $u = 1$, the shear (and moment) distribution is discontinuous at

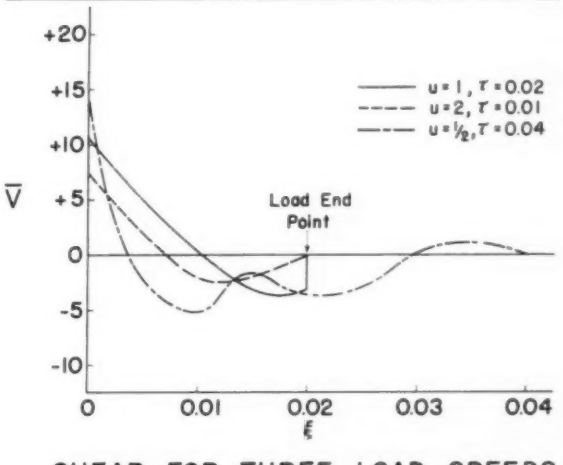

SHEAR FOR THREE LOAD SPEEDS

FIG. 3.

$\tau = \xi$. Comparing deflection curves at equal load length, the deflection is larger for $u < 1$, as it should be.

The absorption of energy by the beam as well as the energy spectrum, as functions of u and τ are being investigated.

On a Stress Tensor for Turbulence

Willis H. Braun
Lewis Flight Propulsion Laboratory, NACA, Cleveland, Ohio
January 24, 1955

THE REYNOLDS EQUATIONS for steady turbulent shear flows of an incompressible fluid are

$$\rho U_j U_{i,\,j} = \mu U_{i,\,j,\,j} - P_{,\,i} + (-\overline{\rho u_j u_i})_{,\,j} \qquad (1)$$

The U_i are components of the mean velocity; the u_i are fluctuation velocity components. For a solution of these equations to be obtained it is necessary first to find an independent relation between the mean flow quantities and the Reynolds stresses $T_{ji} \equiv -\overline{\rho u_j u_i}$. There are several properties required of such a relation:

(1) The formulation of the stresses must be a tensor. Hence, it should be composed of sums of products of tensor quantities such as the mean velocity components and their gradients and gradients of the mean pressure. No quotients or reciprocals of tensor components are allowed for they have no meaning in a tensor formulation. Reciprocals of invariants formed from the tensor quantities are permitted, but, because of the regular nature of the mean flow, it is assumed such functions are expanded in power series of the tensor components. The net result is to bring the expression for the stress back to the stated form.

(2) It must be consistent with the boundary conditions. There are two boundary conditions on the mean velocity—requiring that it vanish at solid boundaries and attain a maximum at some other surface. Therefore, the equation of motion should be of second order. This, in turn, requires that no derivative of the mean velocity higher than the first appear in the stress tensor.

(3) The magnitude of a stress component should remain invariant while its sign undergoes a change due to the reflection of a coordinate that corresponds to one of the directions associated with that component. If a coordinate is reflected which does not correspond to either direction associated with the stress, then the component should change neither in magnitude nor in sign.

In addition to satisfying (1), (2), and (3), it is desirable that part of the stress tensor should represent a dissipative process. That part is expected to take the form of an irreversible process in a fluid—namely, the sum of products of diffusion coefficients and powers of the gradient of the velocity. In general, there should also be a portion of the stress which performs reversible work.

The effects of requirements (1), (2), and (3) can be simply illustrated by examining the fully-developed turbulent flow between two infinite, parallel flat plates. Let x_1 be the Cartesian coordinate parallel to the plates and in the direction of the mean velocity U_1, and let x_2 be perpendicular to the plates. The component of turbulent shear stress which acts to retard the flow is T_{21}, and according to (1) and (2) it should be of the form

$$T_{21} = A_{2112}U_1U_{1,\,2} + A_{211212}U_1(U_{1,\,2})^2 + \ldots + A_{21112}U_1^2U_{1,\,2} + A_{2111212}U_1^2(U_{1,\,2})^2 + \ldots \qquad (2)$$

Because the pressure gradients are either extremely small or constant, their contribution to the stress is assumed to be negligible. The $A_{ij}\ldots$ are tensor coefficients of proper dimensions, some of which are found to vanish by (3). The shear stress is then

$$T_{21} = (A_{21112}U_1^2 + A_{2111112}U_1^4 + \ldots)U_{1,\,2} + (A_{2111212}U_1^2 + A_{21111212}U_1^4 + \ldots)(U_{1,\,2})^2 + \ldots \qquad (3)$$

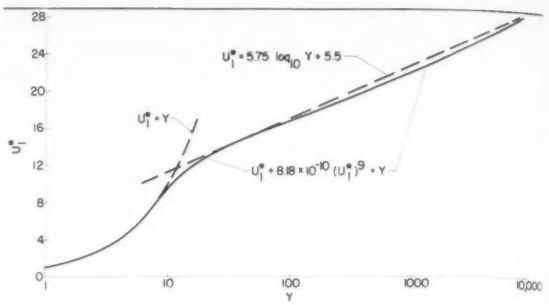

FIG. 1.

Eq. (3) resembles the general formulation of an irreversible process. The eddy diffusion coefficients, which are the terms in parentheses, are associated with the relative mean velocity between the fluid and the solid boundary. Their dependence on a velocity difference rather than on a velocity gradient corresponds to the production of the stresses by the turbulent motions which are of such scale that the mean velocity changes appreciably over one eddy. The classical form of a dissipative process involves only terms linear in the velocity gradient. According to reference 1 the classical generalization of Eq. (3) for the dissipative stresses should be a deviator tensor

$$(T_{ij})_D = (\alpha_{ijklrs}U_kU_l + \alpha_{ijklmnrs}U_kU_lU_mU_n + \ldots)U_{r,\,s} - (1/3)\delta_{ij}(\alpha_{ppklrs}U_kU_l + \alpha_{ppklmnrs}U_kU_lU_mU_n + \ldots)U_{r,\,s} \qquad (4)$$

The portion of the stress tensor which does reversible work has normal components only and is associated with the turbulent pressure.

$$(T_{ij})_R = -(1/3)\overline{\rho u_m u_m}\,\delta_{ij} \equiv -\pi\delta_{ij} \qquad (5)$$

Because the mean velocity gradient is associated with the dissipative portion of the stress, the turbulent pressure will be represented as a function of the mean velocity components alone.

$$\pi = \beta_{ij}U_iU_j + \beta_{ijkl}U_iU_jU_kU_l + \ldots \qquad (6)$$

The total turbulent stress is the combination of Eqs. (4) and (5),

$$T_{ij} = (T_{ij})_D - \pi\delta_{ij} \qquad (7)$$

The coefficients $\alpha_{ij}\ldots$ and $\beta_{ij}\ldots$ must in general depend upon the dimensionless parameters of the flow, on whether the boundaries are solid or fluid and on the shape of the boundaries if solid. These are the factors that determine the history of the flow and, hence, the turbulent structure at a point. At present it appears that the coefficients and their parameters' dependence can only be ascertained from experimental data. Consequently, the stress formulation [Eqs. (4), (6), and (7)] seems to have no immediate applicability in the sense of predicting mean velocity profiles in flows not already experimentally investigated. Nevertheless, it may be of value in suggesting correlations of experimental data.

In this regard the application of Eq. (4) to fully-developed pipe flow yields a new expression for the universal velocity profile near the wall. The primary dimensionless parameter of the flow is the Reynolds Number based on shear stress velocity and radius, $Re = \rho U^*L\mu^{-1}$. The shear stress (using the mixed tensor) is obtained from Eq. (4) by performing a dimensional analysis of the $\alpha_{ijk}\ldots$ and introducing dimensionless variables. The resulting form is

$$T_2{}^1 = \rho(U^*)^2 \sum_{n=1}^{\infty} f_n(Re)\,(u_1^*)^{2n}u_{1,\,2}^* \qquad (8)$$

where $u_1^* \equiv U_1/U^*$ and the $f_n(Re)$ are unspecified functions. The integrated equation of motion is then

$$u_1^* + u_1^*Re\sum_{n=1}^{\infty}\frac{1}{2n+1}f_n(Re)\,(u_1^*)^{2n} = \frac{1}{2}Re(1-r^2) \qquad (9)$$

Comparison with experiment[2] indicates that the leading terms

in the sum in Eq. (9) are integral powers of $(u_1^*)^8\ Re^{-1}$. Then near the wall Eq. (9) reduces to

$$u_1^* + a(u_1^*)^9 = y \tag{10}$$

where $y = Re(1 - r)$ and r is the dimensionless radial coordinate of the pipe. Eq. (10) for the mean velocity profile near the wall is compared with the logarithmic law (with constants as given in reference 3) in Fig. 1. It varies smoothly from the linear law, $u^* = y$, in the laminar region to a nearly logarithmic curve where the turbulent stress predominates.

REFERENCES

[1] Anderson, Orson L., *Conditions for the Derivation of the Stress Deviator Tensor*, American Journal of Physics, Vol. 20, No. 4, April, 1952.

[2] Laufer, John, *The Structure of Turbulence in Fully Developed Pipe Flow*, NACA TN 2954, June, 1953.

[3] Schlichting, H., *Lecture Series "Boundary Layer Theory" Part II—Turbulent Flows*, NACA TM 1218.

The Obukhoff Spectrum of Homogeneous Isotropic Turbulence

Knox Millsaps

Chief, System Dynamics Research Branch, Wright Air Development Center, ARDC, Wright-Patterson AFB, Ohio

January 31, 1955

A. M. OBUKHOFF[1] HAS SUGGESTED that the inertial transfer term in the spectral equation for homogeneous isotropic turbulence may be given in terms of the spectral distribution by postulating that the microcomponents of the turbulence constitute a Reynolds stress which produces a mean rate of shear in the macrocomponents of the turbulence. It is naturally assumed that the Reynolds stress is proportional to the energy in the microcomponents and that the mean rate of shear in the macrocomponents is effectively measured by the root mean square of the rate of strain of the macrocomponents. The Obukhoff postulate when applied to the universal equilibrium situation leads to the following spectral equation:

$$\epsilon = 2\nu \int_0^k k^2 F(k)\, dk + \gamma\sqrt{2} \int_k^\infty F(k)\, dk \left[\int_0^k k^2 F(k)\, dk\right]^{1/2}$$

wherein the customary notation[2] has been used. This integral equation is usually solved by numerical methods, and a closed solution does not appear to have been obtained. Consequently, it may be interesting to note that the substitution used by J. Bass[3] in his treatment of the Heisenberg spectrum may be employed and reduces the integral equation to a cubic algebraic equation. The resulting closed solution is

$$F(k) = \frac{1}{3k^2}\,[A + B]^{-2/3}\,[A' + B'] + \frac{1}{3k^2}\,[A - B]^{-2/3}\,[A' - B'] + \frac{2\nu^2 k}{3\gamma^2}$$

for

$$0 \le k \le \left(\frac{\epsilon\gamma^2}{4\nu^3}\right)^{1/4}$$

and

$$F(k) = 0 \quad \text{for} \quad (\epsilon\gamma^2/4\nu^3)^{1/4} < k < \infty$$

where

$$A = \frac{k^4}{432\gamma^6}\,(27\epsilon^2\gamma^4 + 18\epsilon\gamma^2\nu^3 k^4 + 2\nu^6 k^8)$$

$$B = \frac{\epsilon k^4}{48\gamma^3}\left[\frac{27\epsilon^2\gamma^2 + 4\epsilon\nu^3 k^4}{3}\right]^{1/2}$$

and the primes denote differentiation with respect to k.

REFERENCES

[1] Obukhoff, A. M., *On the Distribution of Energy in the Spectrum of Turbulent Flow*, Comp. Rend. Acad. Sci. U.S.S.R., Vol. 32, p. 19, 1941.

[2] Batchelor, G. K., *The Theory of Homogeneous Turbulence*, Cambridge University Press, p. 103, 1953.

[3] Bass, J., *Sur les Bases Mathématiques de la Théorie de la Turbulence d'Heisenberg*, Comp. Rend. Acad. Sci. Paris, Vol. 228, p. 22, 1949.

On the Normal Force Produced by Multifinned Tail Assemblies in Supersonic Flow

J. Leith Potter, William D. Murphree, and Norman M. Shapiro

Research Division, Ordnance Missile Laboratories, Redstone Arsenal, Huntsville, Ala.

February 7, 1955

ALTHOUGH REASONABLY SATISFACTORY METHODS have been devised for the calculation of normal forces on tail assemblies having two equally loaded fins 180° apart, very little progress has been made toward solution of the corresponding multifin problem where four or more fins may be acting. Two reports[1, 2] dealing with the subject have come to the attention of the authors. The earliest of these is by Luther and Jaeger and contains experimental results for several families of four-, six-, and eight-fin tails. The second report, by Miles, is a theoretical analysis using slender body theory. The latter report includes generalized results and apparently represents the only study of its type. However, the limitations of slender body theory are such that the writers, while appreciating the value of this work, wished to study the problem further. For this reason, it was decided that a brief but systematic supersonic tunnel program would be conducted for the purpose of obtaining additional experimental data on the lift of multifinned tail assemblies and that this would be followed by an attempt to generalize the data in a form suitable for design purposes. This note presents the data obtained thus far and a tentative proposal for an interference parameter which successfully correlates all the experi-

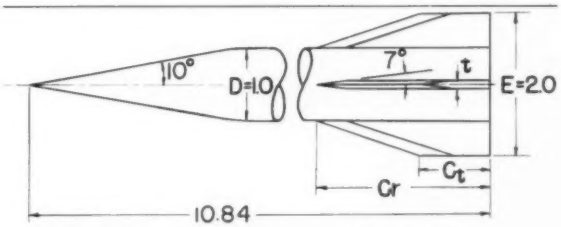

$C_r/C_t = 3.0$ $\quad D/E = 0.5$ $\quad t/C_r = 0.04$

CONFIGURATION	n (NUMBER OF FINS)	C_r
A	0	0
B	4	3.6
C	4	3.0
D	4	2.4
E	4	1.8
F	4	1.2
G	6	3.6
H	6	3.0
I	6	2.4
J	6	1.8
K	6	1.2
L	8	3.6
M	8	3.0
N	8	2.4
O	8	1.8
P	8	1.2

ALL DIMENSIONS IN INCHES OR DEGREES

FIG. 1. Finned bodies tested at Ordnance Missile Laboratories.

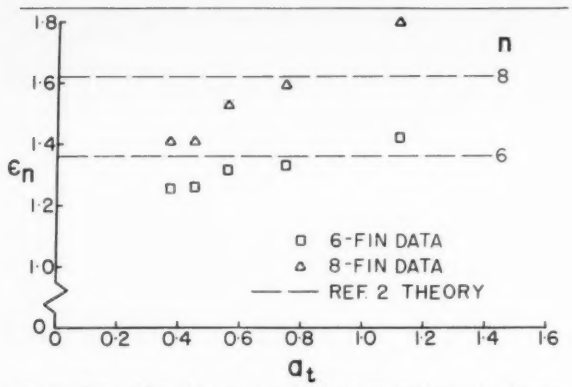

FIG. 2. Comparison between predictions of slender body theory and some experimental data for clipped-delta plan forms.

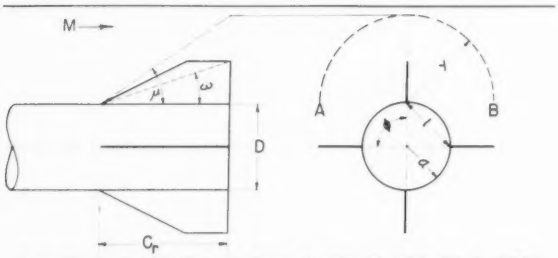

FIG. 3.

mental data in reference 1 as well as that secured by the authors' experiments.

The models tested in the Redstone 7- by 7-in. tunnel are described on Fig. 1. A trapezoidal or clipped-delta plan form was chosen in order to provide for subsonic and supersonic leading edges with adequate fin area for easily measured forces. The body was made as long as possible considering test section size, and calculations by the method of characteristics indicated that the nose should have negligible influence on the flow at the fin locations when angles of attack are small. In the test program already completed, all models were mounted with two fins in the pitch plane—i.e., the four-, six-, and eight-fin configurations had two, four, and six effective fins, respectively. Measurements of normal force and pitching moment were made at angles of attack equal to 0, ±1, ±2, ±4, and +6 degrees with numerous repetitions to verify accuracy. Reynolds Number based on free-stream conditions was close to 1.94×10^6 per in. during all tests and Mach Number was 2.86. A description of the NOTS experiments with fins of rectangular plan form is given in reference 1 and will not be repeated here.

The performance of finned bodies will be discussed in terms of the quantity $C_{N\alpha}$ which is the slope of the normal force coefficient curve at zero angle of attack. The writers determined values of $C_{N\alpha}$ by plotting (C_N/α) as a function of the angle of attack, α, and fairing a curve through $\alpha = 0$. After this, the finless or bare body value, $C_{NB\alpha}$, was subtracted from $C_{N\alpha}$ to give $C_{NT\alpha}$, which represents the total contribution of the fins including all interference effects. Having these data from experiments, the next step is to compare results with Miles' theory.[2] This is done on Fig. 2, where

$$\epsilon_n = C_{NT\alpha}\ (n \text{ fins})/C_{NT\alpha}\ (4 \text{ fins})$$

and

$$a_t = \tan \omega/\tan \mu$$

the angles being defined on Fig. 3.

Referring to Fig. 2, it is evident that the theory may be used for predicting approximate levels of the ratio, ϵ_n, but there are features of the data not recognized by slender body theory. For example, the detrimental effects of fin-on-fin interference may be reduced when the overlap of pressure fields is lessened. Considerations such as this led the senior author to formulate the interference parameter described below.

The intention in this case was merely to search for any significant trend in the data when plotted as a function of some parameter which reflects the degree of mutual interference between fins. As a simple first step, the ratio of a particular Mach cone radius, y, to the length between fin roots, l, was selected. (See the notation shown on Fig. 3.) This ratio is

$$I = (y/l) = c_r/[\beta D \sin (\pi/n)]$$

where

$\beta = \sqrt{M^2 - 1}$
$n \geq 2$, total number of fins

Presumably the body-on-fins and fins-on-body interference components differ depending on the number of fins, but it will be seen later that the parameter, I, at least partially compensates these effects.

In addition, $C_{NT\alpha}$ of the six- and eight-finned tails was adjusted for the reduced angle of attack and projected area of the fins not positioned in the horizontal plane. If α_e represents the geometric angle of attack of a rolled fin with zero incidence, it may be shown that

$$\alpha_e = \sin^{-1} (\sin \alpha \cos \phi)$$

where

α = angle of attack of nonrolled fins
ϕ = angle of roll from horizontal

Effective projected area of a rolled fin was obtained by multiplying panel area by the cosine of ϕ. These adjustments are meant to remove the penalties simply due to multifinned tails not having all fins operating at maximum angle of attack and not having all individual fin normal forces acting in the total normal force direction. The remaining differences between tails similar except for number of fins should be chargeable to interference effects. To summarize, in the present case where $\alpha \to 0$ and 2 fins on each tail are ineffective,

$$\alpha_e\ (4 \text{ fins}) = \alpha$$
$$S_e\ (4 \text{ fins}) = 2S_f$$
$$\alpha_e\ (6 \text{ fins}) = 0.866\alpha$$
$$S_e\ (6 \text{ fins}) = 3.46S_f$$

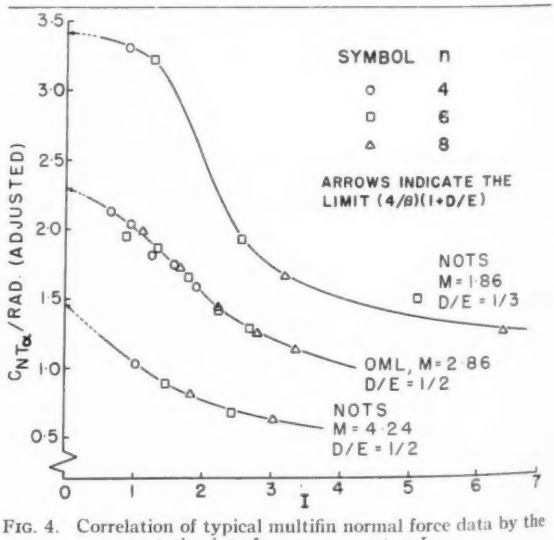

FIG. 4. Correlation of typical multifin normal force data by the tentative interference parameter, I.

$$\alpha_e\,(8\text{ fins}) = 0.805\alpha$$
$$S_e\,(8\text{ fins}) = 4.83S_f$$

All values of $C_{NT\alpha}$ used hereafter are based on α_e and S_e, the latter symbol representing total effective fin area. S_f is the area of one fin.

The clipped-delta data and typical examples of the NOTS rectangular-fin data are shown on Fig. 4. Considering the normal scatter in experimental data of this type, the parameter, I, is very effective. On the strength of evidence shown on Fig. 4, it appears that relatively accurate values of $C_{NT\alpha}$ for six- and eight-finned tails can be obtained merely by plotting available four-fin data as a function of I. Pending further analysis, a stronger conclusion will not be suggested, but the apparent lack of better methods for dealing with the problem seems to warrant this preliminary report.

References

[1] Luther, M. L., and Jaeger, B. F., *Effects of Varying the Number of Fins on Fin-Stabilized Supersonic Rockets*, U.S. Naval Ordnance Test Station NAVORD Report 1900, August, 1951.

[2] Miles, John W., *Interference Factors for Slender Finned Bodies*, U.S. Naval Ordnance Test Station NAVORD Report 2023, April, 1953.

Note on Velocity Fluctuations in Equilibrium Turbulent Shear Flow Along Solid Boundaries*

Heinrich B. Helmbold
School of Engineering, University of Wichita, Wichita, Kan.

February 8, 1955

RECENTLY TWO CAREFULLY PERFORMED experimental investigations have been published by J. Laufer[1] and P. S. Klebanoff[2] which reveal common features of fully-developed turbulent flow in pipes and plane boundary layers with zero pressure gradient. It may be expected that these features are characteristic not only of these special types of flow but of equilibrium turbulent shear flow along solid boundaries in general.

* This study was performed under Office of Naval Research Contract Nonr 201(01).

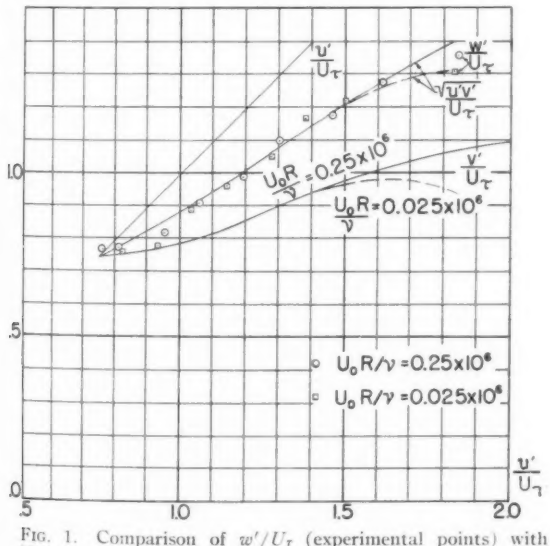

FIG. 1. Comparison of w'/U_τ (experimental points) with $\sqrt{u'v'}/U_\tau$ (curve) as deduced from faired experimental curves of u'/U_τ, and v'/U_τ for pipe flow (see reference 1).

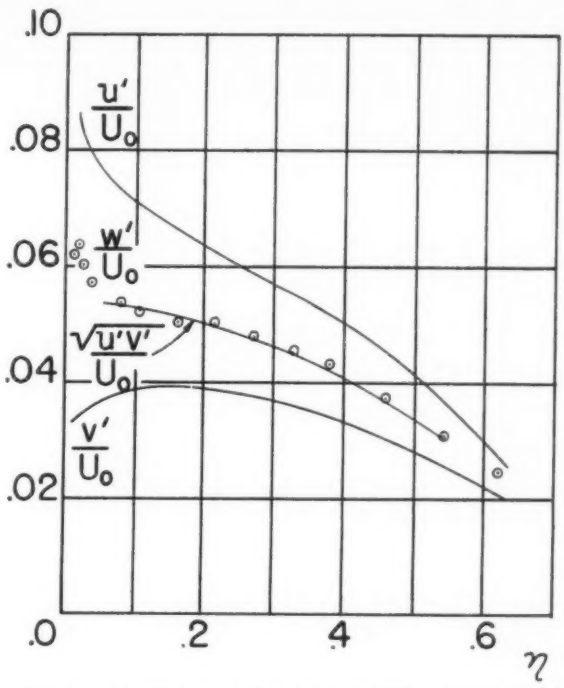

FIG. 2. Comparison of w'/U_0 (experimental points) with $\sqrt{u'v'}/U_0$ (curve) as deduced from faired experimental curves of u'/U_0 and v'/U_0 for plane boundary layer flow with no pressure gradient (plane wall, see reference 2).

(a) The root-mean-square values of velocity-fluctuation components are interconnected by the relationship (Figs. 1 and 2)

$$w' = \sqrt{u'v'} \qquad (1)$$

within the ranges of

$0.1 < \eta \leq 1.0$ in the pipe (independent of Reynolds Number)

and

$0.1 < \eta < 0.5$ in the plane boundary layer (intermittency factor $\gamma < 1$ for $\eta > 0.33$)

Here η denotes the nondimensional distances from the wall, referred to the pipe radius R and to that distance δ_0 from the flat plate where the shear-correlation coefficient vanishes ($\delta_0 = 1.2\delta$ in Klebanoff's notation), respectively. Whether the range of validity for the plane boundary layer actually is restricted by intermittency in the outer region of the layer, or if it merely seems so because of a falsifying effect of the intermittency on the measurements, remains open to discussion.

(b) The ratios of the root-mean-square velocity-fluctuation components in a plane parallel to the mean velocity and perpendicular to the walls of the pipe and flat plate are a "universal" function of the nondimensional distance from the walls (Fig. 3) in the form

$$v'/u' = k + 0.37\sqrt{\eta} \qquad (2)$$

The constants and ranges of validity are dependent on Reynolds Number;

$k = 0.43$ (pipe), $0.05 < \eta < 0.5$, $U_0R/\nu = 0.25 \times 10^6$
$k = 0.45$ (pipe), $0.15 < \eta < 0.6$, $U_0R/\nu = 0.025 \times 10^6$
$k = 0.44 \pm 0.01$ (plane wall), $0.08 < \eta < 0.6$, $U_1\,\delta_0/\nu = 0.1 \times 10^6$

The significant point about Eq. (2) is not the special function chosen for the representation of the experimental values, but the existence of a "universal" function $v'/u' = f(\eta)$. For greater distances, $\eta > 0.5$, the function deviates from Eq. 2 and tends to $f(1) = 1$ in the center of the pipe. The apparent difference

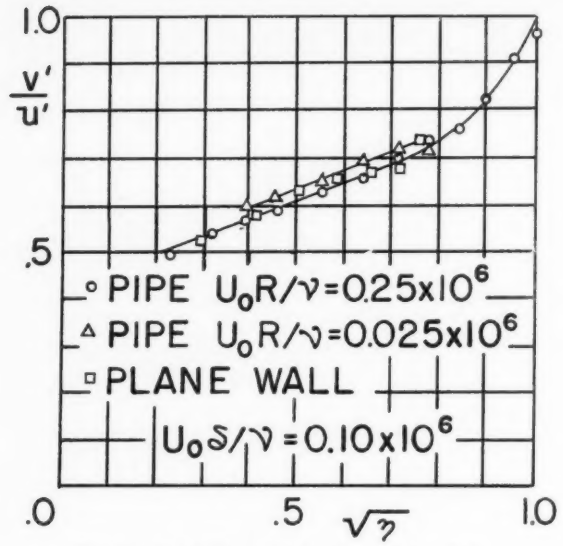

FIG. 3. The "universal" function $v'/u' = f(\eta)$.

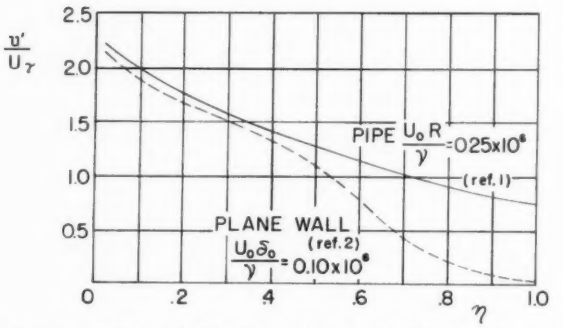

FIG. 4. Lateral distribution of u'/U_τ for pipe and plane wall

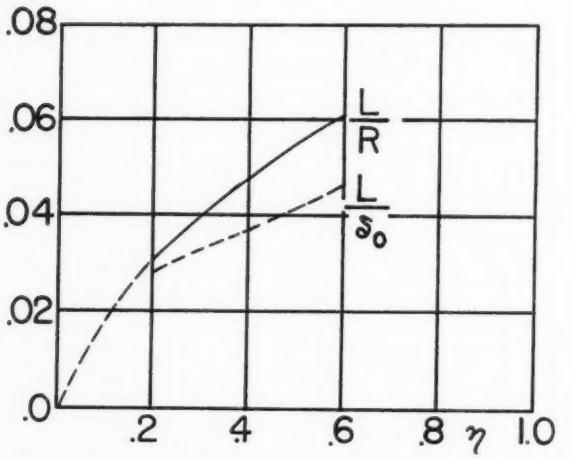

FIG. 5. Lateral distribution of turbulence scales in pipe (L/R) and plane wall (L/δ_0) flows.

between the functions for pipe and plane boundary layers in this region is subject to the same considerations about intermittency effects mentioned above.

(c) To complete the description of the field of velocity fluctuations in that region where these two cases are strictly comparable—i.e., where intermittency does not interfere ($0.1 < \eta < 0.33$)—it also may be stated that the longitudinal fluctuations u'/U_τ are approximately the same with the pipe flow and the plane-wall boundary layer at sufficiently high Reynolds Number (Fig. 4). Together with the statements (a) and (b) this means that in an important region of both flows the kinematic properties of the fluctuation fields are essentially the same; the only major difference is the magnitude of the shear correlation coefficients, about 0.42 with the pipe flow and 0.50 with the boundary layer at high Reynolds Numbers. In other words, the fluctuation fields agree essentially with respect to the intensities. However, they are much different with respect to the scales as can be seen by comparing the nondimensional quantities $L/R = [\overline{uv}/u'(dU/d\eta)]$ for the pipe and $L/\delta_0 = [\overline{uv}/u'(dU/d\eta)]$ for the plane wall (see Fig. 5). The length L can be interpreted as a measure in the y-dimension of the large eddies in turbulent motion.

REFERENCES

[1] Laufer, John, *The Structure of Turbulence in Fully Developed Pipe Flow*, NACA TN 2954, June, 1953.

[2] Klebanoff, P. S., *Characteristics of Turbulence in a Boundary Layer with Zero Pressure Gradient*, NACA TN 3178, July, 1954.

Limitations of Linear Theory in Predicting the Pressure Distribution on Triangular Wings

Elliott D. Katzen

Aeronautical Research Scientist, NACA, Ames Aeronautical Laboratory, Moffett Field, Calif.

February 11, 1955

THE PURPOSE OF THIS NOTE is to call attention to the fact that even for relatively thin, low aspect ratio wings the local surface slopes may be sufficiently large so that linear theory cannot be used for calculating the lift distribution, even at angles of attack as small as 3°. Experimental measurements that illustrate this were made on a triangular wing 5 per cent thick with an aspect ratio of 4, at a Mach Number of 3.36. The wing was tested in the 1- by 3-ft. supersonic wind tunnel at the NACA Ames Laboratory. The semispan wing was a reflection-plane model mounted on a boundary-layer bypass plate. The wing section, plan form, and positions of the pressure orifices are shown in Fig. 1. The wing was composed of similar sections of 5 per cent thickness ratio in the stream direction. Each section was a circular arc to the maximum thickness point at mid-chord and a parabolic arc from the mid-chord point to the blunt trailing edge. The trailing-edge thickness was 50 per cent of the maximum thickness. As a result of this wing geometry, the thickness distribution was not conical with respect to the apex in that the ratio of local thickness to chord was not constant along rays from the apex. Therefore, the pressures due to wing thickness at zero angle of attack were not constant along rays from the apex.

If linear theory is applicable, the pressure distribution due to angle of attack (lifting pressure) is independent of that due to wing thickness at zero angle of attack. On this basis, the wing pressures can be considered as the sum of the pressures due to wing thickness at zero angle of attack (thickness pressures) and those on a flat-plate wing of the same plan form at angle of attack. Since the flat-plate pressures due to angle of attack should be constant along rays from the apex, it follows that if linear theory is applicable for the complete wing, the pressure due to angle of attack should be constant along rays from the apex regardless of

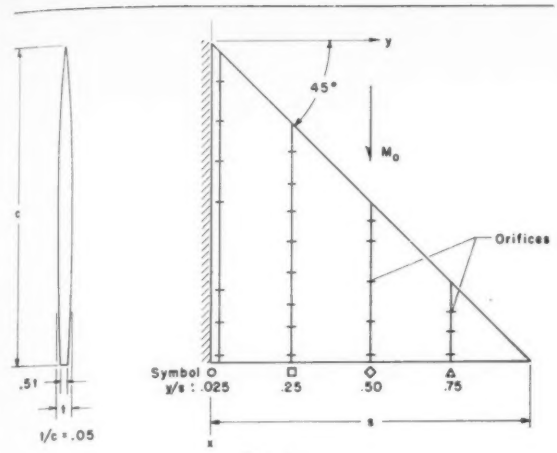

FIG. 1.

whether or not the thickness pressures are conical with respect to this point.

The lifting pressures are shown as a function of the direction of rays from the apex in Fig. 2. It can be seen that there is poor agreement between linear theory and experiment; the lifting pressures are not at all constant along these rays.

A more complete understanding of the nonlinear effects on the outboard portion can be obtained by reconsidering the geometry of the wing and the pressures. The wing is a cone with respect to the tip; the geometry can be described by directions from this point since there is no characteristic length in the problem. Therefore, the wing pressures should be constant along rays from the tip for that part of the wing forward of the region of influence of the apex. If the thickness and lifting pressure distributions are plotted as functions of the direction of rays from the tip as in Fig. 3, it can be seen that the thickness and lifting pressures are nearly constant along such rays. Comparison of the results of linear theory and experiment shows good agreement for the thickness case. For the lifting case, however, linear theory indicates a constant value of lift regardless of ray direction, whereas measured values vary systematically with change in ray direction. Apparently the local surface slopes are sufficiently high for this Mach Number to give rise to a nonlinear component of lift in much the same way that nonlinearities are produced on unswept two-dimensional wings of the same section at the same angle of attack. The linear theory predicts constant lifting pressures for the unswept two-dimensional wing. In contrast, the shock-expansion theory accounts for the finite thickness of the section and predicts increased lift at the leading edge and decreased lift at the trailing edge, resulting in a shift in the center of pressure toward the leading edge. It is evident that, as for the unswept, two-dimensional wing, nonlinear solutions that properly account for thickness effects are necessary for accurately predicting the lifting pressures on the triangular wing at a Mach Number of 3.36.

For that part of the wing forward of the region of influence of the apex, a nonlinear solution can be obtained by extension of the shock-expansion method. This has been done by Vincenti, of the NACA Ames Laboratory, who considers the curved surface of the wing as the limit of an infinite number of planar surfaces intersecting along rays passing through the wing tip. The changes in flow across each element, consisting of an intersection and subsequent flat surface, are then found from considerations of geometry and simple-sweep theory. The result, in the limit of the curved surface, is a pair of simultaneous ordinary differential equations whose solution is readily obtained by numerical means. Theoretical curves obtained by this method for the present wing at 0° and 3° angle of attack are shown in Fig. 3. It can be seen that the variation of lifting pressure with ray direction, previously noted, is estimated more accurately by the shock-expansion theory. The differences in absolute value of lifting pressures as estimated and measured may be attributed to small deviations in the model ordinates from the design values; theory indicates qualitatively that this is the case but does not provide a quantitative correction. Despite these differences, it is apparent that even for relatively thin low aspect ratio wings the surface slope may be sufficiently large that linear theory cannot be used for calculating lift distribution and that this is the case for the present 5 per cent thick wing at Mach Number of 3.6 and angle of attack of 3°.

Deviations from linear theory also occur inside the region of influence of the apex. For this region, further development of nonlinear theory is necessary in order to calculate the pressure distribution.

These results have shown an example of the errors involved in superposing thickness and lifting solutions for a triangular wing in the manner assumed to be valid in linear theory. Wings of other plan forms have similar regions for which nonlinear solutions are also needed.

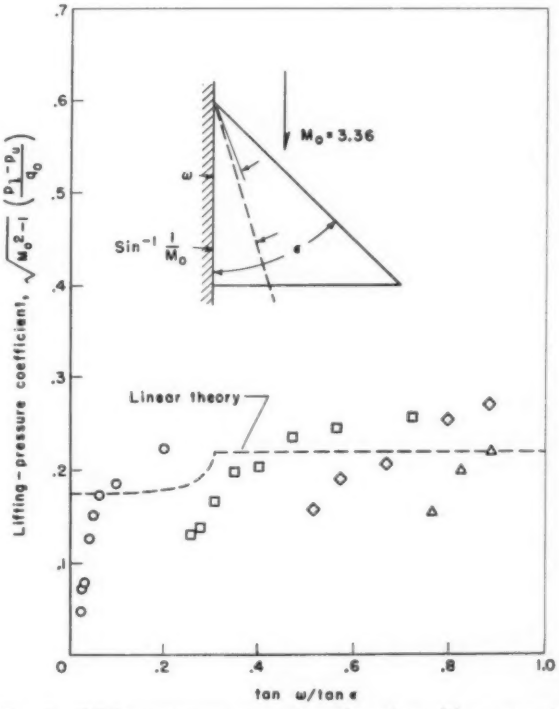

FIG. 2. Lifting pressures on a triangular wing with an aspect ratio of 4 at 3 degrees angle of attack.

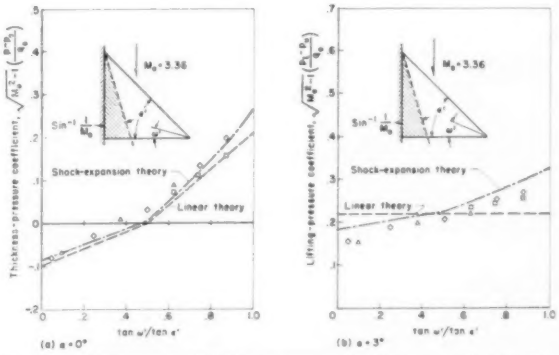

FIG. 3. Thickness and lifting pressures for that part of the wing forward of the region of influence of the apex.

A New Method of Solution of Equation of Compressible Flow

Ezio Betti
Laboratorio di Aerodinamica, Scuola Applicazione Aeronautica, Florence, Italy
February 28, 1955

We consider the two-dimensional equation of compressible flow in which the parameter m is introduced:

$$\frac{\partial^2\varphi}{\partial x^2}\left(1 - m\frac{V_x^2}{a^2}\right) + \frac{\partial^2\varphi}{\partial y^2}\left(1 - m\frac{V_y^2}{a^2}\right) - 2\frac{\partial^2\varphi}{\partial x\partial y}\frac{V_xV_y}{a^2}m = 0 \tag{1}$$

φ is the potential function

$$V_x = \partial\varphi/\partial x \qquad V_y = \partial\varphi/\partial y \qquad a^2 = a_0^2 - [(\gamma - 1)/2](V_x^2 + V_y^2)$$

a_0 is the sound velocity at rest. For $m = 0$ the equation is that of incompressible flow and for $m = 1$ the equation is that of compressible flow. We try to determine the compressible flow, subsonic or supersonic, around a given airfoil by utilizing the solution of incompressible flow around the same airfoil and proceeding in the following manner:

We subdivide the interval 0, 1 of m parameter in n partial intervals of size μ; the corresponding values of m are indicated with m_1, m_2, . . . m_i, . . . m_i; (where $m_{i+1} - m_i = \mu$, $m_n = 1$). The generic function, solution of Eq. (1) with $m = m_i$ is indicated φ_i and the difference $\varphi_i - \varphi_{i-1} = \mu X_i$.

We utilize the equations obtained by neglecting the terms in μ^2 and higher in the following.*

$$\frac{\partial^2(\varphi_{i-1} + \mu X_i)}{\partial x^2}\left\{1 - \frac{m_i}{a^2(m_i)}\left[\frac{\partial(\varphi_{i-1} + \mu X_i)}{\partial x}\right]^2\right\} + \frac{\partial^2(\varphi_{i-1} + \mu X_i)}{\partial y^2}\left\{1 - \frac{m_i}{a^2(m_i)}\left[\frac{\partial(\varphi_{i-1} + \mu X_i)}{\partial y}\right]^2\right\} -$$
$$2\frac{m_i}{a^2(m_i)}\frac{\partial^2(\partial_{i-1} + \mu X_i)}{\partial x\partial y}\frac{\partial(\varphi_{i-1} + \mu X_i)}{\partial x}\frac{\partial(\varphi_{i-1} + \mu X_i)}{\partial y} - \frac{\partial^2\varphi_{i-1}}{\partial x^2}\left\{1 - \frac{m_{i-1}}{a^2(m_{i-1})}\frac{\partial\varphi_{i-1}{}^2}{\partial x^2}\right\} -$$
$$\frac{\partial^2\varphi_{i-1}}{\partial y^2}\left\{1 - \frac{m_{i-1}}{a^2(m_{i-1})}\frac{\partial\varphi_{i-1}{}^2}{\partial y^2}\right\} + \frac{2m_{i-1}}{a^2(m_{i-1})}\frac{\partial^2\varphi_{i-1}}{\partial x\partial y}\frac{\partial\varphi_{i-1}}{\partial x}\frac{\partial\varphi_{i-1}}{\partial y} = 0 \tag{2}$$
$$(i = 1, 2, \ldots n)$$

The simplified equations are indicated with the number (3) between the brackets and the above equations with (2). The difference method will be used to determine $\bar{X}_1$ of the first of linear partial differential equations (3), φ_0 being the solution of incompressible flow. Then from the knowledge of $\varphi_1 = \varphi_0 + \mu\bar{X}_1$ using the second of (3) will be determined $\bar{X}_2$ and so continuing $\bar{X}_3$, $\bar{X}_4$, . . . $\bar{X}_n$. The solution of the last equation (3) will result: $\varphi_n = \varphi_0 + \mu\bar{X}_1 + \mu\bar{X}_2 + \ldots \mu\bar{X}_n$. Now when $\mu \to 0$, that one will be as the solution of equations of compressible flow because the difference between (2) and (3) resides in the terms of order μ^2 and higher neglected in the equations (3). The importance of the terms will be made extremely small decreasing the size of intervals—namely, for $\Delta\mu \to 0$.

* $a^2(m_i) = a_0^2 - [(\gamma - 1)/2][(\partial\varphi_i/\partial x)^2 + (\partial\varphi_i/\partial y)^2]$

On Use of the General Bending Formula

W. P. Rodden
Missiles Division, The RAND Corporation, Santa Monica, Calif.
February 14, 1955

The general unsymmetrical bending formula for plane stress, σ, given by the simultaneous solution of the three equations of section equilibrium without the simplification of centroidal coordinates offers a reasonable savings in computing time and memory space required for stress calculations on a high-speed digital computer.

Writing the equilibrium equations about arbitrary reference axes, x and y, we obtain the applied axial load,

$$P = \int \sigma dA \tag{1}$$

where dA is an element of section area, the applied bending moment about the x axis,

$$M_x = -\int \sigma y dA \tag{2}$$

and the applied bending moment about the y axis,

$$M_y = -\int \sigma x dA. \tag{3}$$

Substituting the plane stress relationship,

$$\sigma = Bx + Cy + D \tag{4}$$

the equilibrium equations become

$$BQ_y + CQ_x + DA = P \tag{5}$$
$$BI_{xy} + CI_x + DQ_x = -M_x \tag{6}$$
$$BI_y + CI_{xy} + DQ_y = -M_y \tag{7}$$

where

$$A = \int dA,\ Q_x = \int y dA,\ Q_y = \int x dA,\ I_x = \int y^2 dA,\ I_y = \int x^2 dA,\ I_{xy} = \int xy dA$$

The simultaneous solution of Eqs. (5), (6) and (7) yields the following expressions for the coefficients:

$$B = (1/\Delta)[M_x(Q_xQ_y - I_{xy}A) + M_y(I_xA - Q_x^2) + P(Q_yI_x - Q_xI_{xy})] \tag{8}$$

$$C = (1/\Delta)[M_x(I_yA - Q_y^2) + M_y(Q_xQ_y - I_{xy}A) + P(Q_xI_y - Q_yI_{xy})] \tag{9}$$

$$D = (1/\Delta)[-M_x(Q_xI_y - Q_yI_{xy}) - M_y(Q_yI_x - Q_xI_{xy}) + P(I_{xy}^2 - I_xI_y)] \tag{10}$$

where

$$\Delta = A(I_{xy}^2 - I_xI_y) + Q_x(Q_xI_y - Q_yI_{xy}) + Q_y(Q_yI_x - Q_xI_{xy}). \tag{11}$$

Although these expressions for the coefficients are somewhat more lengthy than the corresponding ones in the usual unsymmetrical bending formula, the computing effort saved by avoiding the calculation of the centroidal coordinates of typical complex aircraft wing and fuselage structures is extremely worth while.

The centroidal moments of inertia needed in deflection calculations are obtained from the transfer formulas:

$$I_{x_o} = I_x - \bar{y}Q_x \tag{12}$$

$$I_{y_o} = I_y - \bar{x}Q_y \tag{13}$$

$$I_{xy_o} = I_{xy} - \bar{y}Q_x \tag{14}$$

where $\bar{x} = Q_y/A$ and $\bar{y} = Q_x/A$.